

https://dspace.org/

mRNA-mediated delivery of anti-HIV-1 multispecific antibodies as a passive immunisation strategy

O'Connor, Caitlyn

2024

University of the Witwatersrand, Johannesburg

https://hdl.handle.net/10539/46879

O'Connor, Caitlyn . (2024). mRNA-mediated delivery of anti-HIV-1 multispecific antibodies as a passive immunisation strategy [Master`s dissertation, University of the Witwatersrand, Johannesburg]. WIReDSpace. https://hdl.handle.net/10539/46879

Downloaded from a DSpace repository. https://dspace.org/

mRNA-mediated delivery of anti-HIV-1 multispecific antibodies as a passive immunisation strategy.

Caitlyn O'Connor



A dissertation submitted to the Faculty of Health Sciences,
University of the Witwatersrand, Johannesburg
In fulfilment of the requirements for the degree of
Master of Science in Medicine

Johannesburg, July 2024

Declaration.

UNIVERSITY OF THE WITWATERSRAND JOHANNESBURG

FACULTY OF HEALTH SCIENCES

PLAGIARISM DECLARATION TO BE SIGNED BY ALL HIGHER DEGREE STUDENTS

SENATE PLAGIARISM POLICY: APPENDIX ONE

I Caitlyn O'Connor (Student number: 1842025) am a student registered for the degree of Master of Science in Medicine by Dissertation in the academic year 2024.

I hereby declare the following:

- I am aware that plagiarism (the use of someone else's work without their permission and/or without acknowledging the original source) is wrong.
- I confirm that the work submitted for assessment for the above degree is my own unaided work except where I have explicitly indicated otherwise.
- I have followed the required conventions in referencing the thoughts and ideas of others.
- I understand that the University of the Witwatersrand may take disciplinary action against me if there is a belief that this is not my own unaided work or that I have failed to acknowledge the source of the ideas or words in my writing.
- I have included as an appendix a report from "Turnitin" (or other approved plagiarism detection) software indicating the level of plagiarism in my research document.

Signature: CO'Connor Date: 11/07/2024

Publications and presentations arising from this study.

Conference presentations:

Caitlyn J. O'Connor, Abdullah Ely, Maria A. Papathanasopoulos, Mark A. Killick. mRNA-mediated delivery of anti-HIV-1 broadly neutralising multispecific antibodies as a potential strategy for HIV-1 prevention. Oral presentation at: Molecular Biosciences Research Thrust; 7 December 2023; University of the Witwatersrand Parktown Campus, Johannesburg, South Africa.

Caitlyn J. O'Connor, Abdullah Ely, Maria A. Papathanasopoulos, Mark A. Killick. mRNA-mediated delivery of anti-HIV-1 broadly neutralising multispecific antibodies as a potential strategy for HIV-1 prevention. Poster presented at: Keystone Symposia, HIV Vaccines, Immunoprophylaxis and Drugs; 6-10 June 2023; Keystone, Colorado, USA.

Abstract.

HIV-1 broadly neutralising antibodies (bNAbs) show great promise at both reducing viraemia and preventing HIV-1 infection, however, their application may ultimately be limited due to high manufacturing costs and the requirement for combination-based therapies. This project describes the development of *in vitro* transcribed (IVT)-mRNA delivery of multispecific antibodies as a potential cost-effective, passive immunisation strategy for the prevention of HIV-1 infection. Previously described bispecific (Bi-scFv and Bi-NAb) and trispecific (Tri-NAb) antibodies combining VRC01/PGT121 and VRC01/PGT121/10E8 paratopes, respectively (>95% neutralisation coverage *in vitro* against a 208 pseudovirus panel), with geometric mean IC50 titres <0.4 µg/mL), were selected for development. Antibody-encoding DNA plasmid constructs, engineered with T7-IVT mRNA transcription compatibility, were generated. The bispecific antibodies comprise the variable regions connected with linker peptides, both with and without an Fc domain (Bi-scFv and Bi-NAb, respectively) as previously described. The Tri-NAb DNA constructs were designed to express the Tri-NAb from co-transfection (Co-T) with separate Bi-NAb and 10E8 encoding constructs as well as from a novel single open reading frame (sORF) encoding the entire multispecific antibody sequence in a single polycistronic construct. Parental (PGT121, VRC01, and 10E8) and multispecific antibodies were expressed from DNA constructs by transient transfection in mammalian 293F cells, purified and biochemically characterised. Multispecific antibody-encoding mRNA transcripts were IVT from linearised DNA, purified of dsRNA, enzymatically capped (5' Cap1 structure), and transfected into 293F cells. The conformation, assembly, and functionality of the purified antibodies and mRNA-transfected cell culture supernatants were assessed *in vitro* against a panel of 17 HIV tier 2 pseudoviruses. Purified multispecific antibodies demonstrated improved neutralisation potency and coverage compared to the parental monoclonal antibodies, as expected. Encouragingly, unpurified mRNA-expressed multispecific antibodies matched the neutralisation coverage of purified antibodies (94%), with sufficient multispecific antibody titres to generate inhibitory dilution factors conferring 80% neutralisation (median ID80) >150: Bi-scFv (1 427), Bi-NAb (655), Tri-NAb Co-T (327), and Tri-NAb sORF (166). These data provide proof-of-concept of the utility of this HIV-1 multispecific antibody delivery strategy for passive immunisation to prevent HIV-1 infection and provide the basis for advancement into preclinical development.

Acknowledgements.

I would like to express my deepest gratitude and appreciation to all the people who made it possible for me to complete this project.

To my supervisor, Dr. Mark Killick, thank you for all the technical expertise, writing, and presentation skills that you have patiently taught me, for always being available to discuss our experiments and results, and for constantly challenging and encouraging me to do more and critically engage with my results. Thank you for your friendship, guidance, motivation, reassurance, and support that have enabled all the experiences and opportunities I have been afforded during this project. I hope that I continue to grow into the scientist you have inspired and shaped me to be.

To my co-supervisor, Prof. Maria Papathanasopoulos, thank you for your support and encouragement of my scientific endeavours, and for allowing me the fortunate opportunity of presenting at an international conference. I greatly appreciate all you have done for me.

Thank you Prof. Elena Libhaber for your guidance and assistance with the statistical analysis of our results.

To my friends and colleagues in the HIV Pathogenesis Research Unit, especially Hanna, Nikita, Mel, Adri, and Mark, thank you for all the fun times filled with laughter, interesting conversations, comradery, and encouragement that have made this experience so enjoyable.

To my family and friends, thank you for always encouraging and supporting me on this journey. To my parents, Ros and Mike, thank you for everything you have done and continue to do to help me achieve the opportunities I want in life. To my sister, Michaela, and Ross, thank you for always being there for me, and for your reassurance during some stressful times.

Lastly, thank you to the funders who have made this research possible: research funding was provided by the Poliomyelitis Research Foundation (PRF grant 21/71) and the Faculty of Health Sciences, University of the Witwatersrand. Student funding was provided through the Postgraduate Merit Award from the University of the Witwatersrand, the PRF (grant 22/61), and the National Research Foundation (NRF grant PMDS22070230651).

Table of contents.

Declaration. i

Publications and presentations arising from this study. ii

Abstract. iii

Acknowledgements. iv

List of Figures. x

List of Tables. xiii

List of Abbreviations. xiv

Chapter 1. Introduction. 1

1.1 The HIV-1 global pandemic. 1

1.2 HIV-1 structure and life cycle. 1

1.2.1 HIV-1 virion structure. 1

1.2.2 HIV-1 life cycle. 2

1.2.3 HIV-1 pathogenesis and disease progression. 4

1.3 HIV-1 treatment and prevention with ART. 5

1.4 HIV-1 broadly neutralising antibodies. 6

1.4.1 Development of anti-HIV-1 antibodies. 6

1.4.2 HIV-1 epitope targets for bNAbs. 7

1.4.2.1 The CD4 binding site. 7

1.4.2.2 The V1/V2 glycan loops of gp120. 8

1.4.2.3 The V3 glycan supersite of gp120. 8

1.4.2.4 The silent face of gp120. 9

1.4.2.5 The gp120-gp41 interface 9

1.4.2.6 The gp41 fusion peptide. 9

1.4.2.7 The membrane-proximal external region of gp41. 9

1.5 Passive immunisation of HIV-1 bNAbs. 10

1.5.1 HIV-1 bNAb passive immunisation-mediated protection in animal models. 11

1.5.2 bNAb modifications to increase serum half-life. 12

1.5.3 The HIV-1 AMP trials. 13

1.5.4 Combination bNAb infusion for HIV-1 prevention. 14

1.6 HIV-1 multispecific antibodies. 17

1.6.1 Engineering multispecific antibodies. 17
1.6.1.1 Fv-only (variable domain/variable fragment) multispecific antibodies. 17
1.6.1.2 Fab-based multispecific antibodies. 18
1.6.2 Multispecific antibodies targeting HIV-1. 20
1.7 Strategies for vectored bNAb expression *in vivo*. 23
1.7.1 Cost of bNAb production for passive infusion. 23
1.7.2 AAV vectored immunoprophylaxis. 24
1.7.2.1 AAV delivery of HIV-1 bNAbs. 25
1.7.3 IVT-mRNA expression. 26
1.7.3.1 The 5' Cap. 27
1.7.3.2 The 5' UTR. 28
1.7.3.3 The coding sequence. 28
1.7.3.4 The 3' UTR. 29
1.7.3.5 The poly-A tail. 29
1.7.3.6 Reducing mRNA immunogenicity. 29
1.7.4 IVT-mRNA delivery and expression of HIV-1 bNAbs. 30
1.8 Justification for the current study. 31
1.8.1 The HIV-1 multispecific antibody selection for the current study. 31
1.8.2 IVT-mRNA expression of multispecific antibodies. 33
1.9 Aim and objectives. 36
Chapter 2. Materials and Methods. 37
2.1 Reagents used in this study. 37
2.2 General laboratory techniques. 39
2.3 Multispecific antibody constructs. 39
2.3.1 Bispecific antibody construct design. 39
2.3.2 Bispecific antibody cloning into the pmRNA expression vector. 39
2.3.2.1 Bi-NAb antibody construct. 39
2.3.2.2 Bi-scFv antibody construct. 41
2.4 Silencing the *Bpi*I restriction site in the CH2 domain of the Bi-NAb construct. 42
2.4.1 Screening pmRNA_Bi-NAb colonies with silenced *Bpi*I restriction sites. .. 43
2.5 Tri-NAb construct design. 43
2.5.1 Generating complementary knob-into-hole mutations. 43
2.5.1.1 Confirming the presence of the CH3 hole mutations. 44
2.5.1.2 Cloning the Bi-NAb_Ho sequence into the pmRNA expression vector. 44

2.5.2 Generating the Tri-NAb single open reading frame (Tri-NAb sORF) construct. 45
2.5.3 Improving endogenous furin processing of the 10E8_Kn construct. 47
2.5.3.1 Site-directed mutagenesis of the 10E8_Kn furin sequence. 47
2.5.3.2 Cloning 10E8_Kn into the pmRNA expression vector. 48
2.5.3.3 Improving endogenous furin processing of the 10E8_Kn in the Tri-NAb_sORF construct. 49
2.6 Sub-cloning the firefly luciferase sequence into the pmRNA expression vector. 50
2.7 Recombinant antibody expression and purification. 51
2.7.1 General 293F cell line maintenance. 51
2.7.2 Antibody expression. 52
2.7.3 Assessing furin cleavage efficiency by small-scale mammalian cell transfections. 53
2.7.4 Antibody Purification. 53
2.7.4.1 Protein A affinity chromatography. 53
2.7.4.2 Immobilised metal-ion affinity chromatography. 55
2.7.4.3 Size exclusion chromatography. 56
2.7.5 Computation of the multispecific antibody molecular weight and predicted N-linked glycosylation. 57
2.7.5.1 Calculating antibody molecular weight from native SEC profiles. 57
2.7.5.2 Antibody molecular weight determination under reducing conditions. 58
2.7.5.3 Predicted antibody molecular weight and N-linked glycosylation sites. 58
2.8 *In vitro* transcription (IVT) of mRNA encoding multispecific antibody constructs. 58
2.8.1 IVT mRNA transcript production. 58
2.8.2 IVT mRNA transcript purification. 59
2.8.3 Capping purified IVT mRNA. 61
2.8.4 Antibody expression from IVT mRNA. 61
2.9 Antibody HIV-1 pseudovirus *in vitro* neutralisation. 63
2.9.1 Maintenance of the HEK293 and TZM-bl cell lines. 63
2.9.2 HIV-1 pseudovirus production. 64
2.9.2.1 Determining the HIV-1 pseudovirus titres. 65
2.9.3 HIV-1 *in vitro* neutralisation assay. 65
2.9.3.1 Determining the percentage viral inhibition. 66
2.9.3.2 Correcting for the antibody molarity difference. 67

2.10 Quantification of IVT-mRNA-expressed antibodies. 68
2.10.1 ELISA..... 68
2.10.2 Western blot densitometry. 70
2.10.3 IC/ID Neutralisation data estimation of multispecific antibody concentration. 71
2.11 Statistical analysis. 71
Chapter 3. Results. 73
3.1 Generation of bispecific antibody expression constructs. 73
3.2 Silencing of the Bi-NAb CH2 domain *Bpi*I restriction site to prevent premature mRNA transcript truncation. 76
3.3 Generating the Tri-NAb expression constructs. 79
3.3.1 Heterologous heavy chain assembly through complementing knob-into-hole mutations in the 10E8 and Bi-NAb constructs. 79
3.3.2 Generating the Tri-NAb sORF construct. 83
3.4 Small-scale transfection and assessment of multispecific antibody expression *in vitro*. 86
3.4.1 Inefficient endogenous furin processing of 10E8_Kn and Tri-NAb_sORF constructs. 87
3.4.2 Improved endogenous furin processing and cleavage of the 10E8_Kn construct. 90
3.4.3 Sub-cloning of the 10E8_Kn_Δfurin and luciferase reporter into the pmRNA expression vector. 91
3.4.4 Improved endogenous furin processing and cleavage of the Tri-NAb sORF. 94
3.5 Biochemical and functional characterisation of expressed and purified parental and multispecific antibodies from DNA constructs. 97
3.5.1 Recombinant antibody expression and purification. 97
3.5.2 Biochemical and functional characterisation of expressed and purified parental and multispecific antibodies from DNA constructs. 99
3.6 Functional *in vitro* neutralisation of HIV-1 was achieved by the multispecific antibodies. 103
3.7 IVT mRNA transcript production, purification, and expression. 107
3.7.1 Production and purification of IVT-mRNA expression cassettes. 107
3.7.2 Multispecific antibody expression from IVT-mRNA transcripts. 107
3.8 Assessment of mRNA-expressed multispecific antibody functionality and inhibition. 111
3.9 Relative quantification of the mRNA-expressed multispecific antibodies. 114

Chapter 4. Discussion. 117

4.1 Generation of multispecific antibody expression constructs. 117

4.2 Recombinant antibody expression, purification, and biochemical characterisation. 122

4.3 Functional *in vitro* neutralisation of HIV-1 by the multispecific antibodies. 125

4.4 IVT mRNA transcript production and multispecific antibody expression. 130

4.5 IVT-mRNA-expressed multispecific antibodies exhibit high neutralisation titres with broad *in vitro* HIV-1 neutralisation coverage. 133

4.6 Expression discrepancy between the Co-T and sORF expressed Tri-NAb. .. 136

4.7 Future prospects of mRNA-multispecific antibody delivery for HIV-1 prevention. 138

4.8 Conclusion. 141

References. 143

Appendix A: General laboratory techniques and Kit protocols. 164

Appendix B: Supplementary result figures. 178

Appendix C: Ethics waiver. 186

List of Figures.

Chapter 1. Introduction.

Figure 1.1. The HIV-1 genome and virion structure 2

Figure 1.2. The HIV-1 life cycle 3

Figure 1.3. Schematic representation of the HIV-1 Env antibody responses during HIV-1 infection in the absence of antiretroviral therapy 4

Figure 1.4. HIV-1 Env trimer epitopes targeted by various classes of broadly neutralising HIV-1 antibodies 9

Figure 1.5. Multispecific antibody formats of increasing complexity are engineered using various technologies 19

Figure 1.6. HIV-1 multispecific antibody constructs used in this study 35

Chapter 3. Results.

Figure 3.1 Generation and evaluation of bispecific antibody constructs 75

Figure 3.2. Silencing the Bi-NAb CH2 domain *Bpi*I restriction site to prevent premature mRNA transcript truncation 78

Figure 3.3. Generating the pmRNA_Bi-NAb_Ho construct containing the CH3 hole mutations required for heterologous heavy chain assembly and Tri-NAb production 81

Figure 3.4. Generating the Tri-NAb single open reading frame (sORF) construct 85

Figure 3.5. Multispecific antibody expression and processing of F2Aopt-containing constructs (pMin_10E8_Kn and pmRNA_Tri-NAb_sORF) *in vitro* 89

Figure 3.6. Improved endogenous furin processing and cleavage following alterations to the furin site in the F2Aopt of the 10E8 Kn construct 93

Figure 3.7. Improved endogenous furin processing and cleavage of the Tri-NAb single open reading frame (sORF) following modification of the furin cleavage site in the F2Aopt 96

Figure 3.8. Conformational and purity assessment of expressed HIV-1 broadly neutralising parental and multispecific antibodies 102

Figure 3.9. Neutralisation profile (breadth and potency) comparison of purified parental and multispecific antibodies against a panel of 17 tier 2 HIV-1 pseudoviruses 106

Figure 3.10. IVT-mRNA-mediated multispecific antibody expression *in vitro* 110

Figure 3.11. Neutralisation profile (breadth and potency) comparison of IVT-mRNA expressed multispecific antibodies against a panel of 17 tier 2 HIV-1 pseudovirus 113

Appendix A: Supplementary methods.

Figure A1. Plasmid maps for the final pmRNA expression constructs encoding the multispecific antibodies (Bi-scFv, Bi-NAb, Bi-NAb_Ho, 10E8_Kn, and Tri-NAb_sORF, as well as green fluorescent protein (GFP) and firefly luciferase (Fluc) (controls for mRNA-mediated expression, and pMin_iMAb_Ho as an assembly control 167

Appendix B: Supplementary result figures.

Figure B1. Recombinantly expressed multispecific and parental antibodies were purified by standard affinity chromatography procedures 171

Figure B2. Molecular weight protein standard calibration curve 172

Figure B3. Relative migration distance of the protein molecular weights 172

Figure B4. Parental and multispecific purified antibody viral inhibition profiles against a panel of 17 tier 2 HIV-1 pseudoviruses 174

Figure B5. Neutralisation IC50 breadth and potency comparison of purified parental and multispecific antibodies against a panel of 17 HIV-1 pseudoviruses 175

Figure B6. IVT-mRNA expressed multispecific antibody viral inhibition profiles against a panel of 17 tier 2 HIV-1 pseudoviruses 176

Figure B7. Neutralisation ID50 breadth and potency comparison of IVT-mRNA expressed multispecific antibodies against a panel of 17 HIV-1 pseudoviruses 177

Figure B8. Affinity chromatography purification of HIV-1 Env gp120FVC Monomer glycoprotein 177

Figure B9. Representation of the multispecific antibody standard curves used to relatively quantify the mRNA-expressed multispecific antibody titres 178

Figure B10. Western blot images analysed by densitometry to quantify the amount of mRNA-expressed multispecific antibodies in the clarified cell culture supernatant .. 178

List of Tables.

Chapter 1. Introduction.

Table 1.1. HIV-1 broadly neutralising antibodies (bNAbs) (both individual and combinations) that are in early phase 1 and 2 human clinical trials 16

Table 1.2. HIV-1 multispecific antibodies for therapeutic reduction in viraemia or prevention of HIV-1 infection 22

Chapter 3. Results.

Table 3.1. Recombinant antibody expression and purification yields 98

Table 3.2. Relative quantification of the concentration of mRNA-expressed multispecific antibodies 116

Appendix A: Supplementary methods.

Table A1. Primers and thermocycling conditions used in this study 165

Table A2. Composition of SDS-PAGE gel to cast two 1 mm gels 166

Appendix B: Supplementary result figures.

Table B1. Molecular weights of the parental and multispecific antibodies 173

List of Abbreviations.

α: alpha (or anti- in the context of secondary antibodies)

Δ: delta, altered sequence in the context of this study

μ: micro

Ψ: pseudouridine

293F: FreeStyle 293 cells

4dCD4: soluble human CD4 receptor

AAV: adeno-associated virus

ADA: anti-drug antibody

AGTRU: Antiviral Gene Therapy Research Unit

AIDS: acquired immunodeficiency syndrome

AMP: antibody-mediated prevention

A_n: absorbance

ANOVA: analysis of variance

APS: Ammonium Persulfate

ARE: adenylate/uridylate-rich elements

ART: antiretroviral therapy

ARV: antiretroviral

AU: adenine-uracil

BLI: BioLayer Interferometry

bNAbs: broadly neutralising antibodies

bp: base pairs

BSA: bovine serum albumin

CA: capsid proteins

cART: combined antiretroviral therapy

Cat.: catalogue number

CCR5: C-C chemokine receptor type 5

CD4: clusters of differentiation 4

CD8: clusters of differentiation 8

CD4bs: CD4 binding site

CDRH3: third complimentary-determining region of the heavy chain

CH: constant heavy

CHO: Chinese hamster ovary

CL: constant light

CMV: cytomegalovirus

Co-T: co-transfection

CXCR4: C-X-C chemokine receptor type 4

Da: Dalton

DEAE: diethylaminoethyl

DEPC: diethylpyrocarbornate

DMEM: Dulbecco's Modified Eagle's Medium

DMSO: dimethyl sulfoxide

DNA: deoxyribonucleic acid

DPBS: Dulbecco's phosphate buffered saline

dsRNA: double-stranded RNA

DTT: dithiothreitol

E2A: equine rhinitis A virus 2A

E. coli: *Escherichia coli*

ECL: enhanced chemiluminescence

EDTA: ethylenediamine tetraacetic acid

eGFP: enhanced green fluorescent protein

EGFR: epidermal growth factor receptor

ELISA: enzyme-linked immunosorbent assay

env: HIV-1 envelope gene

Env: HIV-1 envelope glycoprotein

ER: endoplasmic reticulum

F2A: foot-and-mouth disease virus 2A

Fab: fragment antigen-binding region

FBS: Foetal Bovine Serum

Fc: fragment crystallisable

FcRn: neonatal receptor

Fluc: firefly luciferase

FOR: forward

Fv: variable domain

G4S: glysine-4-serine

GC: guanosine-cytosine

GFP: green fluorescent protein

G. nivalis: *Galanthus nivalis*

GMT: geometric mean titre

Gp: glycoprotein

Gp120FVC M: gp120 founder virus consensus C monomer

HAART: highly active antiretroviral therapy

HC: heavy chain

HEK293: Human Embryonic Kidney 293 cells

HEPES: 4-(2-hydroxyethyl)-1-piperazineethanesulfonic acid

His: histidine

HIV-1: human immunodeficiency virus type 1

Ho: hole

HPRU: HIV Pathogenesis Research Unit

HPTN: HIV Prevention Trials Network

HRP: horseradish peroxidase

HV: heavy variable

HVTN: HIV Vaccine Trials Network

IC50: inhibitory concentration for 50% viral inhibition

IC80: inhibitory concentration for 80% viral inhibition

ID50: inhibitory dilution for 50% viral inhibition

ID80: inhibitory dilution for 80% viral inhibition

I.D.: internal diameter

IDA: iminodiacetic acid

IgG: immunoglobulin G

IM: intramuscular

iMAb: Ibalizumab

IMAC: immobilised metal-ion affinity chromatography

IN: integrase

INSTIs: integrase strand transfer inhibitors

IRES: internal ribosome entry sites

ITR: inverted terminal repeat

IV: intravenous

IVT: *in vitro* transcription

Kav: ratio between the elution volume of a molecule and the column volume

Kb: kilobase

kDa: kilo-Dalton

kg: kilogram

KIH: knob-into-hole

kL: kilolitre

KLD: kinase, ligase, *Dpn*I reaction

Kn: knob

LB: Luria Broth

LC: light chain

LC-MS/MS: liquid chromatography mass-spectrometry/mass spectrometry

LNP: lipid nanoparticle

LV: light variable

m1Ψ: N^1-methyl-pseudouridine

M7G: 7-methylated guanosine

m: milli-

M: molar

mm: millimetres

MA: matrix proteins

mAb: monoclonal antibody

mg: milligram

miRNA: micro RNA

mL: millilitre

MMP: methyl α-D mannopyranoside

MPER: membrane-proximal external region

MPM 6: Microplate Manager 6

mRNA: messenger RNA

Mw: molecular weight marker

n: nano-

N/A: not available or not applicable

NAbs: neutralising antibodies

NC: nucleocapsid proteins

NHLS: National Health Laboratory Service

NHP: non-human primate

NICD: National Institute for Communicable Diseases

NIH: National Institute of Health

NNRTIs: non-nucleoside reverse transcriptase inhibitors

NRTIs: nucleoside reverse transcriptase inhibitors

NSG: NOD-scid gamma mice

NTC: no template control

ORF: open reading frame

P2A: porcine teschovirus-1 2A

PBS: phosphate buffered saline

PBS-T: Tween-20 prepared in PBS

PCR: polymerase chain reaction

PDB: Protein Data Bank

PEIMAX: Polyethylenimine “Max”

PEP: post-exposure prophylaxis

pg: picograms

PI: Protease inhibitors

PIC: pre-integration complex

PKR: protein kinase

PLWH: people living with HIV

PNGS: potential N-linked glycosylation sites

Poly-A: poly-adenylation

PR: protease

PrEP: pre-exposure prophylaxis

PRR: pattern recognition receptors

rAAV: recombinant adeno-associated virus

REV: reverse

Rf: relative migration distance

RLU: relative luminescence units

RNA: ribonucleic acid

RNA Pol II: RNA polymerase II

Rpm: revolutions per minute

RT: reverse transcriptase

SAM: S-adenosylmethionine

SARS-CoV-2: severe acute respiratory syndrome coronavirus 2

SC: subcutaneous

scFv: single-chain variable fragment

SDM: site-directed mutagenesis

SDS-PAGE: sodium dodecyl sulphate-polyacrylamide gel electrophoresis

SEC: size-exclusion chromatography

SHIV: simian-human immunodeficiency virus

SIV: simian immunodeficiency virus

S.O.C.: Super Optimal broth with Catabolite repression

sORF: single open reading frame

SP: secretion signal peptide

SRP: signal recognition particle

ssRNA: single-stranded RNA

T/F: transmitted/founder virus

T2A: thosea asigna virus 2A

TCID50: tissue culture infectious dose to achieve 50% infection

TEMED: N, N, N', N'-tetramethylethylene-diamine

TLR3: toll-like receptor 3

TMB: 3, 3', 5, 5' – tetramethylbenzidine

tRNA: transfer RNA

UTC: untransfected control

UTP: uridine 5'-triphosphate

UTR: untranslated region

UV: ultraviolet

Vc: geometric column volume

Ve: elution volume

VH: variable heavy

VHH: variable heavy domain of heavy chain

VL: variable light

Vo: column void volume

WB: western blot

Chapter 1. Introduction.

1.1 The HIV-1 global pandemic.

The human immunodeficiency virus type 1 (HIV-1) global pandemic has been a major public health issue for over 40 years and the progression to acquired immunodeficiency syndrome (AIDS) has claimed 40.4 million lives so far (1–3). HIV-1 remains a leading cause of death and disease, especially in sub-Saharan Africa (4–7). In 2022, there were approximately 39 million people living with HIV-1 (PLWH) globally, with 1.3 million new infections (2,3). Years of research have unpacked the structure, life cycle, and pathogenesis of this virus which has and continues to be crucial in developing treatment and prevention strategies to slow the spread of HIV-1 and reduce its morbidity and mortality.

1.2 HIV-1 structure and life cycle.

1.2.1 HIV-1 virion structure.

HIV-1 is a retrovirus, belonging to the *Retroviridae* family, and classified as a member of the *Lentiviridae* genus. HIV-1 is an enveloped virus enclosed in a lipid bilayer derived from the modified host cell membrane and contains a 9.8 kb positive-sense ribonucleic acid (RNA) genome, comprising nine genes encoding multiple proteins (8). The Gag polyprotein is proteolytically cleaved to generate the matrix (MA), capsid (CA), nucleocapsid (NC), and p6 proteins (8,9). The Gag-Pol polyprotein contains the viral enzymes protease (PR), reverse transcriptase (RT), and integrase (IN). The *env* gene encodes the secretion signal peptide (SP), and glycoproteins (gp) gp120 and gp41 (8,9). The remaining sequences encode regulatory proteins (Tat and Rev) (10) and accessory proteins (Nef, Vpr, Vif, and Vpu) (11). The HIV-1 structural proteins are all derived from the Gag polyprotein of immature virions, which is proteolytically cleaved during virion assembly to generate mature virions. The processed proteins reassemble, generating the distinct layers of the mature virion: the MA remains associated with the inner viral layer, the NC coats the viral RNA genome, and the CA assembles to form the capsid surrounding the nucleocapsid and associated virally-encoded enzymes (12,13). The surface envelope glycoprotein (Env) is a trimer, composed of three non-covalently associated heterodimers of gp120 (that interact with

host cell receptors) and gp41 (a transmembrane component that mediates viral- and target host cell- membrane fusion) (14) and is the target for antibodies during an immune response (15).

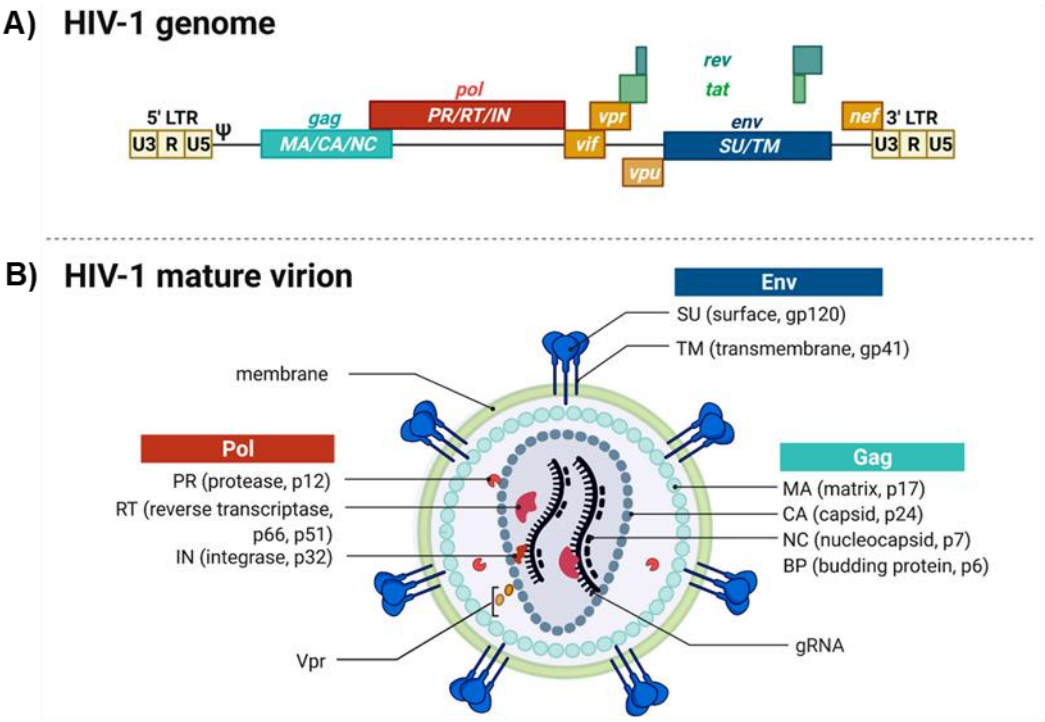


Figure 1.1. The HIV-1 genome and virion structure. (A) Schematic overview of the HIV-1 genome that comprises open reading frames for nine genes (*gag, pol, vpr, vif, vpu, env, rev, tat, nef*). **(B)** The mature HIV-1 virion comprises structural proteins that are proteolytically cleaved from the Gag polyprotein (matrix, capsid, nucleocapsid, and p6) and viral enzymes (protease, reverse transcriptase, and integrase). Env encodes for the surface gp120 and transmembrane gp41 proteins. Figure obtained from van Heuvel *et al.* (9).

1.2.2 HIV-1 life cycle.

HIV-1 infects cells via receptor-mediated entry and targets cells that present the clusters of differentiation 4 (CD4) receptor and C-C chemokine receptor type 5 (CCR5) or C-X-C chemokine receptor type 4 (CXCR4) co-receptors (e.g. human T helper cells and microglia cells) (16,17). The HIV-1 life cycle has an early and late stage. The early stage begins with infection of a host cell and ends with viral genome integration into the host DNA genome. The late stage is the post-integration period until viral maturation (18). Briefly, the HIV-1 virion Env glycoprotein spikes engage the host cell CD4 and CCR5/CXCR4 co-receptor, triggering conformational rearrangements that enable the viral and host cell membrane fusion and release of the viral core into the host cell cytoplasm (19). The viral capsid begins uncoating and trafficking to the

nucleus (20,21) where the viral genome is reverse-transcribed to generate the pre-integration complex (PIC) (22). Uncoating and reverse transcription are completed after nuclear import and before nuclear integration (20,23,24). The capsid localises the PIC to transcriptionally active sites within the host chromatin and PIC-associated integrase facilitates the integration of viral transcripts into the host genome resulting in the integrated provirus (25–27). Host cell RNA polymerase II (RNA Pol II) mediates proviral transcription, generating viral messenger RNA (mRNA) transcripts that are exported from the nucleus and provide the template for viral protein production, such as the Gag polyprotein which is localised to the plasma membrane (28). Viral protein components are combined with genome-length RNA to form immature viral particles that bud from the host cell and have intact Gag polyproteins coating the host-derived viral membrane (29). Finally, the immature virions undergo protease-mediated maturation where viral protease cleaves the Gag polyprotein into its smaller, functional subunits (30), forming the viral capsid to create an infectious HIV-1 viral particle that can restart the HIV-1 life cycle (31).

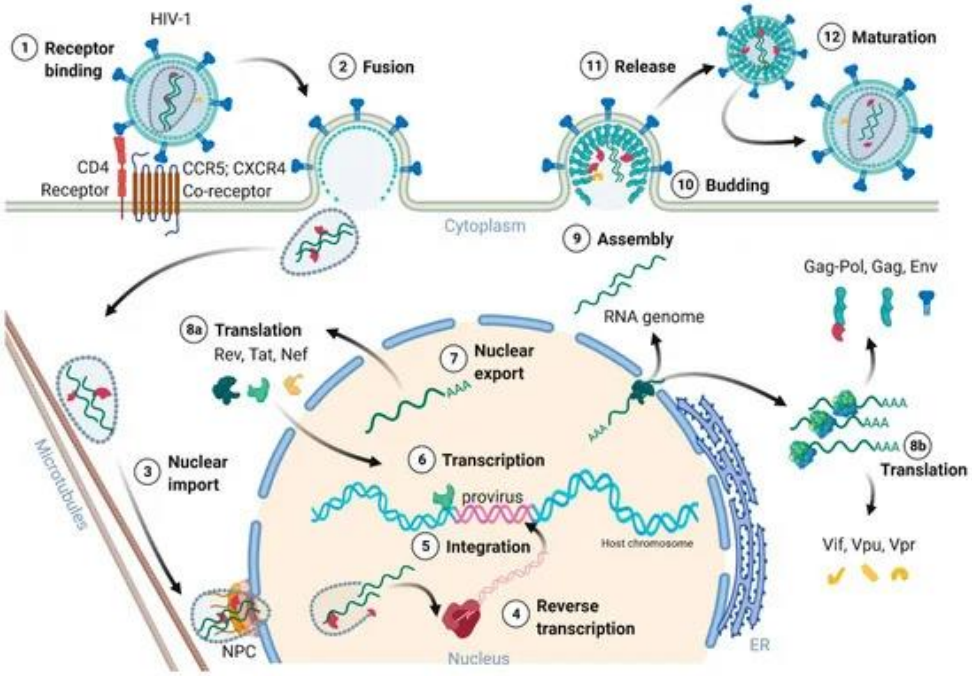


Figure 1.2. The HIV-1 life cycle. 1) The HIV-1 envelope glycoprotein binds to the receptors on the host cell surface. 2) The virion and cellular membranes fuse and the viral capsid is released into the cytoplasm. 3) The viral capsid passes through the nuclear pore complex (NPC) into the nucleus. 4) The capsid partially uncoats and the viral gRNA is reverse transcribed into the provirus. 5) The provirus is integrated into highly active chromosomal regions in the host genome. 6) The provirus genes are transcribed. 7) Viral mRNAs are exported from the nucleus. 8) Viral mRNA translation occurs in the cytoplasm. 9) Nascent HIV-1 particles assemble at the cell membrane. 10) Immature HIV-1 particles bud from the cell membrane and 11) are released from the host cell. 12) The viral particle matures into infectious HIV-1 virions. Figure obtained from van Heuvel *et al.* (9).

1.2.3 HIV-1 pathogenesis and disease progression.

HIV-1 infection and transmission across mucosal membranes is predominantly established by a single transmitted/founder (T/F) virus (~75-80%) with the remaining 20-25% of infections occurring from two-to-five distinct T/F viral variants (32,33). T/F viruses have a specific viral phenotype based on the co-receptor used for entry and the tropism of the cell (33), with viral tropism being shown to influence the infection outcome and the duration of disease progression (34). In the absence of antiretroviral (ARV) therapy (ART), the typical HIV-1 infection progresses in three main phases: 1) an initial acute infection; 2) a prolonged asymptomatic period; and 3) a final rapid increase in viral load accompanied by a simultaneous drop in healthy $CD4^+$ T cells and the progression to AIDS (35,36). Acute HIV-1 infection can last approximately 2 to 10 weeks. Active viral replication results in high plasma viraemia and a decrease in circulating $CD4^+$ T cells, where patients present with fever and flu-like symptoms approximately 2 to 4 weeks after infection (37). Initially, HIV-1 replicates rapidly and peaks at 3 to 4 weeks post-exposure, in the absence of an immune response or ART (38,39). However, this phase may take up to 3 months after infection until seroconversion occurs and HIV-1-specific antibodies are detected within the patient's serum (40). HIV-1 replication then spontaneously declines for several months, the viral load decreases dramatically and the circulating $CD4^+$ T cells return to near-normal levels. A viral set point or steady state of viral replication is reached (which determines disease progression) and an asymptomatic latent phase is experienced for 7 to 10 years (36,41). Following this latent period, the viral load rapidly increases with a simultaneous decrease in $CD4^+$ T cell count to <200 cells/mm^3 increasing a patient's susceptibility to opportunistic infections and progression to AIDS (42). Due to the high viral loads experienced during the early (can last for up to 3 months after seroconversion) and late stages of HIV-1 infection (10 to 19 months before death), these periods are associated with high rates of transmission (43).

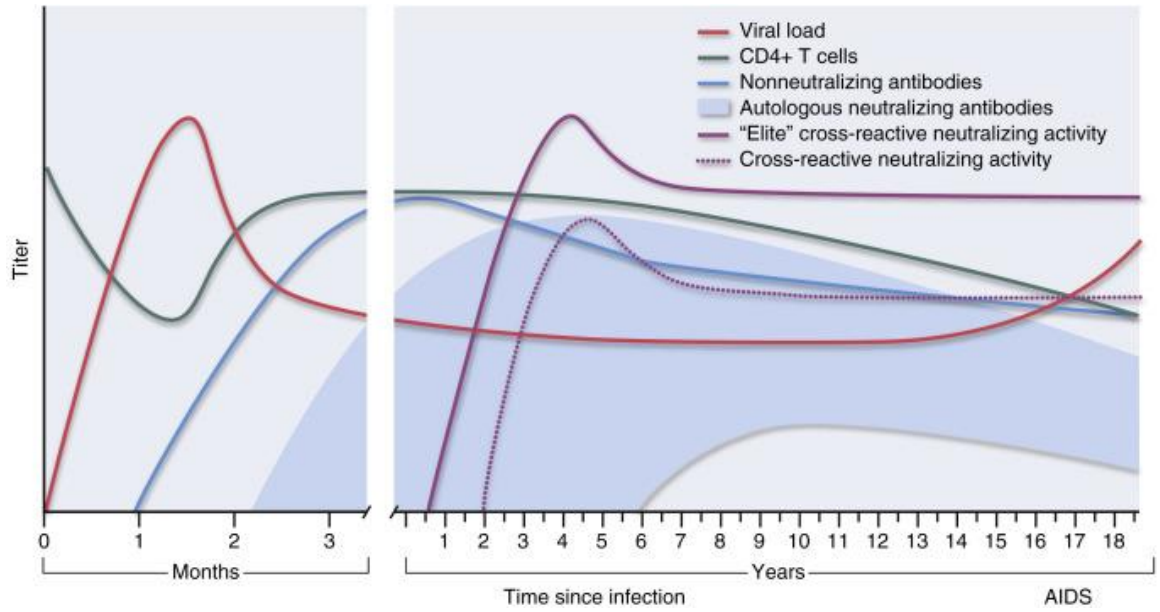


Figure 1.3. Schematic representation of the HIV-1 Env antibody responses during HIV-1 infection in the absence of antiretroviral therapy. HIV-1 infection has an acute phase, a prolonged asymptomatic period, and a final increase in viral load and decrease in $CD4^+$ T cells and progression to AIDS. It can take up to three months after infection for seroconversion to occur and for autologous HIV-1 specific antibodies to be present. Cross-reactive/broadly neutralising antibodies take years to develop. Figure obtained from Silvestri and Cartwright (40).

Understanding the HIV-1 virion structure, life cycle, and disease progression has provided targets for active immunisation strategies and treatment to prevent and treat HIV-1 infection respectively. So far, all attempts to generate a prophylactic vaccine have failed (44,45) and current biomedical prevention strategies involve male circumcision, ART-based treatment, and antibody passive immunisation, which will be the focus of this study.

1.3 HIV-1 treatment and prevention with ART.

Knowledge of the HIV-1 life cycle has identified various targets for ARV interventions and enabled the development of ART to manage this chronic illness and has greatly reduced the morbidity, mortality, and incidence of HIV-1 and resulted in better patient survival, prognosis, and quality of life (46–48). HIV-1 therapy utilises combined ART treatment (cART, which combines ARV drugs from different drug classes) and highly active ART (HAART) to suppress HIV-1 replication. The commonly used ARV drug classes include: nucleoside reverse transcriptase inhibitors (NRTIs), non-nucleoside reverse transcriptase inhibitors (NNRTIs), protease inhibitors (PIs), and integrase strand transfer inhibitors (INSTIs), with each drug class targeting key enzymes within

the different stages of the HIV-1 replication cycle (49). HIV-1 therapy has mostly been focused on individual ART treatment, however, long-acting ARV drugs demonstrate improved success of ART and enabled its expansion to include prevention strategies that reduce transmission risk, such as pre-exposure prophylaxis (PrEP) and post-exposure prophylaxis (PEP) (50,51). The effective prevention of HIV-1 infection has been demonstrated using PrEP, where ARV drugs are taken by an uninfected individual who is at risk for acquiring HIV-1 infection, in serodiscordant couples (52,53).

Unfortunately, HIV-1 drug resistance resulting from the genetic mechanisms (54) or the epidemiology (55) of HIV-1, threatens the long-term success of ART (56). HIV-1 has great genetic variability due to the high rate of HIV-1 RT processing errors during viral replication, which can introduce mutations that confer ARV drug resistance (54,57). HIV-1 drug resistance mutations can be transmitted between people, or be acquired through drug selection pressure (55). Poor drug adherence and non-compliance (due to factors such as drug toxicity) accelerate treatment failure resulting from the emergence of drug-resistant virus that may impact the protection achieved by PrEP in these patients (58,59). Therefore, alternative HIV-1 prevention strategies that complement the existing repertoire and address some of the limitations of cART may offer further benefits in limiting HIV-1 transmission and ending the global HIV-1 pandemic (60).

1.4 HIV-1 broadly neutralising antibodies.

1.4.1 Development of anti-HIV-1 antibodies.

The elicitation of neutralising antibodies (NAbs) from infection or vaccination is an important component of immunological protection from viral infections. Autologous neutralising HIV-1 antibodies arise approximately 1 to 3 months after infection (in the absence of ART) and select for the viral escape mutations (15). During the early stages of HIV-1 infection in the absence of ART, there is the continuous emergence of functional viral envelope that changes and competes against the rapidly evolving neutralising antibody response. However, these early NAbs are specific for the autologous patient's virus and do not cross-neutralise heterologous primary isolates (15). Eliciting broadly neutralising antibodies (bNAbs), capable of neutralising different HIV-1 subtypes and diverse circulating isolates, is desirable but the development of bNAbs is rare and evolves over time. bNAbs have a high frequency of somatic

mutations and are only developed by approximately 10-30% of HIV-1 infected individuals, with 10-15% producing high serum levels of broad and potent bNAbs (61–63). The rarity of bNAbs is largely due to the multiple antibody evasion mechanisms of the HIV-1 Env (64,65). The Env protein displays sophisticated structural heterogeneity, limiting the accessibility and masking functional epitopes to divert antibody responses to non-functional surface epitopes, thus ensuring non-neutralising antibody responses (64,65). HIV-1 Env also has a high mutation rate (RT has no proof-reading mechanism), enabling its rapid evolution in response to immune selection pressure (15,66) and generating incredible genetic diversity within an individual during the course of infection and across different global populations (67). HIV-1 Env is heavily glycosylated, generating a glycan shield that sterically blocks accessibility of antibodies to target epitopes, evades antibody recognition by resembling 'self', and shifting surface glycosylation patterns through acquired mutations that further hinder antibody neutralisation potential (68–70).

1.4.2 HIV-1 epitope targets for bNAbs.

Despite these viral defence mechanisms, numerous broadly neutralising and potent monoclonal antibodies (mAbs) have been isolated from multiple infected donors and have enlightened the HIV-1 Env target epitopes (71–76). HIV-1 bNAbs target relatively conserved, functional epitopes on the surface of the HIV-1 Env trimer (77). The different Env epitopes targeted by the bNAb subtypes and the proposed mechanism resulting in neutralisation are discussed briefly (77–79). Where possible and unless stated otherwise, examples of each bNAb subtype that have reached human passive immunisation clinical trials are provided with the inhibitory concentration for 50% viral inhibition (IC50 - µg/mL) and coverage (percentage of "X" number of viruses) indicated in brackets (80).

1.4.2.1 The CD4 binding site.

The CD4 binding site (CD4bs) is located in a cavity at the interface between gp120 inner and outer domains and is required for HIV-1 to bind to the host cell CD4 primary receptor, thus, it is a conserved immune target with multiple N-linked glycans (81,82). Antibodies targeted against this site can prevent viral interaction with CD4 and host-cell entry. bNAbs to the CD4bs take longer to develop during infection, have the highest level of somatic hypermutation, and tend to have the best combination of

breadth and potency compared to the other bNAb specificities (78). There are two identified CD4bs bNAb classes: CD4 mimics which have heavy chains encoded by variable heavy (VH)1-2 of VH1-46 that contact the CD4bs; and third complimentary-determining region of the heavy chain (CDR H3)-dependent bNAbs (VRC01-class antibodies) that utilise the CDR H3 loop to interact with the CD4bs (83). Examples include (78) (IC50 (μg/mL), coverage % of 'x' virus test panel): VRC01 (0.329, 91% of 196), VRC07-523, and VRC07-523LS (0.047, 96% of 179 (84)), 3BNC117 and 3BNC117-LS-J (0.097, 85% of 198), N6 (0.038, 98% of 181 (85)).

1.4.2.2 The V1/V2 glycan loops of gp120.

The V1 and V2 loops are found at the distal end of each gp120 molecule and form an Env trimer V2 apex that is thought to maintain the metastability of the Env spike (77,86). The V1/V2 loops rearrange after CD4 engagement to fully expose the otherwise shielded V3 loop and co-receptor binding site. The V1/V2 loops are the most variable on Env, and conserved regions surrounding the loops are covered by glycans (e.g. N160 glycan) (77). bNAbs within this class penetrate the glycan shield using long CDR H3 loops and are believed to stabilise Env trimer and prevent the structural changes, thereby neutralising the virus (87). bNAbs to the V2 apex are some of the most potent antibodies described, but fail to reach the breadth of other antibody classes (88). Examples (78): PGDM1400 (0.017, 81% of 194), PG9 (0.118, 84% of 200), CAP256-VRC26.25 (0.001, 57% of 200 (89)).

1.4.2.3 The V3 glycan supersite of gp120.

The V3 glycan supersite of gp120 is located near the V1/V2 region. The V3 loop region contains a highly conserved motif positioned between two N-linked glycans that are targets for bNAbs (N301 and N332) (90), with all known bNAbs targeting the N332 glycan (77,91). The conservation at the V3 loop base is believed to be due to its crucial role in CCR5 co-receptor recognition (92). Therefore, bNAb neutralisation is likely mediated by preventing V3 loop/co-receptor binding or conformational changes that occur post-binding to enable membrane fusion (93). Examples (78): PGT121 (0.48, 66% of 200), 10-1074 (0.039, 68% of 200).

1.4.2.4 The silent face of gp120.

The Env silent face of gp120 is the highly glycosylated region across from the CD4bs, and the epitope mainly includes the N262, N295, and N448 glycans on a single gp120 monomer (70). Antibodies against this epitope are suggested to neutralise HIV-1 by preventing Env conformational changes required for full receptor binding and host cell entry (70). Neutralisation may also include the N262 glycan that is observed to be important for CD4-mediated viral entry (94). Examples that have not reached human clinical trials: VRC-PG05 (0.8, 27% of 208 (70)) and SF12 (0.2, 62% of 119 (95)).

1.4.2.5 The gp120-gp41 interface.

The glycoprotein gp120-gp41 interface is located below the gp120 lobe. Diverse bNAbs target this epitope, some with non-overlapping epitopes and different glycan dependencies (96). Some bNAbs target gp120, or gp41 individually but most are specific for the assembled Env trimer and depend on gp120-gp41 cleavage. The neutralisation mechanism includes preventing the conformational changes needed for membrane fusion which destabilises the trimer and encourages dissociation (96,97). bNAbs 8ANC195 (1.115, 66% of 200 (78)) and 35O22 (0.033, 62% of 181 (98)) are examples, however to date, no antibody from this class has reached human clinical trials.

1.4.2.6 The gp41 fusion peptide.

The fusion peptide of gp41 is critical for initiating the viral-host membrane fusion process and is located at the N-terminus of gp41. In the prefusion Env conformation, it is exposed and located in a hydrophobic region of the Env trimer (99). bNAbs to this epitope interact with the fusion peptide N-terminal residues and some also interact with complex glycans (e.g. N88) at the gp120-gp41 interface and have similar binding approaches to gp120-gp41 interface bNAbs (77). Examples that have not reached human clinical trials include (78): VRC34.01 (0.310, 49% of 179), and PGT151 (0.023, 72% of 200).

1.4.2.7 The membrane-proximal external region of gp41.

The membrane-proximal external region (MPER) on gp41 is part of the fusion machinery and is required for host cell entry by facilitating membrane fusion (100). This epitope is a challenging target since bNAbs typically recognise both a viral

membrane lipid component and a transient Env conformation, made possible by their long CDR H3 loops (101). Due to the high level of conservation and linear nature of the target epitope, these MPER-targeting bNAbs are among the most broadly neutralising (101). The most prominent bNAb within this class that has reached human clinical trials is 10E8 (0.299, 98% of 199) (78).

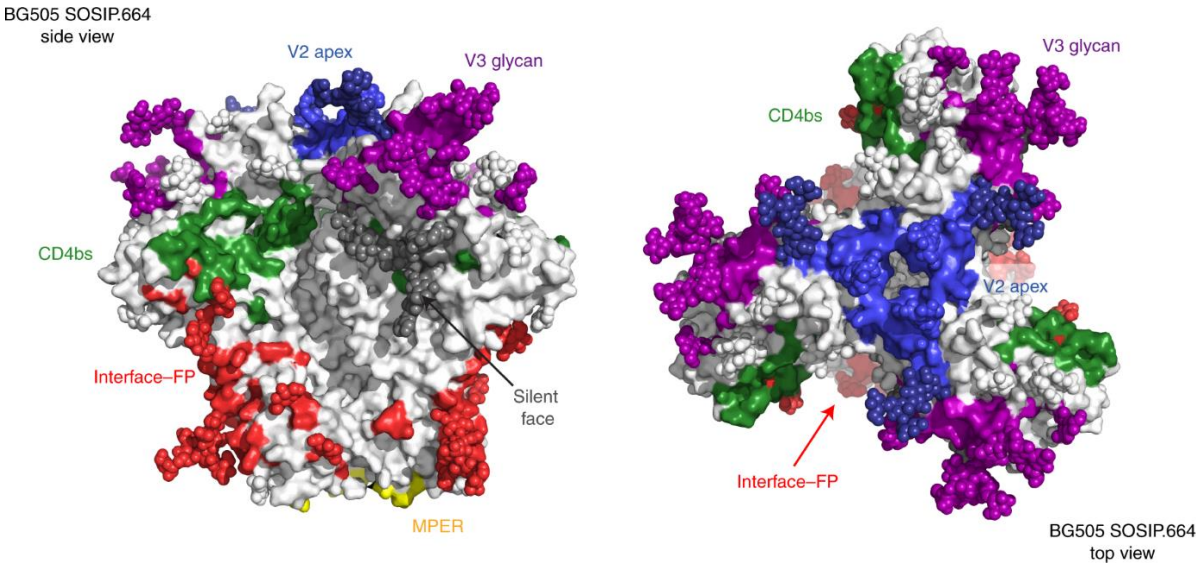


Figure 1.4. HIV-1 Env trimer epitopes targeted by various classes of broadly neutralising HIV-1 antibodies. The HIV-1 Env trimer (BG505 SOSIP.664) has various epitope targets for bNAbs: V1/V2 glycan loop (V2 apex - blue), V3 glycan supersite (purple), CD4 binding site (CD4bs – green), gp120-gp41 interface and gp41 fusion peptide (FP - red), membrane-proximal external region (MPER – yellow), and silent face (grey). Images obtained from Sok and Burton (78).

1.5 Passive immunisation of HIV-1 bNAbs.

The desired result for a preventative vaccine against HIV-1 is to elicit bNAbs that can neutralise heterologous HIV-1 strains and prevent infection (102–104). Multiple vaccine strategies to elicit bNAbs have been tested in clinical trials, including the administration of gp120 antigen or adenovirus vectored delivery of Env protein-encoding genes. However, to date, all active immunisation strategies have failed to elicit bNAb responses or display efficacy in human clinical trials, reviewed and summarised in (44,45). Therefore, in the absence of an effective prophylactic vaccine, novel biomedical prevention and therapeutic strategies capable of preventing HIV-1 transmission are of critical importance and have the potential to end the HIV-1 global pandemic. Passive immunisation of bNAbs is the main candidate for novel immune-based therapy and prevention strategies (105). Advantageously, bNAbs can enable host clusters of differentiation 8 $(CD8)^{+}$ T-cell immunity via the antibody fragment

crystallisable (Fc) domain for more vigorous suppression of viral replication as well as the clearance of viral reservoir cells, which cannot be achieved with cART (106). Pre-clinical evaluation in murine and non-human primate (NHP) models of HIV-1 infection, as well as human clinical trials, have demonstrated the efficacy of bNAbs for both PrEP and the therapeutic control of viraemia in patients with antibody-sensitive viruses in the absence of ART (59,107–109). The following sections will focus on bNAb passive immunisation as a prevention strategy for HIV-1.

1.5.1 HIV-1 bNAb passive immunisation-mediated protection in animal models.

The humanised mouse model has been utilised to characterise the protection efficacy of HIV-1 bNAbs. Humanised mice are immunodeficient mice that are transplanted with human haematopoietic and lymphoid cells or tissues, enabling them to be infected with HIV-1 and investigate the efficacy of HIV-1 prevention strategies with human immune cells (110). This *in vivo* model has been used to demonstrate initial proof-of-concept of anti-viral protection by HIV-1 bNAbs when passively infused as single antibodies. Multiple bNAbs at various doses (e.g., b12 (2, 10, 50 mg/kg), PGT126 (10 or 50 mg/kg), PG16 (0.05 and 0.2 mg/kg), VRC01 (20 mg/kg)) have shown partial or complete protection within this model (111–115). The humanised mouse model advantageously enables *in vivo* experimental intervention and sampling but there are several disadvantages and limitations to this model's utility in assessing bNAb efficacy. The small size and blood volume of the mice restrict blood sampling volume and frequency, and the reduced lifespan of the mice due to the development of graft versus host disease can limit long-term bNAb efficacy studies. These mice may also have incomplete immune reconstitution and lack robust innate and adaptive immune responses (110). Regardless of these limitations, the humanised mouse model is important for the initial *in vivo* evaluation of HIV-1 bNAbs before progressing to larger animal studies.

The NHP model provides a more relevant model of human HIV-1 infection given their natural susceptibility to chimeric simian-human immunodeficiency viruses (SHIVs) expressing HIV-1 Env on a simian immunodeficiency virus (SIV) backbone without the need for immune-modifications (116,117). The protective efficacy of multiple HIV-1 bNAbs when passively immunised before vaginal, rectal, and oral SHIV challenge has been demonstrated in macaques, reviewed (105). Numerous bNAbs (CD4bs: VRC01,

3BNC117, VRC07; V3 glycan site: PGT121, 10-1074; V2-glycan site: PGDM1400, CAP256-VRC26.25; and MPER: 10E8) are currently in advanced clinical development because they have displayed levels of protection against SHIV infection (118–123). The observed level of protection strongly correlates with the bNAb potency against the specific SHIV strain and the durability of serum bNAb levels (119,121). Recently, a meta-analysis was performed of data from 18 bNAb protection studies passively infusing a total of 242 NHPs with 16 different bNAbs (targeting CD4bs, V1/V2 glycan, V3-glycan, and MPER) infused at a range of doses (0.05 to 50 mg/kg) and challenged with eight SHIV strains (124). It demonstrated that serum neutralisation titre on the day of SHIV challenge was strongly associated with the bNAb protective efficacy in NHPs, and suggests that serum neutralisation titre against the infecting HIV-1 strain will be an important determinant of bNAb protection in humans (124).

These studies reflect the NHP HIV-1 challenge models' utility in determining the factors contributing to HIV-1 protection in humans. However, several limitations should be considered: 1) the limited genetic diversity of SHIVs compared to the circulating HIV-1 strains and the variable SHIV-sensitivity to bNAbs, 2) the infection rate per SHIV challenge in the model may differ from natural human HIV-1 infection, 3) interspecies immunoglobulin G (IgG) variability could result in inefficiencies of human bNAbs to activate NHP innate immune effector functions, and 4) the elicitation of an autologous antibody response against the passively infused human bNAb within macaques leading to decreased efficacy (105,119,125–127). Despite these limitations, the NHP model remains the best animal model for bNAb protection studies and is instrumental in investigating the safety and protection efficacy of bNAb passive immunisation before progressing to human clinical trials.

1.5.2 bNAb modifications to increase serum half-life.

HIV-1 bNAbs that have demonstrated HIV-1 neutralisation *in vitro*, and prevention efficacy in animal models have progressed to explore the possibility of antibody-mediated prevention (AMP) of HIV-1 infection in humans.

To improve the bNAb half-lives in circulation, various IgG Fc region modifications have been made to reduce *in vivo* catabolism by improving affinity for the neonatal receptor (FcRn) (128). The FcRn plays a role in IgG transport and homeostasis (129,130). Under acidic pH (<6.5) but not at physiological pH 7.4, FcRn binds to the Fc portion of

IgG with high affinity. After endocytosis, free IgG is degraded in the lysosome but FcRn-bound IgG avoids degradation and is recycled into the extracellular space and maintained in circulation with a prolonged half-life (129,130). Salt bridges between anionic FcRn residues and protonated IgG Fc residues (positions 117, 132, 137, and 310, 435, 436, respectively) stabilise the hydrophobic interactions, therefore, mutagenesis of these Fc regions can increase the IgG circulation half-life (128). VRC01 had the constant heavy 2 or 3 (CH2 or CH3) regions modified to increase FcRn binding affinity. Multiple mutations were compared, and the LS mutation (M428L/N434S) in VRC01-LS displayed the best improvement in serum half-life in NHPs and was three-fold longer than VRC01 (131). Therefore, the LS mutation has been incorporated in many HIV-1 bNAbs to increase the recirculation of functional IgG.

Multiple bNAbs from different subclasses have been tested in phase 1 human clinical trials to determine the safety, tolerability, and pharmacokinetic profiles in HIV-1 infected and uninfected participants and have been deemed to be safe and well tolerated, with no anti-drug antibody (ADA) responses reported (Table 1.1). Thus far, only VRC01 (targeting the CD4bs) has advanced to HIV-1 protection efficacy studies and will be discussed in more detail.

1.5.3 The HIV-1 AMP trials.

The AMP trials were a collaborative effort between the HIV Vaccine Trials Network (HVTN) and the HIV Prevention Trials Network (HPTN) (132). Following studies that demonstrated the safety and tolerability of CD4bs-targeting antibody VRC01 in HIV-1-uninfected individuals and modest anti-viral effects in HIV-1-infected viraemic individuals (60,133,134), the potential of VRC01 to prevent HIV-1 infection was explored. The AMP trials were divided into two sub-studies receiving the same regimens, HVTN 704/HPTN 085 (2 699 at-risk cisgender men and transgender persons in the Americas and Europe - NCT02716675) and HVTN 703/HPTN 081 (1 924 at-risk women in sub-Saharan Africa - NCT02568215) (135). A total of 10 infusions of VRC01 at 10 or 30 mg/kg were administered every 8 weeks (a total of 20 months). Overall, VRC01 infusion offered no protection against HIV-1 acquisition compared to the saline-infused placebo groups, with the HVTN 704/HPTN 085 and HVTN 703/HPTN 081 displaying estimated prevention efficacies of 26.6% and 8.8% respectively.

While these results were disappointing, factoring in viral VRC01-sensitivity proved to be a crucial analysis and gleaned important determinants of antibody protection. Pooled trial data showed that regardless of the VRC01 dose, the prevention efficacy of VRC01 against sensitive HIV-1 isolates (*in vitro* sensitivity to VRC01 with an IC80 <1 μg/mL) was 75.4% (135). Therefore, against highly sensitive HIV-1 isolates, VRC01 was associated with a lower risk of HIV-1 infection with 75% protection over the 20 month period, demonstrating a key proof-of-principle that bNAbs can prevent HIV-1 infection in humans (135). However, these data also demonstrated the importance of viral antibody susceptibility to determine antiviral activity, especially when there are circulating bNAb-resistant viruses. In this regard, *in vitro* neutralisation sensitivity is an important biomarker to be considered. Corey ***et al***. (135) defined the required serum neutralisation titre for protection, which can be evaluated *in vitro* using an IC80 cutoff of <1 μg/mL to predict the clinical potency of antibodies. bNAbs displaying superior potency and neutralisation coverage than VRC01 are currently in clinical development (e.g. N6, 3BNC119, and VRC07) but it remains to be seen whether this defined cutoff (<1 μg/mL) for protection translates to other bNAbs or if this threshold is maintained with repeated passive infusions (80). Nonetheless, these results provide the current benchmark for bNAb protection from HIV-1 infection and this cutoff should be considered when screening the neutralisation potency of HIV-1 bNAbs. The AMP trials results also highlighted the importance of neutralisation breadth and the requirement of combinations of bNAbs to provide sufficient coverage for *in vivo* protection. Cognoscente of this, the neutralisation breadth of bNAb combinations should be considered based on their *in vitro* neutralisation data and in animal models for improved HIV-1 prevention.

1.5.4 Combination bNAb infusion for HIV-1 prevention.

HIV-1 bNAb infusion within HIV-1 infected patients has been shown to result in the emergence of bNAb-resistant viral strains with molecular signatures that escape bNAb neutralisation, resulting in viral rebound (136–138). This viral bNAb resistance can emerge due to the bNAb selection pressure on the virus or exist within the myriad of circulating viruses in the human population (pre-existing bNAb resistance) (139–141). To address the challenges of bNAb breadth and potency, and associated bNAb resistance, combinations of different bNAbs can be formulated to collectively target multiple Env epitopes. While individual HIV-1 antibody monotherapy failed to protect

from SHIV infection due to escape mutations, combination bNAbs provided complete protection from mixed SHIV challenge (142,143). Additionally, combinations of bNAbs can effectively maintain viral suppression in antibody-sensitive patients and limit viral escape from individual bNAb selection pressure (previous studies have shown that no individuals developed resistance to both co-administered antibodies) (59,108). Triple and quadruple bNAb combinations have achieved even higher efficacy at neutralising HIV-1 *in vitro* (144). In this way, it is unlikely for an individual to have pre-existing antibody resistance affecting multiple paratopes, and if selection pressure results in viral isolates that escape one antibody, the remaining antibody or antibodies should retain their activity and effectively neutralise the viral isolates that remain sensitive to them.

Various combinations of HIV-1 bNAbs targeting different epitopes have been tested or are in early phase 1 clinical trials (Table 1.1). Double and triple bNAb co-infusions have displayed their safety and tolerability in humans, with no pharmacokinetic interactions occurring among the bNAbs (Table 1.1) (59,145–148). Different doses have been administered in the respective studies, resulting in serum antibody titres ranging from ~10 to >100 μg/mL and half-lives of ~10 to 50 days (Table 1.1). The pharmacokinetics of the antibody titres required for protection and antibody longevity in circulation are dependent on both the dose and the antibody/combination, thus requiring extensive testing and optimisation. The efficacy of bNAb combinations at preventing HIV-1 infection in humans has not reached clinical efficacy testing, however, as suggested by the AMP trials data, diverse and broad bNAb combinations are believed to be required for HIV-1 prevention and are key for future research.

Table 1.1. HIV-1 broadly neutralizing antibodies (bNAbs) (both individual and combinations) that are in early phase 1 and 2 human clinical trials.

bNAb epitope & identifier	Dose (mg/kg)	Half-life (days)	Serum titre (μg/mL)	Main clinical outcome	Reference
Individual bNAb administration					
CD4bs					
VRC01	10 or 30	15	N/A	Phase 2b: Pooled groups had estimated prevention efficacies of 8.8% and 26.6%, sensitive isolates 75.4%.	NCT02165267 (135)
VRC01-LS	5, 20, 40	71	40, 180, 326	Phase 1b: safe, well tolerated, 4-fold greater half-life.	NCT02599896 (149)
VRC01	N/A	N/A	N/A	Recruiting, analytical treatment interruption study.	NCT04860323/NCT04801758 (150)
VRC07-523	1, 5, 20, 40 & 2.5, 5, 20	38 & 40	14, 57, 148, 272 & 42.2, 80.3, 353.6	Phase 1b: Safe and well tolerated across a range of doses, no anti-drug antibodies detected	NCT03015181 (151) (152)
3BNC117	1, 3, 10, 30	17	>1, >10, >10, >100	Phase 1b: safe and effective at reducing viraemia	NCT02018510 (137)
N6-LS	5, 20, 40	44	32, 95, 254	Phase 1b: safe and well-tolerated	NCT03538626 (153)
VRC07	5×10^{10}, 5×10^{11}, 2.5×10^{12} vector genomes/kg	N/A	>1	Phase 1b: safe, some participants developed anti-drug antibody responses. Proof of AAV-bNAb expression in humans	NCT03374202 (154)
MPER					
10E8	N/A	N/A	N/A	Suspended due to reactogenicity	NCT03565315 (155) (156)
V1/V2 glycan loop					
PGDM1400	3, 10, 30	20.7	~≥100	Phase 1b: safe and well-tolerated	NCT03205917 (146)
PG9 *AAV first in human	4×10^{12}, 4×10^{13}, 8×10^{13}, 1.2×10^{14} vg/kg	N/A	Not detected (ELISA LOD 2.5)	Phase 1b: safe, well tolerated, higher dose required in future	NCT01937455 (157)
CAP256-VRC26.25	5, 10	43	1.5, 3.95	Phase 1b: safe and well-tolerated	PACTR202003767867253 (145)
V3 glycan loop					
PGT121	3, 10, 30	22	N/A	Phase 1b: safe, well tolerated, viral suppression in 2 individuals for 168 days	NCT02960581 (158)
10-1074	3, 10, 30	24	>100	Phase 1b: safe and well tolerated, reduce viraemia	NCT02511990 (138)
Gp120 silent face					
2G12	10	16.5	238	Phase 1b: safe and well-tolerated	(159)
Combinations of bNAbs co-administered					
PGT121 (V3 glycan) PGDM1400 (V1/V2 glycan) VRC07-523LS (CD4bs)	PGT121 & PGDM1400: 3, 10, 30 Triple: 20	PGT121 & PGDM1400: 20.2 and 17.4 Triple: 11.8, 11, 29.3	~≥100	Phase 1b: safe and well tolerated, first report of triple HIV-1 antibody administration in humans	NCT03205917 (146)
3BNC117 (CD4bs) 10-1074 (V3 glycan)	Together: 10 each; 8 weeks Separate: 3, 10	3BNC117: 18, 13.7, 15 10-1074: 23.3, 19.9, 22.2	3BNC117: >10, <10, >10 10-1074: >100, >10, ~100	Phase 1b: safe and well-tolerated	NCT02824536 (147) (healthy adults) NCT02825797 (59) (viraemic individuals)
	Together:30, 7 doses	14.9, 20.3	3.5, 28.3	Phase 1: viral suppression for ~20 weeks	NCT03526848 (160)
VRC07-523LS (CD4bs) PGT121 or 10-1074 (V3 glycan) PGDM1400 (V1/V2 glycan)	Double or triple: 20 each	52.9, 32.2, 27.5, 25.4	>100, >10, >100, >10	Phase 1a: safe and well tolerated, no pharmacokinetic interactions among bNAbs	NCT03928821 (148)
VRC07-523LS (CD4bs) PGT121.141.LS (V3 glycan)	N/A	N/A	N/A	Trial completed and results submitted	NCT04212091
3BNC117-LS (CD4bs) 10-1074-LS-J (V3 glycan)	N/A	N/A	N/A	Active, no results posted	NCT04173819 (147)
CAP256V2LS (V1/V2 glycan) VRC07-523LS (CD4bs)	10, 20	43, 66	6, 10	Phase 1b: safe and well-tolerated	PACTR202003767867253 (145)

CD4bs, CD4 binding site; MPER, membrane-proximal external region; AAV, adeno-associated virus; ELISA LOD, enzyme-linked immunosorbent assay limit of detection; N/A: not available.

1.6 HIV-1 multispecific antibodies.

As an alternative to infusing combinations of bNAbs to address the issues surrounding neutralisation breadth and bNAb resistance, multispecific antibodies have been engineered to comprise two or more HIV-1 entry-targeting moieties in a single antibody molecule.

1.6.1 Engineering multispecific antibodies.

Natural antibodies are monospecific in that they target a single epitope and thus require combinations of antibodies to include additional specificities and increase coverage. To simplify this, multispecific antibodies can be engineered to create a single molecule that can recognise different epitopes on the same or different antigen. Multispecific antibodies have diverse applications in diagnostics, imaging, prophylaxis, and therapy, with initial therapeutic applications focused on effector cell retargeting for cancer therapy, reviewed in (161). Multispecific antibodies are engineered by employing various technologies, reviewed in (162–164). Here, we will focus on the main strategies that have been utilised to engineer HIV-1 multispecific antibodies with improved potency and breadth, reviewed in (165).

Native IgG antibodies contain identical heavy and light chain domains in both antibody arms to form a single paratope binding region on each arm. Multispecific antibodies incorporate multiple paratopes in different ways by linking variable heavy (VH) and variable light (VL) domains together and placing separate VH/VL domains in tandem, linking VH/VL domains to the IgG heavy chain N- or C-terminus, different heavy chain/light chain (HC/LC) combination pairing, or a combination of these approaches (Figure 1.5). This is achieved by combining multiple methodologies and technologies, the main concepts of which are summarised below.

1.6.1.1 Fv-only (variable domain/variable fragment) multispecific antibodies.

The simplest bispecific antibodies are made from single antibody variable domains (Fv) as the antigen binding unit (dAbs). The dAbs consist mainly of VH, VL, or other variable domains such as variable heavy domain of heavy chain (VHH) derived from the heavy-chain only antibodies of camelids (166,167). Naturally in humans and other mammal species, VH and VL domains must be paired to reconstitute the paratope and facilitate target epitope binding. There are some cases of VH and VL that comprise the

full binding capability of the antibody (168). However, in most circumstances, the VH and VL domains need to be engineered to have sufficient antigen binding capabilities in isolation (169), and connecting multiple domains with linkers can create multivalent molecules with multiple specificities (164). Single-chain variable fragment (scFv) antibodies are made by connecting constituent variable genes VH and VL of an antibody with linker peptides (like Gly4Ser). The order of the variable domains separated by the linker sequence can be altered, e.g. VH-VL vs VL-VH (170). Tandem-scFv antibodies combine the variable genes of two antibodies, joined by linker peptides (170). All these 'variable-only' formats combine multiple antigen-binding moieties and generally omit the Fc region. Lacking an Fc region can circumvent issues of chain association but as a consequence results in reduced plasma half-life since they cannot have Fc-FcRn-mediated protection from catabolism (162).

1.6.1.2 Fab-based multispecific antibodies.

Fv-only antibodies lack the native fragment antigen-binding region (Fab) architecture that provides stability to the interactions of heavy- and light-chain constant domains (CH1 and CL). The absence of these stabilising domains can compromise the stability or solubility of the Fv fragments, leading to aggregation (171). Additionally, incorporating an Fc domain is advantageous as it enables additional immune effector functions and improved serum half-life (172). A challenge with full antibody Fab moieties for multispecific antibodies is ensuring the correct HC/LC pairing when there are multiple at play, thus creating the need to direct cognate HC/LC pairing to assemble homogenous multispecific antibodies (173).

CrossMab technology was developed to enforce the correct HC/LC association in multispecific heterodimer IgG antibodies (174). This is achieved by exchanging/crossing different domains within the Fab-fragment: exchange of either Fab domain (CrossMab^{Fab} format), exchange of only the variable VH-VL domains (CrossMab^{VH-VL} format), or the exchange of the constant-heavy and -light (CH1-CL) domains (CrossMab^{CH1-CL} format) can facilitate the correct HC/LC pairing within bispecific conformations (175). Issues with these methods includes the formation of by-products. The CrossMab^{Fab} format can form non-functional monovalent antibodies and Fab fragment side products, and the CrossMab^{VH-VL} format can form an undesirable by-product via association between the VL-CH1 containing heavy chain

and the original VL-CL light chain (174,175). While these by-products can be removed with chromatographic techniques, the CrossMab$^{CH1\text{-}CL}$ format does not have any undesirable by-products generated as there is no interaction between respective original light chain and novel VL-CH1 light chain (175).

In contrast to CrossMab technology which enables correct chain association to form multispecific antibodies, knob-into-hole (KIH) technology enables correct heterodimerisation of different antibody heavy chains to generate multispecific antibodies (175,176). KIH uses the sterically complimented T366W 'knob' mutation and the T366S, L368A, and Y407V 'hole' mutations in the CH3 domains of respective antibody heavy chains that resulted in knob-hole heterodimerisation efficiency of ~87% (177). Correct association was further enforced, achieving a ~95% heterodimerisation rate, by introducing an inter-chain disulphide bond through the addition of the S354C knob mutation and Y349C hole mutation (178).

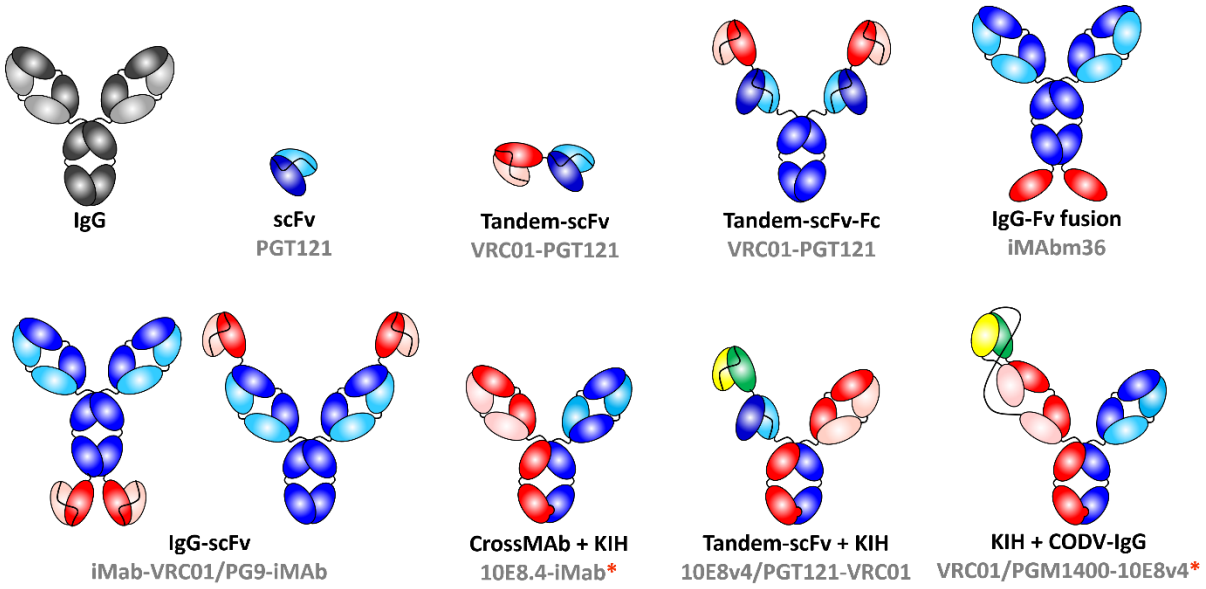


Figure 1.5. Multispecific antibody formats of increasing complexity are engineered using various technologies. *Indicates currently in clinical development. Figure adapted from Padte *et al.* (165). scFv, single chain variable fragment; CrossMab, constant heavy (CH1) and constant light (CL) domain exchange (CH-CL); KIH, knob-into-hole.

1.6.2 Multispecific antibodies targeting HIV-1.

Numerous HIV-1 multispecific antibodies have been developed using a myriad of assembly technologies. Multispecific antibodies have been developed for HIV-1 viral reservoir clearance strategies where incorporated bNAb paratopes are used to redirect immune effector functions. Strategies include the targeting of the viral reservoirs through redirecting $CD8^+$ T cell activity (179–182), HIV-1-specific natural killer cell activity (183), or endocytosis and lysosomal degradation through co-targeting of the epidermal growth factor receptor (EGFR) (184). Selected HIV-1 multispecific bNAb conformations that exhibit enhanced neutralisation breadth and potency, making them best suited for HIV-1 prevention strategies, are described in detail below.

Multispecific antibodies that combine multiple antibody Env-directed paratopes or Env-CD4 host cell receptor targeting paratopes into a single antibody conformation have been described. These conformations have applications for both HIV-1 therapy and prevention, which require broad neutralisation coverage to combat the emergence of bNAb resistance or counter diverse circulating viral swarms. Various bispecific and trispecific HIV-1 antibodies have been developed using combinations of multispecific antibody engineering techniques, summarised in Table 1.2. Importantly, several of the multispecific antibody conformations have demonstrated synergistic enhancement in potency compared to the parental antibody combinations (185–192) (Multispecific antibodies indicated with (*) in Table 1.2), promoting their progression in preclinical and clinical development.

In humanised mice, HIV-1 multispecific antibodies have displayed therapeutic efficacy at reducing viraemia (189,190) and preventing infection upon HIV-1 challenge (185,193). Additionally, the safety and pharmacokinetics as well as potent SHIV protection of HIV-1 multispecific antibodies have been shown in macaques (188,194). Importantly, HIV-1 bispecific (10E8v4/iMAb) and trispecific (VRC01/PGDM1400/10E8v4) antibodies have progressed to phase 1 human clinical trials to test the safety, tolerability, pharmacokinetics, and antiviral activity of these multispecific antibodies, summarised below.

NCT03875209 (completed, results not posted or published) – 10E8v4/iMAb bispecific antibody has progressed to phase 1b human trials in HIV-1-uninfected and infected adults. In this dose-escalation trial, HIV-1-uninfected participants received once-off

doses of 0.3 mg/kg (intravenous - IV) and 1 mg/kg (IV or subcutaneous - SC), and once-off IV doses of 3, 10, 30 mg/kg. HIV-1-infected participants also received a once-off IV dose of 10 and 30 mg/kg (195).

NCT05890963 (recruiting) – 10E8v4/iMAb bispecific antibody alone or in combination with VRC07-523LS mAb for treatment in HIV-infected adults. This is currently in the recruiting stage for an open-label phase 1b clinical trial enrolling PLWH who are ART-naïve or have been off ART for >24 weeks. Participants will receive a single dose of 10E8v4/iMAb at 600 mg IV/intramuscular (IM) or 1800 mg IV, as well as combining 10E8v4/iMAb 1800 mg IV and VRC07-523LS 1200 mg IV (196).

NCT03705169 (completed, results not posted or published (197)) – SAR441236 (VRC01/PGDM1400/10E8v4 trispecific antibody with Fc-region LS mutations for half-life extension). This trispecific antibody has previously provided complete protection from SHIV challenge in macaques (194), and progressed to a phase 1b study in ART-treated PLWH. Escalating IV or SC single doses were administered, from 0.3-10 mg/kg, or 4 doses at 30 mg/kg IV every 12 weeks. SAR441236 was safe and well tolerated and had a half-life of 38 days which is consistent with traditional HIV-1 IgG antibodies incorporating half-life extension modifications. From these results, it was predicted that 30 mg/kg IV every 12 weeks could result in a median steady-state serum trough of 74 µg/mL (198). An arm of the study was terminated as the planned number of viraemic participants was not met.

There has been great interest and progress in the development of HIV-1 multispecific antibodies. Passively infusing a single multispecific construct is simpler and favourable over combinations of bNAbs, and in some instances provides improved breadth and/or potency over that of the individual parental antibodies (185–187,189–192). This potential for synergy and overall enhancement in the potency and/or breadth of multispecific antibodies provides a further advantage over combination bNAb infusions.

Table 1.2. HIV-1 multispecific antibodies for therapeutic reduction in viraemia or prevention of HIV-1 infection.

Reference	Antibody paratopes	Conformation	Best performer	Potency (mean IC50 µg/mL)	Breadth % (Number of viruses)	Models tested in
Pace *et al*., 2013 (186)	PG9/iMAb PG16/iMAb	scFv linked to iMAb IgG N-terminal	PG9/iMAb * PG16/iMAb *	0.004 0.0027	100 (118)	*In vitro*
Sun *et al*., 2014 (187)	iMAbm36	Linked to C-terminus	iMAbm36 *	<10	96 (118)	*In vitro*
Asokan *et al*., 2015 (188)	VRC07/10E8, VRC07/PGT121, VRC07/PG9-16, 10E8/PG9-16	CrossMab KIH	VRC07/PG9-16 *	0.055	97 (206)	*In vitro*. Rhesus macaques, 10 mg/kg, half-life 10 days
Bournazos *et al*., 2016 (189)	IgG1: 3BNC117/10-1074, PG16/10/10-1074, PG16/PGT121, PG16/PGT128. IgG3C: 3BNC117/10-1074, PGT151/10-1074, 3BNC117/PGT135, 8ANC195/PGT128, PGT151/10E8, 8ANC195/10-1074, 3BNC117/10E8, PG16/10-1074, CH103/8ANC195, 10E8/10-1074	CrossMab KIH	3BNC117/10-1074 – IgG3C 3BNC117/PGT135 – IgG3C*	0.110 0.036	95.8 (120) 93.3 (119)	*In vitro*. *In vivo*, 3BNC117/PGT135 – IgG3C reduced viraemia in HIV-1-infected humanised mice
Huang *et al*., 2016 (190)	PGT121/iMAb, PGT121/P140, 3BNC117/iMAb, 3BNC117/P140, PGT128/iMAb, PGT128/P140, PGT151/iMAb, PGT151/P140, 10E8/iMAb, 10E8/P140	CrossMab KIH	10E8v2.0/iMAb *	0.002	100 (118)	*In vitro*. NGS mice: improved therapeutic reduction in viral load over combination (weekly dose bispecific 0.5 mg), 0.2 mg protective from infection.
Xu *et al*., 2017 (194)	VRC01/10E8, PGT121/VRC01, VRC01/PGDM1400-10E8v4, N6/PGDM1400-10E8v4	scFv-IgG KIH	N6/PGDM1400-10E8v4	<0.02	99.5 (208)	*In vitro*. Potent SHIV protection in macaques, 5 mg/kg.
Khan *et al*., 2018 (199)	10E8fv-N6fv, m36.4-PRO140, 10E8/PGT121/PGDM1400, 10E8Fab/PGDMfv/PRO140fv	scFv, scFv-IgG	10E8Fab/PGDMfv/PRO140fv	0.007	98 (109)	*In vitro*
Steinhardt *et al*., 2018 (200)	Bi-scFvdVRC01/PGT121, Bi-NAbdVRC01/PGT121, 10E8/Bi-NAbdVRC01/PGT121,	scFv, scFv-IgG, scFv IgG and IgG KIH	VRC01/PGT121/10E8	0.063	99.5 (208)	*In vitro*
Wu *et al*., 2018 (193)	PGT128/Hu5A8	Tandem scFv-IgG	PGT128/Hu5A8	0.073	100 (124)	*In vitro*. Humanised mice: sterile protection (10 mg/kg), complete viraemia control and eliminates HIV-1 infection (AAV)
Moshoette *et al*., 2019 (191)	iMAb/CAP256, 10E8/iMAb	CrossMab KIH	iMAb/CAP256 *	<0.001	100 (20)	*In vitro*
Strokappe *et al*., 2019 (201)	J3-11F1F, 3E3-11F1F, J3-2E7, 3E3-2E7, J3-1F10, 3E3-1F10	Bispecific VHH	3E3-11F1F	~10, (4.65 nM)	100 (6)	*In vitro*
Davis-Gardner *et al*., 2020 (192)	CAP256.VRC26.25/10-1074, PGT145/10-1074, CAP256.VRC26.25/PGT121, AP256.VRC26.25/PGT128 PGT145/10-1074, PGT145/PGT121, PGT145/PGT128	scFv & full IgG arm, with and without KIH, full IgG arms with KIH	CAP256.VRC26.25 scFv/PGT128 *	0.0128	100 (15)	*In vitro*
Moshoette *et al*., 2022 (202)	iMAb/N6	CrossMab KIH	iMAb/N6	0.0475	100 (21)	*In vitro*
Liang *et al*., 2023 (185)	iMAb/PRO140/10E8, iMAb/PRO140/PGDM1400, iMAb/PRO140/PGT121	Variable regions on IgG, linked third Fab on N-terminus	iMAb/PRO140/PGDM1400 *	0.05	100 (23)	*In vitro* In humanised mice, 1 mg/kg protective from viral challenge

* Indicates the multispecific antibody is better than parental antibodies. scFv, single chain variable fragment; IgG, immunoglobulin G, KIH, knob-into-hole; VHH, variable heavy-heavy; AAV, adeno-associated virus.

1.7 Strategies for vectored bNAb expression *in vivo*.

1.7.1 Cost of bNAb production for passive infusion.

Monoclonal antibody therapy effectively treats many conditions. Although it depends on the type of mAb and the application, mAb therapy is generally considered to be expensive (the average mAb therapy cost per year in 2018 was $97 731 (203)). Published costing on HIV-1 bNAb passive immunisation was difficult to find and, unfortunately, the most recent and relevant cost per dose of VRC01 administered in the AMP trials was not available. Antibody passive immunisation costs are based on many factors, including mAb production and purification, cold-chain storage, and personnel (204). The cost to produce a mAb (cost of production and purification only (cost of goods), all-inclusive purchase cost was not available) in 2022 ranged from $95-200/g, which far exceeds the estimated cost of $10/g required for global mAb access (205). Unfortunately, this global mAb access price may be unachievable as cost modelling on mAb production in high-titre very large-scale production facilities (12-25 kL bioreactors) suggested that ~$20-40/gram is likely the lowest achievable cost (206). Product royalties, the significant cost of new facilities, purification procedures, and clinical trial validation suggests that alternative mAb production hosts are unlikely to be cheaper per gram than the standard optimised Chinese hamster ovary (CHO) mammalian cell line (206).

We estimate the cost of mAb passive immunisation for HIV-1 based on the cost of goods price range of $95-200/g (205) and the study parameters of the AMP trial (30 mg/kg administered every 8 weeks, ~6.5 times per year) (135). We assert the following cost of goods (note that the final purchase price would likely be significantly greater): for an average 60 kg female ($171-360 per dose and $1 112-2 340 per year), and an average 80 kg male ($228-480 per dose and $1 482-3 120 per year).

Therefore, whilst passive infusion of HIV-1 bNAbs has demonstrated proof-of-principle for both therapy and prophylaxis the cost prohibits its large-scale global rollout and it is unlikely to be a viable option in resource-limited countries with the highest HIV-1 prevalence and greatest need for HIV-1 prevention (4–7). Thus, alternative, more cost-effective HIV-1 prevention strategies or passive immunisation approaches are required. To this end, antibody gene transfer techniques that deliver antibody-encoding nucleotide sequences to tissues for *in vivo* HIV-1 bNAb expression and secretion are

being explored in earnest (207). Gene transfer can be mediated by different vector systems, such as viral vectors, naked deoxyribonucleic acid (DNA), or mRNA (207). Naked DNA and lentiviral vectors have disadvantages (electroporation delivery, and safety concerns due to replication-competencies, respectively) (207–210) that have restricted their use in humans and will not be discussed here. We will focus on adeno-associated virus (AAV) vector delivery of bNAbs, which are currently the best-studied gene therapy vector in humans (211), and the newer approach of mRNA delivery of bNAbs.

1.7.2 AAV vectored immunoprophylaxis.

AAVs are small non-enveloped viruses, packaging a 4.7 kb single-stranded DNA genome, that require helper viruses (e.g. adenovirus) to replicate. AAVs can infect different cell types, the specificity of which is determined by the cell tropism of the viral capsid (212,213). Currently, there are over 100 AAV serotypes and capsids documented, making this a powerful tool for therapeutic gene delivery *in vivo* (214). Advantageously, AAVs have an established safety profile in humans from their use in previous HIV-1 vaccine strategies and more recently in the severe acute respiratory syndrome coronavirus 2 (SARS-CoV-2) vaccines, reviewed by (44,215). The viral vector-based SARS-CoV-2 vaccines produced by AstraZeneca and Johnson & Johnson were reasonably cost-effective under the not-for-profit model during the SARS-CoV-2 pandemic, at $5.3/dose and $10/dose, respectively (216). They are no longer available in the United States and the updated, for-profit prices are not available (217).

Although AAV gene transfer vectors have been widely used, there are important considerations and disadvantages. AAVs have a limited transgene carrying capacity, restricted at a standard 4.5 kb transgene size with larger transgenes of ~5 kb substantially reducing the transduction efficiency (218). Space-efficient bicistronic antibody encoding constructs that enable efficient full-length HIV-1 bNAb expression, by incorporating self-cleaving 2A peptides rather than dual-promoters have been developed (discussed in more detail later – section 1.8.2) (154,211,219,220).

Additionally, natural AAV exposure results in pre-existing immunity and the global seroprevalences range from 30 to 60% depending on the AAV serotype (221,222), which reduces the AAV transduction efficiencies in these individuals and may limit

large-scale use (223,224). AAVs can also stimulate an adaptive immune response against the viral capsid proteins or the transgene that severely limits the transgene expression and reduces the effectiveness of re-administration of multiple doses (223,224).

1.7.2.1 AAV delivery of HIV-1 bNAbs.

Recombinant AAV (rAAV) vector-mediated delivery of HIV-1 bNAbs has been effective in humanised mouse and NHP models. rAAV8 delivery of HIV-1 antibodies (b12, VRC01, and VRC07-G54W) in humanised mice generated antibody serum titres of 45-313 μg/mL that were protective from viral challenge (219,220). In macaques, rAAV1, 2, or 8 delivery of bNAbs (4L6 5L7, or N4 immunoadhesin, lgG1 4L6 or 5L7, simianised VRC07, and rhesus eCD4-Ig) generated protective antibody serum titres (17-270 μg/mL) (225–228). Importantly, ADA responses against the expressed antibodies developed in multiple macaques, greatly reducing the efficacy (226–228). A favourable property of IM rAAV-mediated antibody delivery is the longevity of antibody expression. Single IM AAV-delivered SHIV antibody administration to macaques resulted in one animal that successfully maintained 240-350 μg/mL anti-SHIV antibody for over 6 years, with no ADA response, and was protected from repeated SHIV challenges (229). Another study reported sustained AAV-encoded expression of two HIV-1 antibodies (50-150 μg/mL) in an infected macaque for over 2 years, with an abrupt decline in plasma viraemia (230). This demonstrates the low turnover in muscle cell tissue (231) that can enable a long-term stable source of antibody expression *in vivo* following AAV delivery (229).

rAAV delivery of HIV-1 bNAbs has progressed to early phase 1b clinical trials to assess the safety of dose escalation (Table 1.1). The first-in-human trial used a rAAV1 cassette dual-promoter system encoding the HIV-1 bNAb PG9 (157). Unfortunately, PG9 was not detected in the serum, likely due to the PG9 ADA that was present in the high-dose groups, in combination with the detected anti-AAV1 antibodies and AAV1-specific T-cell responses (157). A more recent clinical trial administered a bicistronic AAV8 vector encoding for HIV-1 bNAb VRC07 heavy- and light-chains to HIV-1 infected adults which was shown to be safe and well-tolerated (154). Maximal serum VRC07 titres >1 μg/mL were detected, and 4/8 individuals maintained stable near-maximum serum VRC07 titres for up to 3 years of follow-up. Unfortunately, ADA

responses occurred in 3 individuals and appeared to decrease the serum VRC07 production (154).

Therefore, comprehensive AAV HIV-1 bNAb delivery in humanised mice, NHPs and humans displayed safety and efficacy in long-term antibody expression *in vivo*. However, ADA responses and anti-AAV responses have been elicited in macaques and humans using this method which greatly reduces the serum antibody titres and thus the efficacy for protection (154,226–228). Additionally, the size constraint of the transgene may restrict the antibody conformations that can be delivered using this strategy, since antibody sequences are quite large and encoding multispecific full antibodies in AAV vectors may not always be possible.

1.7.3 IVT-mRNA expression.

In vitro transcribed (IVT) mRNA expression cassettes present an attractive means of vector-mediated delivery and *in vivo* heterologous antibody expression (232). IVT mRNA vectors are advantageous compared to DNA- and viral-based systems, since mRNA only requires direct uptake into the cytosol for immediate protein expression without the need for prior DNA entry into the nucleus, negating the risk of insertional mutagenesis (233,234). IVT mRNA has demonstrated therapeutic activity in multiple cancers and protein replacement therapies (235,236) and mRNA vaccines created a new era in vaccinology, highlighted by the rapid production of effective and safe mRNA vaccines against SARS-CoV-2 (237,238). This platform is also relatively cost-effective, based on the estimated commercial cost of the Pfizer-BioNTech SARS-CoV-2 vaccine, initially purchased at far reduced prices during the SARS-CoV-2 pandemic (average purchase price of $20.69 per dose (216)) but sold at $120/dose in 2023 (216,239,240).

The mRNA cost per dose for *in* vivo delivery and expression of HIV-1 bNAbs/multispecifics would depend on the concentration required to achieve protective serum titres *in* vivo, which are currently unknown for HIV-1. We performed mRNA-mediated antibody delivery costing calculations under the following assumptions: the current Pfizer-BioNTech SARS-CoV-2 vaccine cost per dose ($120 (216,239,240)) with the AMP trials administration schedule (6.5x a year (135)), giving an estimated yearly purchase cost of $780. This is more cost-effective than the estimated antibody passive immunisation cost and the mRNA production costs may decrease over time as this technology matures and there is increased

business/manufacture competition. An additional important consideration for antibody passive immunisation strategies is the ease of administration. Large passive infusion doses of 30 mg/kg of antibody need scaled and slow IV administration to limit infusion reactions (241,242) while mRNA is compatible with a simplified injection administration protocol.

IVT mRNA is produced by different RNA polymerase species (T7, T3, and SP6 polymerases) that overcome the 200 base pair (bp) length restrictions of chemical RNA synthesis and can achieve long transcripts with high yields (243). The T7 RNA polymerase, derived from the T7 bacteriophage, is frequently used because of its high specificity and RNA synthesis activity (244). T7 polymerase recognises the conserved T7 promoter DNA sequence (TAATACGACTCACTATAGGG) to initiate transcription and generate full-length RNA transcripts. The downstream sequence (starting with the 5' untranslated region (UTR)) may affect the T7 promoter activity and should be placed after the conserved T7 promoter sequence (245). IVT with T7 RNA polymerase yields high transcript production, however, there is also nonspecific synthesis of double-stranded RNA (dsRNA) byproducts which can stimulate the immune system (discussed later – section 1.7.3.6) (246).

The IVT mRNA expression platform is cheaper, faster, simpler, and a more controlled reaction than recombinant antibody production and purification for passive infusion. IVT mRNA is a synthetic single-stranded RNA (ssRNA) transcript engineered to mimic naturally occurring mRNAs (235). Thus, there are key mRNA aspects/structural elements that can be optimised for improved mRNA stability, transfection, and expression efficiency and are crucial to achieving its full therapeutic potential (235,243) which are described briefly below.

1.7.3.1 The 5' Cap.

Eukaryotic mRNAs all have an evolutionarily conserved 5' 7-methylated guanosine (m7G) cap linked to the first RNA nucleotide via a 5'-5' triphosphate bridge. It is required to modulate nuclear export, pre-mRNA splicing, RNA stability, protection from 5' to 3' exonuclease cleavage, and for efficient initiation of translation (recruits translation factors) for protein synthesis (247–249). The Cap0 (m7GpppN) structure is an early processing event that naturally occurs co-transcriptionally and can be altered by attaching additional methyl groups to the first and/or second transcribed nucleotides

to generate a Cap1 (m7GpppNm) or Cap2 (m7GpppNmNm) structure, respectively (250). The immune system can recognise non-self RNAs (dsRNA lacking a Cap1 or Cap2 methylation structure) through pattern recognition receptors (PRR) (251). Thus while both the Cap0 and Cap1 structures are required for efficient *in vitro* translation, the Cap1 is required to evade an immune response *in vivo* (247,251). IVT mRNAs can be synthetically capped in different ways. The T7 RNA polymerase IVT reaction initiates transcription with guanosine triphosphate that can then be post-transcriptionally, enzymatically capped and methylated, usually using the Vaccinia capping enzyme (Cap0) and 2'O-methyltransferase (Cap1), respectively (247,252). Alternatively, cap analogues can be incorporated co-transcriptionally during the IVT reaction which reduces the number of manufacturing steps (252). Enzymatic capping allows complete RNA capping but cap analogues can have <100% capping efficiency (247).

1.7.3.2 The 5' UTR.

The 5' UTR mRNA section (~100 to 200 nucleotides (253)) is upstream of the coding region, it is not translated but is a critical binding site for ribosomes to initiate translation, therefore the 5' UTR is optimised to improve stability or increase translation efficiency (243,254). The 5' UTR sequence is generally adenine-uracil (AU)-rich which promotes secondary structure formation that impedes or engages the binding of ribosomes and regulatory factors that control gene expression (255). Additionally, most eukaryotic 5' UTRs include a Kozak consensus sequence (GCCRCCAUGG – where R is a purine (A or G)) that contains the AUG start codon (underlined) to initiate translation (255).

1.7.3.3 The coding sequence.

The open reading frame (ORF) coding sequence encodes for the protein of interest. It is the largest portion of the transcript, thus modulating this region via codon optimisation is important as this affects the overall mRNA stability and translation capacity (256). The transfer RNA (tRNA) species determine the overall translation rate, and optimising codon usage to replace rare tRNA species with common tRNA species can affect the fidelity of translation and efficiency of protein production (257). Modified nucleosides are widely used to reduce innate immune activation (discussed later – section 1.7.3.6) but this may affect the overall translation, with contrasting reports of

impeded and enhanced translation with modified nucleosides (258–260). Therefore, the dynamic translation mechanisms for different sequences resulting from codon optimisation and base modification need to be considered and evaluated on an independent basis.

1.7.3.4 The 3' UTR.

The 3' UTR mRNA regulatory element is crucial for targeting transcripts to specific cellular compartments which is essential for mRNA localisation and protein synthesis (261). Since microRNAs (miRNA) bind to the 3' UTR to silence mRNA expression, mRNAs can be designed to have cell-specific translation and activity by artificially including miRNA binding sites within the 3' UTR (262,263). Additionally, reducing unstructured 3' UTR sequences can facilitate the poly-adenylation (poly-A) tail binding to translation machinery and enhance translation (264).

1.7.3.5 The poly-A tail.

The poly-A tail is characterised by a long repetitive stretch of adenosine nucleotides at the 3' end of mRNA. Generally, longer poly-A tails (>100 bp) provide better protection of the coding sequence from deadenylating and degrading enzymes and thus result in more stable mRNA (265), although stable mRNAs exhibiting shorter poly-A tails have been documented (266). Interactions between poly-A binding proteins and other translation initiation proteins regulate mRNA stability and translation efficiency (267). The poly-A structure can be synthesised using an enzymatic reaction with recombinant poly-A polymerase that extends the IVT mRNA transcript but this lacks the control and precision of incorporating a fixed-length tail that is preferred for clinical applications (235,268). Alternatively, a long "A" sequence stretch is encoded in the DNA template vector (which can be stabilised by a short UGC linker, as used by the current Pfizer/BioNTech SARS-CoV-2 vaccine, which controls the length of the resulting poly-A tail (269).

1.7.3.6 Reducing mRNA immunogenicity.

Chemically modified nucleosides reduce innate immune activation by exogenous mRNA (270). Substituting uridine (complete or partial replacement) with modified nucleosides (pseudouridine (Ψ) or N^1-methyl-pseudouridine (m1Ψ)) has shown enhanced protein translation and expression with low immune stimulation (271–274).

Alternatively, whole sequence engineering, which optimises the codon usage and chooses the most appropriate regulatory sequence (5' and 3' UTRs) for a specific target and application, has demonstrated increased translation and decreased immune stimulation without the need for modified nucleosides (275). Additionally, guanine-cytosine (GC)-rich transcripts are more optimally translated compared to AU-rich transcripts, and increasing the mRNA transcript GC content may help synthetic mRNAs evade targeted degradation by the adenylate/uridylate-rich elements (AREs)-binding proteins and protect them from endonuclease digestion (276–279).

T7 RNA polymerase can synthesise dsRNA byproducts from full-length RNA transcripts through erroneous 3' extension, and the large amount of smaller oligonucleotides that result from the abortion of initiation can prime RNA synthesis and generate dsRNA (244,246,280–283). dsRNA is a common identifier of viral infections and its presence is actively censored by dsRNA-binding proteins (284). When dsRNA enters human cells an immune response is activated, dsRNA-dependent enzymes are activated and inhibit protein synthesis, and dsRNA sensors such as Toll-like receptor 3 (TLR3) are stimulated and release various cytokines (285). Therefore, for improved and efficient translation of administered mRNA and to limit the activation of cytokine production (*in vitro* or *in vivo*), contaminating dsRNA must be removed from the IVT mRNA (286). Alternatively, thermostable T7 RNA polymerase has been engineered to produce IVT mRNA transcripts with improved fidelity, that lack dsRNA byproducts and display reduced activation of the innate immune system (287,288).

1.7.4 IVT-mRNA delivery and expression of HIV-1 bNAbs.

HIV-1 mRNA-based vaccines have tested many delivery systems, including electroporation, cationic micelles, cationic nanoemulsion, poly (lactic acid) nanoparticles, cationic lipid nanoparticles (LNPs), and *ex vivo* loading of dendritic cells, reviewed by (289). IVT-mRNA encoding combinations of various HIV-1 viral proteins electroporated into dendritic cells was the first strategy tested in phase 1/2 clinical trials as a therapeutic vaccine in HIV-1 infected individuals. These studies demonstrated vaccine safety and the induction of transient antigen-specific $CD8^+$ and $CD4^+$ T cell responses but there was no evidence of viraemic control (289–295). Recently, the emphasis has been on the mRNA-LNP platform, since the safety and immunogenicity were tested in people receiving the SARS-CoV-2 vaccines (296,297).

mRNA-LNPs encoding HIV-1 Env antigens have been tested in mice, rabbits, and NHPs and induced robust $CD8^+$ and $CD4^+$ T cell responses as well as developed antibodies and neutralising antibodies (298–300).

The mRNA-LNP platform has also successfully been used for HIV-1 bNAb passive immunisation (234,301). Pardi *et al*. (234) injected humanised mice with LNP-encapsulated mRNA encoding VRC01 heavy- and light-chains (co-administered separate mRNAs). Systemic administration of 1.4 mg/kg of mRNA yielded plasma VRC01 titres of ~170 µg/mL 24 hours post-administration, and weekly injections of 1 mg/kg maintained trough VRC01 levels >40 µg/mL. Interestingly, the plasma VRC01 titres were higher in mice receiving mRNA-LNPs than in mice that received a large bolus (28 mg/kg) of VRC01 antibody protein (mean plasma titres of 204 and 123 µg/mL, respectively). Importantly, the translated antibody from a single injection of VRC01-mRNA-LNP protected humanised mice from IV HIV-1 challenge (234). Co-administration of mRNA-LNPs encoding PGDM1400 and PGT121 scFv-Fc and N6 IgG antibodies resulted in co-expression in mice (301). Individual bNAb administration (0.5 mg/kg) resulted in titres >73 µg/mL 24 hours after administration and it was extrapolated that a single 1 mg/kg dose (0.3 mg/kg of each bNAb) could maintain trough levels >10 µg/mL/antibody for up to 90 days (301).

Therefore, this evolving mRNA-LNP delivery platform has demonstrated utility as both an HIV-1 active and passive immunisation strategy, but only mRNA-LNP-mediated passive immunisation has provided protection from HIV-1 infection in mice and may represent a more cost-effective delivery strategy than passive infusion of antibodies.

1.8 Justification for the current study.

Passive immunisation of HIV-1 bNAbs can prevent HIV-1 infection but requires combinations of bNAbs to reduce viral escape. Multispecific antibodies are desirable over combinations of antibodies since they have simplified manufacturing procedures and facilitate simultaneous engagement of multiple paratopes which can improve the antibody binding avidity and may enhance the neutralisation breadth and potency.

1.8.1 The HIV-1 multispecific antibody selection for the current study.

In a study conducted by Steinhardt *et al*. bispecific and trispecific antibody constructs were rationally designed and optimised that target the HIV-1 viral Env (200). The

bispecific antibodies comprise two HIV-1 bNAbs, VRC01 which targets the CD4bs (mean IC50 0.33 μg/mL, 91% breadth against 190 viruses (72)), and PGT121 which targets the V3 region N332 glycan (median IC50 0.03 μg/mL, 70% breadth against 162 viruses (91)). Tandem variable heavy and light chains of these two bNAbs (VRC01 and PGT121) were joined together by (G4S)n flexible linker sequences (200). Env and bNAb high-resolution x-ray crystallography structures available in the Protein Data Bank (PDB - https://www.rcsb.org/) were used to select the bNAb combination and determine the optimal G4S linker length for an inter-protomer binding model whilst avoiding unfavourable steric hindrances. This design facilitates intra-spike crosslinking of Env, where bispecific antibodies bind and cross-link adjacent protomers within the same HIV-1 Env trimer (200). The tandem variable regions of VRC01 and PGT121 were joined by an additional (G4S)n flexible linker sequence to create the Bi-scFv, which lacks an Fc domain, thus it is unable to modulate additional immune effector functions and has a reduced serum half-life (162,200). To address these limitations, the Bi-scFv was fused to an IgG1 Fc region (using a linker peptide) to create the Bi-NAb capable of affecting additional immune functions (172,200). The most favourable molecular topology and linker peptide sequences were determined (VRC01-5xGSG-PGT121) and BioLayer Interferometry (BLI) confirmed the simultaneous engagement of both epitopes and the functionality of each antibody arm. Additionally, the bivalent binding nature of the Bi-scFv/Bi-NAb and Env trimer were confirmed and was consistent with the design for inter-protomer crosslinking (200). Lastly, the best Bi-NAb topology was paired with the 10E8 bNAb, targeting the MPER (mean IC50 0.35 μg/mL, 98% breadth against 181 viruses (302)) via knob-into-hole technology to generate the heterodimeric Tri-NAb (200). BLI confirmed that the Tri-NAb recognised and bound all three cognate bNAb epitopes on HIV-1 Env (200). Finally, the neutralisation capacity of the multispecific antibodies was assessed against a comprehensive 208 virus panel with diverse HIV-1 Env strains. The Bi-scFv, Bi-NAb, and Tri-NAb multispecific antibodies demonstrated overall improved neutralisation breadth and potency (geometric mean IC50 (breadth): 0.400 μg/mL (molar corrected) (94.7%), 0.380 μg/mL (95.1%), and 0.071 μg/mL (99.5%), respectively) than all their respective parental antibodies (VRC01 0.492 μg/mL (90.4%), PGT121 0.566 μg/mL (63.9%), and 10E8 0.338 μg/mL (97.6%)) (200).

Importantly, these broadly neutralising multispecific antibody constructs described by Steinhardt *et al*. (200) had key aspects that favoured our selection for IVT-mRNA-mediated delivery *in vitro.* The bispecific antibody conformations incorporate antibody variable domains linked in tandem produce a single open reading frame (sORF) encoding region, conducive to translation from a single mRNA transcript. Additionally, the optimised molecular topology of the bispecific antibody constructs had been validated, with further neutralisation coverage achieved when combined with the third Env-targeting paratope of the 10E8 bNAb. Therefore, we did not have to optimise the bispecific topology and could focus on the mRNA-delivery requirements. These constructs also provided increasing multispecific antibody complexity, from Bi-scFv to Bi-NAb to Tri-NAb which was of interest for us in evaluating delivery by the IVT-mRNA expression platform. Therefore, we utilised the best molecular topology of the previously described Bi-scFv, Bi-NAb, and Tri-NAb antibodies (200) (Figure 1.6) and explored the possibility of IVT-mRNA expression of multispecific antibodies *in vitro*.

1.8.2 IVT-mRNA expression of multispecific antibodies.

The bispecific antibodies (Bi-scFv and Bi-NAb) were available in sORF conformations which easily facilitated mRNA production (Figure 1.6). However, the Tri-NAb was originally expressed by transient co-transfection of three plasmid constructs (the Bi-NAb ‘knob’, 10E8 heavy chain ‘hole’ and 10E8 light chain) in mammalian 293F cells to generate a heterologous dimer via KIH assembly (200). Co-administration of mRNA encoding HIV-1 antibody heavy- and light-chain or different scFvs has been done previously and yielded antibody titres in mice (234,301). However, assembling a polycistronic construct in which multiple antibody-encoding genes are placed in tandem to yield a sORF that can be transcribed into a single mRNA may be simpler and have improved expression than co-transfection. For this purpose, we designed a novel and distinguishing Tri-NAb polycistronic construct encoding the Bi-NAb and 10E8 heavy and light chain as a sORF to compare Tri-NAb expression from co-transfection and the sORF constructs (Figure 1.6).

Strategies for multiple gene co-expression from a single vector include using multiple promoters, fusion proteins, proteolytic cleavage sites, internal ribosome entry sites (IRES), and “self-cleaving” 2A peptides between genes (303). IRES have been used to express antibody heavy- and light-chain from a single vector (304), however, the

reduced translation efficiency of the second ORF and the large size (~500 nucleotides) of IRES (305) were unfavourable limitations for our purposes. Self-cleaving 2A peptides are preferable since they are smaller in size (18-22 amino acids long) and have more balanced cleavage efficiency of genes up- and downstream of the 2A peptide (306). Self-cleaving 2A peptides have been identified in some picornavirus genomes, “2A” refers to the specific viral polyprotein region and different viral 2As have been named after their derived virus: F2A (foot-and-mouth disease virus 2A), E2A (equine rhinitis A virus 2A), P2A (porcine teschovirus-1 2A) and T2A (thosea asigna virus 2A) (307,308). The C-terminus of 2A self-cleaving peptides has a highly conserved “NPGP” amino acid sequence where “cleavage” occurs through a ribosomal skipping mechanism (309). During translation, the ribosome skips synthesising at the 2A peptide C-terminus causing cleavage between the glycine and proline residues (306,310,311). This mediates the cleavage of polypeptides during translation in eukaryotic cells and separates the 2A peptide from the downstream peptide (312). However, this results in the remaining 2A peptide sequence being fused to the C-terminus of the upstream protein and the proline residue attached to the N-terminus of the downstream protein (308). Some studies have shown a negative effect of the 2A peptide fused to the C-terminus of the upstream protein, which can be avoided by incorporating a furin cleavage site before the 2A peptide sequence to remove the 2A-derived amino acid residues by endogenous furin cleavage *in vivo* (313). Furin is a highly conserved eukaryotic endoprotease localised in the Golgi (314), through the preferential consensus motif Arg.X.Arg/Lys.Arg (RXK/RR), furin efficiently processes and cleaves precursor proteins (315). Thus furin cleavage before the 2A sequence can remove the 2A peptide residues and limit the potential adverse effects (313).

Polycistronic vectors separating HIV-1 antibody heavy- and light-chain sequences with furin-F2A self-cleaving peptides have been used in AAV vectored immunoprophylaxis (219,220). Therefore, we incorporated self-cleaving 2A peptides combined with furin motif sequences to generate the polycistronic Tri-NAb construct (Tri-NAb sORF). Importantly, we used a furin-F2A self-cleaving peptide to separate the 10E8 knob heavy- and light chains (a construct previously generated and available in our lab (191,202)). Thus, our Tri-NAb expressed from co-transfection (Co-T) was from two plasmid constructs, Bi-NAb_hole and 10E8_knob encoding plasmids (Figure 1.6), and

not three plasmid constructs as described by Steinhardt *et al*. (200). The novel Tri-NAb sORF tricistronic construct incorporated an additional furin/self-cleaving 2A peptide to separate respective Bi-NAb hole and 10E8 knob antibody encoding regions (Figure 1.6).

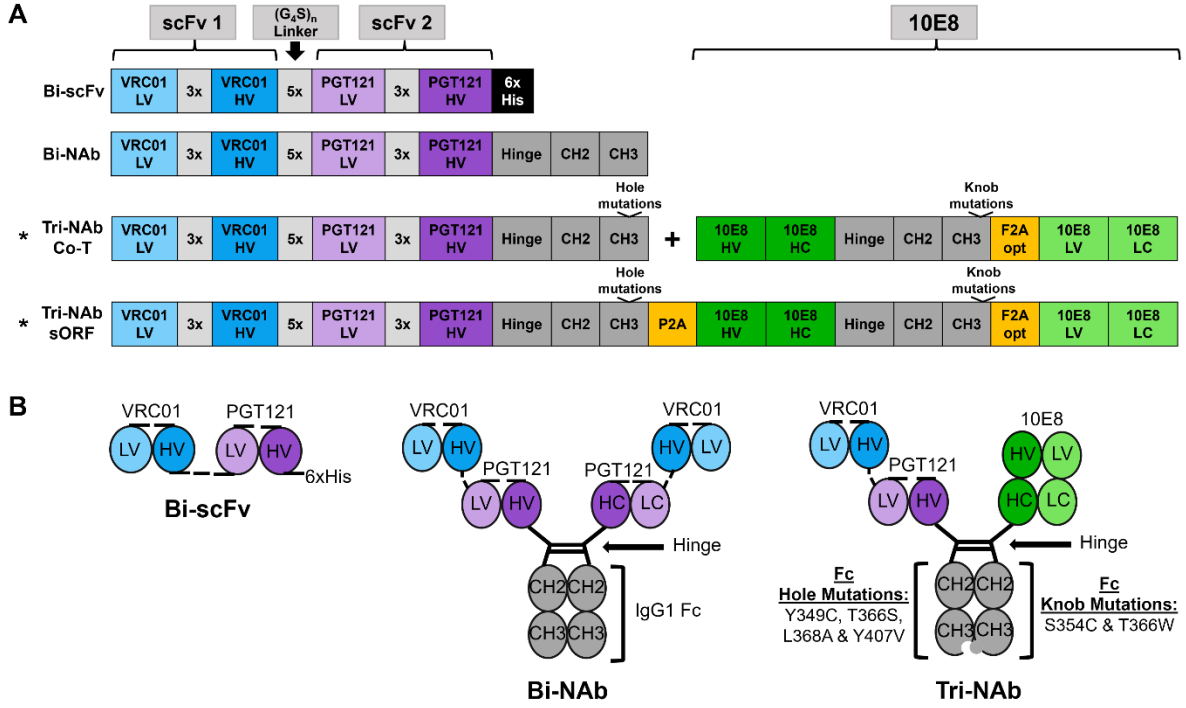


Figure 1.6. HIV-1 multispecific antibody constructs used in this study. The bispecific antibody constructs (Bi-scFv and Bi-NAb) are designed as previously described by Steinhardt *et al.* (200). The trispecific antibody combination is as described by Steinhardt *et al.* (200) but the constructs are designed as single open reading frames (sORF) for expression by co-transfection (Co-T) and from the complete polycistronic sORF. **(A)** Schematic presentation of the multispecific antibody constructs. **(B)** Schematic diagram of the molecular configurations of the multispecific antibodies used in this study. * Indicates constructs that are unique to this dissertation.

1.9 Aim and objectives.

In the absence of an effective prophylactic HIV-1 vaccine, passive immunisation of HIV-1 bNAb combinations can be used to prevent infection, unfortunately, the associated cost may restrict its large-scale use, especially in the resource-limited countries where HIV-1 predominates. HIV-1 multispecific antibodies with enhanced neutralisation breadth combined with IVT mRNA expression could present a simpler, more cost-effective biomedical intervention strategy for prophylactic antibody delivery. To our knowledge, there are no published findings reporting IVT-mRNA-mediated delivery of full-length HIV-1 multispecific bNAbs as a potential prevention strategy against HIV-1. Therefore, the aim of this project was to develop an IVT-mRNA strategy for the *in vitro* expression of HIV-1 bispecific and trispecific antibodies as a potential passive immunisation strategy against HIV-1.

This was achieved using the following objectives:

1) To design HIV-1 bispecific antibody (Bi-scFv and 'full' antibody Bi-NAb with an Fc domain) and trispecific antibody (Tri-NAb, via co-transfection (Co-T) and a sORF) DNA template constructs compatible with *in vitro* transcription of mRNA expression transcripts.
2) To validate and compare the antibody encoding DNA constructs by biochemical characterisation, functional neutralisation and conformation assessment of expressed and purified multispecific antibodies (Bi-scFv, Bi-NAb and Tri-NAbs) relative to the parental antibodies PGT121, VRC01 and 10E8.
3) To transcribe, purify and characterise the respective multispecific-mRNA encoding transcripts *in vitro.*
4) To evaluate and compare the *in vitro* expression, conformational assembly, and functional neutralisation of the mRNA-translated multispecific antibodies Bi-scFv, Bi-NAb and the Tri-NAbs (Co-T and sORF).

Chapter 2. Materials and Methods.

2.1 Reagents used in this study.

The pmRNA_GFP expression vector encoding green fluorescent protein (GFP) and psiCheck_Hbx_Fluc plasmid encoding firefly luciferase (Fluc) were generously donated by Prof A. Ely (Antiviral Gene Therapy Research Unit (AGTRU), Faculty of Health Sciences, University of the Witwatersrand).

The pMin_10E8 and pMin_iMAb single plasmids encoding bNAbs 10E8 and Ibalizumab (iMAb) respectively were available in the HIV Pathogenesis Research Unit ((HPRU), Faculty of Health Sciences, University of the Witwatersrand). These constructs were produced by modification of the original pMin plasmid (generously donated by Dr. A. Balazs (219,220)) to remove the cytomegalovirus (CMV) promoter and inverted terminal repeat (ITR) flanking regions to optimise *in vitro* antibody expression. The corresponding 10E8 and iMAb heavy- and light-chains, incorporating the knob and hole mutations, respectively, within the Fc portion were synthesised and inserted into the pMin vector (pMin_10E8_Kn and pMin_iMAb_Ho) as described (191,202).

The pCI-neo_4dCD4 plasmid expressing a C-terminal His tagged soluble human CD4 receptor was available in the HPRU and was used as a control for His-tagged protein detection.

The pcDNA 3.1-furin plasmid encoding the sequence of the furin protease was originally obtained from Dr. J.P. Moore (316) and was available in the HPRU (317).

The $gp120_{FVC}$ monomer construct, pcDNA3.1gp120FVCm was available in the HPRU (318).

The PGT122 mAb (generously donated by Dr. Peter Kwong (Vaccine Research Centre, National Institute of Allergy and Infectious Diseases, National Institute of Health, Bethesda, Maryland, USA) and was available in the HPRU) is a somatic variant of the PGT121 mAb and was used as a control in small-scale expression studies until the PGT121 constructs were obtained. The PGT121 mAb heavy- and light-chain encoding DNA plasmids were generously donated by Prof. Penny Moore (SA MRC Antibody Immunity Research Unit, University of the Witwatersrand; Centre

for HIV and STIs, National Institute for Communicable Diseases (NICD) of the National Health Laboratory Service (NHLS)).

The following reagents were obtained through the National Institute of Health (NIH) HIV Reagent Program, NIAID, NIH (contributor in parenthesis): antibody expression vectors (complimenting heavy- and light-chain) encoding parental antibodies VRC01 mAb Catalogue number (Cat.) ARP-12035 and ARP-12036 (Drs. X. Wu, ZY. Yand, Y. Li, G. Nabel and J. Mascola (319)), and 10E8v4 mAb, Cat. ARP-12866 and ARP-12867 (Dr. P. Kwong (320)). Reagents for HIV-1 pseudovirus production including: TZM-bl (JC53-bl) reporter cell line Cat. ARP-8129 (Drs. J. Kappes and X. Wu, Tranzyme Inc. (321–326)), HIV-1 pSG3$^{\Delta env}$ Non-infectious Molecular Clone, Cat. ARP-11051 (Drs. JC. Kappes and X. Wu (68,321,327)), and 17 complementing HIV-1 Env plasmids comprised primarily of the Panel of Global HIV-1 Env Clones, HRP-12670, contributed by Dr. David Montefiori (328) (original contributor/s in parenthesis): HIV-1 Env Expression Vectors: 25710*, Cat. ARP-11505 (Drs. R. Paranjape, S. Kulkarni, H. Tang and D. Montefiori (328,329)), 398F1*, Cat. ARP-12652 and 246F3*, Cat. ARP-12658 (Drs. C. Williamson, G. Bandawe and D. Montefiori (328)), CE0217*, Cat. ARP-12660 and CE1176*, Cat. ARP-12657 (Drs. R. Swanstrom, Li-H. Ping, J. Anderson and D. Montefiori (328)), CH119*, Cat. ARP-12659 (Drs. K. Hong, Y. Shao and D. Montefiori (328)), TRO11*, Cat. ARP-11023 (M. Li, F. Gao and D. Montefiori (328,330)), X2278*, Cat. ARP-12654 and X1632*, Cat. ARP-12656 (M. Thomson, A. Revilla, E. Delgado and D. Montefiori (328,331)), CNE8*, Cat. ARP-12653 and CNE55*, Cat. ARP-12661 (L. Zhang, H. Shang and D. Montefiori (328,332)), BJOX002000*, Cat. ARP-12655 (F. Gao and D. Montefiori (328)), Du172.17, Cat. ARP-11307 (Drs. D. Montefiori, F. Gao, S. Abdool Karim and G. Ramjee (333,334)) Du422.1, Cat. ARP-11308 (Drs. D. Montefiori, F. Gao, C. Williamson and S. Abdool Karim (333,334)), CAP210.2.00.E8, Cat. ARP-11317 (Drs. L. Morris, K. Mlisana and D. Montefiori (334)), QH343.21M.ENV.A10, Cat. ARP-11896 (Dr. J. Overbaugh (335,336)) and Ce2103_E8, Cat. ARP-13363 (Drs. D. Montefiori, R. Swanstrom, LH Ping, and J. Anderson (337,338)). (* indicates the Panel of Global HIV-1 Env Clones).

Unless stated otherwise, all chemicals used were obtained from Merck (Merck Group, Darmstadt, Germany) or ACE Chemicals (Associated Chemical Enterprises Pty Ltd, Johannesburg, South Africa).

2.2 General laboratory techniques.

General laboratory techniques, commercially available kit protocols, thermocycling conditions, and primer sequences used in this study are available in the appendix methods (Appendix A).

2.3 Multispecific antibody constructs.

2.3.1 Bispecific antibody construct design.

Previously reported multispecific antibody configurations incorporating VRC01/PGT121 paratopes as tandem single-chain variable fragments alone, for the Bi-scFv and Bi-NAb constructs, and in combination with 10E8 to generate the Tri-NAb, were designed according to the methods described by Steinhardt *et al.* (200). The Bi-NAb antibody construct containing the variable regions interspaced with tetraglycine-serine peptide linker sequences (G4S) ('x' representing the number of repeats incorporated) in the following order: VRC01 delta E1I2/V3S light chain variable region, 3x GSG linker sequence, the VRC01 heavy chain variable region, 5x GSG linker sequence, the PGT121 light chain variable region, 3x GSG linker sequence, the PGT121 heavy chain variable region, and a GSG linker sequence linking the hinge, CH2/CH3 Fc region (Figure 1.6). This Bi-NAb sequence was codon-optimised for mammalian cell expression and synthesised by GenScript (GenScript Biotech Corporation, Piscataway, NJ, USA), incorporating additional flanking sequences on the 5' end (including a *Kpn*I restriction site, a 5' UTR with a T7 promoter sequence, and a secretion signal peptide) as well as on the 3' end (two stop codons (tga tga) and the *Apa*I restriction site. The *Kpn*I and *Apa*I restriction sites were used for directional sub-cloning procedures below.

2.3.2 Bispecific antibody cloning into the pmRNA expression vector.

2.3.2.1 Bi-NAb antibody construct.

The Bi-NAb sequence and flanking regions were provided in the pUC57-Mini holding plasmid from GenScript (GenScript Biotech Corporation, Piscataway, NJ, USA) and the DNA pellet was resuspended in nuclease-free water to a concentration of 0.2 µg/µL. The Bi-NAb sequence was sub-cloned into the pmRNA expression vector using the restriction endonuclease sites *Kpn*I and *Apa*I present in both the Bi-NAb sequence

and the pmRNA plasmid. Restriction digests of 2 µg of pUC57-Mini_Bi-NAb and pmRNA_GFP plasmid DNA were performed with 2 µL of each FastDigest *Kpn*I and *Apa*I enzyme prepared in 10x FastDigest Green Buffer (Thermo Fisher Scientific, Waltham, MA, USA) diluted to 1x in a final volume of 20 µL and incubated at 37°C for 1 hour. Digest reactions were resolved on a 0.8% agarose gel (prepared and resolved as described in Appendix A4) and the Bi-NAb insert sequence (2 374 bp) and the pmRNA backbone sequence (3 638 bp) were extracted using the QIAquick Gel Extraction Kit (Qiagen, Hilden, Germany) as described in the Appendix A2.1.

The gel-purified fragments were ligated using T4 DNA Ligase (New England Biolabs, Ipswich, MA, USA) using 100 ng total DNA and a ratio of insert to backbone of 3:1 (Bi-NAb: pmRNA = 3:1) and incubated at room temperature for 10 minutes. DH5α chemically competent bacteria (prepared as described in Appendix A1) (50 µL) were transformed with 5 µl (1/10 volume of DH5α cells) of the ligation reaction, incubated on ice for 20 minutes, heat-shocked at 42°C for 45 seconds (GLS Aqua 12 Plus water bath - Grant Instruments, Cambridgeshire, UK), and placed back on ice for 5 minutes. An hour outgrowth step was performed at 37°C, 200 rpm in 200 µL of S.O.C. Medium (2% tryptone, 0.5% yeast extract, 10 mM NaCl, 2.5 mM KCl, 10 mM MgCl2, 10 mM MgSO4, and 20 mM glucose - Invitrogen, Thermo Fisher Scientific, Waltham, MA, USA), and 1/10 of the outgrowth culture volume was plated onto carbenicillin (100 µg/mL)-containing LB nutrient agar plates and incubated at 37°C overnight. Single colonies were selected and inoculated into 6 mL Luria Broth (LB) Medium (1% tryptone, 0.5% yeast extract, and 170 mM NaCl) containing 100 µg/mL carbenicillin and incubated overnight at 37°C, 200 rpm. A 100 µL aliquot of each colony culture was stored at 4°C and the remaining culture had the plasmid DNA of the colonies extracted using the High Pure Plasmid Isolation Kit (Roche Group, Basel, Switzerland) according to the manufacturer's instructions (described in Appendix A2.3). Isolated colony plasmid DNA was screened by restriction double digest of 500 ng, alongside 500 ng of control pmRNA_GFP DNA, with 0.5 µL of each FastDigest *Kpn*I and *Apa*I enzyme prepared with 2 µL of 10x FastDigest Green Buffer (Thermo Fisher Scientific, Waltham, MA, USA) in a final volume of 20 µL, and incubated for 15 minutes at 37°C. Digests were resolved on a 0.8% agarose gel (as previously described) to analyse the banding pattern. A single positive pmRNA_Bi-NAb clone was expanded from the 100 µL culture sample into a starter culture of 5.5 mL of carbenicillin-containing LB media

and incubated at 37°C, 200 rpm for 8 hours. The starter culture was expanded 1: 1 000 into 150 mL of carbenicillin-containing LB medium and cultured overnight at 37°C, 200 rpm in a 500 mL Erlenmeyer flask. Bacterial glycerol stocks were prepared by adding glycerol to a final concentration of 25% and stored at -80°C. The pmRNA_Bi-NAb plasmid DNA was isolated using a modified alkaline-lysis method followed by ion exchange chromatography using the QIAGEN Plasmid Maxi Kit (Qiagen, Hilden, Germany) according to the manufacturer's instructions (described in Appendix A2.4).

2.3.2.2 Bi-scFv antibody construct.

The Bi-scFv expression construct was generated from the Bi-NAb sequence using primers that amplified out the tandem-scFv sequence but excluded the Fc region using the Q5® High-Fidelity 2x Master Mix (New England Biolabs, Ipswich, MA, USA) for the polymerase chain reaction (PCR). The amplicon extended from the minimal CMV promoter and incorporated the 5' *Kpn*I restriction site (using the CMV_FOR primer) to the end of the PGT121 heavy chain variable region, excluded the Fc region, and incorporated a six histidine residue encoding region (His tag), followed by stop codon and 3' terminal *Apa*I restriction site to facilitate sub-cloning via the reverse primer (Bi-scFv_REV – Appendix Table A1). The PCR product (1 696 bp) was purified using the GeneJET PCR Purification Kit (Invitrogen, Thermo Fisher Scientific, Waltham, MA, USA) according to the manufacturer's instructions (described in Appendix A2.2). The purified PCR product was digested (1 µg) with 1 µL of each FastDigest enzyme, *Kpn*I and *Apa*I, prepared with 2 µL of 10x FastDigest Green Buffer (Thermo Fisher Scientific, Waltham, MA, USA) in a final volume of 20 µL and incubated at 37°C for 1 hour. The digested Bi-scFv fragment was re-purified using the GeneJET PCR Purification Kit (Invitrogen, Thermo Fisher Scientific, Waltham, MA, USA) to remove restriction enzymes and cleavage products, and sub-cloned into the pmRNA backbone (prepared in section 2.3.2.1) using compatible restriction ends (*Kpn*I and *Apa*I). Ligation and transformation procedures were performed as previously described in section 2.3.2.1. Individual colonies were inoculated into 6 mL of carbenicillin-containing LB media, cultured at 37°C, 200 rpm overnight, and the plasmid DNA was extracted using the High Pure Plasmid Isolation Kit (Roche Group, Basel, Switzerland) as previously described. Extracted plasmid DNA samples were screened by *Kpn*I and *Apa*I restriction double digest as described in section 2.3.2.1. Following screening, culture samples taken before the DNA Mini plasmid isolation corresponding to a

positive clone was expanded by inoculating 5.5 mL of carbenicillin-containing LB media at a ratio of 1:100. Cultures were grown at 37°C, 200 rpm for 8 hours. This starter culture was expanded (1: 1 000) into 150 mL carbenicillin-containing LB media at 37°C, 200 rpm overnight. Residual starter culture volume was used to generate glycerol stocks by adding glycerol to a final concentration of 25% and stored at -80°C. The 150 mL cultures were used for plasmid DNA isolations using the QIAGEN Plasmid Maxi Kit (Qiagen, Hilden, Germany) as described previously.

2.4 Silencing the *Bpi*I restriction site in the CH2 domain of the Bi-NAb construct.

The Bi-NAb encoding sequence contained an additional *Bpi*I restriction site in the corresponding C-terminus of the CH2 domain of the Fc region that required silencing prior to mRNA transcription. The pmRNA construct contains a functional *Bpi*I restriction site at the 3' terminus of the poly-A signal which is used to linearise the DNA plasmid template to improve mRNA transcript production by resulting in a specific poly-A tail sequence length of 46 nucleotides. Targeted-*Bpi*I silencing was achieved by synonymous mutation of the *Bpi*I restriction site in pmRNA_Bi-NAb using the Q5® Site-Directed Mutagenesis (SDM) Kit (New England Biolabs, Ipswich, MA, USA) according to the manufacturer's instructions with the following modifications. The SDM reaction was performed using the primer set BpiI_SDM_FOR and BpiI_SDM_REV and the cycling conditions provided in Appendix, Table A1. The BpiI_SDM_FOR primer incorporated a single nucleotide mutation (1959G>A) on the 5' terminus to silence the *Bpi*I restriction site without altering the lysine amino acid. The SDM product was resolved on a 0.8% agarose gel and the 6 012 bp fragment was purified using the QIAquick Gel Extraction Kit (Qiagen, Hilden, Germany) as described previously, to remove lower molecular weight non-specific bands. Approximately 40 ng (2 µL) (as estimated from the resolved molecular weight marker on the agarose gel) of the Bi-NAb SDM product was added to the kinase, ligase, *Dpn*I (KLD) reaction and incubated at room temperature for 15 minutes. The transformation was performed according to the manufacturer's instructions as follows. The supplied ultra-chemically competent DH5α cells were transformed with 5 µL of the total KLD reaction, incubated on ice for 30 minutes, heat shocked at 42°C for 30 seconds, and returned to ice for a further 5 minutes. An hour outgrowth was performed at 37°C, 200 rpm in 950 µL of Super Optimal broth with Catabolite repression (S.O.C.), 1/10 of the outgrowth volume was plated onto carbenicillin-containing LB agar plates and incubated overnight at 37°C.

2.4.1 Screening pmRNA_Bi-NAb colonies with silenced *Bpi*I restriction sites.

Single colony inoculates were cultured in 6 mL of carbenicillin-containing LB media at 37°C, 200 rpm overnight and the plasmid DNA was extracted using the High Pure Plasmid Isolation Kit (Roche Group, Basel, Switzerland), as described previously. Isolated colony plasmid DNA was screened by restriction digest of 500 ng, alongside 500 ng of original pmRNA_Bi-NAb and pmRNA_GFP DNA as appropriate controls, with 0.5 µL of *Bpi*I prepared in 2 µL of 10x Buffer G (with BSA) (Thermo Fisher Scientific, Waltham, MA, USA) in a final volume of 20 µL, incubated at 37°C for 1 hour. Digests were resolved on a 0.8% agarose gel to analyse the banding pattern. The introduction of the synonymous mutations within the Fc portion in combination with the removal of the *Bpi*I restriction site in the CH2 domain was confirmed by Sanger sequencing using the CH3_Ho_FOR and CH3_Ho_REV primers (Appendix Table A1) and performed by Inqaba Biotech (Inqaba Biotech, Johannesburg, South Africa). A glycerol stock of culture taken prior to the DNA plasmid isolation, corresponding to the confirmed pmRNA_Bi-NAb construct with the silenced *Bpi*I restriction site in the CH2 region was expanded (1:1 000) into 150 mL carbenicillin-containing LB media and cultured at 37°C, 200 rpm overnight. The plasmid DNA was isolated using the QIAGEN Plasmid Maxi Kit (Qiagen, Hilden, Germany) as described previously. The resultant pmRNA_Bi-NAb construct with the silenced *Bpi*I restriction site was now compatible with mRNA production and was used in all downstream antibody expression and characterisation experiments.

2.5 Tri-NAb construct design.

2.5.1 Generating complementary knob-into-hole mutations.

The Tri-NAb was generated by assembling the Bi-NAb and the bNAb 10E8 antibody heavy- and light-chains through the specific introduction of knob-into-hole mutations in the complimenting Fc regions (200). This ensures that the ‘knob’ (Kn) mutations (S354C and T366W) in the 10E8 CH3 domain (pMin_10E8_Kn construct already generated by our research unit – (191,202)) assembles with the complimenting ‘hole’ (Ho) mutations (Y349C, T366S, L368A and Y407V) introduced into the corresponding CH3 domain of the IgG1 Fc arm of the Bi-NAb to allow expression of the Tri-NAb (PGT121/VRC01/10E8) (200). Hole mutations were introduced in the Bi-NAb construct using Gibson assembly (339,340). A 390 bp region encompassing the hole

mutations was amplified from the iMAb_Ho template construct ((pMin_iMAb_Ho) previously reported by our research group (341)) using CH3_Ho_FOR and CH3_Ho_REV primers (Appendix Table A1). The CH3_Ho fragment was assembled in place of the existing CH3 region by linearising the pUC57-Mini_Bi-NAb (experimentally found to have improved amplification over the pmRNA_Bi-NAb – data not shown) using the Bi-NAb_Linear_FOR and Bi-NAb_Linear_REV primer sets, and the cycling conditions described in Appendix Table A1. Assembly of amplicons was achieved through 21 bp homologous overlap on both the corresponding 5' and 3' ends. Fortuitously, the amplified CH3_Ho region included the CH2 C-terminal encoding region without the erroneous *Bpi*I restriction site, and thus did not require further correction as was done in section 2.4.1. The amplified, linearised DNA was resolved on a 0.8% agarose gel and the pUC57-Mini_Bi-NAb backbone (3 889 bp) and CH3 Ho (390 bp) bands were extracted using the QIAquick Gel Extraction Kit (Qiagen, Hilden, Germany) as described previously. Gibson Assembly of the two fragments was performed using the NEBuilder Hifi DNA Assembly Kit (New England Biolabs, Ipswich, MA, USA) according to the manufacturer's instructions, using a total of 100 ng DNA, a vector to insert ratio of 1:2 (pmRNA_Bi-NAb: CH3 Ho = 1:2) and incubated at 50°C for 15 minutes. Transformation and plating were performed as described above using DH5α competent cells (described in section 2.3.2.1).

2.5.1.1 Confirming the presence of the CH3 hole mutations.

Resulting individual selected colonies were cultured in 6 mL carbenicillin-containing LB media at 37°C, 200 rpm overnight, and the plasmid DNA was extracted using the High Pure Plasmid Isolation Kit (Roche Group, Basel, Switzerland), as described previously. Extracted plasmid DNA samples were screened by *Kpn*I and *Apa*I restriction double digest as described in section 2.3.2.1. Finally, the presence of the hole mutations was confirmed by performing in-house Sanger sequencing as described in Appendix A5, using the CH3_Ho_Screen_FOR and CH3_Ho_REV primers (Appendix Table A1).

2.5.1.2 Cloning the Bi-NAb_Ho sequence into the pmRNA expression vector.

The confirmed Bi-NAb_Ho encoding sequence was directionally sub-cloned using *Kpn*I and *Apa*I restriction sites into the pmRNA expression vector as described in section 2.3.2.1. Selected colonies were cultured in 6 mL of carbenicillin-containing LB

media at 37°C, 200 rpm overnight. The plasmid DNA was isolated using the High Pure Plasmid Isolation Kit (Roche Group, Basel, Switzerland) as described previously. Extracted plasmid DNA samples were screened by *Kpn*I and *Apa*I restriction double digest as described in section 2.3.2.1 or *Bpi*I single digest as described in section 2.4.1. The *Kpn*I/*Apa*I digest confirmed the correct assembly of the construct while the *Bpi*I digest indicated that the CH3 hole segment was present as this did not contain an additional *Bpi*I restriction site so the plasmid DNA would be linearised. A confirmed pmRNA_Bi-NAb_Ho transformed colony was inoculated from a glycerol stock (1: 1 000) into 150 mL carbenicillin-containing LB media and cultured in a 500 mL Erlenmeyer flask at 37°C, 200 rpm overnight. The plasmid DNA was isolated using the QIAGEN Plasmid Maxi Kit (Qiagen, Hilden, Germany), as described previously, and was used in combination with the 10E8_Kn sequence to produce the Tri-NAb by co-transfection in 293F cells (Section 2.7.2).

2.5.2 Generating the Tri-NAb single open reading frame (Tri-NAb sORF) construct.

A sORF construct for the expression of the Tri-NAb antibody was produced by insertion of a furin cleavage peptide sequence in combination with a self-cleaving 2A peptide sequence (P2A) in frame and downstream of the Bi-NAb_Ho encoding sequence followed by the 10E8_Kn encoding sequence (Figure 1.6). The modified furin sequence (RRRRRR) in combination with the P2A cleavage peptide were chosen because they have been shown to result in improved processing and cleavage (303,309,342), and the P2A has demonstrated this improvement in multiple human cell lines *in vitro* as well as in mice *in vivo* (306). The three fragments (pmRNA_Bi-NAb_Ho, P2A cleavage peptide, and 10E8_Kn) were assembled by Gibson Assembly using the respective primers provided in Appendix Table A1. The pmRNA_Bi-NAb_Ho backbone (6 006 bp) was amplified using primers Bi-NAb_Ho_linear_FOR and Bi-NAb_Ho_linear_REV that linearised the construct at the 3' terminus of the Bi-NAb encoding sequence, eliminating the stop codons. The 10E8_Kn sequence (2 322 bp) was amplified from the pMin_10E8_Kn sequence described above (section 2.5.1). The forward 10E8_Kn_linear_FOR primer incorporated a 21 bp overlap with the P2A cleavage peptide on the 5' end, whilst the reverse 10E8_Kn_linear_pmRNA_REV primer sequence maintained the 10E8_Kn construct's stop codon and incorporated a 21 bp homologous overhang for compatible assembly with the pmRNA backbone (Appendix Table A1). Amplified fragments were resolved on a 0.8% agarose gel and

were extracted using the QIAquick Gel Extraction Kit (Qiagen, Hilden, Germany) as described previously. The interlinking P2A encoding peptide sequence (93 bp) was generated using the Q5® High-Fidelity 2x Master Mix (New England Biolabs, Ipswich, MA, USA) with an overlapping primer strategy. The forward Cleavage_peptide_FOR primer sequence (54 bp) and reverse Cleavage_peptide_REV primer sequence (59 bp), which have 20 bp complimentary overlap on their respective 3' ends, were used to generate the template P2A DNA. Briefly, 1 µM of each primer was combined with the Q5® High-Fidelity 2x Master Mix (New England Biolabs, Ipswich, MA, USA) and allowed to anneal and extend to complete the polymerase reaction (Appendix Table A1). The generated P2A DNA template was analysed on a 1.5% agarose gel to confirm the correct size, and 200 pg of the P2A template DNA was amplified using the primers Cleavage_peptide_AMP_FOR and Cleavage_peptide_AMP_REV (Appendix Table A1) to ensure compatibility in the Gibson assembly reaction. P2A DNA products were purified using the GeneJET PCR Purification Kit (Invitrogen, Thermo Fisher Scientific, Waltham, MA, USA) as previously described.

The three fragments were assembled using the NEBuilder Hifi DNA Assembly Kit (New England Biolabs, Ipswich, MA, USA) to generate a single 8 379 bp product. A total of 100 ng of DNA was used at a ratio of pmRNA_Bi-NAb_Ho: 10E8_Kn: P2A cleavage peptide of 1:2:5. The reaction was incubated at 50°C for 30 minutes before *E. coli* DH5α cell transformation and plating of the transformed bacteria were performed as previously described (section 2.3.2.1). Selected colonies were cultured overnight at 37°C, 200 rpm in 6 mL of carbenicillin-containing LB media, and the plasmid DNA was extracted using the High Pure Plasmid Isolation Kit (Roche Group, Basel, Switzerland) as previously described. Extracted plasmid DNA samples were screened by *Kpn*I and *Apa*I restriction double digest as described in section 2.3.2.1 and with 0.5 µL of each FastDigest *Kpn*I and *Not*I, prepared with 2 µL 10x FastDigest Green Buffer (Thermo Fisher Scientific, Waltham, MA, USA) in final volumes of 20 µL, incubated for 15 minutes at 37°C and resolved on a 0.8% agarose gel. Targeted in-house Sanger sequencing, as described previously, of presumptive constructs was performed to confirm the Bi-NAb_Ho-P2A cleavage peptide-10E8_Kn transition sequences using the single CH3_Ho_Screen_FOR primer (Appendix Table A1).

2.5.3 Improving endogenous furin processing of the 10E8_Kn construct.

2.5.3.1 Site-directed mutagenesis of the 10E8_Kn furin sequence.

The 10E8_Kn F2Aopt furin encoding sequence (amino acid sequence RKRR) used to separate the heavy- and light-antibody chains following translation was altered to six consecutive arginine residues (RRRRRR - sequence shown to improve cleavage (343)) using site-directed mutagenesis. Non-overlapping SDM primers were designed to remove the lysine (K) (omitted from the reverse primer – 10E8_Kn_furin_SDM_REV) and incorporate an additional three arginine residues (R) (on the 5' end of the forward primer – 10E8_Kn_furin_SDM_FOR, Appendix Table A1). The SDM reaction was performed using the Q5® Site-Directed Mutagenesis Kit (New England Biolabs, Ipswich, MA, USA) according to the manufacturer's instructions. A linearised amplicon with incorporated mutations was amplified from the pMin_10E8_Kn template (6 183 bp), resolved on a 0.8% agarose gel, extracted, and purified using the QIAquick Gel Extraction Kit (Qiagen, Hilden, Germany), as previously described, to remove the smaller non-specific bands. Purified SDM product (25 µL) was concentrated by DNA precipitation, with the addition of 1/10 the volume (2.5 µL) 3 M sodium acetate and one volume (27.5 µL) isopropanol, incubated at room temperature for 15 minutes and centrifuged at 13 000 x g for 15 minutes at 4°C to pellet the DNA. The supernatant was carefully discarded, and the DNA pellet was washed with one volume (27.5 µL) of chilled 70% ethanol and centrifuged at 13 000 x g for 15 minutes at 4°C. The ethanol supernatant was discarded, and the DNA pellet was resuspended in 5 µl nuclease-free water.

The KLD reaction was performed according to the manufacturer's instructions, except a greater amount of PCR product DNA (4 µl) generated above was used in the reaction to maximise transformation efficiency and incubated at room temperature for 15 minutes. The transformation was performed as described above (section 2.4) using DH5α chemically competent bacteria and 1/10 of the outgrowth volume was plated on carbenicillin-containing LB agar plates and incubated overnight at 37°C. Selected colonies were cultured in 6 mL carbenicillin-containing LB media and the plasmid DNA was extracted using the High Pure Plasmid Isolation Kit (Roche Group, Basel, Switzerland) according to the manufacturer's instructions. Colonies were screened by Sanger Sequencing in-house using the primer set 10E8_Kn_CP_seq_FOR and

10E8_Kn_CP_seq_REV (Appendix Table A1) as described above. A sequence confirmed pMin_10E8_Kn_Δfurin clone was expanded by inoculating 50 mL of carbenicillin-containing LB media with 100 µL of a glycerol stock (25% glycerol, stored at -80°C) and cultured overnight at 37°C in a 250 mL Erlenmeyer flask. The plasmid DNA was extracted and purified using the QIAGEN Plasmid Midi Kit (Qiagen, Hilden, Germany) as described previously. Small-scale transient mammalian cell transfections were performed in the presence and absence of supplemental furin to confirm improved proteolytic *in vitro* furin cleavage. Refer to Section 2.7.3 below for details. Except where stated, hereafter, 10E8_Kn denotes the construct with the improved furin cleavage sequence.

2.5.3.2 Cloning 10E8_Kn into the pmRNA expression vector.

To enable 10E8_Kn mRNA transcript production, the 10E8_Kn was sub-cloned out of the pMin vector and into the pmRNA expression vector using Gibson Assembly. This cloning method was necessary as restriction cloning using *Kpn*I and *Apa*I was incompatible since the 10E8_Kn sequence contains an additional *Apa*I restriction site in the 10E8_Kn heavy chain constant region. The 10E8_Kn insert was amplified using the primers; 10E8_Kn_linear_pmRNA_FOR and 10E8_Kn_linear_pmRNA_REV (Appendix Table A1), each with 21 bp homologous overlap with the pmRNA vector to enable assembly. The pmRNA backbone was amplified using primers; Bi-NAb_Ho_linear_FOR and pmRNA_linear_REV (Appendix Table A1). The amplicons were purified using the GeneJET PCR Purification Kit (Invitrogen, Thermo Fisher Scientific, Waltham, MA, USA) as described above. The two fragments were assembled using the NEBuilder Hifi DNA Assembly Kit (New England Biolabs, Ipswich, MA, USA) according to the manufacturer's instructions, using a total of 50 ng DNA and a vector to insert ratio of 1:2 (pmRNA: 10E8_Kn_Δfurin = 1:2) and incubated at 50°C for 15 minutes. Transformation and plating were performed as described above (section 2.3.2.1). Resulting single colonies were inoculated into 6 mL carbenicillin-containing LB media and grown overnight at 37°C. The plasmid DNA was extracted using the High Pure Plasmid Isolation Kit (Roche Group, Basel, Switzerland). Extracted plasmid DNA samples were screened by *Kpn*I and *Apa*I restriction double digest as described in section 2.3.2.1. Digests were resolved on a 1% agarose gel to confirm the insertion of the 10E8_Kn encoding region within the pmRNA vector. Confirmation of the furin sequence modification and the 5' termini were confirmed by

in-house Sanger sequencing, as described previously, using the primers; CMV_FOR, 10E8_Kn_CP_seq_FOR, and 10E8_Kn_CP_seq_REV (Appendix Table A1). A confirmed pmRNA_10E8_Kn transformed colony was expanded into 150 mL carbenicillin-containing LB media from a glycerol stock (1: 1 000) and cultured at 37°C, 200 rpm overnight. The plasmid DNA was isolated using the QIAGEN Plasmid Maxi Kit (Qiagen, Hilden, Germany) as previously described, and was used in combination with the pmRNA_Bi-NAb_Ho construct to produce the Tri-NAb by co-transfection (see section 2.7.3 below for details).

2.5.3.3 Improving endogenous furin processing of the 10E8_Kn in the Tri-NAb_sORF construct.

Modification of the furin cleavage site within the F2Aopt sequence of the 10E8_Kn in the pmRNA_Tri-NAb_sORF construct was performed by SDM using the Q5® Site-Directed Mutagenesis protocol and primer sets described previously (section 2.5.3.1) (Appendix Table A1). The resulting SDM product (8 385 bp) was resolved on a 0.8% agarose gel and extracted using the QIAquick Gel Extraction Kit (Qiagen, Hilden, Germany) as previously described. The DNA was precipitated using a sodium acetate/isopropanol protocol, the KLD reaction, and the bacterial cell transformation were performed as described above (section 2.5.3.1). Selected colonies were cultured overnight at 37°C, 200 rpm in 6 mL of carbenicillin-containing LB media, and the colony plasmid DNA was extracted using the High Pure Plasmid Isolation Kit (Roche Group, Basel, Switzerland). Extracted plasmid DNA samples were screened by restriction double digests with *Kpn*I and *Apa*I, and *Kpn*I and *Not*I, as described in section 2.5.2. Targeted in-house Sanger sequencing of a screened positive construct was performed using primers; CMV_FOR, CH3_Ho-Screen_FOR, 10E8_Kn_CP_seq_FOR, and 10E8_Kn_CP_seq_REV (Appendix Table A1). These primers were used to confirm the specific transition regions from pmRNA into the Bi-NAb-encoding sequence, inclusion of the Bi-NAb hole mutations within the CH3 region, correct assembly of the Bi-NAb_Ho-P2A cleavage peptide-10E8_Kn transition, and modification of the furin sequence within the 10E8_Kn F2Aopt region respectively. A sequence-confirmed construct with the improved furin sequence is hereafter referred to as the pmRNA_Tri-NAb_sORF. A single pmRNA_Tri-NAb_sORF construct was expanded from a glycerol stock (1: 1 000) overnight at 37°C in 150 mL of carbenicillin-containing LB media and the plasmid DNA was extracted using the QIAGEN Plasmid Maxi Kit (Qiagen, Hilden,

Germany) as previously described. Small-scale transient mammalian cell transfections were performed in the presence or absence of supplemental furin to confirm improved proteolytic *in vitro* furin cleavage. Refer to Section 2.7.3 for details.

2.6 Sub-cloning the firefly luciferase sequence into the pmRNA expression vector.

The firefly luciferase (Fluc) expression construct was included as a control to optimise mRNA-mediated expression *in vitro* with the potential to also be a control for *in vivo* mRNA-mediated expression in preclinical testing (unfortunately, this aspect was not part of this study). The Fluc sequence was sub-cloned from the psiCheck_Hbx_Fluc plasmid into the pmRNA expression vector by Gibson assembly. The Fluc sequence (1 695 bp) was amplified out of the psiCheck_Hbx_Fluc plasmid using Fluc_FOR and Fluc_REV primers (Appendix Table A1) that each incorporated 21 bp homologous overlap with pmRNA for compatible assembly. The pmRNA vector (3 638 bp) was amplified using the Bi-NAb_Ho_linear_FOR and pmRNA_linear_REV primers that linearised the vector to remove the GFP-encoding sequence to be replaced with the Fluc sequence. The amplicons were purified using the GeneJET PCR Purification Kit (Invitrogen, Thermo Fisher Scientific, Waltham, MA, USA) as described previously. The two fragments were assembled using the NEBuilder Hifi DNA Assembly Kit (New England Biolabs, Ipswich, MA, USA) according to the manufacturer's instructions, using a total of 50 ng DNA and a vector to insert ratio of 1:2 (pmRNA: Fluc = 1:2) and incubated at 50°C for 15 minutes. Transformation and plating were performed as described above (section 2.3.2.1). Resulting single colonies were inoculated into 6 mL carbenicillin-containing LB media and grown overnight at 37°C. The plasmid DNA was extracted using the High Pure Plasmid Isolation Kit (Roche Group, Basel, Switzerland). Extracted plasmid DNA samples were screened by *Kpn*I and *Apa*I restriction double digest as described in section 2.3.2.1 and resolved on a 1% agarose gel to confirm insertion of the Fluc encoding region within the pmRNA. Confirmation of the pmRNA_Fluc sequence at the 5' termini was confirmed by in-house Sanger sequencing using the CMV_FOR primer (Appendix Table A1). A confirmed pmRNA_Fluc construct was inoculated into 50 mL carbenicillin-containing LB media from a glycerol stock (1: 1 000) and cultured at 37°C, 200 rpm overnight. The plasmid DNA was isolated using the QIAGEN Plasmid Midi Kit (Qiagen, Hilden, Germany), as

described previously, and stored at -20°C. All final pmRNA plasmid maps used for DNA and mRNA expression are available in the Appendix (Figure A1).

2.7 Recombinant antibody expression and purification.

2.7.1 General 293F cell line maintenance.

The FreeStyle 293F cell line (Thermo Fisher Scientific, Waltham, MA, USA) was maintained in Corning® 50 mL or 125 mL Polycarbonate Erlenmeyer Flasks with a vent cap (Corning Inc., Corning, NY, USA) in Gibco FreeStyle™ 293 Expression Medium at a volume not exceeding 1/5 the volume of the flask. The 293F cells were incubated at 37°C in 5% CO_2 (Forma Series II, Water Jacketed CO_2 Incubator - Thermo Fisher Scientific, Waltham, MA, USA) at 130 rpm on a shaking platform (VWR Advanced Digital Shaker – VWR, Radnor, PA, USA). The 293F cells were passaged twice a week and reseeded in 1/5 the flask volume in Gibco FreeStyle™ 293 Expression Medium (Thermo Fisher Scientific, Waltham, MA, USA) at a concentration of 0.5 x 10^6 cells/mL and cultured to a maximum concentration of 4 x 10^6 cells/mL. Cell viability was assessed by trypan blue exclusion and enumeration by diluting a 15 µL cell culture sample 1:1 with trypan blue solution (0.4% trypan blue, 0.81% NaCl, 0.06% K_2HPO_4, 0.2 µm filtered – Sigma Life Science, Merck Group, Darmstadt, Germany) and a total of 15 µL was loaded onto the haemocytometer and counted using the Countess II FL (Life Technologies, Thermo Fisher Scientific, Waltham, MA, USA). The cells were maintained in a single seeding-flask which was cleaned of debris once a week using a Nunc™ Cell Scraper (Thermo Fisher Scientific, Waltham, MA, USA). The 293F cell line was discarded into Virkon at passage number 35 or when a cell viability of <70% was recorded.

Freezer stocks were made when 293F cells were at a low passage number with >90% viability. The cell culture was enumerated as described above, and the volume equivalent to 50 x 10^6 viable cells was collected into a Nunc™ 15 mL Conical Sterile Polypropylene Centrifuge tube (Thermo Fisher Scientific, Waltham, MA, USA), centrifuged at 300 x g for 5 minutes to gently pellet the cells and the media supernatant was discarded. The cell pellet was gently resuspended in 5 mL freezing mix (90% FreeStyle Expression Medium, 10% dimethyl sulfoxide (DMSO), 0.2 µm filtered) yielding a final concentration of 1 x 10^7 cells/mL. The cell suspension was divided into five 1 mL aliquots in Nunc™ 1.8 mL CryoTube™ Vials (Thermo Fisher Scientific,

Waltham, MA, USA) and placed in a CoolCell® LX freezing unit (Biocision, Larkspur, CA, USA) to control the freezing rate (-1°C/minute) when placed in the -80°C freezer. The following day, the cryovials were transferred to liquid nitrogen for long-term storage.

293F cell line freezer stocks were brought up by rapid thawing in a 37°C water bath and diluted into warm Gibco FreeStyle™ 293 Expression Medium (Thermo Fisher Scientific, Waltham, MA, USA) in a new Corning® Polycarbonate Erlenmeyer Flask with vent cap (Corning Inc., Corning, NY, USA), ensuring the DMSO was diluted to <1%. Cells were maintained and passaged as described above.

2.7.2 Antibody expression.

Parental and multispecific antibodies were expressed by transient transfection of the PGT121, VRC01, and 10E8v4 heavy and light chain plasmids or Bi-scFv, Bi-NAb, and Tri-NAb sORF or co-transfected with 10E8_Kn and Bi-NAb_Ho plasmids (Tri-NAb Co-T), respectively, in FreeStyle 293 F cells. A scalable transfection protocol reported by Raymond *et al*. (344) was used for a Greiner CELLSTAR® multiwell 12-well culture plate (Greiner Bio-One, Kremsmunster, Austria - cell culture volume of 1 mL) up to a Corning® 500 mL Polycarbonate Erlenmeyer Flasks with vent cap (Corning Inc., Corning, NY, USA - cell culture volume of 100 mL). The 293F cells were seeded 24 hours prior to transfection at 0.75 x 10^6 cells/mL at ≥80% viability, with the culture passage number not exceeding 30. Cells were transfected with a total of 1 µg of DNA per mL of cell culture, complexed with Polyethylenimine “Max” (PEIMAX - Polysciences Inc., Warrington, PA, USA) (DNA: PEI = 1:3 (w:w)) made up to 10% of the final volume of the transfection in FreeStyle™ 293 Expression Medium (i.e., 100 mL cell suspension transfected with 100 µg DNA/ 300 µg PEI in a final volume of 10 mL). DNA/PEI complexes were vortexed briefly, incubated at room temperature for 5 minutes to allow complexing before being added to the cells. For small-scale transfections performed in 6 and 12 well plates, the culture supernatant was harvested 48 hours post-transfection by centrifugation of the culture media at 2 000 x g for 5 minutes. For larger-scale production in 50-, 250- or 500-mL Erlenmeyer flasks, culture supernatants were harvested at 72 hours by centrifugation at 300 x g for 5 minutes. The culture supernatant was harvested from the cell pellet and centrifuged for an additional 10 minutes at 1 000 x g and the clarified culture supernatant was stored at

4°C. Cell pellets were reseeded to a final cell concentration of 2 x 10^6 cells/mL in fresh FreeStyle™ 293 Expression Medium and cultured for an additional 72 hours. At 144 hours, cell culture supernatants were harvested by centrifugation at 1 000 x g for 15 minutes. Combined 72- and 144-hour clarified cell culture supernatants were stored at 4°C until protein purification.

2.7.3 Assessing furin cleavage efficiency by small-scale mammalian cell transfections.

The improvement in cleavage of the pMin_10E8_Kn_Δfurin, pmRNA_10E8_Kn_Δfurin, and the pmRNA_Tri-NAb_sORF_Δfurin construct were confirmed by performing small-scale mammalian cell transfections in the presence or absence of supplemental furin. Freestyle 293F cells were seeded 24 hours prior to transfection at 0.75 x 10^6 cells/mL at ≥80% viability in Greiner CELLSTAR® multiwell 6-well culture plate (Greiner Bio-One, Kremsmunster, Austria - a total volume of 2 mL). A total of 1.5 µg of DNA per mL of cell culture was used, with an experimentally optimised ratio of antibody DNA to furin DNA of 2:1 (data not shown). Where antibody construct co-transfections were performed to produce multispecific antibody conformations (Tri-NAb Co-T, iMAb/10E8), the antibody DNAs were used at a 1:1 ratio (thus an overall ratio of antibody DNA 1: antibody DNA 2: furin DNA = 1:1:1). The DNA was complexed with PEIMAX (Polysciences Inc., Warrington, PA, USA) (DNA: PEI = 1:3 (w:w)) made up to 10% of the final volume of the transfection (0.2 mL) in FreeStyle™ 293 Expression Medium. DNA/PEI complexes were vortexed briefly, incubated at room temperature for 5 minutes to allow complexing before being added to the cells. The culture supernatant was harvested 48 hours post-transfection by centrifugation at 2 000 x g for 5 minutes and the clarified cell culture supernatant was analysed by western blot as described in Appendix A7.

2.7.4 Antibody Purification.

2.7.4.1 Protein A affinity chromatography.

PGT121, VRC01, 10E8v4, Bi-NAb, and Tri-NAb antibodies with IgG1 Fc domains were purified using Protein A affinity chromatography. Supernatants were 0.8 µm filtered (Pall Corporation, Port Washington, NY, USA) and incubated with 1 mL of packed Pierce™ Protein A Agarose (Thermo Fisher Scientific, Waltham, MA, USA) per 200 mL clarified cell culture supernatant at 4°C overnight. A magnetic stirrer was used to

maintain the Protein A agarose in suspension. Luer Lock, non-jacketed, liquid chromatography columns (internal diameter (I.D.) x L 2.5 cm x 10 cm (total volume ~50 mL - Merck Group, Darmstadt, Germany) were cleaned and primed with 50 mL of binding buffer (0.02 M Sodium phosphate, pH 7.0). The antibody-bound protein A agarose resin (1 mL) was collected by passing the culture supernatant through the column. The resin was washed with 2 x 50 resin bed volumes (100 mL) of binding buffer and eluted in 2 x 2.5 resin bed volumes of elution buffer (0.1 M glycine-HCl, pH 2.7) into a vessel containing 10% (v/v) of neutralising buffer (1 M Tris-HCl, pH 9.0). Following the elution, the resin was washed with 50 column volumes of binding buffer, re-incubated with the culture supernatant flow-through for an additional 2-4 hours before performing a second round of antibody purification. The combined eluates were 0.2 µm filtered (Pall Corporation, Port Washington, NY, USA), buffer exchanged into 1x Gibco™ phosphate buffered saline (PBS) (0.001 M KH_2PO_4, 0.150 M NaCl, 0.003 M Na_2HPO_4-$7H_2O$, pH 7.4 - Thermo Fisher Scientific, Waltham, MA, USA) and concentrated to 0.3 – 1.0 mL final volume using an Amicon Ultra 50 kDa molecular weight cut-off concentrator (Merck Group, Darmstadt, Germany) centrifuged at 3 000 x g. Purified antibodies were quantified using the Pierce™ BCA Protein Assay Kit (Thermo Fisher Scientific, Waltham, MA, USA) according to the manufacturer's instructions. Bovine serum albumin (BSA) protein assay standards were prepared from 2 mg/mL to 62.5 µg/mL, and antibody protein samples were diluted 2-6x in 1x Gibco™ PBS (Thermo Fisher Scientific, Waltham, MA, USA). BSA standards and samples (20 µL) were added to a Nunc™ 96 well PolySorb plate (Thermo Fisher Scientific, Waltham, MA, USA) and incubated with 200 µL of BCA working reagent (50:1, BCA Reagent A:B) at 37°C, 300 rpm for 30 minutes on an orbital plate shaker (THERMOstar Microplate incubator, BMG Labtech, Ortenberg, Germany). The plate was allowed to cool for 10 minutes at room temperature and the absorbance was measured at A_{570nm} on the BioRad iMark™ microplate reader (BIO-RAD Laboratories, Hercules, CA, USA). Protein concentrations of the unknown samples (correcting for the dilution factor) were interpolated from their A_{570nm} against the derived BSA standard curve generated on the Microplate Manager 6 software (MPM 6). Purified and concentrated antibodies were supplemented with glycerol to a final concentration of 25% (v/v) to improve stability, snap-frozen in liquid nitrogen, and stored at -80°C until testing.

The parental PGT121, Bi-NAb, and Tri-NAb antibodies were observed to be prone to precipitation when using the standard Protein A chromatography protocol described above, resulting in reduced yields of purified protein. Alternative chromatography buffers were explored, and the optimal combination that reduced the occurrence of visible precipitation was achieved using 2 x 50 column volumes of 1x Gibco™ PBS (Thermo Fisher Scientific, Waltham, MA, USA) wash buffer; 2 x 5 column volumes of elution buffer (0.1 M glycine, 0.15 M NaCl, 5% glycerol, pH 3.0); and 10% (v/v) neutralising buffer (1M Tris-HCl, pH 8.0). All buffers and eluate were maintained on ice to reduce the precipitation of the antibodies. The eluate was dialysed in SnakeSkin® Dialysis Tubing (Thermo Fisher Scientific, Waltham, MA, USA) against 2 L of 1x Gibco™ PBS (Thermo Fisher Scientific, Waltham, MA, USA) overnight, 0.2 µm filtered (Pall Corporation, Port Washington, NY, USA) and concentrated to a volume of 0.3 – 1 mL using Amicon Ultra 50 kDa molecular weight cut-off concentrators and quantified using the Pierce™ BCA Protein Assay Kit as described above. Purified and concentrated antibodies were supplemented with glycerol to a final concentration of 25% (v/v) to improve stability, snap-frozen in liquid nitrogen, and stored at -80°C.

2.7.4.2 Immobilised metal-ion affinity chromatography.

The Bi-scFv antibody fragment was purified using immobilised metal-ion affinity chromatography (IMAC) via it's C-terminal 6x His tag. Iminodiacetic acid cross-linked 4% beaded agarose (IDA) (Merck Group, Darmstadt, Germany) was rinsed with 3 x 20 resin bed volumes of MilliQ water and charged by incubating the resin in a resin-bed volume of 250 mM Nickle(II) sulphate hexahydrate at room temperature for 20 minutes on a rotary shaker (HulaMixer ® Sample Mixer - Life Technologies, Thermo Fisher Scientific, Waltham, MA, USA; orbital 20 rpm for 15s; reciprocal 45° for 10s; and vibro/pause 3° for 5s). The resin was collected by centrifugation at 2 000 x g for 2 minutes and the charging solution was discarded. The resin was washed with 3 x 20 resin bed volumes of MilliQ water before final resuspension to 50% aqueous charged resin slurry (IDA-Ni^{2+}) in 1x Gibco™ PBS (Thermo Fisher Scientific, Waltham, MA, USA). The supernatant was 0.8 µm filtered (Pall Corporation, Port Washington, NY, USA) and incubated with 2 mL packed IDA-Ni^{2+} charged resin per 200 mL culture supernatant at 4°C overnight using a magnetic stirrer to maintain the resin in suspension. Luer Lock, non-jacketed Liquid chromatography columns (I.D. x L 2.5 cm x 10 cm - Merck Group, Darmstadt, Germany) were cleaned and primed with 50 mL

of wash buffer (0.02 M Na_3PO_4, 0.5 M NaCl, pH 7.4). The IMAC resin was collected by passing the culture supernatant through the primed column, and the flow-through was retained for a second round of purification. The resin was washed with 2 x 20 resin-bed volumes of wash buffer followed by 2 x 20 resin-bed volumes of wash buffer containing 0.05 M imidazole and incubated in 5 resin-bed volumes of elution buffer (0.02 M Na_3PO_4, 0.5 M NaCl, 0.2 M $C_3N_2H_4$ (imidazole), pH 7.4) for 5 minutes at room temperature prior to the eluate being collected. The resin was re-equilibrated with 2 x 20 resin-bed volumes of wash buffer and re-incubated with the culture supernatant flow-through for an additional 2-4 hrs before the second round of protein purification. The combined eluate was 0.2 µm filtered (Pall Corporation, Port Washington, NY, USA), buffer exchanged into 1x Gibco™ PBS (Thermo Fisher Scientific, Waltham, MA, USA), and concentrated to a final volume of 1 mL at 3 000 x g using an Amicon Ultra 10 kDa molecular weight cut-off concentrator and quantified using the Pierce™ BCA Protein Assay Kit as described in section 2.7.4.1. Purified and concentrated Bi-scFv antibody was supplemented with glycerol to a final concentration of 25% (v/v), snap-frozen in liquid nitrogen, and stored at -80°C.

2.7.4.3 Size exclusion chromatography.

Conformational heterogeneity and isolation of monomeric isoforms of the affinity-purified antibodies were performed using size exclusion chromatography (SEC) on a HiLoad 16/600 Superdex 200pg column (Cytiva, Marlborough, MA, USA) using the AKTA fast protein liquid chromatography (FPLC) UPC-900 system (Amersham Biosciences, GE Healthcare - Cytiva, Marlborough, MA, USA) with UNICORN 5.20 software. The HiLoad 16/600 Superdex 200pg column void volume was determined based on the elution volume for Blue Dextran 2000, prepared as per the manufacturer's instructions. Chromatographic separation and a calibration curve for the HiLoad 16/600 Superdex 200pg column were generated using a mixture of low and high molecular weight (MW) standard proteins (aprotinin (6 500 Da), ribonuclease A (13 700 Da), carbonic anhydrase (29 000 Da), ovalbumin (44 000 Da), conalbumin (75 000 DA), aldolase (158 000 Da), ferritin (440 000 Da)) as per the manufacturer's recommendations (Cytiva, Marlborough, MA, USA). The Blue Dextran and protein standards were resolved at a flow rate of 1 mL/min on the pre-equilibrated HiLoad 16/600 Superdex 200pg column in 1x Gibco™ PBS (Thermo Fisher Scientific, Waltham, MA, USA).

Purified antibodies at concentrations ranging from 2-5 mg/mL were injected onto a 1x Gibco™ PBS (Thermo Fisher Scientific, Waltham, MA, USA) pre-equilibrated HiLoad 16/600 Superdex 200pg column and resolved at a flow rate of 1 mL/min in 1x Gibco™ PBS (Thermo Fisher Scientific, Waltham, MA, USA). The eluted fractions containing monomeric antibody conformations were 0.2 µm filtered (Pall Corporation, Port Washington, NY, USA) and concentrated to 1 mL using Amicon Ultra 50 kDa or 10 kDa molecular weight cut-off concentrators, as above, at 3 000 x g, and quantified using the Pierce™ BCA Protein Assay Kit as described in section 2.7.4.1. Pure monomeric antibodies were supplemented with glycerol to a final concentration of 25% (v/v), snap-frozen, and stored at -80°C. Purity was analysed by sodium dodecyl sulphate-polyacrylamide gel electrophoresis (SDS-PAGE) on NuPAGE™ 4-12% Bis-Tris gels (Invitrogen, Thermo Fisher Scientific, Waltham, MA, USA) under reducing (+dithiothreitol (DTT)) and non-reducing (-DTT) conditions (described in Appendix A6).

2.7.5 Computation of the multispecific antibody molecular weight and predicted N-linked glycosylation.

2.7.5.1 Calculating antibody molecular weight from native SEC profiles.

From the SEC profiles, the retention volume of the antibodies was compared to that of the MW standard proteins with known sizes to determine the relative molecular weight of the native monomeric antibody conformations. The MW standard calibration curve (as described by Cytiva, Marlborough, MA, USA) was generated from the calculated Kav values for each protein standard using the equation:

$$\boldsymbol{Kav} = \frac{(\boldsymbol{Ve} - \boldsymbol{Vo})}{(\boldsymbol{Vc} - \boldsymbol{Vo})}$$

where Vo= column void volume, Ve= elution volume, and Vc= geometric column volume.

The calibration curve of Kav versus log (molecular weight (Da)) was generated on Microsoft excel (Microsoft Corporation, Redmond, WA, USA). The corresponding Kav values for each antibody were calculated and substituted into the calibration curve equation to calculate the antibody's molecular weight.

2.7.5.2 Antibody molecular weight determination under reducing conditions.

Purified parental and multispecific antibodies were resolved under reducing conditions (+DTT) on NuPAGE™ 4-12% Bis-Tris gels (Invitrogen, Thermo Fisher Scientific, Waltham, MA, USA), as described previously. The relative migration distance (Rf) of the resolved polypeptides and the molecular weight marker bands were calculated using the equation:

$$\boldsymbol{Rf = \frac{migration\ distance\ of\ the\ protein\ (mm)}{migration\ distance\ of\ the\ dye\ front\ (mm)}}$$

The molecular weight marker standards were plotted as log (molecular weight (kDa)) versus Rf value using Microsoft excel (Microsoft Corporation, Redmond, WA, USA) to generate the standard curve. The corresponding Rf values for each antibody polypeptide were calculated and substituted into the standard curve equation to calculate the molecular weight of the respective antibody polypeptides.

2.7.5.3 Predicted antibody molecular weight and N-linked glycosylation sites.

The predicted molecular weights of the parental and multispecific antibody polypeptides were computed from their respective amino acid sequences (excluding the secretion signal peptide sequence) using the online "Protein Molecular Weight" tool (https://www.bioinformatics.org/sms/prot_mw.html).

The predicted N-linked glycosylation sites, based on the antibody amino acid sequences, were determined using the "NetNGlyc – 1.0, N-linked glycosylation sites in human proteins" online tool (345). This server predicts N-glycosylation sites in human proteins by examining Asn-Xaa-Ser/Thr sequences. The presence of these sequences is predicted as potential sites for N-linked glycosylation but may not necessarily be glycosylated *in vitro*.

2.8 *In vitro* transcription (IVT) of mRNA encoding multispecific antibody constructs.

2.8.1 IVT mRNA transcript production.

IVT mRNA expression cassettes were generated from the pmRNA DNA plasmids described above. Homogenous mRNA transcripts of defined length were produced from the T7 promoter sequence positioned at the 5' terminus of the coding sequence

and had a 46-nucleotide poly-A sequence incorporated on the 3' terminus following DNA template linearisation. The DNA constructs encoding the multispecific antibodies (bispecific: Bi-scFv and Bi-NAb; trispecific: Tri-NAb sORF and 10E8_Kn/Bi-NAb_Ho combination for the co-transfection production of the Tri-NAb) or the GFP and Fluc controls for mRNA-mediated expression were linearised at the single *Bpi*I restriction site located downstream of the poly-A sequence. Overnight digests (16 hours) of 20 µg of pmRNA DNA plasmid with 0.6 µL (6 units) *Bpi*I prepared in Buffer G (with BSA) (Thermo Fisher Scientific, Waltham, MA, USA) to a final volume of 50 µL were performed at 37°C. A 100 ng sample of the linearised DNA was resolved on a 0.8% agarose gel, prepared and resolved as described in Appendix A4, and the remaining linear DNA was purified using the GeneJET PCR Purification Kit (Thermo Fisher Scientific, Waltham, MA, USA) as described previously. mRNA transcripts were produced using the TranscriptAid T7 High Yield Transcription Kit according to the manufacturer's instructions (Thermo Fisher Scientific, Waltham, MA, USA). The components were combined at room temperature in the specified order: diethylpyrocarbornate (DEPC)-treated water (up to 20 µL), 4 µL of 5x TranscriptAid Reaction Buffer, 8 µL of an equal mix of ATP/CTP/GTP/UTP (each 100 mM), 1 µg of template DNA, and 2 µL of TranscriptAid Enzyme Mix. The reaction was mixed, spun briefly to collect the droplets, and incubated at 37°C for 2 hours. Samples of the IVT-mRNA transcripts were diluted 20-40-fold in DEPC-treated water, 3 µL was prepared in 2x RNA Loading Solution (Thermo Fisher Scientific, Waltham, MA, USA), heated at 70°C for 10 minutes to denature the RNA secondary structure, chilled on ice for 3 minutes, and resolved on a 1% agarose gel with ethidium bromide along with RiboRuler™ RNA Ladder (Thermo Fisher Scientific, Waltham, MA, USA) that had been denatured in parallel with the samples (Appendix A4).

2.8.2 IVT mRNA transcript purification.

IVT mRNA transcripts were purified using a standard lithium chloride (LiCl) precipitation protocol (Thermo Fisher Scientific, Waltham, MA, USA), by adding 0.5 volume of chilled 7.5 M LiCl (LiCl final concentration of 2.5 M) to the mRNA transcript solution, precipitated at -20°C for 1 hour, and centrifuged at 16 000 x g for 15 minutes at 4°C. The RNA pellet was washed in 0.2 mL chilled 70% ethanol, centrifuged at 16 000 x g for 15 minutes at 4°C, and resuspended in 100 µL nuclease-free water. dsRNA contaminants were removed from IVT mRNA transcripts using Pierce™ Spin

Cups with a Cellulose Acetate Filter (Thermo Fisher Scientific, Waltham, MA, USA) and cellulose fibres (Cat. C6288, Sigma Aldridge - Merck Group, Darmstadt, Germany) to bind the dsRNA as previously described, which has been shown to result in increased translation and eliminate immunoreactivity *in vivo* (286). Briefly, the cellulose was pre-washed in a chromatography buffer (0.01 M 4-(2-hydroxyethyl)-1-piperazineethanesulfonic acid (HEPES) (pH 7.2), 0.1 mM ethylenediamine tetraacetic acid (EDTA), 0.125 M NaCl, and 16% (v/v) ethanol) to make a 0.2 g cellulose/mL slurry. After mixing the cellulose slurry at room temperature for 10 minutes, 0.14 g cellulose slurry was transferred to a spin cup, centrifuged for 60 seconds at 14 000 x g and the flow-through was discarded. The cellulose was resuspended in the spin cup in 0.5 mL fresh chromatography buffer, mixed for 5 minutes, centrifuged for 60 seconds at 14 000 x g and the flow-through was discarded. IVT mRNA (100 to 500 µg) diluted in chromatography buffer (final volume of 0.5 mL) was added to the spin cup containing pre-washed cellulose and incubated with vigorous shaking on the HulaMixer ® Sample Mixer (Life Technologies, Thermo Fisher Scientific, Waltham, MA, USA) (orbital 20 rpm for 15s; reciprocal 45° for 10s; and vibro/pause 3° for 5s) at room temperature for 30 minutes to maximise dsRNA contact with the cellulose. The spin cup was centrifuged for 60 seconds at 14 000 x g to harvest the unbound ssRNA contained within the flow-through from the contaminating dsRNA bound to the cellulose. The cellulose was discarded from the spin cup and replaced with fresh pre-washed cellulose, and collected single-stranded IVT mRNA flow through was transferred back into the upper chamber of the spin cup, and the purification procedure was repeated. The purified ssRNA was recovered from the filtrate using the lithium chloride precipitation procedure described above and the RNA pellet was resuspended in 50 µL nuclease-free water. The purified RNA was quantified by ultraviolet (UV) absorption at A_{260nm} on the NanoDrop® Spectrophotometer ND-1000, software version 3.8.1 (Thermo Fisher Scientific, Waltham, MA, USA) which was initiated with and blanked against nuclease-free water, diluted to 2 µg/µL and aliquots were stored at -80°C prior to capping. Samples of the purified IVT-mRNA transcripts were diluted in DEPC-treated water to 100 ng/µl, 10 µl was prepared in 2x RNA Loading Solution (Thermo Fisher Scientific, Waltham, MA, USA) and heated at 70°C for 10 minutes to denature the RNA secondary structure. Samples were chilled on ice for 3 minutes prior to resolving 500 ng on a 1% agarose with ethidium bromide for visualisation, as described in Appendix

A4. RiboRuler™ RNA Ladder (Thermo Fisher Scientific, Waltham, MA, USA) was prepared and denatured in parallel and resolved with the samples for size estimation.

2.8.3 Capping purified IVT mRNA.

The single-stranded, purified IVT mRNA transcripts were enzymatically capped in a single reaction using the Vaccinia Capping System (New England Biolabs, Ipswich, MA, USA) and methylated using the mRNA Cap 2'-O-methyltransferase (New England Biolabs, Ipswich, MA, USA) resulting in a 5' Cap1 structure, according to the manufacturer's instructions but scaled up two-fold. A 2 µg/µL aliquot of purified RNA was thawed on ice, 10 µL (20 µg total RNA) was diluted in nuclease-free water to a final volume of 28 µL, heated at 65°C for 5 minutes and placed on ice for 5 minutes. The denatured uncapped RNA was added to the one-step capping and methylation reaction, comprising of the following reagents added in the specified order: 4 µL of 10x Capping Buffer, 2 µL of GTP (10 mM), 2 µL of S-adenosylmethionine (SAM - 4 mM diluted in DEPC-treated water from 32 mM stock), 2 µL of Vaccinia Capping Enzyme, and 2 µL of mRNA Cap 2'-O-methyltransferase to a final volume of 40 µL. The reaction was incubated at 37°C for 1 hour. Capped IVT mRNA transcripts were recovered using the lithium chloride precipitation protocol as described above (section 2.8.2), the capped RNA pellet was resuspended in 20 µL nuclease-free water, quantified by UV absorption at A_{260nm} on the NanoDrop® Spectrophotometer ND-1000, software version 3.8.1 (Thermo Fisher Scientific, Waltham, MA, USA) and stored at -80°C at a concentration of 0.5 µg/µL until transfections.

2.8.4 Antibody expression from IVT mRNA.

Multispecific antibodies were expressed in FreeStyle 293F cells by transient transfection with purified, capped IVT mRNA encoding the GFP or Fluc controls, Bi-scFv, Bi-NAb, Tri-NAb sORF, and Bi-NAb_Ho with 10E8_Kn (Tri-NAb Co-T). Cells were seeded into Greiner CELLSTAR® multiwell 6-well culture plate (Greiner Bio-One, Kremsmunster, Austria - cell culture volume of 2 mL) 24 hours prior to transfection at 0.75 x 10^6 cells/mL at ≥80% viability, with the culture passage number not exceeding 30. Cells were transfected with 1 µg of mRNA per mL of cell culture, complexed with Lipofectamine™ MessengerMAX™ Transfection Reagent (Thermo Fisher Scientific, Waltham, MA, USA) according to the manufacturer's instructions (mRNA: Lipofectamine MessengerMAX = 1:3). Transfection complexes were made up to 10%

of the final volume of the transfection reaction in FreeStyle™ Expression Medium (i.e., 2 mL cell suspension transfected with 2 µg mRNA/ 6 µg Lipofectamine MessengerMAX in a final volume of 200 µL). The transfection complexes were made in a two-step process. A Lipofectamine MessengerMAX/FreeStyle Expression Medium mix (6 µL in 94 µL) was incubated at room temperature for 10 minutes before being combined with the mRNA that had been diluted in FreeStyle Expression Medium (4 µL (2 µg) in 96 µL). Combined mRNA/Lipofectamine MessengerMAX complexes were vortexed briefly and incubated at room temperature for 5 minutes before being added to the cells. The cell culture supernatant was harvested 72 hours post-transfection by centrifugation at 2 000 x g for 5 minutes. Clarified cell culture supernatant was 0.45 µm filtered (Pall Corporation, Port Washington, NY, USA), aliquoted, and stored at 4°C short term or snap frozen in liquid nitrogen and stored at -80°C long term prior to quantification and performing *in vitro* neutralisation assays.

The clarified cell culture supernatant was analysed for expressed and secreted multispecific antibodies by SDS-PAGE followed by western blot, developed using α-Penta-His-HRP (1: 2 000) for detection of the His-tagged Bi-scFv and α-Human-IgG-horse-radish peroxidase (HRP) (1: 3 000) for detection of the Bi-NAb and Tri-NAb (as described in Appendix A7). As the GFP and Fluc controls for mRNA-transfection are not secreted into the supernatant (lack a secretion signal peptide), the cell lysates were evaluated for expressed protein. The harvested cell culture pellets were resuspended in 0.5 mL of Glo Lysis buffer (Promega Corporation, Madison, WI, USA) and incubated for 5 minutes at room temperature to lyse the 293F cells. Lysate was centrifuged at 2 000 x g for 5 minutes to pellet the cell debris and 50 µL of lysate, in triplicate per transfection culture, were transferred to a white 96-well plate. Fluorescence was measured using the Promega Glomax Explorer luminometer (Promega Corporation, Madison, WI, USA) at an excitation wavelength of 488 nm and an emission wavelength of 507 nm. Subsequently, equal volumes (50 µL per well) of Bright Glo Luciferase reagent (Promega Corporation, Madison, WI, USA) was added to the 96-well white plate to determine luminescence from luciferase expression and quantified using the Promega Glomax Explorer luminometer (Promega Corporation, Madison, WI, USA). The measured florescence and relative luminescence units (RLU) for each transfection lysate were plotted using GraphPad Prism 8.

2.9 Antibody HIV-1 pseudovirus *in vitro* neutralisation.

2.9.1 Maintenance of the HEK293 and TZM-bl cell lines.

The HEK293T (available in the HPRU) and TZM-bl cell lines were maintained at 37°C in 5% CO_2 (Forma Series II, Water Jacketed CO_2 Incubator - Thermo Fisher Scientific, Waltham, MA, USA) in Nunc™ EasYFlask™ 75 cm^2 Cell Culture Flasks with filter cap (Thermo Fisher Scientific, Waltham, MA, USA) in 13 mL of Dulbecco's Modified Eagle's Medium (DMEM) (4.5 g/L Glucose, L-glutamine, sodium pyruvate, 3.7 g/L $NaHCO_3$ - PAN Biotech, Aidenbach, Germany) supplemented with 10% Foetal Bovine Serum (FBS - Gibco, Thermo Fisher Scientific, Waltham, MA, USA). The TZM-bl cell's DMEM media also contained 100 U/mL penicillin/ 100 µg/mL streptomycin (PAN Biotech, Aidenbach, Germany). These cell lines were passaged when they were approximately 90% confluent (HEK293T cells - every two or three days, TZM-bl cells – every three to four days). The media was discarded into 1 % Virkon solution (Agluco Pharmaceuticals Pty Ltd, Pretoria, South Africa), and the cells were washed with 4 mL of 1x DPBS (without (w/o) Ca and Mg - PAN Biotech, Aidenbach, Germany) and discarded. To detach the cells from the flask, they were incubated with 1 mL of TrypLE Express Enzyme (1x) (Gibco, Thermo Fisher Scientific, Waltham, MA, USA) at room temperature for 15 or 45 seconds (HEK293T and TZM-bl cells, respectively), the TryPLE Express was discarded and the cells were incubated for an additional 4 minutes at 37°C. The cells were resuspended in 5 mL of complete DMEM and 500 µL (cells were passaged 1/10) was diluted in 13 mL of fresh complete DMEM. Remaining cells were discarded. Culture flasks were discarded after 10 to 20 passages in the same flask. Freezer stocks were made at lower passage numbers when the cells were ~90% confluent by gently pelleting the trypsinised, resuspended cells by centrifugation at 300 x g for 5 minutes. The media supernatant was discarded, and the cell pellet was gently resuspended in 5 mL freezing mix (90% FBS, 10% DMSO, 0.2 µm filtered) and split into 1 mL aliquots in Nunc™ 1.8 mL CryoTube™ Vials (Thermo Fisher Scientific, Waltham, MA, USA) and slowly frozen at -1°C/minute in a CoolCell® LX (Biocision, Larkspur, CA, USA) overnight to -80°C before being moved to liquid nitrogen storage. Cell line freezer stocks were thawed rapidly at 37°C and diluted in 15 mL complete, warm DMEM in a new Nunc™ EasYFlask™ 75 cm^2 Cell Culture Flasks with filter cap (Thermo Fisher Scientific, Waltham, MA, USA). Cell lines were maintained and passaged as described above.

2.9.2 HIV-1 pseudovirus production.

Antibody mediated neutralisation breadth and potency was assessed against a panel of 17, clinically relevant tier 2 HIV-1 pseudoviruses using a single-round HIV-1 pseudovirus infectivity assay in the TZM-bl reporter cell line as described previously (346). The 17 HIV-1 pseudovirus panel comprised the Panel of Global HIV-1 Env Clones (328) supplemented with viruses with the desired resistance profiles. The CATNAP tool under the neutralisation database of the Los Alamos National Laboratory HIV Database (347) was used to determine the resistance profiles of the selected viruses in our panel. These include the PGT121/VRC01 dual sensitive viruses (25710, 398F1, CE0217, CE1176, CH119, TRO11, and X2278); PGT121 resistant viruses (246F3, CNE8, CNE55, and X1632); VRC01 resistant viruses (BJOX002000, Du172.17, and Du422.1); and PGT121/VRC01 dual resistant viruses (CAP210.2.00.E8, QH343.21M.ENV.A10, and Ce2103_E8). HEK293T cells were seeded into Nunc™ EasYFlask™ 25 cm^2 Cell Culture Flasks with filter cap (Thermo Fisher Scientific, Waltham, MA, USA) at 0.25 x 10^6 cells/mL in total 5 mL volume of complete DMEM and transfected when approximately 70% confluent (roughly 24 hours post seeding). Single-round HIV-1 Env pseudotyped viruses were produced by co-transfection of HEK293T cells with a 1:2 ratio with HIV-1 *rev/env* expression plasmids and the *env*-deficient HIV-1 backbone plasmid ($pSG3^{\Delta env}$). A total of 10 µg of DNA (Env: backbone = 1:2) was combined with FuGene HD transfection reagent (Promega Corporation, Madison, WI, USA) at a ratio of DNA:FuGene of 1:3 (30 µL), made up to 10% of the final volume of the transfection (500 µL) in FreeStyle™ Expression Medium (Thermo Fisher Scientific, Waltham, MA, USA), incubated at room temperature for 5 minutes and carefully added to the culture media without disturbing the adhered cells. The media was discarded and replaced with 7 mL of warm, complete DMEM approximately 10-12 hours post-transfection. Pseudovirus-containing culture supernatants were harvested at 48 hours post-transfection, filtered through 0.45 µm filter (Pall Corporation, Port Washington, NY, USA), supplemented to a final concentration of 20% FBS (Gibco, Thermo Fisher Scientific, Waltham, MA, USA), aliquoted into 2 mL screw-cap vials and stored at -80°C. The cell culture was incubated for a further 24 hours in 5 mL of fresh complete DMEM and a second pseudovirus harvest was collected as described above.

2.9.2.1 Determining the HIV-1 pseudovirus titres.

Tissue culture infectious dose to achieve 50% infection (TCID50) of each virus was determined in the TZM-bl cell line as previously described (348). Briefly, serial 5-fold dilutions of pseudovirus, for a total of 11 dilution points, were made in duplicate wells in Nunc™ Edge™ 96-well microplates (Thermo Fisher Scientific, Waltham, MA, USA) in DMEM growth medium to a final volume of 100 µL. Freshly trypsinised TZM-bl cells (1×10^4 cells per well) in DMEM supplemented with diethylaminoethyl (DEAE)-Dextran (to increase the transduction efficiency) to a final concentration of 20 µg/mL were added to each well (100 µL per well). The four outer chambers of the edge of the plate were filled with 2.5 mL of 1x PBS each to reduced evaporation affects, and the plates were incubated at 37°C in 5% CO_2 (Forma Series II, Water Jacketed CO_2 Incubator - Thermo Fisher Scientific, Waltham, MA, USA) for 48 hours. Following the incubation, the media was aspirated from the wells and 80 µL of Glo Lysis buffer (Promega Corporation, Madison, WI, USA) was added to each well and incubated for 5 minutes at room temperature to lyse the TZM-bl cells. Fifty microliters of the cell lysate were transferred to a white 96-well plate and an equal volume of Bright Glo Luciferase reagent (Promega Corporation, Madison, WI, USA) was added to determine luciferase expression and quantified using the Promega Glomax Explorer luminometer (Promega Corporation, Madison, WI, USA). Wells were scored positive where RLU units were 2.5x greater than the background cell-only control wells. The TCID50 was determined using the TCID50 Macro, available on the Los Alamos National Laboratory HIV Database, Standardised Assessments of Neutralising Antibodies for HIV/AIDS Vaccine Development (https://www.hiv.lanl.gov/content/nab-reference-strains/html/home.htm) as previously described (348).

2.9.3 HIV-1 *in vitro* neutralisation assay.

Neutralisation assays were performed by preparing a serial dilution of purified parental (PGT121, VRC01, and 10E8v4) and multispecific antibodies (Bi-scFv, Bi-NAb, Tri-NAb sORF and Tri-NAb Co-T), as well as mRNA-transfected clarified cell culture supernatant including GFP and Fluc controls and multispecific antibodies (Bi-scFv, Bi-NAb, Tri-NAb sORF, and Tri-NAb Co-T). All the purified antibodies, clarified cell culture supernatant, pseudoviruses, and TZM-bl cells were prepared or diluted in complete DMEM containing 100 U/mL penicillin/ 100 µg/mL streptomycin (PAN Biotech,

Aidenbach, Germany). Serial dilutions of purified antibodies were prepared in Nunc™ Edge™ 96-well microplates (Thermo Fisher Scientific, Waltham, MA, USA), starting at a maximum concentration of 25 µg/mL with an eight-point 3-fold dilution series in DMEM. A serial dilution of mRNA-expressed clarified cell culture supernatant was performed, starting at a maximum 10-fold dilution, followed by an eight-point 4-fold dilution series in a Nunc™ Edge™ 96-well microplate (Thermo Fisher Scientific, Waltham, MA, USA). Each antibody or mRNA-transfected cell culture supernatant was performed in duplicate wells per each dilution point. Two hundred TCID50s of pseudovirus prepared in complete DMEM were added to each well of the plate, before filling the four outer chambers of the edge of the plate with 2.5 mL of 1x PBS each and incubating at 37°C in 5% CO_2 for 1 hour. Following the incubation, freshly trypsinised TZM-bl cells were added at 1 x 10^4 cells/well. The TZM-bl cells were prepared in complete DMEM, and to enhance the pseudovirus infectivity in the TZM-bl cells, each well was supplemented with DEAE Dextran to a final assay concentration of 20 µg/mL with a final well volume of 250 µL. Cell-only and virus-only wells were included as appropriate controls, and the plate was incubated for 48 hours at 37°C in 5% CO_2. Luciferase expression was determined 48 hours later, as described above (Section 2.9.2.1) using the Glo Lysis buffer and Bright Glo Luciferase reagent (Promega Corporation, Madison, WI, USA) and quantified using the Promega Glomax Explorer luminometer (Promega Corporation, Madison, WI, USA).

2.9.3.1 Determining the percentage viral inhibition.

Percent viral inhibition, as a reduction in the RLU values achieved by the antibody-containing wells (test wells) corrected for background RLU (less average cell control wells) relative to the background corrected (less average cells control wells) average virus only containing control wells (average virus control wells) was determined using the following equation.

$$\%\ \boldsymbol{Inhibition} = \mathbf{100} - \left(\frac{(\boldsymbol{test\ wells} - \boldsymbol{average\ cell\ control\ wells})}{(\boldsymbol{average\ virus\ control\ wells} - \boldsymbol{average\ cell\ control\ wells})} \times \mathbf{100}\right)$$

Inhibitory concentration (IC) IC50 and IC80 values for the purified antibodies, and inhibitory dilution (ID) ID50 and ID80 values for the mRNA expressed antibodies within the unpurified cell culture medium, were calculated by fitting a non-linear variable slope curve to the duplicate data using the non-linear regression function (log(agonist)

vs response – Find ECanything) in GraphPad Prism 8. IC values represent the antibody concentration (µg/mL) required to reach 50% and 80% pseudovirus inhibition respectively. ID values represent the reciprocal of the serum dilution required to achieve 50% and 80% inhibition respectively. IC/ID50 data were used to estimate the concentration (µg/mL) of mRNA-expressed Bi-scFv, Bi-NAb, and Tri-NAb antibodies within the cell culture supernatant (see section 2.10.3). For the following specified virus/antibody combination (purified antibody assays: 398F1 – 10E8v4 and Tri-NAbs; CNE8 – Bi-scFv; Du172.17 – PGT121, Bi-scFv, and Bi-NAb; CAP210.2.00.E8 – Bi-scFv, Bi-NAb, and Tri-NAbs; and QH343.21M.ENV.A10 – VRC01, Bi-scFv, and Bi-NAb and mRNA-expressed cell culture supernatant assays: CNE55 and CAP210.2.00.E8 – Bi-scFv, Bi-NAb, and Tri-NAbs) the non-linear regression function in GraphPad Prism 8 did not have the favourable sigmoidal curve that reaches a maximum at ~100% and a minimum at ~0% inhibition. As a result, the interpolated IC/ID50 and IC/ID80 values were either under or over-estimated. To correct for this, these calculations were performed using Microsoft excel (Microsoft Corporation, Redmond, WA, USA). For each virus/antibody, the average percentage inhibition vs log(concentration) or average percentage inhibition vs log(dilution factor) were plotted. Three or four data points falling within the linear portion of the curve were used to generate the graph equation which was used to calculate the IC50/80 and ID50/80 values by substituting the y value and solving for x.

2.9.3.2 Correcting for the antibody molarity difference.

The parental antibodies (PGT121, VRC01, and 10E8v4) and the multispecific antibodies (Bi-scFv, Bi-NAb, and Tri-NAb) were observed to have different molecular sizes, thus this molarity difference would affect the number of antibody molecules present per µg of purified, diluted antibody. Antibody molar concentrations were calculated based on the relative molecular weights as determined from their SEC profiles (Section 2.7.5.1) The IC50 and IC80 antibody concentrations were corrected to molarity (nM) prior to statistical analysis.

2.10 Quantification of IVT-mRNA-expressed antibodies.

2.10.1 ELISA.

The gp120$_{FVC}$M construct encoding the inferred Founder virus consensus C sequence (FVC) was previously described and available in our laboratory (318,349). HIV-1 monomeric gp120$_{FVC}$ monomer Env was recombinantly expressed by transient transfection of 293F cells using 1 µg/mL DNA complexed with PEI, cultured, and harvested as described in section 2.7.3. Harvested culture supernatant containing the expressed Env glycoprotein was purified using an optimised *Galanthus (G.) nivalis* lectin-affinity chromatography procedure and SEC as previously described (318). Briefly, 200 mL culture supernatant was incubated with 2 mL of *G. nivalis* lectin cross-linked to 4% beaded agarose (Merck Group, Darmstadt, Germany) on a magnetic stirrer overnight. The resin was collected in Luer Lock, non-jacketed Liquid chromatography columns (I.D. x L 2.5 cm x 10 cm - Merck Group, Darmstadt, Germany). The collected resin was washed with 50 resin-bed volumes (100 mL) of 0.65 M NaCl in 1x DPBS (Thermo Fisher Scientific, Waltham, MA, USA), 25 resin-bed volumes (50 mL) of 1.0 M NaCl in DPBS, and a final 25 resin-bed volumes (50 mL) DPBS wash. Bound Env glycoprotein was eluted from the resin with 2 x 10 mL of DPBS containing 1.0 M methyl α-D mannopyranoside (MMP) (Merck Group, Darmstadt, Germany), 0.45 µm filter-sterilised (Pall Corporation, Port Washington, NY, USA) and concentrated to a final volume of ~1 mL at 3 000 x g using an Amicon Ultra 50 kDa molecular weight cut-off concentrator. Purified and concentrated Env was quantified using the Pierce™ BCA Protein Assay Kit as described in section 2.7.4.1, prior to snap-freezing in liquid nitrogen and storage at -80°C. The purity of the gp120$_{FVC}$M protein was confirmed by SDS-PAGE (as described previously). Subsequently, the purified gp120$_{FVC}$M was further purified using size exclusion chromatography, at a flow rate of 1 mL/min on a HiLoad 16/600 Superdex 200pg column (Cytiva, Marlborough, MA, USA) using the AKTA FPLC UPC-900 system (Amersham Biosciences, GE Healthcare - Cytiva, Marlborough, MA, USA) with UNICORN 5.20 software (as described in section 2.7.4.3). The collected monomeric fractions were concentrated to a final volume of ~0.5 mL at 3 000 x g using an Amicon Ultra 50 kDa molecular weight cut-off concentrator and quantified using the Pierce™ BCA Protein Assay Kit as described in section 2.7.4.1. Purified and concentrated Env was aliquoted, snap-frozen in liquid nitrogen, and stored at -80°C.

Antibody titres of the mRNA expressed Bi-scFv, Bi-NAb, and Tri-NAbs (expressed from co-transfection and sORF) were quantified using an in-house HIV-1 Env $gp120_{FVC}$M specific binding enzyme-linked immunosorbent assay (ELISA). Unless stated otherwise, a working reaction volume in the ELISA assay of 100 µL was used. All washes were performed using the Biotek ELx50 automated microplate washer (BioTek Instruments, Inc., Winooski, VT, USA). Briefly, HIV-1 Env $gp120_{FVC}$ monomer was prepared at 1 µg/mL in 1x Gibco™ PBS (Thermo Fisher Scientific, Waltham, MA, USA) and immobilised at 100 ng per well on a Nunc™ 96 well MaxiSorb plate (Thermo Fisher Scientific, Waltham, MA, USA) overnight at 4°C. The binding buffer solution was aspirated using the (BioTek Instruments, Inc., Winooski, VT, USA), and the wells were blocked with 250 µL of 1% BSA, PBS-T (0.05% Tween 20 prepared in phosphate buffered saline) buffer solution for 1 hour at room temperature. The wells were washed 3 x 300 µl with PBS-T. A 3-fold serial dilution ranging from 10 – 0.004 µg/mL of recombinantly expressed and purified Bi-scFv, Bi-NAb, or Tri-NAb multispecific antibodies were prepared in PBS-T, was added to the gp120 coated wells and allowed to bind for 1 hour at room temperature. In parallel, clarified cell culture supernatant from mRNA transfected 293F cells was diluted 50 and 100 times in PBS-T and 100 µL of the respective dilutions were added to the respective gp120 coated wells and incubated at room temperature for 1 hour. Unbound antibody was removed by washing each well 5 x 300 µl PBS-T. Bound Bi-scFv was detected using 100 µL/well of His-probe HRP conjugate (4 µg/mL - Thermo Fisher Scientific, Waltham, MA, USA), the Bi-NAb or Tri-NAb bound antibodies were detected using 100 µL/well of an anti-Human-IgG (Fc specific)-HRP produced in goat (1: 2 000 - Cat. A0170, Merck Group, Darmstadt, Germany) both prepared in PBS-T, for one hour at room temperature. Each well was washed with 5 x 300 µl PBS-T. Bound primary antibody-secondary HRP-conjugate antibody complexes were detected using 100 µL of chromogenic substrate (1-Step Turbo 3, 3', 5, 5' – tetramethylbenzidine (TMB)-ELISA Substrate Solution - Thermo Fisher Scientific, Waltham, MA, USA) incubated in the dark at room temperature for approximately 10-15 minutes and neutralised with 50 µL 0.5 M H_2SO_4. Absorbance readings were measured at 450 nm on the BioRad iMark™ microplate reader (BIO-RAD Laboratories, Hercules, CA, USA). The Microplate Manager 6 software (MPM 6) was used to generate a standard curve of the prepared serial dilution of Bi-scFv, Bi-NAb, or Tri-NAb. The mRNA-expressed antibody concentrations present in the clarified culture supernatant were determined by interpolating the obtained A_{450nm}

values against the generated standard curve and correcting for the dilution factor. Standards and samples were assayed in triplicate, with the assay being capable of accurately quantifying 0.1 µg/mL of the expressed antibodies (Bi-scFv, Bi-NAb/Tri-NAb) based on the generated standard curve. For visualisation of the standard curves the sigmoidal 4PL equation on GraphPad prism 8 was used on the triplicate 450 nm absorbance readings of each multispecific antibody standards to generate the respective standard curves.

2.10.2 Western blot densitometry.

Antibody titres of the mRNA expressed Bi-scFv, Bi-NAb, and Tri-NAbs (expressed from Co-T and sORF) were also quantified using densitometry analysis of a western blot. Multispecific antibody standards were prepared by performing a 2-fold dilution series of recombinantly expressed and purified antibody, such that a final amount of antibody loaded ranged from 1 – 0.007 µg (Bi-NAb), 1 – 0.062 µg (Tri-NAb), and 3 – 0.187 µg (Bi-scFv). In parallel, clarified cell culture supernatant from mRNA transfected 293F cells were assayed neat (undiluted) and as 2- or 4-fold dilutions prepared in water. The antibody standards and clarified cell culture supernatant were prepared in reducing (+DTT) NuPAGE™ LDS sample buffer, resolved on NuPAGE™ 4-12% Bis-Tris Gels (Invitrogen, Thermo Fisher Scientific, Waltham, MA, USA) and transferred onto HybondTM-C Extra nitrocellulose membranes (Amersham Biosciences, GE Healthcare, Amersham, UK) as described in Appendix A6 and A7. The nitrocellulose membranes were developed using His-Probe-HRP conjugate (4 µg/mL - Thermo Fisher Scientific, Waltham, MA, USA) for the Bi-scFv, or anti-Human-IgG (Fc specific)-HRP produced in goat (1:3 000 - Cat. A0170, Merck Group, Darmstadt, Germany) for the Bi-NAb and Tri-NAb. The membranes were imaged on the ChemiDoc™ MP Imaging System and the Quantity One® software, version 4.6.9 (BIO-RAD Laboratories, Hercules, CA, USA) on the chemiluminescence setting with no filter for maximal exposure, as described previously. Densitometry analysis was performed on the images using the volume rectangle tool and volume analysis report function on the Quantity One® software, version 4.6.9 (BIO-RAD Laboratories, Hercules, CA, USA). The resolved antibody standard bands were identified, and the respective amounts (microgram) of antibody were entered to generate a standard curve. The standard curve was used to compute the corresponding resolved protein bands in the IVT-mRNA-expressed antibody clarified cell culture supernatants. Final IVT-mRNA-

expressed antibody concentration in the clarified cell culture supernatants were estimated once corrected for the dilutions. The standard curves and equations were unavailable for export from the Quantity One® software program.

2.10.3 IC/ID Neutralisation data estimation of multispecific antibody concentration.

The relative concentration of the mRNA-expressed multispecific antibodies was determined by comparing the antibody/virus paired percentage inhibition data generated from the purified multispecific antibody data (IC50) in relation to the mRNA-expressed multispecific antibody inhibition data (ID50), produced using the *in vitro* neutralisation assays. It was reasoned that the IC50 and ID50 values would represent equivalent neutralisation antibody concentrations and that the starting concentration in the undiluted mRNA-expressed clarified cell culture supernatants could be inferred by multiplying the IC50 for the purified antibodies for each virus with the respective ID50 value. Previous studies have quantified human serum antibody titres, following passive bNAb infusion, using TZM-bl neutralisation assays (measure antibody neutralisation activity) and ELISA (measure bound antibody levels) and have shown good agreement between the two assays (108,147,350). Thus, we performed the following calculations:

E.g. mRNA expressed antibody starting concentration (µg/mL) = IC50 µg/mL x ID50 (dilution factor).

For this calculation, it was assumed that the unpurified mRNA-expressed multispecific antibodies display similar conformation assembly and neutralisation activity to the DNA-expressed and purified antibodies. IC50 x ID50 was calculated for each virus, multispecific antibody pair (n=17), excluding the resistant viruses (IC50 >10 µg/mL (Bi-scFv) or >25 µg/mL, ID50 <10). The means and standard deviation were calculated using Microsoft excel (Microsoft Corporation, Redmond, WA, USA) and reported for each multispecific antibody.

2.11 Statistical analysis.

The median antibody IC50 and IC80s (molarity corrected), and the mRNA-expressed multispecific antibody ID50 and ID80s were analysed using the descriptive statistics parameters in GraphPad Prism 8. Scatterplots depicting the median and interquartile range were generated in GraphPad Prism 8. The smaller number of viruses and the

preferential inclusion of resistant strains in the tested viral panel would result in the data being more affected by outliers. Therefore, the data was analysed using the median (rather than the geometric mean) which is more conservative. Comparisons of median neutralisation values (corrected molarity difference IC50 and IC80 values, uncorrected molarity difference ID50 and ID80 values) were performed using a non-parametric, paired one-way analysis of variance (ANOVA) (Friedman test) and two-tailed *p*-value with Dunns correction *post hoc* in GraphPad Prism 8. The following groups were compared for the purified antibody (IC50/IC80): PGT121 vs VRC01 vs 10E8v4, PGT121 vs each multispecific antibody, VRC01 vs each multispecific antibody, 10E8v4 vs Tri-NAbs (Co-T and sORF), and Bi-scFv vs Bi-NAb vs Tri-NAb Co-T vs Tri-NAb sORF. For the mRNA-expressed antibody clarified cell culture supernatants, the ID50 and ID80 values between the multispecific antibodies were compared (Bi-scFv vs Bi-NAb vs Tri-NAb Co-T vs Tri-NAb sORF). Breadth versus potency plots were produced using the survival plots in GraphPad Prism 8 by representing the IC50/IC80 and ID50/ID80 values as zero for resistance or one for neutralisation for each antibody.

Chapter 3. Results.

3.1 Generation of bispecific antibody expression constructs.

The Bi-NAb sequence incorporating tandem scFv VRC01 and PGT121 bNAb domains with optimised interspacing glycine-serine linker sequences, fused to the human Fc domain as reported by Steinhardt *et al.* (200) was synthesised and sub-cloned into the pmRNA expression vector by directional restriction endonuclease digest using *Kpn*I and *Apa*I (Figure 3.1A). Digested pUC57-Mini_Bi-NAb and pmRNA_GFP plasmids (removing the GFP encoding sequence from the pmRNA vector and replacing it with the Bi-NAb sequence) were resolved on an agarose gel and the Bi-NAb insert (2 374 bp) and the pmRNA vector backbone (3 638 bp – Figure 3.1B) were extracted, purified, and ligated together. Single pmRNA_Bi-NAb cultured colonies were screened by restriction digest with *Kpn*I and *Apa*I and resolved on a 0.8% agarose gel. Successful ligation of the Bi-NAb insert into the pmRNA backbone was confirmed as anticipated DNA fragments for the Bi-NAb insert and pmRNA backbone were visible (Figure 3.1C – correct banding pattern displayed by clones 2 and 3). The expression and secretion of the Bi-NAb from the pmRNA_Bi-NAb construct was confirmed and compared to the expression of the parental VRC01, PGT122 (PGT122 is a somatic variant of PGT121 and was used as a substitute for the PGT121 parental antibody until the PGT121 constructs were obtained), and 10E8v4 antibodies (third parental antibody incorporated into the Tri-NAb confirmation, described in section 3.3 below) by transient transfection of mammalian cells. The harvested, clarified cell culture supernatants were resolved by SDS-PAGE under reducing conditions and expressed antibodies detected using anti-human secondary antibody by western blot. The parental antibodies (VRC01, PGT122 and 10E8v4) produced the characteristic heavy- and light-chain banding pattern of ~60 kDa and ~30 kDa respectively (Figure 3.1D). The Bi-NAb resolved as a single polypeptide of ~100 kDa (Figure 3.1D), confirming the correct expression and secretion of the Bi-NAb. A corresponding faint band was observed in the adjacent GFP lane, which most likely represents carryover from the Bi-NAb lane as no antibody expression should result from the pmRNA_GFP transfected cells (Figure 3.1D – lane two).

Having confirmed expression of Bi-NAb, the pUC57-Mini_Bi-NAb construct was used to generate the Bi-scFv by amplification of the tandem-scFv sequence excluding the

Fc region. The position of the amplification primers are presented in Figure 3.1E (red arrows) and the reverse primer was used to incorporate an in-frame six histidine purification tag (6x His-tag) on the C-terminus followed by an *Apa*I restriction site to facilitate sub-cloning into the pmRNA expression vector by directional restriction endonuclease digest using *Kpn*I and *Apa*I (Figure 3.1E). The Bi-scFv amplicon product of 1 696 bp was generated and visualised on an agarose gel (Figure 3.1F). The Bi-scFv insert was sub-cloned into the pmRNA vector using *Kpn*I and *Apa*I endonuclease restriction sites. Selected colonies were cultured, plasmid DNA isolation was performed and subsequently screened by restriction digest with *Kpn*I and *Apa*I and resolved on a 0.8% agarose gel. All three of the selected clones displayed the successful insertion of the Bi-scFv sequence resulting in the anticipated banding pattern observed, Bi-scFv (1 696 bp) and pmRNA (3 638 bp) (Figure 3.1G). The resulting pmRNA_Bi-scFv construct was used to determine the expression and secretion of the Bi-scFv antibody following transient mammalian cell transfection. Clarified culture supernatants were resolved by SDS-PAGE under reducing conditions and detected by western blot using the incorporated C-terminal 6x His tag. The Bi-scFv was successfully expressed and observed to be of the approximate size ~70 kDa (Figure 3.1H). The 4dCD4 His-tagged positive control was detected at the correct approximate size ~56 kDa and the GFP and Bi-NAb negative controls that lack the His tag were not detected (Figure 3.1H), indicating the specific detection of the Bi-scFv that confirmed the correct expression and secretion of the Bi-scFv.

In summary, the pmRNA_Bi-NAb and pmRNA_Bi-scFv constructs were successfully generated with small-scale transfections confirming expression and secretion of the bispecific antibodies. These constructs were advanced into large-scale production to generate sufficient quantities of antibody for *in vitro* characterisation and neutralisation testing.

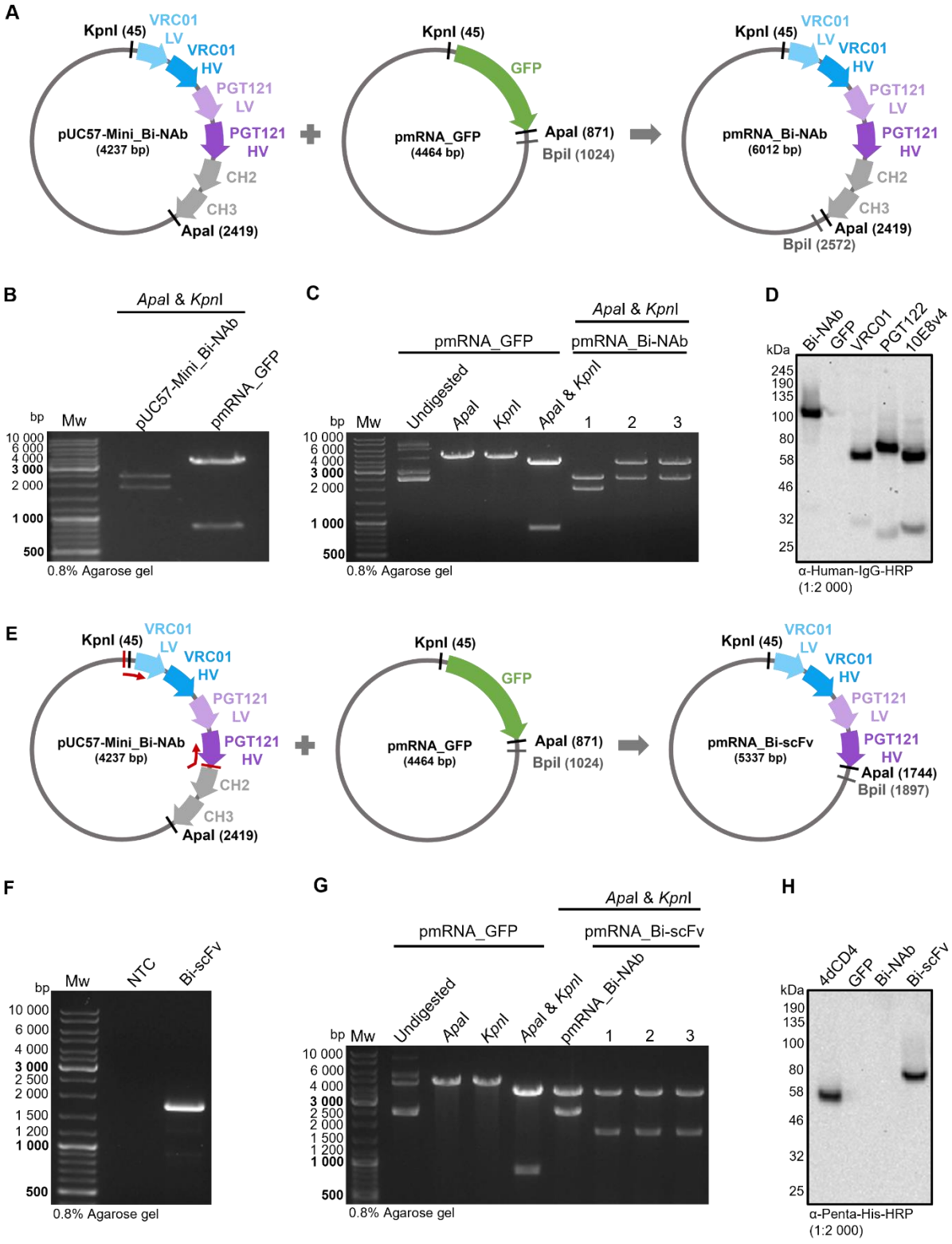

A
KpnI (45)
VRC01 LV
VRC01 HV
PGT121 LV
PGT121 HV
CH2
CH3
ApaI (2419)
pUC57-Mini_Bi-NAb (4237 bp)
pmRNA_GFP (4464 bp)
GFP
ApaI (871)
BpiI (1024)
pmRNA_Bi-NAb (6012 bp)
BpiI (2572)
B
ApaI & KpnI
pUC57-Mini_Bi-NAb
pmRNA_GFP
bp
Mw
10 000
6 000
4 000
3 000
2 000
1 000
500
0.8% Agarose gel
C
pmRNA_GFP
pmRNA_Bi-NAb
Undigested
ApaI
KpnI
1
2
3
D
Bi-NAb
GFP
VRC01
PGT122
10E8v4
kDa
245
190
135
100
80
58
46
32
25
α-Human-IgG-HRP
(1:2 000)
E
pmRNA_Bi-scFv (5337 bp)
ApaI (1744)
BpiI (1897)
F
NTC
Bi-scFv
2 500
1 500
1 200
G
H
4dCD4
α-Penta-His-HRP
(1:2 000)

Figure 3.1. Generation and evaluation of bispecific antibody constructs. (A) Schematic representing the synthesised Bi-NAb sequence (tandem scFv VRC01 and PGT121 domains with a human Fc region) which was subcloned into the pmRNA expression vector by directional restriction endonuclease digest using *Kpn*I and *Apa*I. **(B)** The Bi-NAb (2 374 bp) and pmRNA (3 638 bp) sequences were isolated following double digests with *Kpn*I and *Apa*I and resolved on a 0.8% agarose gel. **(C)** Single pmRNA_Bi-NAb cultured colonies were screened by restriction digest with *Apa*I and *Kpn*I and resolved on a 0.8% agarose gel to confirm assembly of the Bi-NAb insert (2 374 bp) into the pmRNA vector. **(D)** The expression and secretion of the Bi-NAb from the pmRNA_Bi-NAb construct was confirmed and compared to the expression of the parental VRC01, PGT122 (PGT122 is a somatic variant of the parental antibody PGT121), and 10E8v4 (third parental antibody for the Tri-NAb conformation described later) antibody controls by transient transfection of mammalian cells. Reduced clarified cell culture supernatant samples (Bi-NAb and parental antibodies) were resolved on a 10% SDS-PAGE gel, transferred onto a nitrocellulose membrane, and detected using ECL™ anti-human IgG horseradish peroxidase (HRP) linked whole antibody (1: 2 000). The Bi-NAb resolved as a single polypeptide (~100 kDa) and the parental antibodies produced the characteristic heavy- and light-chain banding pattern (~60 kDa and ~30 kDa respectively). **(E)** Schematic representation of the cloning strategy used to generate the Bi-scFv construct. The tandem scFv sequence, excluding the Fc region, was amplified using primers (red arrows) that incorporated a six histidine tag (6x His-tag) and *Apa*I restriction site on the 3' end on the reverse primer sequence, and sub-cloned into the pmRNA expression vector by directional restriction endonuclease digest using *Kpn*I and *Apa*I. **(F)** The Bi-scFv amplicon was visualised on a 0.8% agarose gel (1 696 bp) and was cloned into the pmRNA vector. NTC – no template control amplification PCR reaction. **(G)** Single pmRNA_Bi-scFv cultured colonies were screened by restriction digest with *Apa*I and *Kpn*I and resolved on a 0.8% agarose gel to visualise the Bi-scFv (1 696 bp) and pmRNA (3 638 bp) segments. **(H)** The expression and secretion of the Bi-scFv from the pmRNA_Bi-scFv construct were confirmed by transient transfection of mammalian 293F cells. Clarified cell culture supernatant (Bi-scFv, Bi-NAb, His-tagged positive control human, soluble four domain CD4 (4dCD4) and negative control (green fluorescent protein - GFP)) were resolved on a 10% SDS-PAGE gel, transferred onto a nitrocellulose membrane and detected using α-Penta-His-HRP (1: 2 000). The Bi-scFv was observed at the correct approximate size (~70 kDa). The DNA molecular weight marker (Mw) on agarose gels is the GeneRuler DNA Ladder Mix, ready-to-use SM0333 (Thermo Fisher Scientific, Waltham, MA, USA), the protein ladder on western blots is the Color Protein Standard Broad Range P7712S (New England Biolabs, Ipswich, MA, USA).

3.2 Silencing of the Bi-NAb CH2 domain *Bpi*I restriction site to prevent premature mRNA transcript truncation.

Analysis of the pmRNA_Bi-NAb plasmid sequence revealed an additional *Bpi*I restriction site within the CH2 domain (C-terminus) of the Bi-NAb Fc encoding region. Whilst this additional *Bpi*I restriction site does not affect expression of the antibodies by DNA plasmid transfection (Figure 3.1 D), *Bpi*I is used to linearise the pmRNA template for the *in vitro* mRNA transcription reaction (Figure 3.2A). Failure to silence this additional *Bpi*I restriction site would thus result in premature truncation of the Bi-NAb transcript and protein expression failure (Figure 3.2A). The additional *Bpi*I restriction site was silenced by site-directed mutagenesis (SDM – via a single nucleotide mutation (1959G>A) without altering the lysine amino acid) while retaining the functional *Bpi*I restriction site at the 3' terminus of the poly-A signal (Figure 3.2A). The amplification step of the SDM reaction was performed in both the pUC57-Mini_Bi-NAb and pmRNA_Bi-NAb vectors, with no visible benefit of the starting template vector as both PCR amplification products had a larger non-specific band present (Figure 3.2B). Therefore, the band corresponding to the linear SDM amplicon was extracted from the gel for the pmRNA_Bi-NAb vector (6 012 bp – Figure 3.2B) to continue with

the KLD reaction. Single pmRNA_Bi-NAb_Δ*Bpi*I cultured colonies were screened by restriction digest with *Bpi*I and analysed by agarose gel electrophoresis. Compared to the original pmRNA_Bi-NAb construct that has two *Bpi*I restriction sites, resulting in two bands of 5 513 bp and 499 bp respectively (Figure 3.2C), the SDM clones were found to successfully have silenced the additional *Bpi*I restriction site resulting in linearisation of the pmRNA_Bi-NAb_Δ*Bpi*I following *Bpi*I treatment (Figure 3.2C – all three selected colonies displayed the correct banding pattern). Silencing of the *Bpi*I restriction site within the Bi-NAb CH2 encoding region whilst preserving the native amino acid sequence at this position (EKT) was confirmed by Sanger sequencing (Figure 3.2D). The expression of the Bi-NAb from the pmRNA_Bi-NAb_Δ*Bpi*I was confirmed in small-scale mammalian 293F cell transfection to have been unaltered by the SDM, producing the ~95 kDa Bi-NAb band of identical intensity to that of the original Bi-NAb construct when analysed by western blot (Figure 3.5A). Therefore, the resultant pmRNA_Bi-NAb_Δ*Bpi*I construct should be compatible with mRNA production and is subsequently used to replace the existing pmRNA_Bi-NAb construct in all downstream antibody expression and characterisation experiments (i.e. pmRNA_Bi-NAb henceforth contains the silenced *Bpi*I restriction site in the CH2 domain).

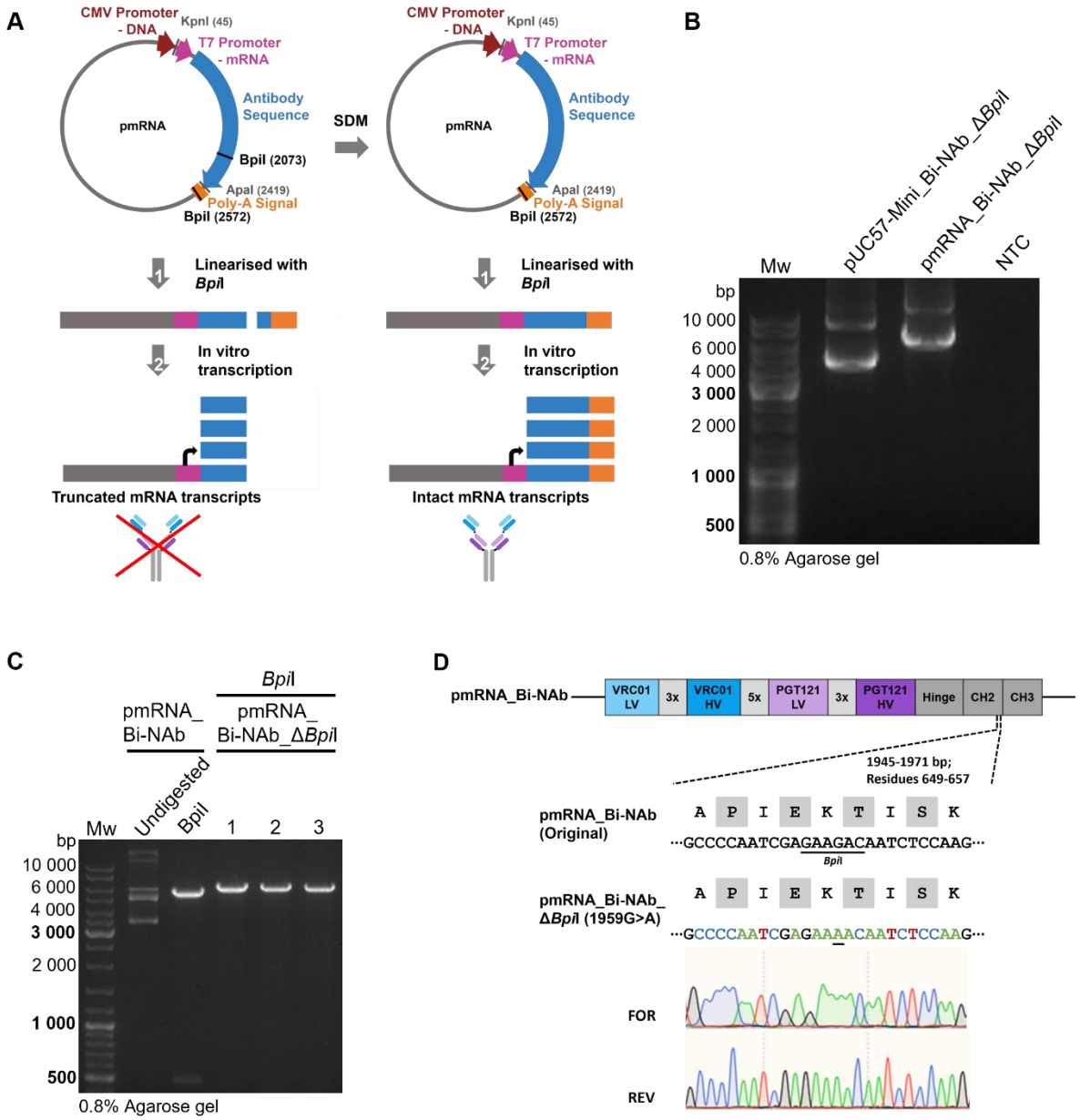


Figure 3.2. Silencing the Bi-NAb CH2 domain *Bpi*I restriction site to prevent premature mRNA transcript truncation. (A) The *Bpi*I restriction site in the poly-adenylation (poly-A) signal is used to linearise the DNA construct for mRNA transcript production. The Bi-NAb sequence was found to contain an additional *Bpi*I restriction site within the C-terminus of the CH2 domain of the Fc region which would result in premature truncation of the Bi-NAb transcript and protein expression failure. Therefore, the additional *Bpi*I restriction site was silenced using site-directed mutagenesis (SDM) while retaining the functional poly-A signal *Bpi*I restriction site. **(B)** The SDM amplification reaction was performed using both the pUC57-Mini and pmRNA vector templates with no discernible difference in amplification efficiency (higher non-specific bands noted in both reactions). The SDM band was extracted from the pmRNA_Bi-NAb (6 012 bp) to perform the kinase, ligase, *Dpn*I (KLD) reaction and transformation. **(C)** Single pmRNA_Bi-NAb_Δ*Bpi*I cultured colonies were screened by *Bpi*I restriction digest and resolved on a 0.8% agarose gel. The additional *Bpi*I restriction site was successfully silenced in all constructs as the single remaining functional *Bpi*I restriction site in the poly-A signal linearised the constructs to 6 012 bp. **(D)** Sanger sequencing was performed (forward (FOR) and reverse (REV) sequencing chromatograms shown) on a pmRNA_Bi-NAb_Δ*Bpi*I construct to confirm abrogation of the *Bpi*I restriction site (1959G>A) in the Bi-NAb CH2 region while preserving the native amino acids at this position (EKT). The DNA molecular weight marker (Mw) on agarose gels is the GeneRuler DNA Ladder Mix, ready-to-use SM0333 (Thermo Fisher Scientific, Waltham, MA, USA).

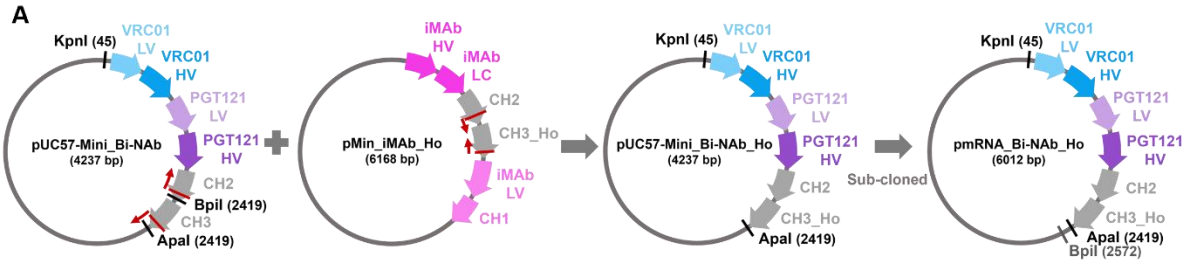
3.3 Generating the Tri-NAb expression constructs.

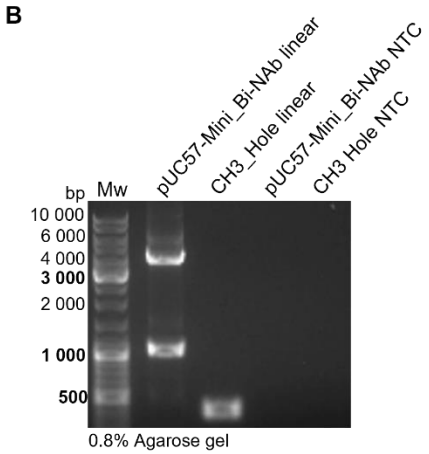
3.3.1 Heterologous heavy chain assembly through complementing knob-into-hole mutations in the 10E8 and Bi-NAb constructs.

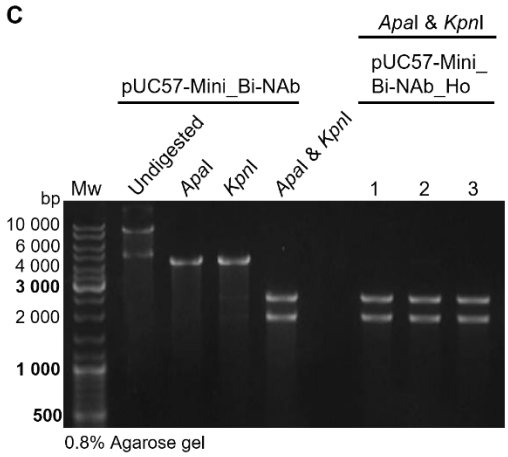
The Tri-NAb construct was generated based on the Tri-NAb described by Steinhardt *et al*. (200) through incorporating the assembly of the Bi-NAb and the 10E8 antibody heavy- and light-chains with the specific introduction of knob-into-hole mutations in the complimenting Fc regions to favour heterodimeric heavy chain assembly. The pMin_10E8_Kn construct containing the knob mutations (S354C and T366W) was already available in our research unit (191,202). The complimenting hole mutations were introduced in the Bi-NAb via the Gibson Assembly mechanism, in which the pmRNA_Bi-NAb construct was linearised and amplified to exclude the CH3 region and substituted with the pMin-iMAb_CH3_Ho region (previously produced in our research unit (191,202)) (Figure 3.3A). As the iMAb CH2 region did not contain a *Bpi*I restriction site, the C-terminal CH2 region was included in the substitution region of the Bi-NAb (Figure 3.3A). The corresponding CH3 hole region, containing the hole mutations (Y349C, T366S, L368A, and Y407V), was amplified (390 bp) from the pMin_iMAb_Ho construct and substituted into the linearised pUC57-Mini_Bi-NAb (3 889 bp – this vector was used as the template since improved amplification was achieved (data not shown) - Figure 3.3B). The resulting pUC57-Mini_Bi-NAb_Ho clones were screened by restriction digest with *Kpn*I and *Apa*I, resolved on an agarose gel, and displayed the correct band sizes for the Bi-NAb (2 374 bp) and pUC57-Mini (1 863 bp) (Figure 3.3C – all three colonies) and were identical to the parental pUC57_Mini_ Bi-NAb construct. This result confirmed an intact Bi-NAb sequence but is unable to confirm that the CH3_Ho region substitution had occurred, given that this would not result in a size difference compared to the original Bi-NAb construct (Figure 3.3C – right side, clones compared to the original). Therefore, a selected pUC57-Mini_Bi-NAb_Ho construct was Sanger sequenced and confirmed the presence of the hole mutations in the CH3 region of the Bi-NAb_Ho (data not shown, however incorporated hole mutations were confirmed in the final construct, data shown below) prior to sub-cloning.

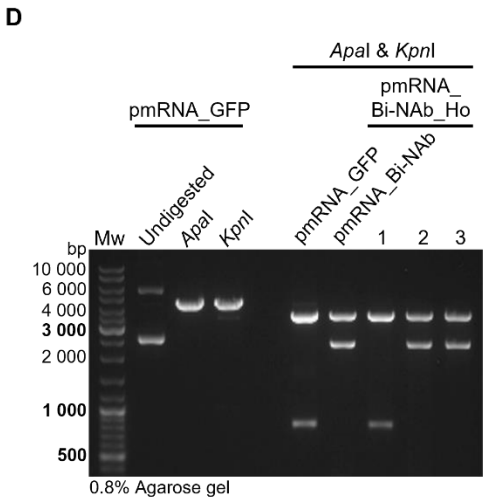
The confirmed Bi-NAb_Ho sequence was sub-cloned into the pmRNA vector using *Kpn*I and *Apa*I restriction sites and individual cultured colonies were screened by restriction digest with *Kpn*I and *Apa*I and compared to the digested backbone control

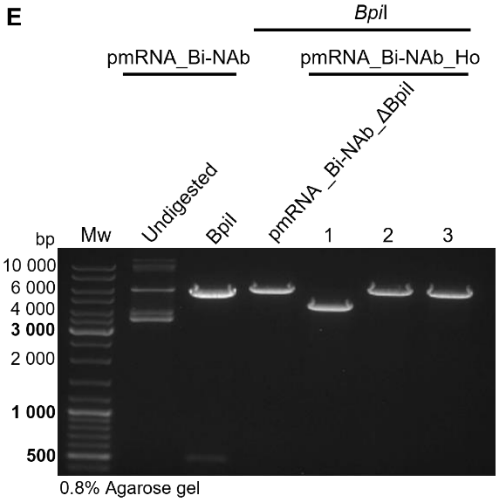
pmRNA_GFP DNA when resolved on an agarose gel (Figure 3.3D). Clone 1 appeared to be pmRNA_GFP backbone vector but the anticipated Bi-NAb_Ho (2 374 bp) and pmRNA (3 638 bp) bands were present in the remaining clones (Figure 3.3D – e.g. clones 2 and 3) indicating successful sub-cloning into the pmRNA vector (Figure 3.3D). To ensure that the *Bpi*I restriction site had been eliminated from the Bi-NAb CH2 region, selected pmRNA_Bi-NAb_Ho colonies were further screened using a *Bpi*I restriction digest and compared to digested pmRNA_Bi-NAb DNA (before and after silencing the CH2 *Bpi*I restriction site) (Figure 3.3E). Clones 2 and 3 were successfully linearised to 6 012 bp (Figure 3.3E), indicating the presence of only a single *Bpi*I restriction site, implying correct incorporation of the CH3 hole-mutation-containing section into the pmRNA_Bi-NAb. As final confirmation, a selected pmRNA_Bi-NAb_Ho construct was sequenced to confirm the presence of the hole mutations (Figure 3.3F) as well as the absence of the *Bpi*I restriction site and retained amino acid sequence (EKT) in the CH2 region of the Bi-NAb_Ho (Figure 3.3G). Taken together, these data confirm the generation of the pmRNA_Bi-NAb_Ho construct which could now be evaluated for Tri-NAb expression by co-transfection with pMin_10E8_Kn construct in mammalian cells.


A
KpnI (45)
VRC01 LV
VRC01 HV
PGT121 LV
PGT121 HV
CH2
CH3
BpiI (2419)
ApaI (2419)
pUC57-Mini_Bi-NAb (4237 bp)
pMin_iMAb_Ho (6168 bp)
iMAb HV
iMAb LC
iMAb LV
CH1
CH3_Ho
pUC57-Mini_Bi-NAb_Ho (4237 bp)
Sub-cloned
pmRNA_Bi-NAb_Ho (6012 bp)
BpiI (2572)


B
pUC57-Mini_Bi-NAb linear
CH3_Hole linear
pUC57-Mini_Bi-NAb NTC
CH3 Hole NTC
bp
Mw
10 000
6 000
4 000
3 000
2 000
1 000
500
0.8% Agarose gel


C
ApaI & KpnI
pUC57-Mini_Bi-NAb
pUC57-Mini_Bi-NAb_Ho
Undigested
ApaI
KpnI
ApaI & KpnI
1
2
3
bp
Mw
10 000
6 000
4 000
3 000
2 000
1 000
500
0.8% Agarose gel


D
ApaI & KpnI
pmRNA_GFP
pmRNA_Bi-NAb_Ho
Undigested
ApaI
KpnI
pmRNA_GFP
pmRNA_Bi-NAb
1
2
3
bp
Mw
10 000
6 000
4 000
3 000
2 000
1 000
500
0.8% Agarose gel


E
BpiI
pmRNA_Bi-NAb
pmRNA_Bi-NAb_Ho
Undigested
BpiI
pmRNA_Bi-NAb_ΔBpiI
1
2
3
bp
Mw
10 000
6 000
4 000
3 000
2 000
1 000
500
0.8% Agarose gel

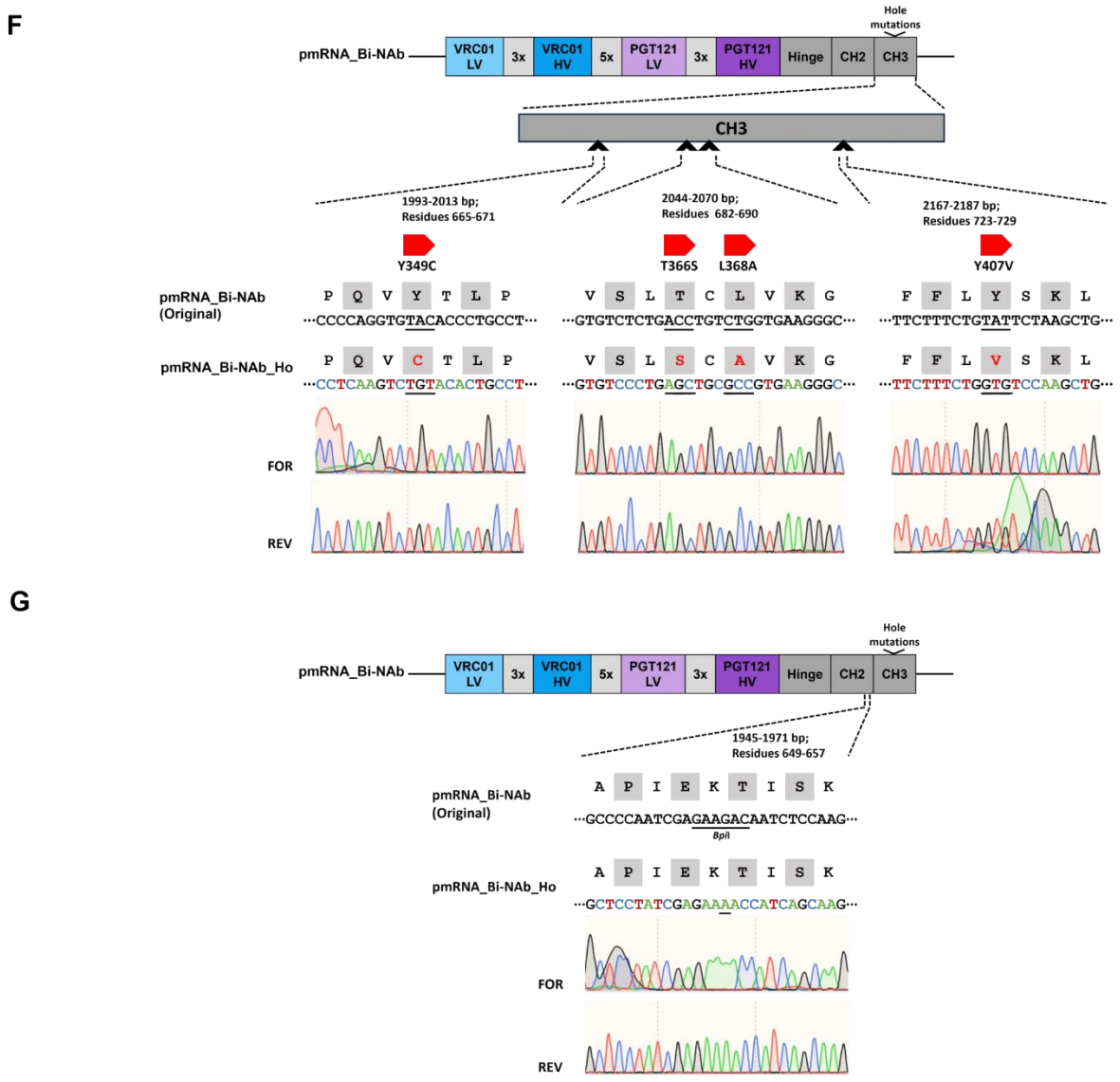


Figure 3.3. Generating the pmRNA_Bi-NAb_Ho construct containing the CH3 hole mutations required for heterologous heavy chain assembly and Tri-NAb production. The Tri-NAb is generated by the assembly of two different antibody heavy chains (Bi-NAb and 10E8) through the specific introduction of knob-into-hole mutations to favour heterodimer assembly. **(A)** Schematic representation of the cloning strategy for replacement of the CH3 region. The CH3 region containing the hole mutations was amplified from the iMAb_Ho template sequence and substituted into the linearised Bi-NAb sequence via Gibson assembly to generate the pUC57-Mini_Bi-NAb_Ho construct and then sub-cloned into the pmRNA vector using the *KpnI* and *ApaI* restriction sites. **(B)** Gibson assembly amplified fragments of the CH3 region containing the 'hole' (Ho) mutations (Y349C, T366S, L368A, and Y407V – 390 bp) and linearised amplified pUC57-Mini_Bi-NAb excluding the corresponding CH3 domain (3 889 bp). **(C)** pUC57-Mini_Bi-NAb_Ho cultured colonies were screened by restriction digest with *Apa*I and *Kpn*I, resolved on a 0.8% agarose gel, and displayed the correct banding pattern (Bi-NAb, 2 374 bp and pUC57-Mini, 1 863 bp). **(D)** The Bi-NAb_Ho sequence was sub-cloned into the pmRNA vector using the *Kpn*I and *Apa*I restriction endonuclease sites and individual cultured colonies were screened (compared to backbone control pmRNA_GFP) by restriction double digest with *Kpn*I and *Apa*I and resolved on a 0.8% agarose gel. Clones 2 and 3 were cloned successfully (correct banding pattern of 2 374 and 3 638 bp present). **(E)** Elimination of the *Bpi*I restriction site in the pmRNA_Bi-NAb through substitution of the CH3_Ho region was confirmed by *Bpi*I digest on selected clones (Clones 2 and 3 reflecting the correct linearisation of the plasmid, 6 012 bp). Sanger sequencing was performed on a pmRNA_Bi-NAb_Ho construct to confirm the presence of the hole mutations in the CH3 region of the Bi-NAb **(F)** as well as the absence of the *Bpi*I restriction site in the CH2 region **(G)**. Forward (FOR) and reverse (REV) sequencing chromatograms are shown. The DNA molecular weight marker (Mw) on agarose gels is the GeneRuler DNA Ladder Mix, ready-to-use SM0333 (Thermo Fisher Scientific, Waltham, MA, USA). NTC, no template control; GFP, green fluorescent protein.

3.3.2 Generating the Tri-NAb sORF construct.

Steinhardt *et al.* (200) expressed the Tri-NAb by co-transfecting mammalian cells with the Bi-NAb 'knob', 10E8 heavy chain 'hole', and 10E8 light chain plasmid constructs that generated a heterologous dimer via KIH assembly. However, for direct mRNA delivery *in vitro* or *in vivo*, having the entire encoding sequence in a sORF that generates a single mRNA transcript may be advantageous in simplifying the delivery process (single versus two or three constructs), provided transfection efficiency or downstream protein expression is not sacrificed. To this end, a Tri-NAb sORF construct was generated. The pmRNA_Bi-NAb_Ho construct was linearised and used as a template, to which a furin/P2A cleavage peptide sequence was inserted followed by the 10E8_Kn sequence (containing sequential heavy and light chain encoding regions, separated by the furin/F2Aopt cleavage peptide sequence). All sequences were cloned in frame using compatible overhangs and Gibson assembly to generate the Tri-NAb_sORF of an anticipated size of approximately 4 000 bp (Figure 3.4A).

The P2A cleavage peptide was synthesised in-house using a primer extension method (Figure 3.4A – 93 bp) followed by amplification yielding a 114 bp insert with compatible overhang with the 3' terminus of the Bi-NAb (Figure 3.4C). The pmRNA_Bi-NAb_Ho construct was linearised to eliminate the stop codon (6 006 bp) and the complete 10E8_Kn encoding region including the stop codon (2 322 bp – with compatible overhangs with the P2A cleavage peptide 5' and pmRNA 3') were amplified in separate reactions (Figure 3.4C). Primer dimers were visible in the 10E8_Kn reactions, but all the no-template controls were negative (Figure 3.4C). The three fragments were assembled via their incorporated compatible overhang regions using a Gibson assembly reaction. The pmRNA_Bi-NAb_Ho construct has a *Kpn*I restriction site at the 5' terminus and *Apa*I and *Not*I restriction sites at the 3' terminus (Figure 3.4A). However, the 10E8_Kn sequence contains an additional *Apa*I restriction site in the heavy chain sequence (Figure 3.4A), therefore, this provides a characteristic banding pattern when the Tri-NAb_sORF is generated. Selected pmRNA_Tri-NAb_sORF colonies were screened by restriction double digests with *Kpn*I and *Apa*I, and *Kpn*I and *Not*I, and resolved on an agarose gel. The anticipated banding patterns of 3 638 bp, 2 943 bp, and 1 798 bp; and 4 933 bp and 3 446 bp, respectively, were observed (e.g., clones 1, 2, and 4 - Figure 3.4D). Clone 3 appeared to be the original pmRNA_Bi-NAb_Ho with unsuccessful assembly (Figure 3.4D – banding pattern comparable to

control pmRNA_Bi-NAb_Ho for both double digests). The Bi-NAb_Ho-P2A cleavage peptide-10E8_Kn transition sequence of a pmRNA_Tri-NAb_sORF construct was confirmed by Sanger sequencing to be intact and in the correct order (Figure 3.4E). The furin-P2A cleavage peptide was synthesised correctly and of the designed amino acid sequence and the transitions from Bi-NAb_Ho and into 10E8_Kn were intact with no frameshifts created from the assembly process (Figure 3.4E). Therefore, the generated pmRNA_Tri-NAb_sORF could now be evaluated for expression of the Tri-NAb antibody and expression levels and heterologous heavy chain assembly compared to the expression of the Tri-NAb by conventional co-transfection procedures (pmRNA_Bi-NAb + pMin_10E8_Kn).

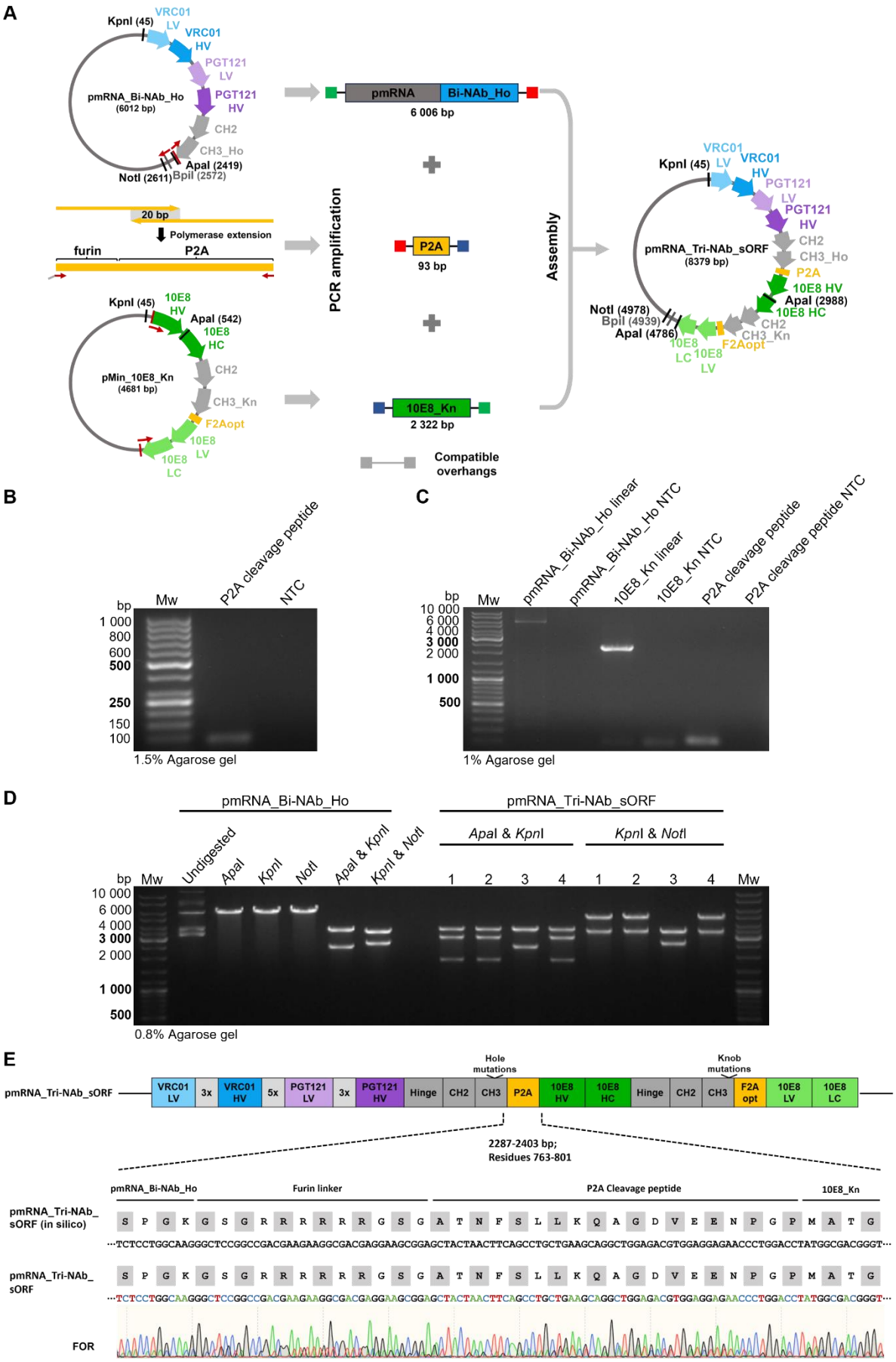

A
KpnI (45)
VRC01 LV
VRC01 HV
PGT121 LV
PGT121 HV
CH2
CH3_Ho
ApaI (2419)
BpiI (2572)
NotI (2611)
pmRNA_Bi-NAb_Ho (6012 bp)
20 bp
Polymerase extension
furin
P2A
PCR amplification
pmRNA
Bi-NAb_Ho
6 006 bp
P2A
93 bp
10E8_Kn
2 322 bp
Compatible overhangs
Assembly
KpnI (45)
10E8 HV
ApaI (542)
10E8 HC
CH2
CH3_Kn
F2Aopt
10E8 LV
10E8 LC
pMin_10E8_Kn (4681 bp)
pmRNA_Tri-NAb_sORF (8379 bp)
P2A
10E8 HV
ApaI (2988)
10E8 HC
NotI (4978)
BpiI (4939)
ApaI (4786)
B
P2A cleavage peptide
NTC
Mw
bp
1 000
800
600
500
250
150
100
1.5% Agarose gel
C
pmRNA_Bi-NAb_Ho linear
pmRNA_Bi-NAb_Ho NTC
10E8_Kn linear
10E8_Kn NTC
P2A cleavage peptide
P2A cleavage peptide NTC
10 000
6 000
4 000
3 000
2 000
1 000
500
1% Agarose gel
D
pmRNA_Bi-NAb_Ho
pmRNA_Tri-NAb_sORF
Undigested
ApaI
KpnI
NotI
ApaI & KpnI
KpnI & NotI
ApaI & KpnI
KpnI & NotI
1 2 3 4 1 2 3 4
0.8% Agarose gel
E
pmRNA_Tri-NAb_sORF
Hole mutations
Knob mutations
VRC01 LV
3x
VRC01 HV
5x
PGT121 LV
3x
PGT121 HV
Hinge
CH2
CH3
P2A
10E8 HV
10E8 HC
Hinge
CH2
CH3
F2A opt
10E8 LV
10E8 LC
2287-2403 bp;
Residues 763-801
pmRNA_Bi-NAb_Ho
Furin linker
P2A Cleavage peptide
10E8_Kn
pmRNA_Tri-NAb_ sORF (in silico)
S P G K G S G R R R R R G S G A T N F S L L K Q A G D V E E N P G P M A T G
···TCTCCTGGCAAGGGCTCCGGCCGACGAAGAAGGCGACGAGGAAGCGGAGCTACTAACTTCAGCCTGCTGAAGCAGGCTGGAGACGTGGAGGAGAACCCTGGACCTATGGCGACGGGT···
pmRNA_Tri-NAb_ sORF
S P G K G S G R R R R R G S G A T N F S L L K Q A G D V E E N P G P M A T G
···TCTCCTGGCAAGGGCTCCGGCCGACGAAGAAGGCGACGAGGAAGCGGAGCTACTAACTTCAGCCTGCTGAAGCAGGCTGGAGACGTGGAGGAGAACCCTGGACCTATGGCGACGGGT···
FOR

Figure 3.4. Generating the Tri-NAb single open reading frame (sORF) construct. The Tri-NAb sORF combines the Bi-NAb and the broadly neutralising antibody 10E8, with the 'hole' (Ho) and 'knob' (Kn) mutations respectively, separated by a P2A cleavage peptide. **(A)** Schematic representation depicting the cloning strategy used to generate the pmRNA_Tri-NAb_sORF by Gibson assembly of the linearised pmRNA-Bi-NAb_Ho and the 10E8_Kn sequence (sequential heavy- and light-chain encoding regions), separated by a furin/P2A cleavage peptide sequence. **(B)** The P2A cleavage peptide template DNA was synthesised using a primer extension method (93 bp) and resolved on a 1.5% agarose gel. **(C)** To facilitate assembly of the three fragments, pmRNA_Bi-NAb_Ho, P2A cleavage peptide, and 10E8_Kn were amplified with primers that incorporate the corresponding overlapping regions and were resolved on a 1% agarose gel for visualisation of the 6 006 bp, 114 bp, and 2 322 bp bands (respectively). **(D)** The three fragments were assembled, and colonies were screened by restriction digests with *Apa*I and *Kpn*I (two *Apa*I restrictions sites present, resulting banding pattern of 3 638 bp, 2 943 bp, and 1 798 bp), and *Kpn*I with *Not*I (resulting banding pattern of 4 933 bp and 3 446 bp), and resolved on a 0.8% agarose gel. The correct banding pattern, indicating successful assembly, was observed for clones 1, 2, and 4. **(E)** A pmRNA_Tri-NAb_sORF construct was Sanger sequenced (forward (FOR) sequencing chromatogram shown) to confirm insertion and assembly of the P2A interspacing sequence. The DNA molecular weight marker (Mw) on agarose gels is the O'GeneRuler 50 bp DNA Ladder, ready-to-use SM1133 **(B)** and the GeneRuler DNA Ladder Mix, ready-to-use SM0333 **(C and D)** (Thermo Fisher Scientific, Waltham, MA, USA). NTC, no template control.

3.4 Small-scale transfection and assessment of multispecific antibody expression *in vitro*.

Small-scale mammalian cell transfections were conducted to assess the expression of Bi-NAb antibody from the pmRNA_Bi-NAb_Δ*Bpi*I construct and the expression and assembly of Tri-NAb by co-transfection (Co-T, pmRNA_Bi-NAb_Ho & pMin_10E8_Kn) or single pmRNA_Tri-NAb_sORF constructs. Following transfection, cell culture supernatants were evaluated under reducing SDS-PAGE/western blot using anti-human Fc specific secondary antibody to detect expression of the antibody heavy chains (Figure 3.5A & B). The anti-human IgG-HRP secondary antibody western blot analysis from this point forward did not have apparent detection of antibody light chain (Figure 3.5A & B), which differs from the previously used anti-human IgG-HRP secondary antibody which did detect light chain (Figure 3.1C). The modified pmRNA_Bi-NAb_Δ*Bpi*I construct demonstrated identical expression with regard to size and intensity of the Bi-NAb antibody when compared to the original pmRNA_Bi-NAb construct. Thereby confirming the introduced mutation to silence the *BpiI* restriction site in the CH2 domain (Section 3.2) did not affect the expression levels of the Bi-NAb antibody (Figure 3.5A). Henceforth, all expressed Bi-NAb contained the silenced *Bpi*I restriction site in the CH2 domain. Tri-NAb antibody expression was evaluated by co-transfection (pmRNA_Bi-NAb_Ho & pMin_10E8_Kn) or by single transfection using the pmRNA_Tri-NAb_sORF construct. The iMAb-10E8 bispecific antibody generated through co-transfection with (pMin_iMAb_Ho & pMin_10E8_Kn) was included as an appropriate expression and assembly control based on our group's previously published data (191). Single transfections of individual constructs (pmRNA_Bi-NAb_Ho, pMin_10E8_Kn, and pMin_iMAb_Ho), as well as 10E8v4

parental (co-transfection), were included as expression controls (Figure 3.5A & B). Co-transfection with pmRNA_Bi-NAb_Ho & pMin_10E8_Kn or pmRNA_Tri-NAb_sORF produced visible banding corresponding to both the Bi-NAb (~95 kDa) and 10E8 heavy chain (~60 kDa) polypeptides. The 10E8 light chain was not detected using the selected anti-human Fc-specific antibody, consistent with the parental 10E8v4 expression analysis (Figure 3.5A & B). There was a noticeable decrease in intensity in both the Bi-NAb and 10E8 heavy chain bands when comparing Tri-NAb expression using the Co-T strategy to the Tri-NAb produced by single Tri-NAb_sORF transfection. This suggests that there may be a decrease in expression efficiency when using a sORF transfection strategy considering total DNA amounts and cell passage number, culture conditions, etc. were controlled for during the transfection procedure (Figure 3.5B). Confirmation of the co-expression and secretion of the Bi-NAb and 10E8 heavy chain polypeptides in the cell cultures media suggest heterologous chain assembly based on our previous published findings. However, the individual transfection controls (pmRNA-Bi-NAb_Ho, pMin_10E8_Kn or pMin_iMab_Ho) suggest homodimeric chain assembly of either Kn or Ho containing heavy chains may assemble and effectively be secreted in the culture supernatant (Figure 3.5A & B). Confirmation of the heterologous heavy chain assembly for production of the Tri-NAb was verified in the large-scale expression analysis below (Section 3.5.2).

3.4.1 Inefficient endogenous furin processing of 10E8_Kn and Tri-NAb_sORF constructs.

During initial mammalian cell expression of the Tri-NAb by co-transfection with pmRNA_Bi-NAb_Ho and pMin_10E8_Kn (and co-transfection with pMin_10E8_Kn and pMin_iMAb_Ho as an assembly control) and from the Tri-NAb_sORF, analysis by western blot revealed that there was an additional band of ~65 kDa present above the anticipated heavy chain bands of ~60 kDa (Figure 3.5A). This additional band was present in the 10E8_Kn or co-transfection combinations with the pMin_10E8_Kn and in the pMin_iMAb_Ho controls as well as the pmRNA_Tri-NAb_sORF transfections, but not in the controls 10E8v4 or Bi-NAb (Figure 3.5A & B). Therefore, it was suspected that there was incomplete furin cleavage occurring within the F2Aopt region that is used to separate the heavy- and light-chain sequences within these pMin constructs (pMin_10E8_Kn and pMin_iMAb_Ho), resulting in a furin-F2Aopt peptide tag (~3.4 kDa) fused to the C-terminus of the 10E8 heavy chain (Figure 3.5C). This high

molecular weight 10E8 heavy chain band was not removed by Protein A affinity chromatography purification in the Tri-NAb Co-T or sORF expressed antibodies (Appendix Figure B1C & D), suggesting that inclusion of the tag does not affect heavy chain assembly and/or antibody secretion. Additionally, there was also a high molecular weight 10E8 light chain band (~35 kDa) visible above the 10E8 light chain band in the expressed Tri-NAb antibodies (Co-T and sORF) (Appendix Figure B1C and D), indicating cleavage at the furin sequence but cleavage failure of the F2Aopt, resulting in a F2Aopt-tag fused to the N-terminus 10E8 light chain (Figure 3.5C). An additional aberrant band (~90 kDa) was present below the Bi-NAb band of the expressed Tri-NAbs (Figure 3.5A & B) which we posited to be a result of complete cleavage failure at both the furin and F2Aopt sequences resulting in 10E8 heavy-light chain fusion peptides (Figure 3.5C). There was no apparent incomplete cleavage occurring in the P2A cleavage peptide furin sequence of the pmRNA_Tri-NAb_sORF construct, as the Bi-NAb band was of the correct approximate size (~95 kDa) with no observed additional higher molecular weight bands that would otherwise suggest inefficient Bi-NAb/10E8 heavy chain processing resulting in P2A cleavage peptide fusion (Figure 3.4B).

The presence of this additional higher molecular weight 10E8 heavy chain band suggests fusion of the F2opt peptide sequence to the C-terminus of the heavy chain antibody constructs (Figure 3.5C). Given that the furin cleavage site is located at the N-terminus of the F2Aopt sequence, with the role of separating the F2A peptide from the antibody heavy chain, failure to remove this sequence (the furin-F2Aopt sequence is estimated to be ~3.4 kDa based on the amino acid sequence) from the 10E8_Kn heavy chain could explain this size of the additional 10E8_Kn heavy chain band observed (Figure 3.5A, B, and C). To examine this further, cleavage efficiency was evaluated through the supplementation of exogenous furin by co-transfection with plasmid encoding the furin protease (pcDNA 3.1-furin - (316,317)). Supplementing with exogenous furin, whilst maintaining antibody encoding construct concentration, clearly demonstrated improved cleavage and eliminated the 10E8 higher molecular weight, heavy chain band when transfected alone (pMin_10E8_Kn – lanes 9 and 10) or in combination with pmRNA_Bi-NAb_Ho or the pmRNA_Tri-NAb_sORF constructs (lanes 5 and 6, and 7 and 8 respectively - Figure 3.5D). We therefore set about to improve the processing of the F2Aopt sequence by endogenous furin without the

requirement for exogenous supplementation, given that it would overcomplicate the proposed *in vivo* mRNA delivery strategy downstream.

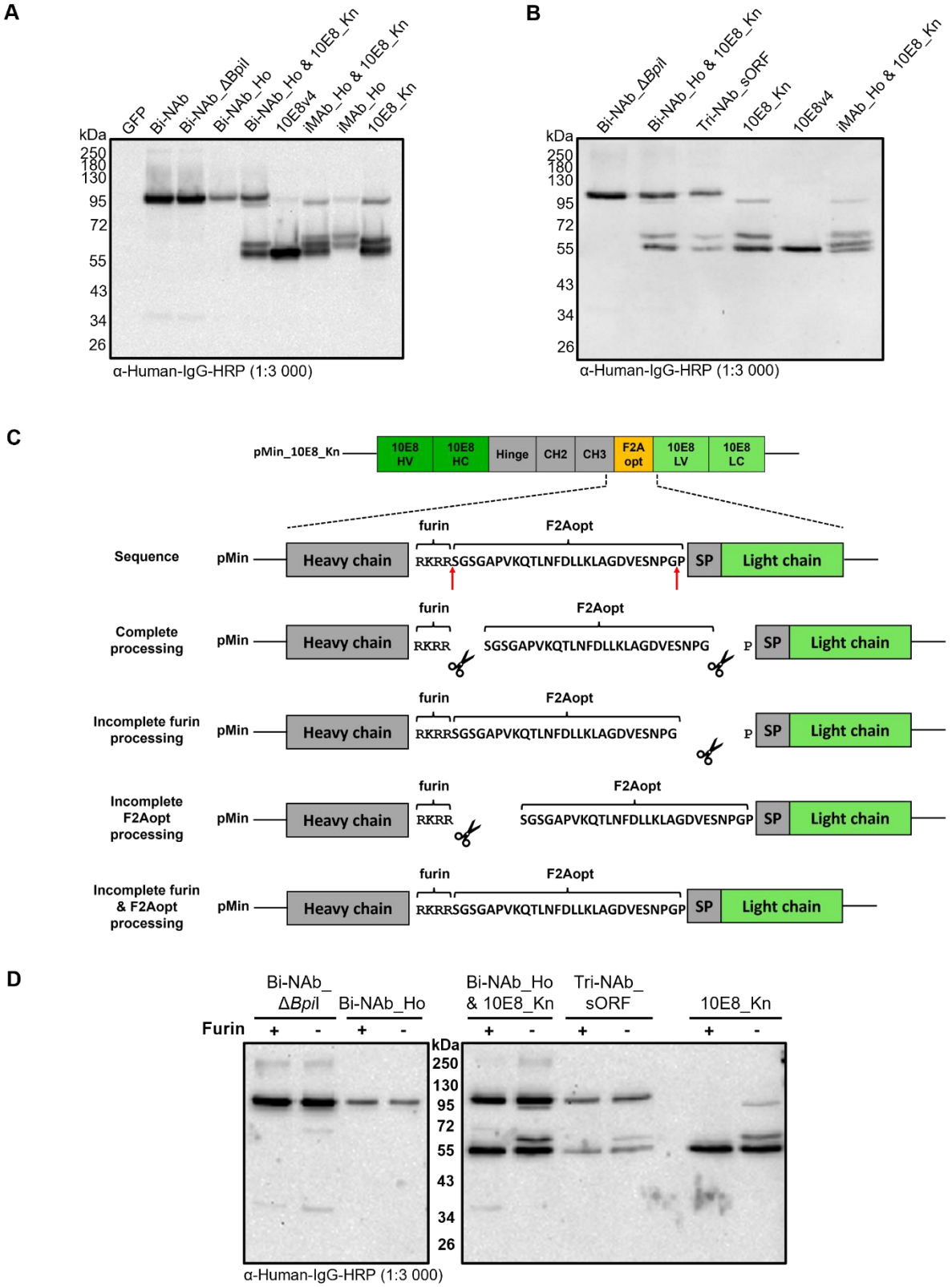


Figure 3.5. Multispecific antibody expression and processing of F2Aopt-containing constructs (pMin_10E8_Kn and pmRNA_Tri-NAb_sORF) *in vitro*. (A) Western blot analysis of cell culture supernatant from initial mammalian cell expression of the 10E8 containing the 'knob' (Kn) mutations alone or in combination with Bi-NAb_Ho or iMAb 'hole' (Ho) (assembly control) displayed an additional high molecular weight band (~65 kDa) above the 10E8_Kn heavy chain (HC) (~60 kDa). **(B)** This additional band above the 10E8_Kn HC band was also observed following transfection of mammalian cells with the pmRNA_Tri-NAb_sORF. **(C)** Schematic representation of the furin-F2Aopt processing between 10E8 heavy- and light-chain, with incomplete processing resulting in various observed additional high molecular weight bands. Complete processing separates the two antibody chains, incomplete furin cleavage results in a furin-F2Aopt peptide (3.4 kDa) attached to the C-terminus of 10E8 HC, incomplete F2Aopt processing results in an F2Aopt peptide fused to the N-terminus of 10E8 LC, and incomplete processing of both furin and F2Aopt results in a 10E8 HC-furin/F2Aopt-LC fusion polypeptide. **(D)** Cleavage efficiency was evaluated by performing mammalian cell transfections in the presence and absence of supplemental exogenous furin (co-transfecting antibody DNA:furin DNA = 2:1). Culture supernatant was analysed by western blot and demonstrated improved cleavage and eliminated the 10E8 higher molecular weight heavy chain band when exogenous supplemental furin was present. All western blots were transferred onto nitrocellulose membranes and developed with α-Human-IgG-Horse Radish Peroxidase (HRP) (1:3 000). The protein ladder is the Color Protein Standard Broad Range P7719S (New England Biolabs, Ipswich, MA, USA). SP, secretion signal peptide.

3.4.2 Improved endogenous furin processing and cleavage of the 10E8_Kn construct.

To improve the endogenous furin cleavage and processing of the 10E8_Kn polypeptide (including expression from the Tri-NAb_sORF construct), the furin recognition sequence was altered. The existing RKRR sequence was modified to an RRRRRR sequence (Δfurin) for enhanced furin recognition through site-specific introduction of additional arginine residues and simultaneous removal of the lysine residue by site-directed mutagenesis. The Δfurin sequence was selected based on previously published findings that demonstrate improved furin cleavage (343). Incorporating the Δfurin sequence into the Tri-NAb_sORF P2A cleavage peptide sequence displayed no observed processing inefficiency compared to the 10E8 F2Aopt sequence (Figure 3.5B).

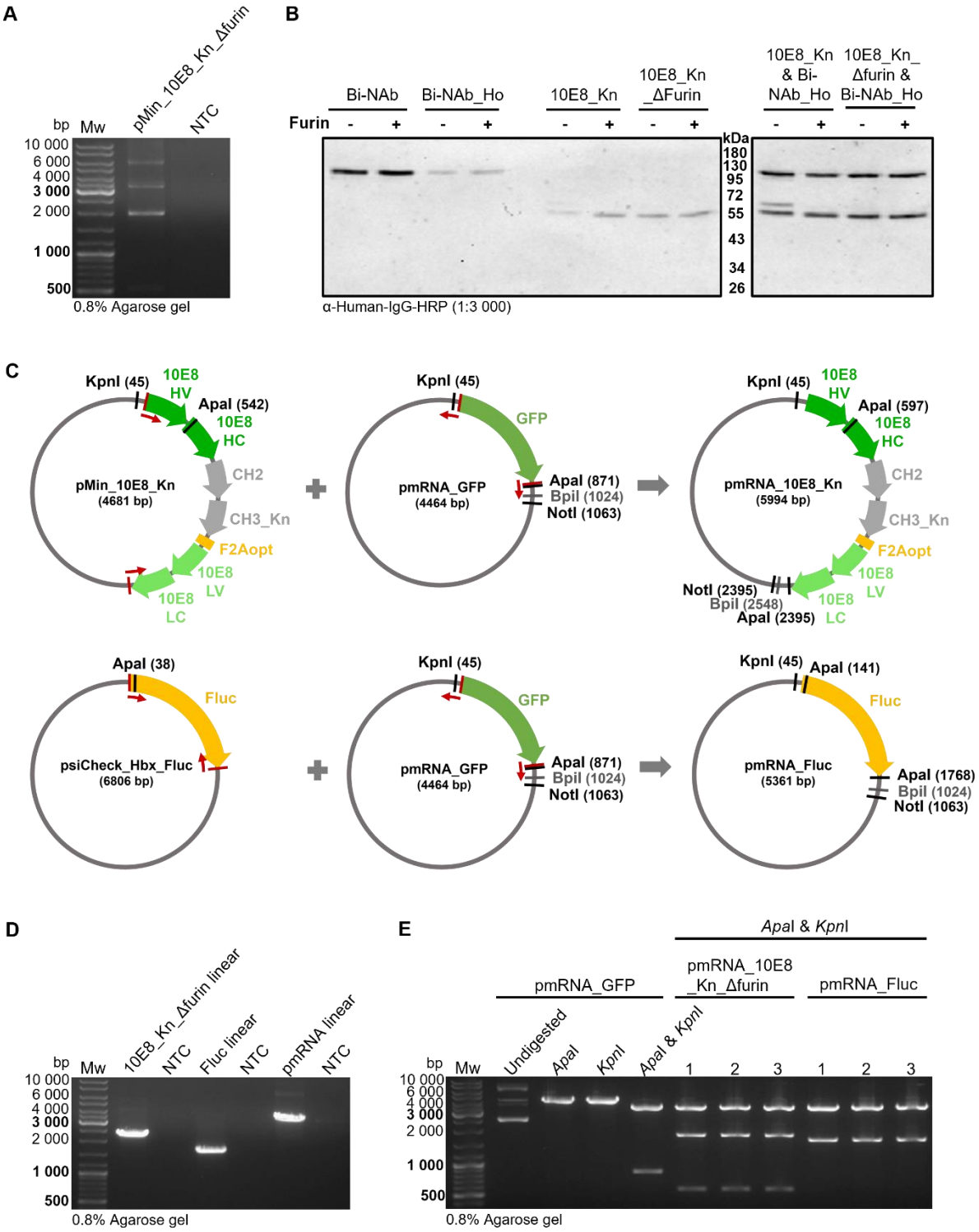
The SDM reaction was initially performed in the pMin_10E8_Kn construct, and the PCR amplicon was resolved on an agarose gel (Figure 3.6A). The SDM product corresponding to 6 183 bp was extracted from the gel to remove the smaller non-specific bands observed (Figure 3.6A) prior to performing the KLD reaction and bacterial transformation. Selected pMin_10E8_Kn_Δfurin clones were sequenced to confirm the alteration of the furin cleavage site (data not shown). Furin cleavage efficiency was then compared between the 10E8 antibody expressed from the original pMin_10E8_Kn construct and the pMin_10E8_Kn_Δfurin construct in the presence and absence of exogenously supplemented furin. The 10E8_Kn transfections (pMin_10E8_Kn or pMin_10E8_Kn_Δfurin) were performed alone or in combination with the pmRNA_Bi-NAb_Ho assembly partner (Figure 3.6B). Modification of the furin

cleavage site (pMin_10E8_Kn_Δfurin) clearly demonstrated improvement both alone and when co-transfected with the Bi-NAb_Ho assembly partner, eliminating the higher molecular, 10E8 heavy chain band (~65 kDa) that is observed when expressed from the original pMin_10E8_Kn construct (Figure 3.6B). Most importantly, supplemental furin was no longer required, and efficient processing was achieved by the endogenously expressed furin (Figure 3.6B, lanes 10E8_Kn_Δfurin and 10E8_Kn_Δfurin & Bi-NAb_Ho). Once again, Bi-NAb_Ho and 10E8_Kn homodimeric heavy chain assembly and secretion into the culture supernatant were detected when transfected in isolation (Figure 3.6B, left panel). However, homodimeric expression was observed to be lower than when compared to the heterologous heavy chain assembly using the complimenting knob-and-hole mutated heavy chains (Tri-NAb) (Figure 3.6B, right panel). Given the success of the modified furin cleavage, the 10E8_Kn_Δfurin sequence was sub-cloned into the pmRNA vector by Gibson assembly for downstream IVT mRNA production and subsequent Tri-NAb expression by co-transfection with Bi-NAb_Ho mRNA transcripts.

3.4.3 Sub-cloning of the 10E8_Kn_Δfurin and luciferase reporter into the pmRNA expression vector.

To facilitate mRNA transcript production, the 10E8_Kn with the altered furin sequence, as well as the firefly luciferase (Fluc) sequence (to serve as an additional IVT mRNA control for downstream *in vitro* expression and characterisation studies), required cloning into the pmRNA expression vector. Since both sequences contained two *Apa*I restriction sites, restriction cloning using *Kpn*I and *Apa*I was incompatible (Figure 3.6C). Gibson assembly was used to assemble the desired encoding sequences into the pmRNA expression vector in place of GFP (Figure 3.6C). The 10E8_Kn_Δfurin sequence was amplified (2 285 bp) from the pMin_10E8_Kn plasmid and sub-cloned into the linearised pmRNA expression vector (3 638 bp – Figure 3.6D). In parallel, the Fluc encoding region was amplified separately (1 695 bp) from the psiCheck_Hbx_Fluc plasmid and sub-cloned into the linearised pmRNA expression vector (3 638 bp - Figure 3.6D). Following the assembly reactions, selected colonies were expanded in liquid culture and screened by restriction double digest with *Kpn*I and *Apa*I and resolved on a 1% agarose gel. All the pmRNA_10E8_Kn_Δfurin constructs displayed the correct band sizes (3 638 bp, 1 804 bp, and 552 bp – Figure 3.6E), thus indicating the correct assembly of the vector and inserts. The pmRNA_Fluc

constructs had the 3 638 bp and 1 627 bp bands present but the 96 bp band could not be resolved or visualised (Figure 3.6E). A pmRNA_10E8_Kn_Δfurin construct and pmRNA_Fluc construct were Sanger sequenced. The furin sequence modification in the 10E8_Kn (Figure 3.6F – right side panel) and the 5' termini Kozak sequence (GCCGCCACCATGG – with the ATG start codon (underlined)) for both the pmRNA_10E8_Kn_Δfurin (Figure 3.6F left side panel) and pmRNA_Fluc (Figure 3.6G) were intact and unaltered during the assembly process. Therefore, the pmRNA_10E8_Kn_Δfurin and pmRNA_Fluc constructs were generated and compatible for DNA and mRNA expression. Henceforth, pmRNA_10E8_Kn refers to the 10E8_Kn_Δfurin sequence with the modified furin sequence (Δfurin – RRRRRR), and the Tri-NAb Co-T was expressed from this construct.


A
pMin_10E8_Kn_Δfurin
bp
Mw
NTC
10 000
6 000
4 000
3 000
2 000
1 000
500
0.8% Agarose gel
B
Bi-NAb
Bi-NAb_Ho
10E8_Kn
10E8_Kn _ΔFurin
10E8_Kn & Bi-NAb_Ho
10E8_Kn_ Δfurin & Bi-NAb_Ho
Furin
kDa
180
130
95
72
55
43
34
26
α-Human-IgG-HRP (1:3 000)
C
KpnI (45)
10E8 HV
ApaI (542)
10E8 HC
CH2
CH3_Kn
F2Aopt
10E8 LV
10E8 LC
pMin_10E8_Kn
(4681 bp)
pmRNA_GFP
(4464 bp)
GFP
ApaI (871)
BpiI (1024)
NotI (1063)
ApaI (597)
pmRNA_10E8_Kn
(5994 bp)
NotI (2395)
BpiI (2548)
ApaI (2395)
ApaI (38)
Fluc
psiCheck_Hbx_Fluc
(6806 bp)
ApaI (141)
pmRNA_Fluc
(5361 bp)
ApaI (1768)
D
10E8_Kn_Δfurin linear
NTC
Fluc linear
pmRNA linear
0.8% Agarose gel
E
ApaI & KpnI
pmRNA_GFP
pmRNA_10E8 _Kn_Δfurin
pmRNA_Fluc
Undigested
ApaI
KpnI
1
2
3
0.8% Agarose gel

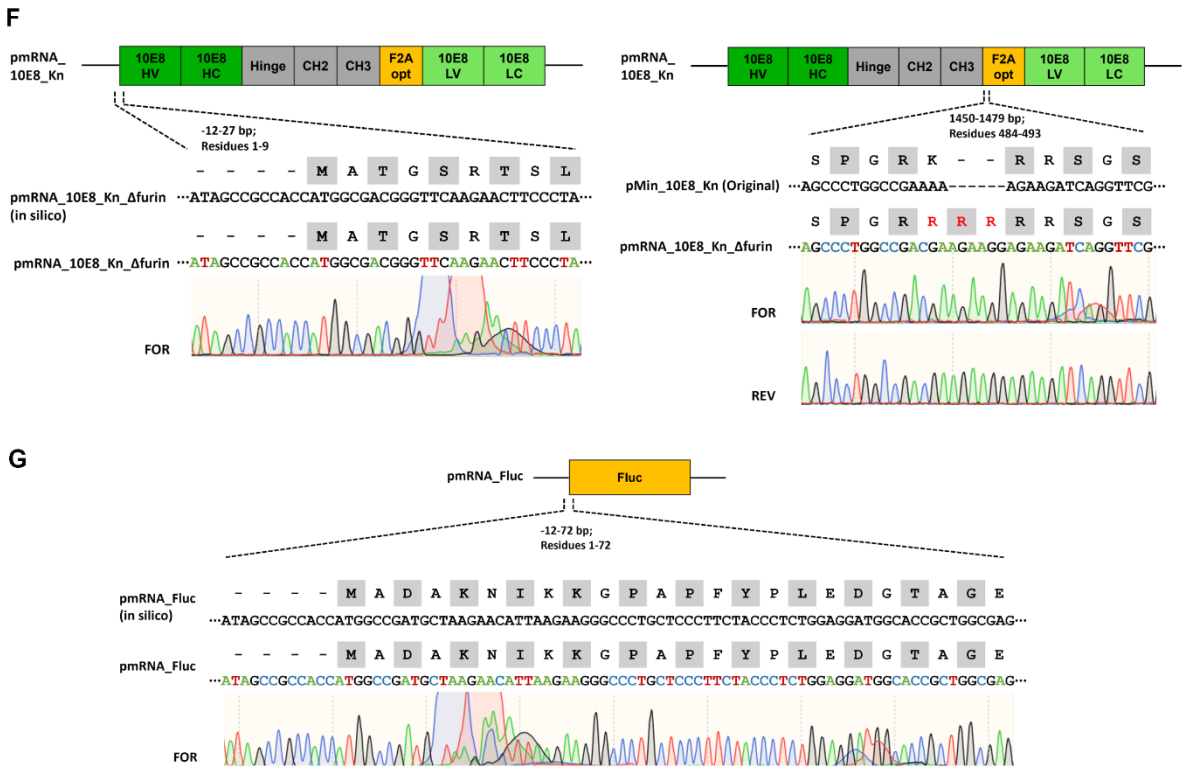


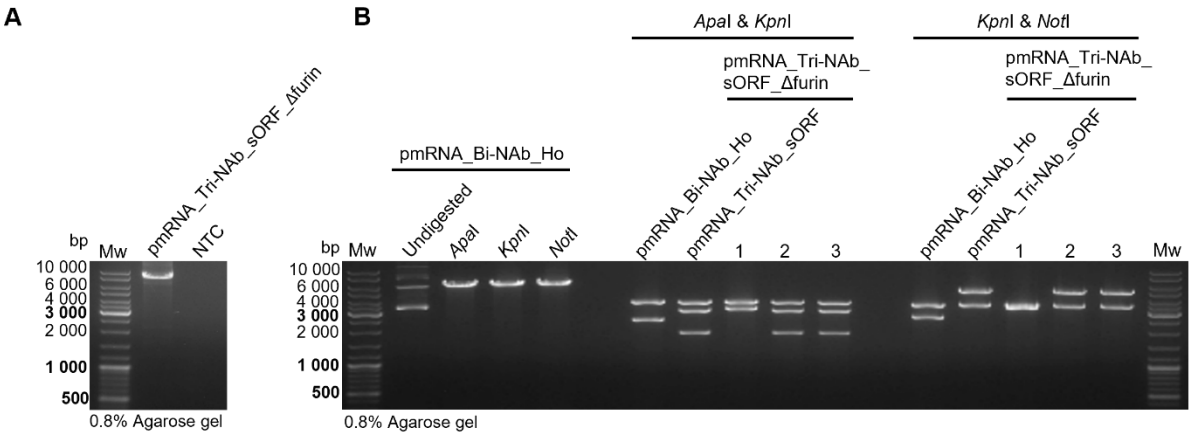
Figure 3.6. Improved endogenous furin processing and cleavage following alteration to the furin site in the F2Aopt of the 10E8_Kn construct. (A) Amplification of the pMin_10E8_Kn construct using site-directed mutagenesis (SDM) primers to modify the furin cleavage site (RRRRRR = Δfurin) within the F2Aopt sequence. The SDM product was resolved on a 0.8% agarose gel and the ~6 000 bp DNA band was extracted and purified from the gel to remove the non-specific bands prior to completing the KLD reaction and bacterial transformation. **(B)** Furin cleavage efficiency in the 10E8_Kn F2Aopt was compared between the original and modified Δfurin constructs in the presence and absence of exogenously supplemented furin (antibody DNA:furin DNA = 2:1) co-transfected in mammalian 293F cells. Compared to the original, the 10E8_Kn_Δfurin construct achieved improved cleavage, no longer requiring supplemental exogenous furin for efficient cleavage. **(C)** Schematic representation of the Gibson assembly strategy used to sub-clone the 10E8_Kn_Δfurin sequence, and the firefly luciferase (Fluc) sequence (to serve as an IVT mRNA control) into the pmRNA expression vector. **(D)** The 10E8_Kn_Δfurin sequence (2 285 bp), Fluc encoding sequence (1 695 bp), and pmRNA expression vector were amplified, incorporating compatible overhang regions for assembly, and resolved on a 0.8% agarose gel. **(E)** Colonies were screened by restriction digest with *Kpn*I and *Apa*I and resolved on a 0.8% agarose gel. The pmRNA_10E8_Kn_Δfurin constructs displayed the correct banding pattern (3 638, 1 804, and 552 bp), as did the pmRNA_Fluc constructs (3 638 and 1 627 bp bands visible, 96 bp band did not resolve). **(F)** Sanger sequencing of pmRNA_10E8_Kn_Δfurin construct was performed and confirmed the 5' terminal Kozak sequence and start codon sequence (GCCGCCACCATGG – with the ATG start codon (underlined)) was unaltered (left) and the Δfurin sequence modification was present (right). **(G)** Sanger sequencing of a pmRNA_Fluc construct demonstrates that the 5' terminus was unaltered during Gibson assembly and the Kozak sequence was present for the initiation of protein transcription. Forward (FOR) and reverse (REV) sequencing chromatograms are shown where available. The DNA molecular weight marker (Mw) is the GeneRuler DNA Ladder Mix, ready-to-use SM0333 (Thermo Fisher Scientific, Waltham, MA, USA). The protein ladder is the Color Protein Standard Broad Range P7719S (New England Biolabs, Ipswich, MA, USA).

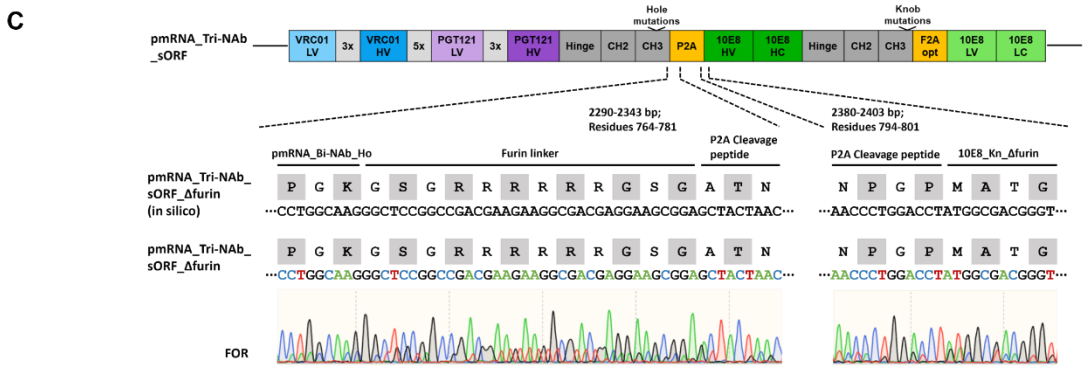
3.4.4 Improved endogenous furin processing and cleavage of the Tri-NAb sORF.

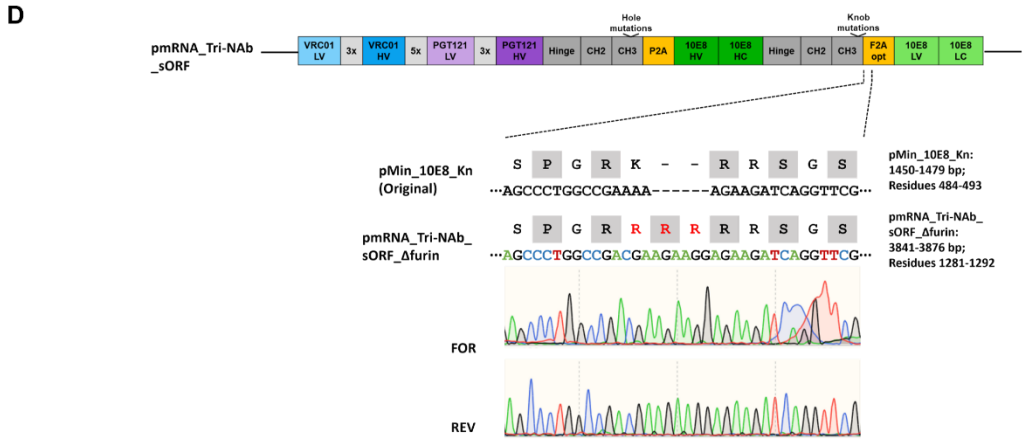
Given the observed improvement in endogenous furin processing in the modified 10E8_Kn_Δfurin, the 10E8_Kn F2Aopt furin sequence in the Tri-NAb_sORF was modified using site-directed mutagenesis as previously described (section 3.4.2). The pmRNA_Tri-NAb_sORF SDM amplification product of 8 385 bp (Figure 3.7A) was

extracted and purified from the agarose gel to perform the KLD and bacterial cell transformation. Selected cultured colonies were screened by restriction double digests with *Kpn*I and *Apa*I which resulted in the anticipated banding pattern of 3 638 bp, 2 943 bp, and 1 804 bp (two *Apa*I restriction sites present), as well as with *Kpn*I and *Not*I which also showed the expected bands of 4 939 bp and 3 446 bp (e.g., clones 2 and 3 resemble the correct banding pattern to that of the pmRNA_Tri-NAb_sORF control - Figure 3.7B). However, the restriction digest analysis is unable to confirm the alternation of the F2Aopt furin sequence as there was no visible change in size. Sanger sequencing was performed on a pmRNA_Tri-NAb_sORF_Δfurin construct and confirmed that the P2A cleavage peptide transitions were unaltered (Figure 3.7C) and that the F2Aopt furin sequence had been modified correctly from the RKRR to RRRRRR sequence (Figure 3.7D). Western blot analysis compared the original Tri-NAb_sORF construct with the modified Tri-NAb_sORF_Δfurin construct following mammalian cell expression in the presence and absence of supplemental exogenous furin. This demonstrated that while there was initially incomplete endogenous furin cleavage of the original F2Aopt sequence (Tri-NAb_sORF), the endogenous processing was improved with the modified furin sequence (Tri-NAb_sORF_Δfurin) and removed the ~65 kDa high molecular weight 10E8_Kn heavy-chain band (Figure 3.7E – right side of the middle pane). As observed for the 10E8_Kn versus 10E8_Kn_Δfurin, both alone and when co-transfected with Bi-NAb_Ho (Figure 3.7E – left and middle left pane, controls for verified furin cleavage efficiency), supplemental furin was no longer required for efficient endogenous cleavage of the 10E8 heavy- and light-chains within the Tri-NAb_sORF_Δfurin (Figure 3.7E). Henceforth, pmRNA_Tri-NAb_sORF refers to the Tri-NAb_sORF_Δfurin containing the modified F2Aopt furin sequence, unless otherwise stated.

Overall, all four multispecific antibody constructs (pmRNA_Bi-scFv, pmRNA_Bi-NAb, co-transfection with pmRNA_Bi-NAb_Ho and pmRNA_10E8_Kn, and pmRNA_Tri-NAb_sORF) were produced and their initial expression and secretion were confirmed in small-scale transfection studies. These constructs were therefore available for larger-scale expression, purification, and subsequent characterisation and functionality studies.


A
pmRNA_Tri-NAb_sORF_Δfurin
bp
Mw
NTC
10 000
6 000
4 000
3 000
2 000
1 000
500
0.8% Agarose gel
B
ApaI & KpnI
KpnI & NotI
pmRNA_Tri-NAb_ sORF_Δfurin
pmRNA_Tri-NAb_ sORF_Δfurin
pmRNA_Bi-NAb_Ho
Undigested
ApaI
KpnI
NotI
pmRNA_Bi-NAb_Ho
pmRNA_Tri-NAb_sORF
1
2
3
pmRNA_Bi-NAb_Ho
pmRNA_Tri-NAb_sORF
1
2
3
Mw
0.8% Agarose gel


C
pmRNA_Tri-NAb _sORF
Hole mutations
Knob mutations
VRC01 LV
3x
VRC01 HV
5x
PGT121 LV
3x
PGT121 HV
Hinge
CH2
CH3
P2A
10E8 HV
10E8 HC
Hinge
CH2
CH3
F2A opt
10E8 LV
10E8 LC
2290-2343 bp; Residues 764-781
2380-2403 bp; Residues 794-801
pmRNA_Bi-NAb_Ho
Furin linker
P2A Cleavage peptide
P2A Cleavage peptide
10E8_Kn_Δfurin
pmRNA_Tri-NAb_ sORF_Δfurin (in silico)
P G K G S G R R R R R R G S G A T N
N P G P M A T G
···CCTGGCAAGGGCTCCGGCCGACGAAGAAGGCGACGAGGAAGCGGAGCTACTAAC···
···AACCCTGGACCTATGGCGACGGGT···
pmRNA_Tri-NAb_ sORF_Δfurin
P G K G S G R R R R R R G S G A T N
N P G P M A T G
···CCTGGCAAGGGCTCCGGCCGACGAAGAAGGCGACGAGGAAGCGGAGCTACTAAC···
···AACCCTGGACCTATGGCGACGGGT···
FOR


D
pmRNA_Tri-NAb _sORF
Hole mutations
Knob mutations
VRC01 LV
3x
VRC01 HV
5x
PGT121 LV
3x
PGT121 HV
Hinge
CH2
CH3
P2A
10E8 HV
10E8 HC
Hinge
CH2
CH3
F2A opt
10E8 LV
10E8 LC
pMin_10E8_Kn (Original)
S P G R K – – R R S G S
···AGCCCTGGCCGAAAA------AGAAGATCAGGTTCG···
pMin_10E8_Kn: 1450-1479 bp; Residues 484-493
pmRNA_Tri-NAb_ sORF_Δfurin
S P G R R R R R R S G S
···AGCCCTGGCCGACGAAGAAGGAGAAGATCAGGTTCG···
pmRNA_Tri-NAb_ sORF_Δfurin: 3841-3876 bp; Residues 1281-1292
FOR
REV

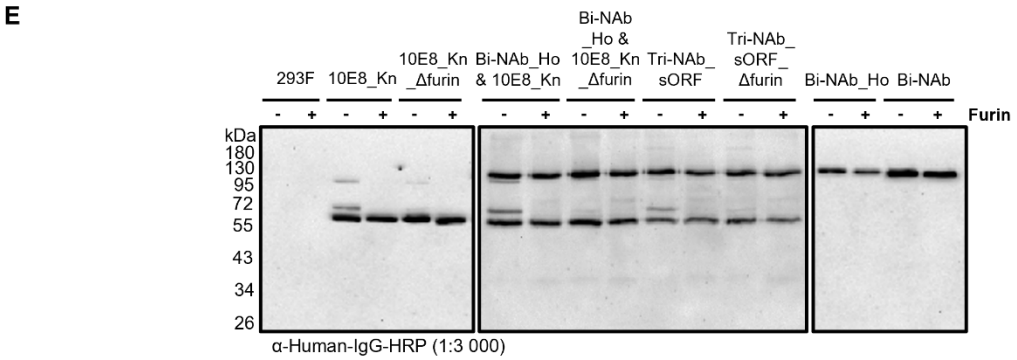

E
293F
10E8_Kn
10E8_Kn _Δfurin
Bi-NAb_Ho & 10E8_Kn
Bi-NAb _Ho & 10E8_Kn _Δfurin
Tri-NAb_ sORF
Tri-NAb_ sORF_ Δfurin
Bi-NAb_Ho
Bi-NAb
- + - + - + - + - + - + - + - + - + - +
Furin
kDa
180
130
95
72
55
43
34
26
α-Human-IgG-HRP (1:3 000)

Figure 3.7. Improved endogenous furin processing and cleavage of the Tri-NAb single open reading frame (sORF) following modification of the furin cleavage site in the F2Aopt. (A) Modification of the furin sequence within the F2Aopt to RRRRRR (Δfurin) of the Tri-NAb_sORF construct using site-directed mutagenesis (SDM) amplification primers to produce 8 385 bp linearised plasmid vector was analysed on a 0.8% agarose gel and extracted to perform the KLD reaction and bacterial cell transformation (no template control (NTC) amplification reaction). **(B)** Selected cultured colonies were screened by restriction digests with *Apa*I and *Kpn*I, as well as with *Kpn*I and *Not*I and 250 ng was resolved on a 0.8% agarose gel. Clones 2 and 3 had the correct banding patterns of 3 638 bp, 2 943 bp, and 1 804 bp (two *Apa*I restriction sites present); and 4 939 bp and 3 446 bp respectively. Sanger sequencing of a pmRNA_Tri-NAb_sORF_Δfurin construct confirmed that the P2A cleavage peptide was unaltered **(C)** and the F2Aopt furin sequence was correctly modified from the RKRR to RRRRRR sequence **(D)** in the Tri-NAb_sORF (forward (FOR) and reverse (REV) sequencing chromatograms are shown where available). **(E)** Western blot analysis of mammalian 293F cell expression in the presence and absence of supplemental exogenous furin demonstrated that the Tri-NAb_sORF_Δfurin had improved cleavage efficiency, removing the high molecular weight 10E8 heavy chain band (~65 kDa), and supplemental furin is no longer required for efficient endogenous furin processing. Western blots were transferred onto a nitrocellulose membrane and developed using α-Human-IgG-HRP (1:3 000). The DNA molecular weight marker (Mw) is the GeneRuler DNA Ladder Mix, ready-to-use SM0333 (Thermo Fisher Scientific, Waltham, MA, USA). The protein ladder is the Color Protein Standard Broad Range P7719S (New England Biolabs, Ipswich, MA, USA).

3.5 Biochemical and functional characterisation of expressed and purified parental and multispecific antibodies from DNA constructs.

3.5.1 Recombinant antibody expression and purification.

Following construct optimisation, and sub-cloning of all constructs into the pmRNA vector backbone, initial small-scale studies confirmed the expression of the predicted antibodies (Figures 3.1D & H, and 3.7E). For further biochemical and HIV-1 *in vitro* functional neutralisation characterisation, large-scale transfections of the parental and multispecific antibodies from the DNA constructs were achieved by transient mammalian cell transfection (293F cell line). Antibody conformations including an Fc portion (VRC01, PGT121, and 10E8v4 parental antibodies, and multispecific antibodies Bi-NAb and Tri-NAb (expressed by co-transfection (Co-T) or sORF) were purified by standard Protein A affinity chromatography. Two rounds of purification were performed on the cell culture supernatants, as antibody was still present in the flow-through after the first incubation and purification, and high antibody yields with good purity were recovered with each elution. An example of the Protein A purification procedure of Bi-NAb, and Tri-NAb Co-T and sORF (before modification of the furin sequence) as determined by SDS-PAGE and/or western blot analysis is in the Appendix (Figure B1A, C & D respectively). The parental antibodies PGT121, VRC01, and 10E8v4 displayed similar results and were not shown. The expressed Bi-scFv was purified using the C-terminal His tag IMAC, washing the resin with increasing concentrations of imidazole which yielded highly pure eluted antibody (Appendix Figure B1B). Consecutive elutions were performed by incubating the resin for 5

minutes with 200 mM imidazole elution buffer for each round of purification to maximise the Bi-scFv yields recovered (Appendix Figure B1B). All antibodies were concentrated and quantified following affinity chromatography purification to determine purified yields of expressed proteins. Expressed and purified antibodies were of the anticipated sizes (results of post-SEC purified antibodies are shown below, Figure 3.8B)

Variations in the purified yield were noted for the different antibodies, however, both parental and multispecific antibody constructs exceeded 5 mg/L purified protein yields following affinity chromatography. Purified antibody yields varied between 6.5 – 8.5 mg/L for VRC01 parental, and the Bi-scFv, Bi-NAb, and Tri-NAb sORF multispecific antibodies (Table 3.1). The 10E8v4 and PGT121 parental antibodies and the Bi-NAb and 10E8 co-transfection produced Tri-NAb (Tri-NAb Co-T) returned approximately 2-fold higher yields ranging from 15.7 – 19.5 mg/L (Table 3.1). Tri-NAb achieved better expression efficiency and yield when produced by co-transfection than from the sORF (Table 3.1) and supports our previously observed differences noted during the small-scale expression experiments which demonstrated darker western blot banding of the Tri-NAb constituents (Bi-NAb and 10E8 heavy chain) produced by co-transfection (Bi-NAb_Ho & 10E8_Kn) versus the Tri-NAb sORF construct (Figure 3.5B and 3.7E). However, the Tri-NAb Co-T was observed to have precipitated after Protein A purification, which was removed by centrifugation prior to SEC purification and thus there was less retained Tri-NAb Co-T after SEC than the Tri-NAb sORF (Table 3.1).

Table 3.1. Recombinant antibody expression and purification yields. The levels of recombinantly expressed parental and multispecific antibodies were obtained after the first-round affinity chromatography purification (Protein A chromatography for 10E8v4, PGT121, VRC01, Bi-NAb, Tri-NAb produced from co-transfection (Co-T) and Tri-NAb produced from single open reading frame (sORF) or immobilised metal-ion affinity chromatography (IMAC) (Bi-scFv). The antibodies subsequently underwent a second purification by size exclusion chromatography and the percentage retained corresponding to the monomeric conformation is indicated.

Antibody	Affinity chromatography (Protein A or IMAC)			Size exclusion chromatography	
	Amount (mg)	Volume (mL)	Yield (mg/L)	Amount (mg)	% Retained post-SEC
10E8v4	9.1	580	15.7	5.8	63.7
PGT121	3.9	200	19.5	3.1	76.9
VRC01	3.8	480	7.9	2.7	71.4
Bi-scFv	3.8	570	6.7	1.6	42.4
Bi-NAb	5.1	600	8.5	5.1	52.9
Tri-NAb Co-T	6.4	400	16.0	6.1	36.6
Tri-NAb sORF	3.9	600	6.5	3.0	50.6

The native conformational heterogeneity of the affinity-purified antibodies was assessed by SEC and the respective monomeric conformations isolated (Figure 3.8A – shaded grey boxes represent respective monomeric conformations) followed by sample concentration and re-quantification. Yields of purified, monomeric antibody conformations (percentage retained) are expressed as a percentage of total protein loaded on the SEC column (affinity chromatography purified amount) (Table 3.1). Parental antibodies, 10E8v4, PGT121, and VRC01 displayed the highest percentage retention of monomeric conformations achieving 63, 76, and 71% respectively. The multispecific antibodies experienced greater losses, with reduced monomeric conformation yields observed (Tri-NAb Co-T = 36%, Bi-scFv = 42%, Tri-NAb sORF = 50.6 % and Bi-NAb = 53% retained - Table 3.1). This is primarily a result of the parental antibodies exhibiting greater homogeneity as observed by the SEC chromatograms that present as a single peak, compared to the multispecific antibodies elution profiles that indicate the presence of higher oligomeric/aggregate conformations (Figure 3.8A). The expressed Bi-NAb and Tri-NAbs (Co-T and sORF) were prone to precipitation during the Protein A affinity chromatography, low pH elution step and post-freeze-thaw cycles for Bi-scFv antibody, and support the greater heterogeneity in the observed SEC chromatograms compared to the purified parental antibodies (Figure 3.8A). Interestingly, while the Tri-NAb Co-T displayed improved expression efficiency/yield following affinity chromatography purification compared to the sORF, lower retention percentages of the final monomeric conformation were obtained for the Co-T compared to the sORF expressed Tri-NAb post-SEC (37% and 51% retained respectively – Table 3.1). Regardless of these losses during purification, sufficient amounts of purified parental and multispecific antibodies were obtained for functional neutralisation assessment.

3.5.2 Biochemical and functional characterisation of expressed and purified parental and multispecific antibodies from DNA constructs.

The multispecific antibodies were observed to be predominantly in the monomeric conformation (highlighted in the grey box – Figure 3.8A) with the Bi-NAb and Tri-NAbs (Co-T and sORF) displaying similar retention volumes to the native monomeric parental antibodies (generally considered to be ~150kDa) (Figure 3.8A), suggesting correct assembly of native-like antibody sized proteins. The antibody molecular weights were calculated from the Kav vs log (MW) calibration curve of the protein

standards (Appendix Figure B2 and Table B1) to be: PGT121 (~196 kDa); VRC01 (~185 kDa); 10E8v4 (~136 kDa); Bi-NAb (~219 kDa), and Tri-NAbs (~187 kDa). Furthermore, the homogeneity of the single symmetrical Tri-NAb peak suggests heterologous heavy chain assembly and not merely expression of separate Bi-NAb and 10E8 antibodies which would have been distinguishable (Figure 3.8A). The Bi-scFv displayed a longer retention volume due to its smaller molecular weight (calculated to be ~60 kDa – Appendix Table B1) and inability to dimerise as it lacks the C-terminal Fc antibody portion (Figure 3.8A).

Polypeptide chain assembly and purity of the parental and multispecific antibodies were confirmed by SDS-PAGE under reducing and non-reducing conditions (Figure 3.8B). The relative migration distance of the molecular weight marker proteins were determined and plotted against the log of the molecular weight to generate a standard curve from which the molecular weights of the resolved parental and multispecific antibodies (reduced conformations only) were determined (Appendix Figure B3). As expected, the bispecific antibodies, Bi-scFv and Bi-NAb, resolve as a single polypeptide under reducing conditions of ~70 and ~95 kDa respectively (Figure 3.8B, left panel and Appendix Table B1). While the Bi-NAb visibly dimerises under non-reducing conditions (~230 kDa) due to the intact Fc region, there is no size shift between native and denatured states for the Bi-scFv due to its inability to dimerise (Figure 3.8B – right panel). The non-reduced Bi-scFv did not resolve into a distinct band, but the size demonstrates this is not due to dimerisation (Figure 3.8B – right panel). The parental antibodies (PGT121, VRC01, and 10E8v4) displayed their characteristic heavy- and light-chain banding pattern of ~60 to 64 kDa and ~30 kDa respectively (Appendix Table B1) when resolved under reducing conditions (Figure 3.8B, left panel) but assemble and dimerise natively (~200 kDa) under non-reducing conditions (Figure 3.8B, right panel). However, it was observed that 10E8v4 had a larger SEC retention volume (and smaller molecular weight) than PGT121 and VRC01, but this data is inconsistent with the SDS-PAGE analysis (Figure 3.8A and B). The delayed elution of 10E8v4 has been reported to result from non-specific interactions of the hydrophobic CDR H3 region of 10E8v4 with SEC resin (351,352). Therefore, the apparent molecular weight of 10E8v4 was adjusted to approximate the size of the other parental antibodies (~190 kDa) (Appendix Table B1) for conversion of neutralisation values into nM (see section 3.6 for details).

The expressed Tri-NAbs (Co-T and sORF) display the characteristic triple banding pattern comprising the Bi-NAb (~95 kDa), 10E8 heavy chain (~60 kDa) and 10E8 light chain (~30 kDa) (Appendix Table B1) under reducing conditions (Figure 3.8B, left panel) and assemble into a native antibody conformation of approximately 220 kDa under non-reducing conditions (Figure 3.8B, right panel). The antibody molecular weights observed were larger than predicted using an online molecular weight calculator, but similar in size to those previously described and published (Appendix Table B1). This discrepancy in the observed versus predicted molecular weights may result from glycosylation at the predicted N-linked glycosylation sites in each of the antibodies (Appendix Table B1). Additionally, all the antibodies were of high purity under reducing conditions, however, various heavy- and light-chain pairing was observed under non-reducing conditions (Figure 3.8B). Therefore, the parental and multispecific antibodies were shown to have high purity and assemble correctly into their quaternary structures and their functionality could be assessed.

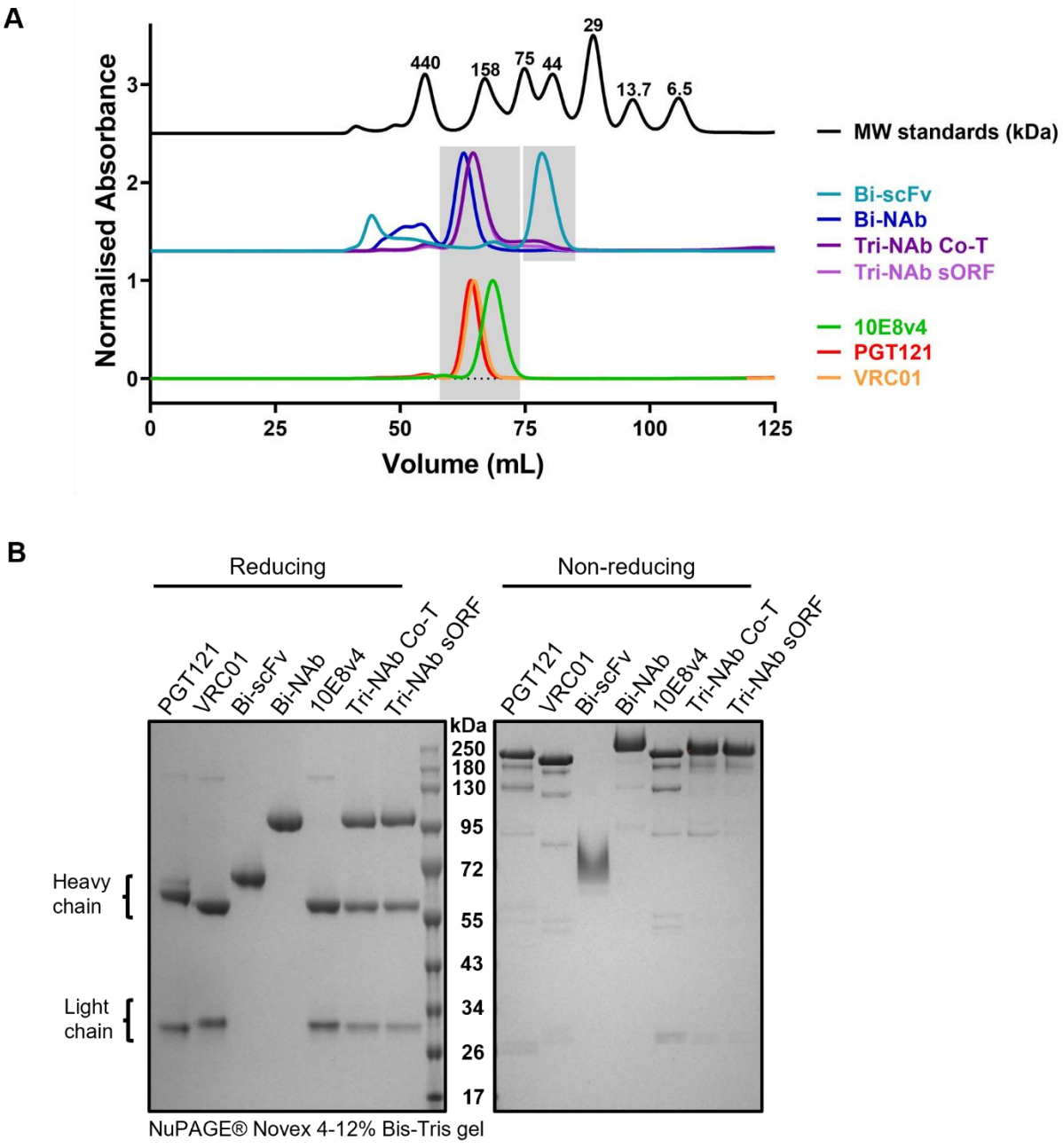


Figure 3.8. Conformational and purity assessment of expressed HIV-1 broadly neutralising parental and multispecific antibodies. (A) Size-exclusion chromatography purification (post primary affinity purification procedures), performed on a HiLoad 16/600 Superdex 200pg column, was used to interrogate the heterogeneity of the purified antibodies and isolate the monomeric conformations of each antibody relative to the molecular weight (MW) standards (~150 kDa for parental, Bi-NAb, and Tri-NAb antibodies, and ~70 kDa for the Bi-scFv as indicated by the grey shaded areas) (y-axis is staggered for chromatogram visualisation and comparison). **(B)** Assessment of antibody purity and conformation by SDS-PAGE. Five micrograms of purified recombinantly expressed antibodies were resolved on a 4-12% Bis-Tris gel under reducing (+dithiothreitol (DTT – left panel) and non-reducing (-DTT – right panel) conditions. Bands were visualised by Coomassie blue/destaining protocols. Parental antibodies (PGT121, VRC01, and 10E8v4) displayed the characteristic heavy- and light chain banding pattern (~60 and ~30kDa respectively) under reducing conditions and ~200 kDa under non-reducing conditions. The bispecific antibodies resolved as a single polypeptide when reduced (Bi-scFv ~70 kDa, Bi-NAb ~95 kDa), with only the Bi-NAb dimerising under non-reducing conditions (~230). The Tri-NAbs displayed the characteristic three banding pattern when reduced (Bi-NAb ~95 kDa, 10E8 heavy chain ~60 kDa, and 10E8 light chain ~30 kDa) that assemble to ~220 kDa under non-reducing conditions. The protein ladder is the Color Protein Standard Broad Range P7719S (New England Biolabs, Ipswich, MA, USA). Co-T, co-transfection, sORF, single open reading frame.

3.6 Functional *in vitro* neutralisation of HIV-1 was achieved by the multispecific antibodies.

Purified parental and multispecific antibodies were assessed for their ability to neutralise a panel of 17 HIV-1 pseudoviruses (inclusive of the global HIV-1 pseudovirus panel) using an in-house single-round HIV-1 pseudovirus infectivity assay. Neutralisation assays were performed using the TZM-bl reporter cell line and the percentage viral inhibition (IC50 and IC80 representing 50% and 80% inhibition percentages respectively) for the purified antibodies were determined (Figure 3.9 and Appendix Figure B4). To account for the differences in size between the antibodies, the IC50 and IC80 values were normalised to nM concentration before statistical analyses (Figure 3.9B & C). Due to the clinical significance of the IC80 values (cutoff of <1 µg/mL (normalised to the molecular weight of a ~150 kDa antibody to be ~6 nM)) to predict the clinical potency of antibodies (135), these results for breadth and potency are discussed while the IC50 results are reported in the Appendix Figure B5.

The PGT121 and VRC01 parental antibodies displayed the expected neutralisation profiles, neutralising sensitive viruses but unable to neutralise their respective resistant viruses or the dual resistant viruses (Figure 3.9A). Interestingly, VRC01 did neutralise 50% of the dual-resistant virus QH343.21M.ENV.A10 at high concentrations but could not reach 80% neutralisation at the maximal tested concentration of 25 µg/mL (Figure 3.9A). The parental antibody 10E8v4 was able to neutralise all 17 HIV-1 pseudoviruses tested which was to be expected given the viruses' sensitivity to this antibody (Figure 3.9A). Overall, PGT121 was observed to be the most potent parental antibody (median IC80 0.187 µg/mL (0.953 nM)) but least broadly neutralising, achieving only 59% coverage (Figure 3.9A, B, and C). Conversely, 10E8v4 has the broadest neutralisation coverage (100%) but the lowest potency (median IC80 2.845 µg/mL (14.92 nM)) (Figure 3.9A, B & C). VRC01 demonstrated slightly improved coverage over PGT121, 65% versus 59% neutralisation coverage, respectively, with a ~10-fold lower median IC80 potency of 1.332 µg/mL (7.185 nM) (Figure 3.9A, B, & C).

Importantly, the multispecific antibodies demonstrate neutralisation of single-PGT121 and -VRC01-resistant viruses, thus confirming the functionality of each antibody paratope in the multispecific antibody conformation and enabling the observed enhanced neutralisation breadth, with the Bi-scFv, Bi-NAb, and Tri-NAb (Co-T and sORF) achieving 94% neutralisation coverage at IC80 <100 nM (25 µg/mL) (Figure

3.9A & B). Ce2103_E8 was the only virus that was not neutralised by the multispecific antibodies despite showing sensitivity to the 10E8v4 parental (IC50 3.136 µg/mL and IC80 11.12 µg/mL) (Figure 3.9A). However, inspection of the neutralisation curves (Appendix Figure B4, Ce2103_E8) indicates that low-level neutralisation activity (0-49%) at the highest concentration tested (25 µg/mL) was obtained but fell short of achieving 50% inhibition. Similarly, reductions in multispecific antibody potency were noted when compared to the parental antibodies for the dual-sensitive and single-resistant pseudoviruses (Figure 3.9A & C). The PGT121 antibody was overall the most potent antibody tested against the selected virus panel, median IC80 0.953 nM (Figure 3.9C) but was only statistically more potent than the Bi-scFv antibody (median IC80 – 3.65 nM) (Figure 3.9C, $p=0.0066$). The multispecific antibodies gained potency from the inclusion of the PGT121 paratope, particularly against VRC01-resistant pseudoviruses, with the Bi-NAb and Tri-NAbs (Co-T and sORF) being statistically more potent ($p<0.001$) than the VRC01 parental antibody (median IC80: VRC01 - 7.185 nM, Bi-NAb – 2.209 nM, Tri-NAb Co-T – 2.869 nM and Tri-NAb-sORF – 3.639 nM (Figure 3.9 A & C)). The Tri-NAbs (Co-T and sORF) were also shown to be statistically more potent than the 10E8v4 parental antibody (median IC80 – 14.92 nM $p<0.02$) (Figure 3.9C). Multispecific antibodies displayed similar potencies (Figure 3.9C) with only the Bi-NAb and Tri-NAb (Co-T) reaching statistically better potency than the Bi-scFv ($p<0.001$ and 0.005, respectively). Similar statistically significant differences in potencies were observed for the IC50 data (Appendix Figure B5B). These data indicate that retention of parental antibody potency is not guaranteed within multispecific conformations, but that improvements in neutralisation breadth are readily attainable.

Synergistic enhanced neutralising potency of multispecific antibodies was observed against several HIV-1 pseudoviruses. The Bi-scFv and Bi-NAb conformations effectively neutralised the dual-resistant strains CAP210.2.00.E8 and QH343.21M.ENV.A10 at IC80 8.716 or 18.25 µg/mL, respectively and 3.37 or 7.36 µg/mL respectively (Figure 3.9A and Appendix B4A). In addition, the multispecific antibodies (Bi-scFv, Bi-NAb and Tri-NAbs (Co-T and sORF)) showed enhanced potency in neutralising PGT121-resistant strain 246F3 compared to parental antibodies, PGT121, VRC01 and 10E8v4 (Figure 3.9A and Appendix B4A). The Tri-NAbs (Co-T and sORF) demonstrated enhanced potency (IC80 ~0.2 µg/mL) (>5 fold)

against the CNE8 virus, compared to the parental VRC01 and 10E8v4 antibodies (1.25 and 2.28 μg/mL respectively), but also the Bi-scFv and Bi-NAb multispecifics (1.88 and 3.03 μg/mL, respectively) (Figure 3.9A and Appendix Figure B4A). These data support the notion that multispecific conformations may develop enhanced potency over the parental antibodies through their ability to engage dual or triple epitopes simultaneously thereby increasing the overall affinity through improved avidity.

Importantly, the multispecific antibodies median IC80 were all <1 μg/mL (Figure 3.9A & C) and were able to neutralise more viruses (>70%) at this concentration compared to the parental antibodies that neutralised only 24-59% of the pseudovirus panel (Figure 3.9A & B). In summary, the functionality of each antibody paratope was confirmed within each multispecific antibody conformation, resulting in improved neutralisation coverage at an IC80 of <1 μg/mL (6 nM) compared to parental antibodies. These data validate the constructs for the expression of functional multispecific antibodies and were advanced into *in vitro* mRNA production and mRNA-mediated antibody expression analyses.

A

	Pseudovirus	Subtype	Purified Antibody IC50 (µg/mL)							Purified Antibody IC80 (µg/mL)						
			Parental Antibodies			Multispecific Antibodies				Parental Antibodies			Multispecific Antibodies			
			PGT121	VRC01	10E8v4	Bi-scFv	Bi-NAb	Tri-NAb Co-T	Tri-NAb sORF	PGT121	VRC01	10E8v4	Bi-scFv	Bi-NAb	Tri-NAb Co-T	Tri-NAb sORF
Dual sensitive	25710*	C	0.018	0.379	0.110	0.051	0.108	0.096	0.102	0.048	1.166	0.369	0.124	0.292	0.231	0.260
	398F1*	C	0.017	0.259	0.521	0.032	0.077	0.011	0.012	0.044	1.088	6.284	0.094	0.186	0.094	0.065
	CE0217*	C	0.007	0.265	0.355	0.013	0.036	0.049	0.051	0.015	1.005	2.681	0.032	0.082	0.122	0.132
	CE1176*	C	0.031	3.181	1.214	0.062	0.142	0.241	0.259	0.067	10.970	4.972	0.183	0.389	0.656	0.682
	CH119*	CRF07_BC	0.037	1.013	2.436	0.092	0.183	0.341	0.324	0.102	2.921	7.514	0.222	0.513	0.811	0.915
	TRO11*	B	0.014	0.260	0.153	0.041	0.079	0.041	0.064	0.045	0.830	0.637	0.100	0.253	0.186	0.190
	X2278*	B	0.024	0.201	0.149	0.042	0.101	0.057	0.059	0.060	0.480	0.940	0.110	0.291	0.200	0.238
PGT121 Resistant	246F3*	AC Recombinant	> 25	0.297	0.605	0.047	0.121	0.151	0.147	> 25	0.850	3.816	0.133	0.334	0.399	0.406
	CNE8*	CRF01_AE	> 25	0.489	0.780	0.644	1.229	0.054	0.049	> 25	1.246	2.279	1.884	3.029	0.225	0.194
	CNE55*	CRF01_AE	> 25	0.373	0.529	1.032	2.995	0.597	0.666	> 25	1.332	2.690	2.332	9.007	2.466	2.357
	X1632*	G	> 25	0.263	0.948	0.146	0.234	0.320	0.363	> 25	0.662	2.845	0.350	0.484	0.936	1.227
VRC01 Resistant	BJOX002000*	CRF07_BC	0.031	> 25	0.910	0.056	0.138	0.166	0.160	0.076	> 25	3.432	0.171	0.352	0.524	0.511
	Du172.17	C	0.126	> 25	0.225	0.184	0.228	0.201	0.281	0.644	> 25	0.594	0.559	0.624	0.538	0.872
	Du422.1	C	0.061	> 25	0.756	0.112	0.351	0.361	0.395	0.187	> 25	2.087	0.386	0.830	0.948	0.896
PGT121/VRC01 Dual resistant	CAP210.2.00.E8	C	> 25	> 25	0.756	2.194	4.377	2.390	3.308	> 25	> 25	3.188	8.716	18.255	11.258	15.213
	QH343.21M.ENV.A10	A	> 25	18.498	2.602	0.959	1.868	1.830	2.033	> 25	> 25	11.440	3.370	7.362	5.936	7.298
	Ce2103_E8	C	> 25	> 25	3.136	> 10	> 25	> 25	> 25	> 25	> 25	11.120	> 10	> 25	> 25	> 25
Number of Viruses			17	17	17	17	17	17	17	17	17	17	17	17	17	17
Total Virus Neutralised			10	12	17	16	16	16	16	10	11	17	16	16	16	16
% Total Virus Neutralised			59	70	100	94	94	94	94	59	65	100	94	94	94	94
% Virus Neutralised <1 µg/mL			59	53	76	82	71	82	82	59	24	24	71	71	76	71
Median (µg/mL)			0.061	0.489	0.756	0.092	0.183	0.201	0.259	0.187	1.332	2.845	0.222	0.484	0.538	0.682
# Median (nM)			0.309	2.638	3.963	1.52	0.837	1.074	1.381	0.953	7.185	14.92	3.65	2.209	2.869	3.639
Geometric Mean (µg/mL)			0.449	1.731	0.622	0.158	0.346	0.235	0.259	0.818	3.655	2.653	0.418	0.903	0.731	0.784
# Geometric Mean (nM)			2.291	9.339	3.260	2.606	1.579	1.256	1.384	4.164	19.720	13.910	6.886	4.121	3.901	4.185

IC50/IC80 Values (µg/mL): 0.001 - 0.01 | 0.01 - 0.1 | 0.1 - 1.0 | 1.0 - 25.0 | > 10 | > 25

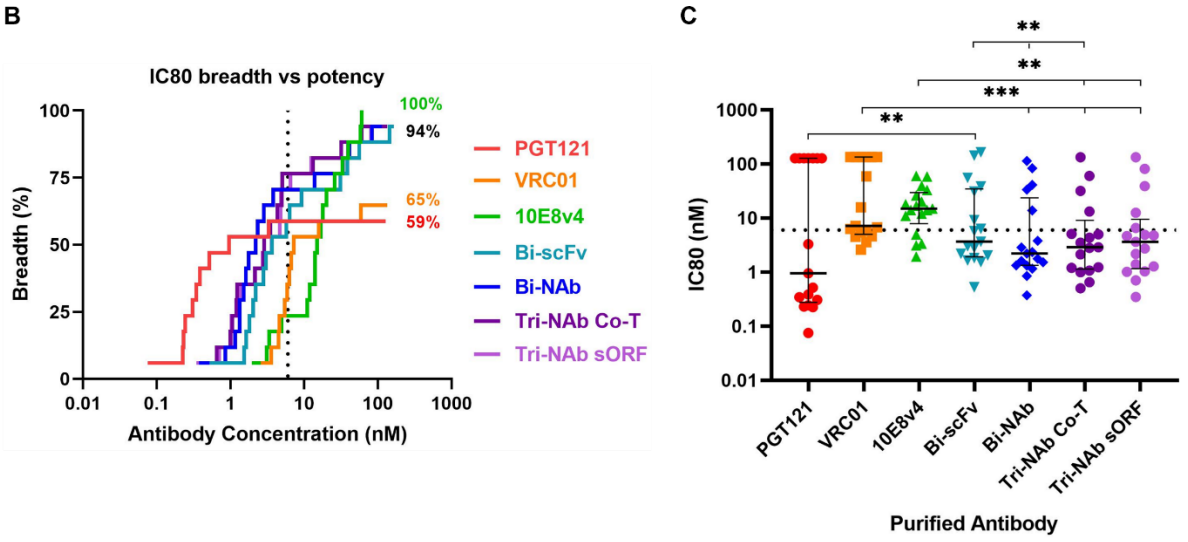


Figure 3.9. Neutralisation profile (breadth and potency) comparison of purified parental and multispecific antibodies against a panel of 17 tier 2 HIV-1 pseudoviruses. (A) IC50/IC80 neutralisation data for the purified monoclonal parental and multispecific antibodies (Bi-scFv, Bi-NAb, and Tri-NAb generated from co-transfection (Co-T) and the single open reading frame (sORF)). Parental monoclonal antibodies demonstrate greater potency against dual-sensitive viruses compared to the multispecific antibodies. However, multispecific conformations achieved enhanced neutralisation breadth, neutralising both single- and dual-resistant viruses. To account for the differences in antibody size, the IC50 and IC80 data were normalised to nM concentration before statistical analyses. **(B)** Breadth-potency curve of parental and multispecific antibody IC80 values (nM) indicating the enhanced neutralisation breadth of the multispecific antibodies over the VRC01 and PGT121 parental antibodies. **(C)** Scatterplots depicting median IC80 values and interquartile range obtained for the parental and multispecific antibodies. Median IC80 values (nM) of parental and multispecific antibodies demonstrate that the multispecific antibodies did not conserve the potency of the PGT121 parental antibody but did have enhanced potency over the VRC01 and 10E8v4 parental antibodies. The Bi-NAb and Tri-NAb Co-T were statistically more potent than the Bi-scFv. The dotted line **(B and C)** indicates the clinical cutoff IC80 of <1 µg/mL, calculated to be ~6 nM for a ~150 kDa antibody. Statistical differences were determined using a Friedman test with Dunns correction post hoc, the level of significance is indicated as follows: * <0.05, ** <0.01, *** <0.001. (A) * Denotes HIV-1 pseudoviruses from the Global Panel of HIV-1 Env reference clones (Cat# 12670), NIH AIDS Reagent Program, and are representative of the globally circulating viruses. # Indicates the median or geometric mean molar corrected antibody concentrations (nM).

3.7 IVT mRNA transcript production, purification, and expression.

3.7.1 Production and purification of IVT-mRNA expression cassettes.

IVT mRNA expression cassettes were generated from *Bpi*I linearised pmRNA DNA plasmids encoding controls for mRNA-mediated expression (GFP (4 464 bp) and Fluc (5 361 bp)) and multispecific antibodies (bispecific: Bi-scFv (5 337 bp) and Bi-NAb (6 012 bp); trispecific: Tri-NAb_sORF (8 385 bp) and for co-transfection with 10E8_Kn (5 994 bp) and Bi-NAb_Ho (6 012)) (Figure 3.10A). mRNA transcripts of the defined length (including a 46-nucleotide poly-A signal for improved mRNA transcript stability) were produced from the linearised DNA templates, denatured, and resolved on an agarose gel to analyse their integrity before purification procedures (data not shown), transcript integrity was observed to be identical pre- and post-cellulose purification – Figure 3.10B). mRNA transcripts were purified of contaminant dsRNA for increased translation efficiency of the retained ssRNA. Purified IVT mRNA samples were denatured and resolved on an agarose gel to evaluate their integrity before performing the capping reactions (Figure 3.10B). Homogenous mRNA transcripts of the anticipated defined sizes were present, GFP (961 bases), Fluc (1 858 bases), Bi-scFv (1 834 bases), Bi-NAb and Bi-NAb_Ho (2 509 bases), 10E8_Kn (2 491 bases), and Tri-NAb_sORF (4 882 bases) (Figure 3.10B), indicating the successful generation of intact mRNA transcripts.

3.7.2 Multispecific antibody expression from IVT-mRNA transcripts.

Purified mRNA transcripts were enzymatically capped (5’ Cap1 structure) which is necessary to protect the mRNA transcripts from decay during transcription. The purified mRNA transcripts were transfected into mammalian 293F cells and the mRNA-mediated expression, polypeptide chain assembly, and secretion of the multispecific antibodies into the cell culture media were confirmed by western blot under reducing and non-reducing conditions, detected with α-Penta-His-HRP (Bi-scFv) or α-Human-IgG-HRP (Bi-NAb and Tri-NAbs - Figure 3.10C & D). Analogous to the antibody banding patterns observed from DNA-expressed and purified antibodies (Figure 3.8B), the multispecific antibodies were observed to be of the anticipated molecular weights and conformations when resolved under reducing conditions (Figure 3.10C). The bispecific antibodies resolved as single polypeptides, Bi-scFv (~70 kDa) and Bi-NAb (~95 kDa), and the Tri-NAbs (Co-T and sORF) displayed the characteristic banding

pattern comprising the Bi-NAb (~95 kDa) and 10E8 heavy chain (~60 kDa) (the 10E8 light chain (~30 kDa), due to the limitations of the secondary antibody used, this light-chain was not detected) (Figure 3.10C). Although the F2Aopt furin sequence had been optimised to improve cleavage efficiency (Figure 3.7), there does appear to be a faint high molecular weight 10E8 heavy chain band (~65 kDa) present in the Tri-NAb sORF but not the Co-T (Figure 3.10C). This may be a result of reduced cleavage efficiency occurring at the F2Aopt furin sequence due to the tandem nature of successive cleavage peptides being present in the sORF construct. A low molecular weight band (~35 kDa) was detected in the Bi-NAb lane (Figure 3.10C – right side pane), while its size approximates that of antibody light chain, due to the structural conformation of the Bi-NAb single polypeptide this is unlikely to be antibody light chain. This band is also visible in the Tri-NAb lanes (Figure 3.10C -right side pane), which is postulated to be the aberrant Bi-NAb band and not 10E8 light chain since the secondary antibody does not detect light chain (Figure 3.10C – right side). The aberrant Bi-NAb band does appear to be specific for the anti-human-IgG detection, suggesting aberrant antibody-related polypeptide which is specific to the Bi-NAb construct as it was not present with the controls (GFP, Fluc nor the Bi-scFv transfected cell culture supernatants - Figure 3.10C). The mRNA-expressed Bi-scFv was not observed to dimerise as expected, with a ~70 kDa band visible under both reducing and non-reducing conditions (Figure 3.10C & D – left side pane). The mRNA-expressed Bi-NAb and Tri-NAbs assembled to their respective ~200 and ~190 kDa conformations under non-reducing conditions, with various observed combinations of heavy- and light-chain pairing (Figure 3.10D – right side pane). These data are consistent with that of the expressed and purified multispecific antibodies (Figure 3.8) and suggest that the mRNA-expressed antibodies achieved comparable assembly.

The detection intensity of the multispecific antibodies indicates that they were expressed efficiently, while the observed intensity of the Bi-NAb was the greatest. The reduced intensity of the Bi-scFv was mostly likely a result of differences in sensitivity of the respective secondary antibodies (Anti-human IgG versus Penta-His) and is not necessarily indicative of differences in expression levels between the multispecific antibodies (Figure 3.10C & D). The transfection efficiency of GFP was confirmed visually (data not shown), however no bands in the GFP or Fluc controls were observed on the western blots as expected (Figure 3.10C & D). This result was

anticipated given that neither protein is secreted into the culture supernatants (constructs lack the secretion signal peptide) nor do these proteins have the anti-human/His-tag epitopes for detection by the secondary antibodies used (Figure 3.10C & D). The GFP and Fluc controls for mRNA transfection had their expression confirmed by analysing the cell lysates for fluorescence at 507 nm and luminescence (Figure 3.10E & F respectively). GFP was efficiently expressed from mRNA transfection and was present in the cell lysate as its fluorescence was greater than 6-fold above the background fluorescence detected for the other cell lysates (Figure 3.10E). Fluc was also efficiently expressed from mRNA transfection and had luminescence detected 10 000-fold greater than the background luminescence of the other cell lysates (Figure 3.10F). Therefore, the expression and conformation of the multispecific antibodies and controls (GFP and Fluc) from mRNA transcripts were confirmed and resembled that of the multispecific antibody DNA-expressed counterparts.

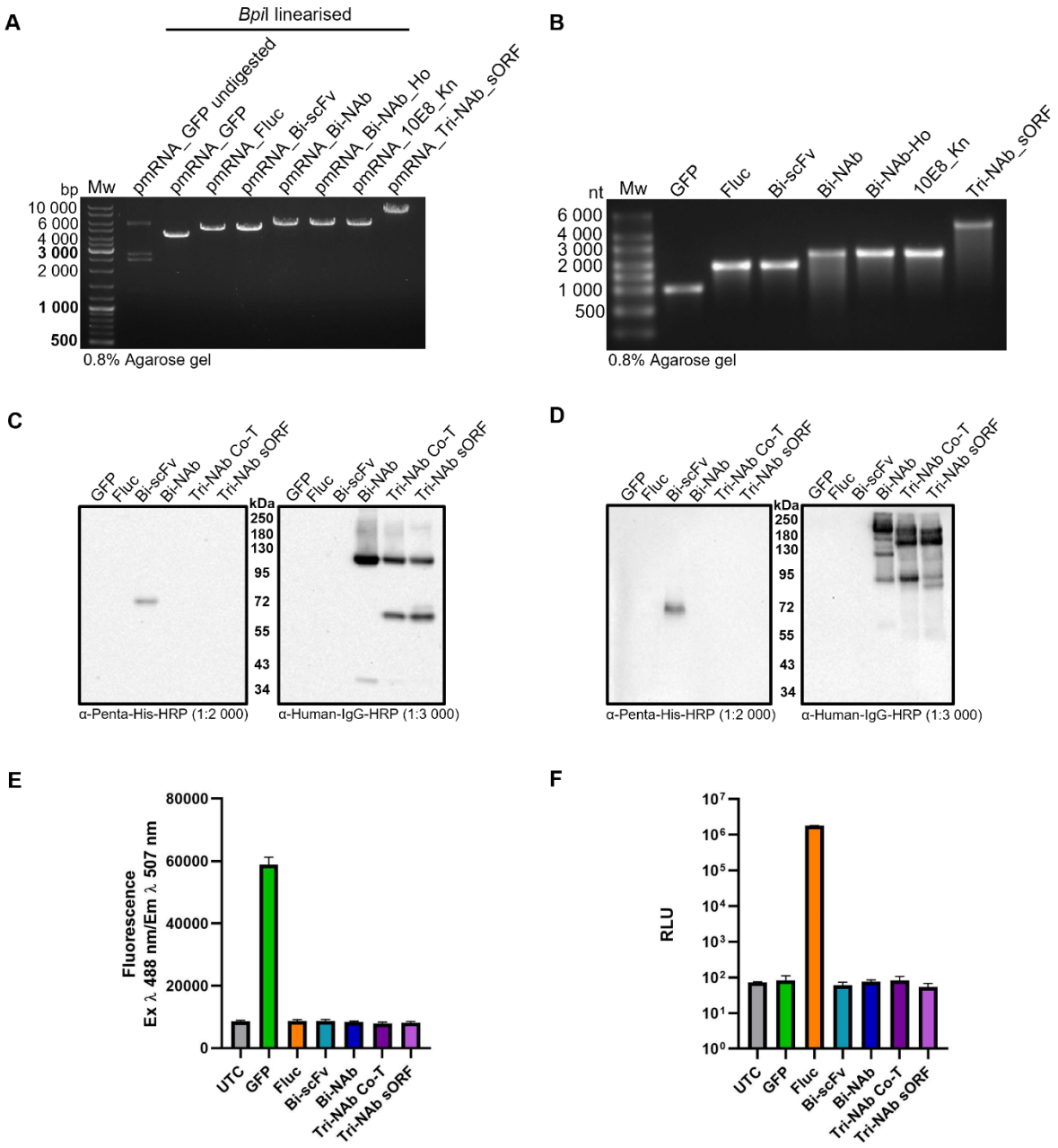


Figure 3.10. IVT-mRNA-mediated multispecific antibody expression *in vitro*. (A) Resolved multispecific antibody, green fluorescent protein (GFP), and firefly luciferase (Fluc) (controls). DNA constructs were linearised with *Bpi*I to serve as templates for mRNA *in vitro* transcription (IVT) reactions. One hundred nanograms of linearised plasmid DNA was resolved on 0.8% agarose gel. Complete digestion was achieved, linearising the DNA constructs to the anticipated sizes (GFP (4 464 bp) and Fluc (5 361 bp)) and multispecific antibodies (bispecific: Bi-scFv (5 337 bp) and Bi-NAb (6 012 bp); trispecific: Tri-NAb_sORF (8 385 bp) and for co-transfection with 10E8_Kn (5 994 bp) and Bi-NAb_Ho (6 012)). **(B)** IVT-mRNA transcripts were generated from linearised DNA, purified of contaminating dsRNA, and 500 ng was denatured prior to the integrity being evaluated by agarose gel electrophoresis on a 1% agarose gel. Homogenous mRNA transcripts of defined length were observed to be intact - GFP (961 bases), Fluc (1 858 bases), Bi-scFv (1 834 bases), Bi-NAb and Bi-NAb_Ho (2 509 bases), 10E8_Kn (2 491 bases), and Tri-NAb_sORF (4 882 bases). Purified IVT-mRNA transcripts were enzymatically capped (5' Cap1 structure), and antibody expression and secretion were confirmed by western blot analysis of unpurified mammalian cell culture supernatants under reducing (+dithiothreitol (DTT) **(C)** and non-reducing (-DTT) conditions **(D)**, following mRNA-transcript transfection in mammalian 293F cells. **(C)** The multispecific antibodies were of the anticipated sizes and conformations, analogous to that of purified antibodies from the DNA transfections – single polypeptide Bi-scFv (~70 kDA) and Bi-NAb (~95 kDa), and Tri-NAbs displaying three bands (Bi-NAb, ~95 kDa, 10E8 heavy chain (~60 kDa) and 10E8 light chain (~30 kDa). **(D)** The Bi-scFv does not dimerise (as expected) but the mRNA-expressed Bi-NAb and Tri-NAb antibodies dimerised and assembled under non-reducing conditions. Fluorescence at 488/507 nm **(E)** and luminescence (relative luminescent units (RLU)) **(F)** of mRNA transfected cell lysates were determined to confirm mRNA-expression of GFP and Fluc, respectively. Western blots were transferred onto nitrocellulose membranes and developed using α-Penta-His-Horse Radish Peroxidase (HRP) (1:2 000) for detection of the Bi-scFv (left side pane) and α-Human-IgG-HRP (1:3 000) for detection of the Bi-NAb and Tri-NAb (right side pane). The RNA ladder (Mw) is the RiboRuler High Range RNA Ladder, ready-to-use SM1823 (Thermo Fisher Scientific, Waltham, MA, USA). The protein ladder is the Color Protein Standard Broad Range P7719S (New England Biolabs, Ipswich, MA, USA). UTC, untransfected control.

3.8 Assessment of mRNA-expressed multispecific antibody functionality and inhibition.

IVT-mRNA expressed GFP and Fluc (controls for mRNA-mediated expression, negative controls for HIV-1 neutralisation) and multispecific antibodies were assessed for their ability to neutralise the previously described panel of 17 HIV-1 pseudoviruses in-house. Neutralisation assays were performed using the TZM-bl reporter cell line. IVT-mRNA multispecific antibodies would ultimately be expressed directly *in vivo* with no purification, therefore, unpurified clarified cell culture supernatant was functionally tested directly for *in vitro* neutralisation. Clarified cell culture supernatants were diluted in the assay to determine the dilution factor corresponding to 50% or 80% viral inhibition (ID50 and ID80 respectively) (Figure 3.11 and Appendix Figure B6). Again, due to the clinical significance of 80% neutralisation metrics (IC80), the ID80 results for breadth and potency are described while the ID50 results are available in the appendix (Appendix Figure B7).

The mRNA-expressed multispecific antibodies achieved high neutralisation titres (median ID80s all >100) and could be diluted up to 6 000x and still achieve 80% neutralisation in exceptional circumstances (Bi-scFv against the dual sensitive virus CE0217 - Figure 3.11A). Given the similarity of the purified multispecific antibodies (Bi-scFv, Bi-NAb, Tri-NAb (Co-T and sORF) potencies (IC80 ~3 nM – Figure 3.9A & C) the differences observed in the ID80 values (Figure 3.11A & C) largely represent differences in protein expression efficiency between the constructs. The smaller Bi-scFv construct achieved the highest relative expression and given that it has the smallest relative molecular weight, produced the highest median neutralising titre (ID80) of 1 427 and was significantly higher than the Tri-NAb produced by Co-T (ID80 362 – $p=0.0002$) or the sORF construct (ID80 166 – $p<0.0001$) (Figure 3.11A & C). The Bi-NAb mRNA construct demonstrated high expression efficiency *in vitro*, achieving a median ID80 neutralising titre of 655, however, this was only found to be significantly higher than the Tri-NAb sORF construct ($p=0.0007$) (Figure 3.11A & C). Tri-NAb sORF mRNA construct resulted in the lowest ID80 titre suggesting the lowest protein expression efficiency, with an approximate 2-fold lower expression efficiency than the co-transfection strategy (Figure 3.11A & C). This finding is consistent with the small- and large-scale DNA expression results (Figure 3.7E and Table 3.1) that

demonstrate the Tri-NAb sORF had lower expression efficiency *in vitro*. Similar statistical differences were observed for the ID50 data (Appendix Figure B7B).

The mRNA-expressed multispecific antibodies once again displayed neutralisation of both single- and dual-PGT121/VRC01-resistant viruses, thus confirming the functionality of each paratope (PGT121, VRC01 and 10E8) within the multispecific conformation and increasing their neutralisation coverage. mRNA-expressed multispecific antibodies inhibited 80% viral infectivity against 94% (Bi-scFv, Bi-NAb, and Tri-NAb Co-T) and 82% (Tri-NAb sORF) at maximum concentration (10-fold dilution) against the 17 HIV-1 viruses (Figure 3.11A & B). This slight decrease in the observed neutralisation coverage of the mRNA sORF expressed Tri-NAb was in the failure to reach 80% neutralisation cut-off for CAP210.2.00.E8 and QH343.21M.ENV.A10 dual resistant strains (Figure 3.11A & B). This indicates that the expression level of the Tri-NAb_sORF was not high enough to achieve 80% neutralisation of these viruses, since they were sensitive to neutralisation at higher concentrations from the DNA-expressed Tri-NAb_sORF (Figure 3.9A) and ID50 for these two viral strains were obtained (Figure 3.11A and Appendix Figure B7A).

Using an arbitrary dilution factor of 100x for comparison (Figure 3.11B - dotted line), the neutralisation data demonstrate that sufficient expression of all four multispecific antibodies was achieved from mRNA constructs. The unpurified cell culture supernatant could be diluted to this extent (100x times) and still inhibit 80% of virus infectivity with >75% neutralisation coverage against the 17 pseudovirus panel tested. The GFP and Fluc mRNA transfected cell controls demonstrate no neutralisation capacity of HIV-1 pseudoviruses as expected (Figure 3.11).

Therefore, in summary, the multispecific antibodies were successfully expressed from IVT-mRNA transcripts, retaining the functional paratopes of each antibody, at sufficiently potent titres to achieve enhanced neutralisation breadth against the viruses tested. Furthermore, the mRNA-expressed multispecific antibodies had a neutralisation coverage comparable to that achieved by the DNA-expressed and purified multispecific antibodies, thus proving the validity of this antibody expression platform *in vitro*.

A

	Pseudovirus	Subtype	Unpurified mRNA Expressed ID50						Unpurified mRNA Expressed ID80					
			Controls		Multispecific Antibodies				Controls		Multispecific Antibodies			
			GFP	Fluc	Bi-ScFv	Bi-NAb	Tri-NAb Co-T	Tri-NAb sORF	GFP	Fluc	Bi-ScFv	Bi-NAb	Tri-NAb Co-T	Tri-NAb sORF
Dual sensitive	25710*	C	< 10	< 10	4997	2292	1105	708	< 10	< 10	1903	824	384	253
	398F1*	C	< 10	< 10	11761	5367	3532	2250	< 10	< 10	3887	1769	1281	681
	CE0217*	C	< 10	< 10	20850	6540	2673	1603	< 10	< 10	6247	2111	1069	562
	CE1176*	C	< 10	< 10	4911	2084	839	408	< 10	< 10	1986	850	361	166
	CH119*	CRF07_BC	< 10	< 10	3103	1257	704	420	< 10	< 10	1374	560	327	194
	TRO11*	B	< 10	< 10	10660	3637	1846	1119	< 10	< 10	3912	1445	677	380
	X2278*	B	< 10	< 10	8871	4523	1755	1020	< 10	< 10	3023	1255	569	287
PGT121 Resistant	246F3*	AC Recombinant	< 10	< 10	5424	3285	1305	660	< 10	< 10	1348	772	297	153
	CNE8*	CRF01_AE	< 10	< 10	600	503	971	949	< 10	< 10	232	153	215	139
	CNE55*	CRF01_AE	< 10	< 10	75	39	44	40	< 10	< 10	26	12	12	12
	X1632*	G	< 10	< 10	2532	1303	560	305	< 10	< 10	954	509	177	106
VRC01 Resistant	BJOX002000*	CRF07_BC	< 10	< 10	4724	1799	1023	692	< 10	< 10	1853	655	388	231
	Du172.17	C	< 10	< 10	4489	2076	1879	966	< 10	< 10	1695	795	653	378
	Du422.1	C	< 10	< 10	3152	1008	694	297	< 10	< 10	1427	433	278	103
PGT121/VRC01 Dual resistant	CAP210.2.00.E8	C	< 10	< 10	242	131	107	67	< 10	< 10	61	34	24	< 10
	QH343.21M.ENV.A10	A	< 10	< 10	272	138	60	31	< 10	< 10	88	33	13	< 10
	Ce2103_E8	C	< 10	< 10	< 10	< 10	< 10	< 10	< 10	< 10	< 10	< 10	< 10	< 10
Number of Viruses			17	17	17	17	17	17	17	17	17	17	17	17
Total Virus Neutralised			0	0	16	16	16	16	0	0	16	16	16	14
% Total Virus Neutralised			0	0	94	94	94	94	0	0	94	94	94	82
% Virus Neutralised >100			0	0	88	88	82	76	0	0	76	76	76	76
Median			< 10	< 10	4489	1799	971	660	< 10	< 10	1427	655	327	166

ID50/ID80 Values: > 10 000 | 10 000 - 1 001 | 1 000 - 101 | 100 - 10 | < 10

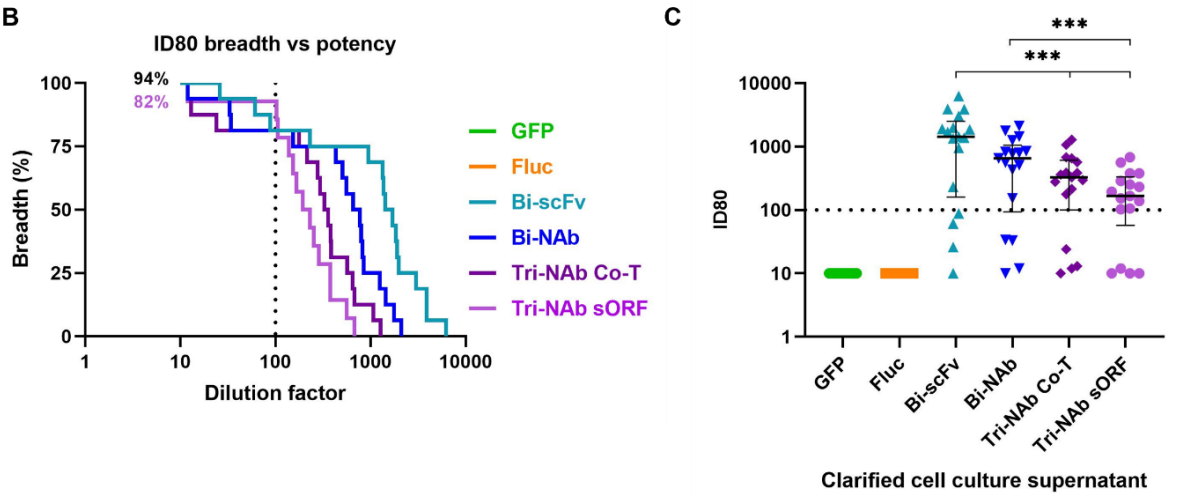


Figure 3.11. Neutralisation profile (breadth and potency) comparison of IVT-mRNA expressed multispecific antibodies against a panel of 17 tier 2 HIV-1 pseudoviruses. (A) ID50/ID80 depicted neutralisation data for IVT-mRNA expressed multispecific antibodies (Bi-scFv, Bi-NAb, and Tri-NAb generated from co-transfection (Co-T) and the single open reading frame (sORF), and controls Green Fluorescent Protein (GFP) and firefly luciferase (Fluc). Multispecific conformations achieved enhanced neutralisation breadth, neutralising both single- and dual-resistant viruses. **(B)** Breadth-potency curve of controls and multispecific antibodies ID80 values indicating the broad neutralisation breadth of the multispecific antibodies. **(C)** Scatter plots depicting median ID80 values obtained for the multispecific antibodies. Median and interquartile ranges (IQR) are shown. Statistical differences were determined using a Friedman test with Dunns correction post hoc, the level of significance is indicated as follows: * <0.05, ** <0.01, *** <0.001. (A) * Denotes HIV-1 pseudoviruses from the Global Panel of HIV-1 Env reference clones (Cat# 12670), NIH AIDS Reagent Program, and are representative of the globally circulating viruses. The dotted line indicates an arbitrary dilution factor of 100x, used for comparison of neutralisation data.

3.9 Relative quantification of the mRNA-expressed multispecific antibodies.

Having demonstrated that mRNA-mediated expression of multispecific antibodies could be achieved *in vitro*, we were interested in quantifying the expression of antibodies into the cell culture media from each construct. To do so, antibody titres of the mRNA-expressed multispecific antibodies were quantified relative to purified multispecific antibody prepared standards using an in-house HIV-1 Env (gp120 founder virus C monomer) specific binding ELISA, densitometry analysis of known antibody standards and unknown cell culture supernatant samples detected by western blotting, and the direct calculation based on the IC50 and ID50 data reported (Table 3.2). HIV-1 Env $gp120_{FVC}$ M was recombinantly expressed and purified using a lectin-affinity chromatography procedure (Appendix Figure B8A) followed by SEC to isolate the monomeric fraction (Appendix Figure B8B) and purified $gp120_{FVC}$ M glycoprotein was used in the ELISA.

The clarified, unpurified cell culture supernatant obtained following mRNA transfection (as was used in the neutralisation assays) was diluted 50x and 100x and quantified relative to each antibody standard curve (Appendix Figure B9). When correcting for the dilution factor, the calculated concentrations were similar between the dilutions, indicating the precision of the quantification. The bispecific IVT-mRNA constructs (Bi-scFv and Bi-NAb) achieved higher antibody expression than the Tri-NAb constructs (Co-T and sORF) (Table 3.2). The Bi-NAb achieved the highest concentration (~22 µg/mL) and thus the best expression, followed by the Bi-scFv (~14 µg/mL) and the Tri-NAbs had the lowest expressed concentration (Co-T, ~10 µg/mL; sORF, ~7 µg/mL) (Table 3.2). However, these low values contradict the neutralisation titre data obtained (Figure 3.11) and suggest an underestimation of antibody concentration by 15-30-fold.

As an alternative method, quantities of IVT-mRNA expressed antibodies were estimated by western blot detection and densitometry measurements relative to purified antibody standards on known concentration (Appendix Figure B10 – standard curves were not available for export). Purified multispecific protein standards of known loaded amounts were resolved against cell culture supernatant (diluted 1, 2, and 4 times) and transferred onto nitrocellulose membranes for analysis (Appendix Figure B10). Quantification by densitometry was less precise than the ELISA, as once the initial dilution was corrected for, the final concentrations varied by as much as 2.3 to

3.4-fold when comparing undiluted (1x) to the 4x diluted samples (Table 3.2). The Bi-scFv had the highest average concentration (across dilution points) (~312 µg/mL), followed by the Bi-NAb (~210 µg/mL) and the Tri-NAbs (Co-T, ~152 µg/mL; sORF, ~121 µg/mL) (Table 3.2). These estimated starting concentrations matched the neutralisation titre data obtained (Figure 3.11). However, the high variability between dilutions was concerning. In an effort to consolidate the data, the mRNA-expressed multispecific antibody concentrations were also determined from their *in vitro* neutralisation data by multiplying the IC50 for each purified multispecific antibody/virus combination by the ID50 of the corresponding clarified cell culture supernatant. Concentrations were averaged and reported in Table 3.2. For this calculation, an assumption is made that the unpurified recombinantly IVT-mRNA-expressed multispecific antibodies shared the assembled conformations and neutralisation functionality of the DNA-expressed and purified multispecific antibodies. Consistent with the densitometry quantification method, the Bi-scFv had the highest mean concentration (~352 µg/mL), followed by the Bi-NAb (~344 µg/mL) and the Tri-NAbs which were ~157 µg/mL for the Co-T and ~100 µg/mL for the sORF (Table 3.2). These concentrations were more closely quantified by densitometry than the ELISA (Table 3.2). Although there were discrepancies with the quantification results, the pattern of expression levels observed was similar, with bispecific antibodies (Bi-scFv and Bi-NAb) having the highest expression levels while the Tri-NAbs were consistently lower (Table 3.2). Additionally, the expression achieved from mRNA transfection for the Tri-NAb sORF was lower than that achieved by the Tri-NAb Co-T (Table 3.2), which is consistent with the lower ID80 neutralisation titres obtained (Figure 3.11) and is analogous to the observed expression levels achieved from DNA transfection (Table 3.1). Final mRNA-expressed multispecific antibody concentrations are estimated to range between ~150-350 µg/mL for the Bi-scFv, ~125-340 µg/mL for the Bi-NAb, and 90-155 µg/mL or 70-100 µg/mL for the Co-T or sORF expressed Tri-NAbs, respectively (Table 3.2).

Regardless of the titres, the mRNA-expressed multispecific antibodies were of the correct assembled conformations, retained the functionality of each paratope and displayed equal neutralisation coverage of the HIV-1 pseudovirus panel to that of the DNA-expressed and purified multispecific antibodies. The levels of mRNA-expressed multispecific antibodies were sufficiently high enough to be diluted >100x and achieve

80% viral inhibition (section 3.8, Figure 3.11C). In summary, these data overall confirm the successful expression of multispecific antibodies from IVT-mRNA constructs *in vitro* result in sufficient titres of functional multispecific antibodies to inhibit viral infection.

Table 3.2. Relative quantification of the concentration of mRNA-expressed multispecific antibodies. Multispecific antibody concentrations were measured by ELISA and western blot (WB) densitometry analysis. The clarified cell culture supernatant was diluted, and the concentration was determined from the respective purified antibody standard curves for each respective method and corrected for the dilution factor (individual dilution point values and the average between the dilution points are shown). The amount (µg) of multispecific antibody in the 9.64 µL loaded (excluding the volume of the sample buffer) quantified by densitometry was converted into the concentration which was corrected for the dilution factor. The concentrations were also determined from the *in vitro* neutralisation values by multiplying the paired virus per multispecific antibody IC50 values by the ID50 values of the mRNA-expressed clarified cell culture supernatant. The average neutralisation concentration per multispecific antibody is reported.

		Bi-scFv	**Bi-NAb**	**Tri-NAb Co-T**	**Tri-NAb sORF**
ELISA (µg/mL)	50x	13.62	21.03	10.07	721
	100x	15.12	24.1	9.43	6.97
	Average concentration	**14.37**	**22.57**	**9.75**	**7.09**
	Standard deviation	1.06	2.17	0.45	0.17
Western blot densitometry (µg/mL)	1x	149.47	126.77	93.67	69.03
	2x	267.59	195.2	141.23	109.61
	4x	519.73	305.24	220.76	184.97
	Average concentration	**312.26**	**209.07**	**151.89**	**121.2**
	Standard deviation	189.13	90.04	64.21	58.83
Neutralisation IC50 x ID50 (µg/mL)	**Average concentration**	**352.4**	**344.2**	**157.1**	**101.3**
	Standard deviation	161	135.3	95.06	65.33

Chapter 4. Discussion.

To end the HIV-1 pandemic, alternative long-lasting biomedical treatment and prevention strategies are required. BNAbs have shown great promise at both reducing viraemia and preventing HIV-1 infection in various animal models and human clinical trials. However, it is clear that combinations of bNAbs are required for effective treatment as they limit viral escape due to antibody selective pressure, whilst offering broader coverage as a preventative strategy to counter the diverse circulating viral swarms within the human population. The major drawback of bNAb combination therapy is the associated increased production cost. Multispecific antibodies are engineered to comprise two or more HIV-1 entry-targeting moieties in a single molecule with the aim of achieving increased potency and neutralisation breadth, while also reducing the cost of antibody production for combination antibody therapy. *In vitro* transcribed (IVT) mRNA expression cassettes that encode multispecific antibodies that achieve clinically relevant antibody titres *in vivo* may represent a further cost-saving benefit. Therefore, HIV-1 multispecific antibodies with enhanced neutralisation breadth combined with IVT mRNA expression could present a cost-effective biomedical intervention strategy for therapeutic or prophylactic antibody delivery.

This dissertation describes the generation of multispecific antibody encoding DNA constructs (Bi-scFv, Bi-NAb, and Tri-NAb), compatible with IVT-mRNA transcript production and details the multispecific antibody expression, biochemical characterisation and neutralisation of clinically relevant HIV-1 pseudoviruses *in vitro*.

4.1 Generation of multispecific antibody expression constructs.

The multispecific antibody sequences were designed as described by Steinhardt *et. al*., 2018 (200). These constructs were selected since the conformation had been rationally designed and optimised to achieve inter-protomer crosslinking using the PGT121 and VRC01 epitopes and demonstrated enhanced neutralisation breadth and coverage (200). The tandem single chain variable fragment (scFv) topology enables expression of the Bi-scFv and Bi-NAb conformations from a sORF making them more amenable to an IVT-mRNA delivery strategy. The Bi-scFv and Bi-NAb DNA constructs were successfully generated and expression of the Bi-scFv and Bi-NAb conformations were confirmed *in vitro* (Figures 3.1D & H). The Bi-NAb construct required synonymous mutation of the *Bpi*I restriction site within the CH2 domain to eliminate

premature truncation and ensure compatibility with the IVT-mRNA reaction (Figure 3.2).

Similarly, the Tri-NAb construct was generated as described by Steinhardt *et al*. (200) by the heterodimeric assembly of the Bi-NAb and the 10E8 antibody heavy- and light-chains through the specific introduction of complimenting Fc region knob-into-hole mutations following co-transfection with the respective antibody plasmids. In addition, we describe the generation of a novel sORF encoding Tri-NAb construct sequence which we hypothesised to be more favourable for mRNA delivery than a co-transfection (Co-T) strategy.

Both Tri-NAb expression strategies (Co-T vs sORF) rely on heterologous heavy antibody chain assembly *in situ*, using the complimenting knob-into-hole mutations. Our co-transfection strategy differed slightly from that originally reported by Steinhardt *et al*., in which the authors used a three-plasmid co-transfection procedure to express the Tri-NAb (Bi-NAb hole, 10E8 knob heavy chain and 10E8 light chain encoding plasmids respectively) (200). The pMin_10E8_Kn construct utilised within this study encodes the 10E8 heavy chain (containing the knob mutations) and light chain in tandem as a sORF, separated by a furin protease/F2A self-cleaving peptide sequence according to the strategy originally developed by Balazs and colleagues (219,220). This strategy has been successfully used to express bNAb and bi-specific bNAbs *in vitro* and *in vivo* (191,202,219,220).

We describe the successful generation of the novel Tri-NAb sORF construct by assembling the 10E8_Kn encoding region downstream of the pmRNA_Bi-NAb_Ho encoding region, interspaced with the modified furin protease cleavage site (RRRRRR) and P2A self-cleaving peptide sequence (Figure 3.4). Small-scale expression of the Tri-NAb was achieved using both the Co-T and sORF strategies, which was confirmed by western blot detection of the secreted Bi-NAb_Ho and 10E8 heavy chains into the culture media (Figure 3.5 A & B, respectively). The 10E8 light chain could not be detected in western blots using the anti-human Fc-specific secondary antibody (as anticipated), and consistent with the 10E8v4 parental bNAb expressed by co-transfection of separate heavy and light encoding constructs in which the light chain fragment was also not detected (Figure 3.5 A & B). Based on our laboratory's previous experience with bi-specific antibody expression using a KIH

heterologous heavy chain assembly strategy (iMAb_Ho and 10E8_Kn included as known assembly control (191,202)), detection of the individual expressed constituents (Bi-NAb_Ho and 10E8_Kn) suggests successful heavy chain assembly. This was confirmed by SEC and SDS-PAGE analysis under reducing and non-reducing conditions (Figure 3.8).

It was noted, however, that knob-knob Fc or hole-hole Fc homodimeric heavy chain assembly and secretion can occur when transfected alone, albeit in lower concentration (based on band intensity) to the heterologous knob-hole heavy chain assembly (Figure 3.5 A & B – lower band intensity of Bi-NAb_Ho and 10E8_Kn only transfections compared to Bi-NAb_Ho & 10E8_Kn or Tri-NAb_sORF). The formation of knob-knob and hole-hole Fc fragment homodimers upon single vector expression, regardless of the presence or absence of the S354C and Y349C cysteine mutations that enforce correct heterodimer assembly, has been described previously (176). Homodimer knob-knob Fc was determined to be structurally altered and destabilised, thus suggesting a disadvantage in formation compared to hole-hole homodimers (176). However, this did not translate to the expression observed in this study where the homodimer 10E8_Kn appeared to display higher expression levels compared to homodimer Bi-NAb_Ho (Figure 3.5D).

In addition, the small-scale Tri-NAb expression analysis by co-transfection or the sORF construct revealed the presence of an additional higher molecular weight band above the 10E8 heavy chain. We were able to demonstrate that this was a result of inefficient proteolytic cleavage by endogenous furin (Figure 3.5D). Performing co-transfections with supplemental exogenous furin improved processing and resulted in the removal of the higher molecular weight 10E8 heavy chain band (Figure 3.5D). It has previously been shown that fusion of the F2A cleavage peptide tag results in a 2-3 kDa shift in the migration pattern of an eGFP reporter protein (311). This is consistent with the shift in migration pattern observed for the 10E8 heavy chain, indicating that the furin sequence was not cleaved efficiently thus the furin-F2Aopt peptide (~3.4 kDa) remained attached to the C-terminus of the 10E8 heavy chain (Figure 3.5A & B). This 10E8 heavy chain-F2Aopt fusion peptide band was not removed during Tri-NAb Protein A purification, however, SEC was not performed, and it is unclear whether SEC would have removed this high molecular weight 10E8 heavy chain (Appendix Figure B1C & D). Additional cleavage inefficiencies occurring in the 10E8 F2Aopt sequence

were also noted. Cleavage failure of both the furin and F2Aopt resulted in a 10E8 heavy-light chain fusion protein of 95 kDa (10E8 HC (61k Da) + 10E8 LC (31 kDa) + F2A (3.4 kDa)) (Figure 3.5 A & B, faint band observed below the Bi-NAb_Ho in the Bi-NAb_Ho & 10E8_Kn co-transfection production of the Tri-NAb). These observed banding patterns resulting from incomplete cleavage at respective furin or 2A recognition sequences are consistent with previous findings (353,354).

Although not readily observable by western blot analysis of small-scale expression experiments, large-scale expression, purification, and concentration of the Tri-NAb displayed an observed N-terminus F2Aopt-tag-10E8 light chain fusion protein (~35 kDa) (Appendix Figure B1C & D). Given the current understanding of the secretory pathway, the presence of the fusion F2Aopt-tag-10E8 light chain peptide is surprising in that it suggests an intact secretion signal peptide (SP) (including the F2Aopt sequence fusion) on the mature, secreted polypeptide, resulting in the presence of an additional higher molecular weight (+ ~5 kDa) light chain (Appendix Figure B1C & D). In mammalian cells, the SP of nascent polypeptides are co-translationally recognised and bound by the signal recognition particle (SRP) while they are still being synthesised by the ribosome (355,356). This induces a translation stalling to provide time for the SRP to deliver the nascent polypeptide chain and associated ribosome to the endoplasmic reticulum (ER) protein translocon (355,356). After arriving at the translocon and before the protein is exported across the ER membrane (which prevents early cytosolic folding of a secreted protein), the SP is cleaved (355,357,358), and polypeptide translation and synthesis resumes (355). Once in the ER, initial glycosylation and protein folding occur, and proteins are exported to the Golgi complex for maturation and secretion (355). Thus, if furin cleavage occurs but F2Aopt processing does not, and the F2Aopt peptide remains fused to the N-terminus of the 10E8 light chain SP (Figure 3.5C), this entire sequence should be removed from the mature secreted protein by the secretory pathway as described above. In this way, only mature (devoid of the SP) 10E8 light chain should be secreted into the cell culture. An extensive review of the literature revealed the presence of intact SPs on both antibody heavy and light chains following excision from SDS-PAGE gels and analysis by liquid chromatography mass-spectrometry/mass-spectrometry (LC-MS/MS) (353). This suggests the possibility that the SP may remain attached to the secreted antibody,

supporting our explanation for the presence of this observed high molecular weight 10E8 light chain band.

During the construct design and *in vitro* optimisations, we were made aware of the furin cleavage inefficiency of the 10E8 heavy chain due to our ability to detect this aberrant processing by western blotting. Incorrect processing of antibody heavy- and light-chain polypeptides from reduced cleavage efficiency is unfavourable as it has been shown to result in aggregation of expressed mAbs (354). While these aggregates can readily be removed by protein purification and clarification methods, mRNA expression directly *in vivo* necessitates the expression of homogenous, monomeric antibodies as there is no opportunity for purification. Thus, optimising the endogenous processing of these interspacing cleavage peptide sequences (furin-F2A) is likely to be an important consideration when advancing such strategies into preclinical and clinical testing.

The furin recognition sequence in the 10E8_Kn-F2Aopt sequence was modified to six consecutive arginine residues (RRRRRR – previously shown to have improved cleavage efficiency (306)) which resolved this processing inefficiency by endogenous cellular furin, and supplemental exogenous furin was no longer required (Figure 3.6B and Figure 3.7E). Therefore, large-scale expression of the Tri-NAb from both Co-T (pmRNA_Bi-NAb_Ho and pmRNA_10E8_Kn) and the pmRNA_Tri-NAb_sORF was performed using constructs with the modified F2Aopt furin sequence. The 10E8 light chain aberrations could not be detected by western blot during initial small-scale expression and were only retrospectively observed following initial Protein A purification once the laboratory work had been completed. Furthermore, despite the advanced nature of the expression of antibodies from constructs incorporating the F2Aopt sequence (154,219,220,228), none of these processing inefficiencies have been documented. Future improvements to or replacement of the F2Aopt sequence may be considered to improve cleavage efficiency. It should be noted that there were no observed furin or P2A processing inefficiencies in the P2A cleavage peptide that separates the Bi-NAb_Ho from the 10E8_Kn encoding region in the Tri-NAb sORF construct. Thus, replacement of the F2Aopt with P2A may resolve the processing issues.

4.2 Recombinant antibody expression, purification, and biochemical characterisation.

The multispecific antibodies were biochemically characterised and their conformation and functional *in vitro* neutralisation were evaluated and compared to the parental antibodies (PGT121, VRC01, and 10E8v4) before progressing to IVT-mRNA expression. This provided validation of the design and functionality of the multispecific antibodies from DNA for comparison with subsequent mRNA-mediated expression.

Parental and multispecific antibodies were recombinantly expressed by large-scale mammalian cell transfection and purified by standard affinity chromatography procedures. PGT121, the Bi-NAb and Tri-NAb antibodies were prone to precipitation upon elution in the low pH elution buffer. Alternative elution buffers were explored including; 0.1 M citric acid buffer, with or without 0.5 M arginine, and increasing the pH to 3.5 (original pH 2.7) that have previously been described to reduce protein precipitation (359–361). No discernible reduction in observed precipitation or improved antibody yield was achieved with these buffers (data not shown). Improvement was achieved by keeping all purification solutions chilled, using a 0.15 M NaCl 1x PBS wash buffer, and eluting in larger volumes of a 0.15 M NaCl, 5% glycerol-containing elution buffer with a moderately higher pH of 3.0. Additionally, all the purified antibodies were noted to precipitate upon freeze-thaw cycles which was improved by supplementing the DPBS solution with 25% glycerol prior to storage.

Antibodies that are prone to precipitation may present a concern *in vivo*. A study estimating the *in vivo* immunogenicity risk of antibodies with poor solubility that precipitate at neutral pH *in vitro* determined that antibody aggregation led to retention at the injection site, resulting in macrophage association and germinal centre localisation with a delay in antibody draining to the lymph nodes (362). However, no overall impact on the immune response in the lymph nodes or systemic exposure of the antibody was noted and it was concluded that poor solubility antibody precipitation delivered subcutaneously may not be of immunogenicity concern (362). However, this apparent lack of immunogenicity of precipitated antibody was reported with subcutaneous delivery, and expressed, circulating antibody aggregates may reduce the efficacy of the antibody therapeutic or have additional clinical impacts. It is unclear whether the multispecific antibodies described herein would precipitate or aggregate in the physiological environment without the initial sudden drop in pH (during the

Protein A elution) triggering the instability. The stability and aggregation of multispecific antibodies infused or endogenously expressed from IVT-mRNA transcripts would have to be explored *in vivo* going forward.

The multispecific antibodies, Bi-scFv, Bi-NAb, and Tri-NAb-sORF displayed reduced expression efficiency and yield (~7-9 mg/mL) compared to the 10E8v4 and PGT121 parental antibodies (16-20 mg/mL) that had the best expression but were similar to the VRC01 parental antibody (~8 mg/mL) (Table 3.1). Interestingly, the expression of the Tri-NAb by co-transfection (Co-T) outperformed the Tri-NAb sORF transfections, by approximately 2.4-fold (Tri-NAb sORF (6.5 mg/L) and Tri-NAb Co-T (16.0 mg/L)) and was comparable to the yield generated by the 10E8v4 and PGT121 parental antibodies (Table 3.1). However, greater precipitation of the Tri-NAb expressed by Co-T was observed during the Protein A chromatography elution step and again when thawed prior to SEC, which greatly reduced the percentage retained after SEC (Co-T (~36%) versus sORF (~50%) - Table 3.1). These antibody yields were sufficient for our purposes, although they were modest compared to other published data. Using the optimised transfection method that was utilised here, large-scale (5 L) expression in a bioreactor achieved chimeric B72.3 monoclonal antibody titres of ~40 mg/L after 72 hours and a maximum of ~100 mg/L after six days (344). Although the type of antibody and scale of production impact the expression and yield, these reported titres are much higher than those achieved in this study. However, small-scale production of HIV-1 trispecific antibodies reported in the literature yielded 5-10 mg/mL (185), which is similar to the expression of the multispecific antibodies reported in this study. The Tri-NAb had better expression efficiency and yield (2.4-fold difference) when produced by co-transfection than from the sORF, which was more profound in DNA expression than from mRNA expression but the proposed reasoning for this will be discussed below.

The multispecific antibodies were observed to be primarily in the monomeric form, but aggregates were noted, particularly for the Bi-scFv and Bi-NAb antibodies which were removed by sample fractionation following SEC. Additionally, the Tri-NAb Co-T precipitated upon thawing and the precipitate was removed by centrifugation prior to SEC resolution, and thus a large aggregate peak is not visible on the SEC profile (Figure 3.8A). The multispecific antibodies displayed similar retention volumes to the native monomeric parental antibodies, which suggests the correct assembly of native-

like antibody-sized proteins. Furthermore, the homogeneity of the single resolved Tri-NAb peak suggests heterologous heavy chain assembly and not merely expression of separate Bi-NAb and 10E8 antibodies (Figure 3.8A). Encouragingly, the expressed Tri-NAbs (Co-T and sORF) produced identical SEC separation profiles and SDS-PAGE banding patterns, confirming the successful expression and processing of the novel Tri-NAb sORF construct generated for this study. The discernible difference in the Bi-NAb and Tri-NAb SEC profiles is likely representative of the heterologous heavy chain assembly of the Tri-NAb construct which presumably allows for a slightly more compact conformation than the homodimeric Bi-NAb heavy chain assembled bispecific conformation (Figure 3.8A). The formation of homodimer by-products (knob-knob or hole-hole) was consistently noted during small-scale expression studies when Bi-NAb_Ho or 10E8_Kn constructs were transfected alone (Figure 3.5A, B, & D, Figure 3.6B, and Figure 3.7E) and may reduce the efficiency of heterodimerisation and potentially threaten the homogeneity of the expressed Tri-NAb antibodies. However, the homogeneity of the single SEC-resolved Tri-NAb peak suggests the presence of uniform conformation through heterologous heavy chain assembly (Figure 3.8A). There was no indication of separate Bi-NAb and 10E8 homodimer antibody expression that would be anticipated to have slightly different elution volumes (additional peaks corresponding to either the Bi-NAb or 10E8v4 elution peaks) but no multiple peak profile was observed (Figure 3.8A). Heavy- and light-chain constituents of multispecific antibodies (Bi-scFv, Bi-NAb, Tri-NAb (Co-T and sORF)) were confirmed by reducing and non-reducing SDS-PAGE analyses (Figure 3.8B).

The larger retention volume observed during elution of 10E8v4 is consistent with previously reported results by our group (191), and others (including comparisons with VRC01) (320,352). The intrinsic hydrophobic nature of the CDR H3 region of 10E8v4 required for paratope engagement has been noted to non-specifically interact with SEC resin, artificially increasing its retention volume and resulting in the apparent smaller molecular weight. The comparative SDS-PAGE analysis were not performed in these studies (351,352) but has previously been reported by our research group (191). Therefore, the apparent molecular weight of 10E8v4 was adjusted to approximate that of the other parental antibodies for conversion of neutralisation data to nM. This non-specific hydrophobic interaction with the SEC resin, mediated through the 10E8 CDR H3 within the purified Tri-NAb antibody may also occur, artificially

reducing the estimated molecular weight. Although the expressed Tri-NAbs displayed a slightly smaller molecular weight compared to the Bi-NAb as determined by SEC (Figure 3.8A), these estimates are consistent with the SDS-PAGE analysis (Figure 3.9B). Based on the generated data we can neither confirm nor refute the potential contribution of the 10E8-mediated hydrophobic interaction in altering the Tri-NAb molecular weight estimate. Therefore, the decision was made not to adjust the molecular weight of the Tri-NAbs, as was done for the 10E8v4 parental antibody.

Slight discrepancies in the observed molecular weights of the parental and multispecific antibodies were noted when compared to the predicted molecular weights based on the amino acid sequence (Appendix Table B1), which may have been as a result of post-transcriptional glycosylation. IgG mAbs have conserved glycosylation at the asparagine position 297 of the Fc region CH2 domain (363,364) and approximately 10-20% of Fab binding regions contain N-linked glycosylation sites (172). A single incorporated glycan can shift the molecular weight by ~2 kDa (365). Using an N-linked glycosylation site predictor, the number of potential N-glycosylation sites (PNGS) were determined for each antibody amino acid sequence (parental and multispecific), across both heavy and light chains where applicable (excluding SP sequence) (Appendix Table B1). The multispecific antibodies, Bi-scFv, Bi-NAb, and Tri-NAb sequences have 3, 4, and 6 PNGS, respectively (Appendix Table B1). While it is not known whether these predicted glycosylation sites are indeed glycosylated, additional glycans may account for the experimentally larger observed sizes (Appendix Table B1). Future work may determine the glycosylation status of the expressed antibodies using PNGase to enzymatically deglycosylate the antibodies and compare them to the untreated antibody (366). Combined, these data confirm the correct assembly of each multispecific antibody into the quaternary structures, where appropriate (e.g. Bi-NAb and Tri-NAb), and that the expressed and purified antibodies were of high purity for their neutralisation functionality to be assessed.

4.3 Functional *in vitro* neutralisation of HIV-1 by the multispecific antibodies.

Viral resistance to PGT121 is associated with mutations resulting in the loss/removal of the N332 glycan (gp120 mutations at position 332 and/or 334), which confers complete resistance (158,367). The V3 loop (position 324-327) is also a critical binding site for V3 glycan bNAbs, therefore, mutations at position 325 (e.g., D325N, D325K

identified in humans following PGT121 passive infusion) may also confer resistance in rebound viruses (158). Most VRC01-resistant viral isolates contain alterations in the V5 region and loop D of gp120 (368). Mutations of structurally defined contact residues in loop D (N terminal to V3 region, residues 278 to 283), the CD4 binding loop (residues 362 to 365), and the V5-β24-α5 region (residues 458 to 467) prevent VRC01-mediated binding and neutralisation (369).

The CATNAP tool (347) was used to determine the resistance profiles of the selected viruses in our panel. Information for CE0217 was not available for our antibodies, and CAP210.2.00.E8 only displayed VRC01-resistance. Based on the resistance and sensitivity profiles observed in our *in vitro* testing (Figure 3.9A), CE0217 was classified as dual-sensitive, and CAP210.2.00.E8 was classified as dual VRC01/PGT121 resistant given that 50% neutralisation by either PGT121 or VRC01 antibody was not achieved at a maximum tested concentration of 25 μg/mL (Figure 3.9A and Appendix Figure B4A). Additionally, QH343.21M.ENV.A10 was predicted and classified as dual VRC01/PGT121 resistant but did demonstrate low-level sensitivity to both antibodies, approaching 50% inhibition at 25 μg/mL (Figure 3.9A and Appendix Figure B4A).

The neutralisation functionality of recombinantly expressed and purified multispecific antibodies was confirmed and compared to the parental antibodies (Figure 3.9). To account for the molarity difference between the antibodies, the SEC-determined native molecular weights were used to standardise the antibody inhibitory concentrations to nM. The multispecific antibodies demonstrated neutralisation of dual PGT121/VRC01-sensitive and single-resistant viruses, confirming the functionality of each antibody paratope that enabled the multispecific antibodies' enhanced neutralisation breadth over PGT121 and VRC01 parental antibodies (Figure 3.9A). Importantly, the multispecificity of the Bi-scFv, Bi-NAb and Tri-NAb facilitated the neutralisation of two of the three dual-resistant viruses (Figure 3.9A) increasing the overall neutralisation coverage of the 17 HIV-1 pseudovirus panel to 94% (Figure 3.9A & B).

Unfortunately, the multispecific antibodies did not always retain the overall potency of the parental antibodies against this pseudovirus panel. This was most notable against dual-sensitive viruses, where the potency of the multispecific antibodies was markedly reduced and did not conserve the potency of the most potent parental antibody, PGT121 (Figure 3.9A). While the median IC50 (0.309 nM) and IC80 (0.953 nM) of

PGT121 were only statistically significantly more potent than the Bi-scFv (Appendix Figure B5B and Figure 3.9C), the limited virus panel tested included ~40% PGT121-resistant viruses which would impact PGT121 median inhibitory concentrations. Previous studies directly comparing the IgG to scFv conformations of PGT121 have shown that the scFv format did not retain the potency of the IgG conformation (average 3.7-fold lower potency) (370,371). It is unclear whether this potency reduction is a result of the loss of epitope bivalency of the scFv conformation compared to IgG, or subtle differences in the paratope structure due to inclusion of the scFv-linker sequences potentially resulting in the observed reduced neutralisation potency and/or breadth compared to IgGs (372). IgG binding is generally believed to be monovalent for most HIV-1 antibodies, due to the spatial distance between epitopes on HIV-1 Env trimer and the distance between adjacent trimers (373). The potential of PGT121 IgG to bind bivalently to the Env spike is yet to be confirmed/determined. Despite monovalent IgG binding, the presence of two binding arms on IgG (versus one in a Fab) may lead to decreases in the off-rate due to avidity effects, overall increasing the binding affinity and neutralisation efficacy and potency (373). Smaller antibody conformations (e.g. scFv) display a general trend of increased off-rates and overall reduced binding affinities compared to their matched IgG conformations in *in vitro* binding assays (374,375), consistent with the inability of the scFv conformations (excluding Bi-scFv strategies) to accommodate bivalency. In our data, the Bi-NAb conformation (PGT121 binding) was unable to restore potency, suggesting loss of bivalency is not solely responsible for the observed potency reduction (Figure 3.9A). However, it should be noted that the bivalent arrangement of the PGT121 paratopes in the Bi-NAb and parental conformations are structurally dissimilar, with a reduced molecular distance spanning between the intramolecular PGT121 paratopes for the Bi-NAb conformation. This constraint may limit active, bivalent engagement of epitopes and the overall potency of the PGT121 paratopes in the Bi-NAb conformation. Alternatively, subtle detrimental differences may arise within the antibody paratope as a result from the inclusion of the scFv peptide-linker modifications. It has been shown that while the PGT121 scFvs retain the ability to interact with their known epitopes, they are more sensitive to single-residue variations of the epitopes (370), suggesting the existence of these subtle differences and impact on neutralisation. Ultimately, the observed inability of the multispecifics to retain the potency of the desired parental antibody could be a combination of the above points, requiring further elucidation

beyond the current scope of the presented work. However, this observation of reduced potency between the multispecifics relative to the most potent parental antibody (PGT121) is consistent with previous studies of various HIV-1 bispecific antibody combinations that failed to recapitulate the neutralisation potency of the parental bNAbs (188–190,202). However, other studies have found remarkable improvements in HIV-1 bispecific (186,187,189,191,192) and trispecific (185,194) antibodies over the parental antibodies, with the improvements in antibody potency being highly synergistic as the bispecific antibodies were shown to be more potent than combinations of the parental antibodies (185–187).

Importantly, the potencies of the multispecific antibodies compared to the parental antibodies reported in this study differ from those reported by Steinhardt *et al.* (200). We report the PGT121 parental antibody as displaying the best overall neutralisation potency (median IC50 0.309 nM) and demonstrate that the Bi-NAb was the most potent multispecific antibody (statistically more potent than the Tri-NAbs - median IC50: Bi-NAb, 0.837 nM versus Bi-scFv (1.52 nM), and Tri-NAb Co-T (1.074 nM) and sORF (1.381 nM)) (Figure 3.9A and Appendix B5B). However, Steinhardt *et al.* demonstrated the Tri-NAb (geometric mean titre (GMT) 0.071 µg/mL) to be the most potent antibody overall, and was statistically more potent than the bispecific antibodies (Bi-scFv (0.400 µg/mL, molar corrected by multiplying by 3) and Bi-NAb 0.380 µg/mL) and all the individual parental antibodies (200). When using the GMT as a comparative measure, our data is consistent with the results reported by Steinhardt *et al.* (200) in that the Tri-NAb (both Co-T and sORF) display the lowest geometric mean titre (Figure 3.9A). However, consistent with our reported statistical analyses, there was not enough evidence to show a significant difference between the Tri-NAbs and PGT121 (the most potent parental antibody), likely due to the relatively small number of viruses in the test panel. Additionally, the bispecific antibody constructs we generated may be different from those used by Steinhardt *et al*., given that we inferred our construct designs based on the reported description only but the amino acid sequences were not published (200). However, it is more plausible that the observed discrepancy in antibody potency and multispecific antibody neutralisation is a result of the differences in the pseudovirus panels, since the panel tested by Steinhardt *et al*. was larger and more diverse than the panel tested in this study (208 vs 17 viruses). Regardless, the general trend of the multispecific antibodies displaying improved neutralisation

coverage over parental antibodies was found in both studies (Figure 3.9 and Appendix B5, and (200)).

Although these multispecific antibody constructs, particularly the VRC01/PGT121 tandem scFv region, were rationally designed to simultaneously engage multiple paratopes (200), the observed synergistic effects were limited to select viruses. The Bi-scFv and Bi-NAb demonstrated potency enhancement against PGT121 resistant virus, 246F3, and dual resistant viruses, CAP210.2.00.E8 and QH343.21M.ENV.A10 (Figure 3.9A). Inspection of the QH343.21M.ENV.A10 demonstrates that there is low-level sensitivity of the virus to both VRC01 and PGT121 parental antibodies (approaching 50% inhibition at 25 µg/mL), whilst CAP210.2.00.E8 and 246F3 show high-level resistance to VRC01 and PGT121, respectively (Appendix Figure B4A). Importantly, Steinhardt *et al*. also reported bispecific antibody neutralisation of dual-resistant viruses, including CAP210.2.00.E8 (200), which is consistent with our results. These data demonstrate that while there is sufficient augmentation of the target epitope to convey resistance to either one or both parental antibodies, there is not complete loss of antibody paratope binding in these instances. Thus, the enhanced potency observed for the bispecifics (Bi-scFv and Bi-NAb) is likely a result of overall improvement in binding affinity through increased avidity provided by the simultaneous engagement of VRC01 and PGT121 paratopes.

The Tri-NAb (Co-T and sORF) demonstrated similar potency enhancement to the Bi-NAb against 246F3 (PGT121 resistant), presumably through the improved avidity provided by the engagement of the VRC01/PGT121 tandem scFv arm. However, the most noticeable enhancement in potency was observed against CNE8 (PGT121 resistant) when compared to the VRC01 or 10E8v4 parental and Bi-NAb multispecific antibodies (Figure 3.9A). This neutralisation result indicates that the combination of the 10E8 with either VRC01 or PGT121 paratopes on the Bi-NAb, promotes dual engagement of the target epitopes (increased avidity) leading to overall increased affinity and potency enhancement. This was not a result of triple epitope engagement, given the relatively poor performance of the Bi-NAb alone (Figure 3.9A). Similarly, a slight potency enhancement of the Tri-NAb was noted compared to the Bi-NAb against X2278 pseudovirus, presumably through a similar 10E8/VRC01 or PGT121 dual engagement, however, in this instance the PGT121 parental antibody produced overall greater potency (Figure 3.9A).

Dual PGT121/VRC01 resistant virus, Ce2103_E8 demonstrated high-level PGT121 and VRC01 resistance, and 10E8v4 requiring >25 μg/mL to achieve 100% viral inhibition. However, inclusion of the 10E8 paratope into the Tri-NAb conformation facilitated 50% inhibition of Ce2103_E8 at the maximum concentration of 25 μg/mL whilst the bispecifics showed no neutralisation activity (Appendix Figure B4A).

Combined this data confirmed the neutralisation functionality of the expressed and purified multispecific antibodies, Bi-scFv, Bi-NAb, and Tri-NAb from their respective DNA constructs and we were confident in advancing the study to explore the *in vitro* multispecific antibody expression via IVT-mRNA.

4.4 IVT mRNA transcript production and multispecific antibody expression.

In vitro transcribed (IVT) mRNA transcripts were generated from the identical pmRNA-plasmid vectors described and characterised above (including the GFP and Fluc controls), by linearising each vector in the poly-A signal region with *Bpi*I restriction enzyme, to define the transcript and poly-A length (Figure 3.10A). Homogenous mRNA transcripts of defined length were generated and confirmed to be of the anticipated sizes (Figure 3.10B). Importantly, the pmRNA_Bi-NAb and Bi-NAb_Ho DNA plasmids linearised to a single band (Figure 3.10A) and the mRNA transcripts were not truncated (Figure 3.10B), thus further validating the successful silencing and replacement, respectively, of the *Bpi*I restriction site in the CH2 domain in the pmRNA_Bi-NAb_Δ*Bpi*I and pmRNA_Bi-NAb_Ho constructs (Figure 3.2 and 3.5, respectively). The Tri-NAb sORF mRNA transcript is consistent with the proposed construct design to generate a sORF encoding Bi-NAb_Ho and 10E8_Kn constructs in tandem resulting in the large transcript size observed (Figure 3.10B).

The IVT mRNA transcripts were purified of contaminating dsRNA using a cellulose purification method previously described, that selectively binds dsRNA to cellulose powder in an ethanol-containing buffer (286). The resulting dsRNA-free, pure mRNA would have improved translation efficiency and limit the activation of cytokine production *in vivo* (286). Purified mRNA transcripts were enzymatically capped (5' Cap1 structure) to protect them from decay during transcription and transfected into mammalian 293F cells (capped mRNA transcripts were experimentally confirmed to be necessary for expression, data not shown). The transfection procedure was initially optimised by varying the nucleic acid quantities of GFP and Bi-scFv mRNA transcripts,

the ratios to Lipofectamine™ MessengerMax™ transfection reagent, and cell culture volumes to determine transfection efficiency and protein expression (data not shown). The manufacturer's recommendations of 1 µg mRNA with a 1:3 ratio per mL of 293F cell suspension was deemed to be optimal for *in vitro* transfection efficiency and expression as this yielded Bi-scFv antibody expression at levels similar to that previously achieved DNA 293F cell transfections (data not shown).

Our data demonstrate that the multispecific antibodies were successfully expressed from IVT-mRNA transcripts following mammalian cell transfection and secreted into the cell culture supernatants, as determined by western blot detection (Figure 3.10C & D). Given the relatively low mRNA-mammalian cell transfection volumes (4 mL) and the proposed mRNA-mediated delivery for antibody expression strategy, the intentional decision was made not to purify the expressed multispecific antibodies from the culture supernatants and examine their expression *in situ*. Thus, expression analysis of the antibodies necessitated the use of western blotting. Analogous to the antibody banding patterns observed from DNA expressed and purified antibodies (Figure 3.8B), the multispecific antibody constituents (where applicable) were observed to be of the anticipated molecular weights when resolved under reducing conditions (Figure 3.10C). Faint banding of approximately ~38 kDa was noted and may be construed as the 10E8 light chain in the resolved Tri-NAb lanes (Figure 3.10C). However, upon closer inspection, this ~38 kDa band was determined to be a by-product of Bi-NAb mRNA transfection (Figure 3.10C) (or pmRNA_Bi-NAb DNA plasmid transfection (Figure 3.5A & D)) that is readily detected by anti-human Fc specific antibody. The identity of this expressed protein is unknown, and the potential impact *in vivo* would require further exploration. The multispecific antibodies with intact Fc domains (Bi-NAb and Tri-NAbs) assembled and dimerised under non-reducing conditions into their corresponding quaternary structures (Figure 3.10D), consistent with results observed for the expressed and purified multispecific antibodies (Figure 3.8B).

mRNA-mediated Tri-NAb expression levels were indistinguishable by western blot analysis between the Co-T and sORF strategies (Figure 3.10C), demonstrating similar transfection and expression efficiency were achieved. However, it was noted that the Tri-NAb expressed from the mRNA sORF construct displayed reduced intracellular furin protease cleavage resulting in a faint band consistent with the 10E8 heavy chain-

F2Aopt fusion protein as described prior to furin cleavage site modification (Figure 3.7E). This 10E8 heavy chain-F2Aopt fusion species was not evident in the mRNA Co-T expressed Tri-NAb (Figure 3.10C). We hypothesised that despite successful modification of furin protease cleavage (Δfurin) in both the pmRNA_10E8_Kn and pmRNA_Tri-NAb_sORF constructs (Figure 3.7), having the dual furin sites in the sORF expressed peptide compared to only a single furin site within the expressed Bi-NAb_Ho & 10E8_Kn Co-T combination, may have resulted in the reduced processing efficiency observed. A known limitation of polycistronic constructs is the reduced cleavage efficiency of successive 2A cleavage peptides (303) which may also be true for multiple furin cleavage sequences within polycistronic vectors. The available literature on the use of multiple furin sequences in a single polycistronic vector encoding antibody or reporter sequences is limited. Tricistronic vectors using the same furin sequence with different 2A peptides to separate viral structural proteins could not clearly show the efficiency of furin-mediated removal of the 2A peptides (376), but another study separating cardiac transcription factors reported no reduced cleavage efficiency of the second furin sequence (377). Therefore, the observed reduced furin cleavage in the Tri-NAb sORF is more likely to be due to the adjoining F2Aopt sequence rather than its position within the polycistronic construct, since the same furin sequence motif has demonstrated reduced cleavage efficiency when combined with an F2A than with a P2A peptide sequence (354). It is possible that the incomplete cleavage may have still occurred after F2Aopt-furin modification during large-scale DNA Tri-NAb sORF expression and was removed during SEC purification as evaluations were only performed post-SEC purification (Figure 3.8). Since the mRNA-expressed antibodies were not purified, this may explain why the 10E8 heavy chain-F2Aopt band was once again seen in the Tri-NAb sORF but this would require further exploration and experimental validation. Inefficiency of the F2Aopt sequence with respect to 10E8 heavy and light chain processing (F2Aopt-10E8-light chain fusion) could not be verified given the inability to detect the expressed light chain by western blot (Figure 3.10C) and would also require further exploration.

Overall, the expression of the multispecific antibodies and the controls from the generated IVT-mRNA were confirmed *in vitro*. The mRNA-expressed multispecific antibodies were deemed to be in the correct conformations and functional HIV-1 pseudovirus neutralisation could be determined.

4.5 IVT-mRNA-expressed multispecific antibodies exhibit high neutralisation titres with broad *in vitro* HIV-1 neutralisation coverage.

The neutralisation functionality of the IVT-mRNA expressed multispecific antibodies in unpurified, clarified cell culture supernatants were confirmed against the panel of 17 tier 2 HIV-1 pseudoviruses. We demonstrate that abundant expression of the multispecific antibodies was achieved *in vitro* from IVT-mRNA delivery that resulted in *in vitro* titres that could be diluted ~160-1 420 fold (Median ID80 values) whilst retaining 80% viral inhibition of 82-94% of the viruses tested (Figure 3.11A). The IVT-mRNA expressed multispecific antibodies recapitulated the broad neutralisation breadth achieved by the recombinantly expressed and purified multispecific antibodies (compare Figure 3.9B and Figure 3.11B), reiterating the functionality and correct assembly (where appropriate, e.g. Bi-NAb and Tri-NAb) of the unpurified multispecifics *in vitro.* The Bi-scFv, Bi-NAb and Tri-NAb Co-T exhibited 94% neutralisation coverage at ID80 of 10 (Figure 3.11A & B). The sORF expressed Tri-NAb demonstrated a slight reduction in coverage, neutralising 82% at an ID80 of 10 (Figure 3.11A & B). The slightly lower expressed titre resulted in failure to achieve 80% neutralisation of dual resistant strains, CAP210.2.00.E8 and QH343.21M.ENV.A10 at minimum 10-fold dilution tested (Figure 3.11A & B).

Given the similarity in the calculated median IC50 (~1.2 nM) and IC80 (~3 nM) obtained for the recombinantly expressed and purified multispecific antibodies (Figure 3.9A & C) offers insight into the significant difference in ID50 and ID80 titres observed between multispecifics expressed from mRNA (Figure 3.11A & C). These observed differences are largely a result of differences in protein expression from the different mRNA constructs and the relative molecular weights of the expressed proteins. The Bi-scFv demonstrated the highest median ID80 titres, which were 2 to 8.8-fold greater than mRNA-expressed Bi-NAb, Tri-NAb Co-T and sORF titres, but were only shown to be significantly higher than the Co-T and sORF expressed Tri-NAbs (Figure 3.11C). These high titres may be explained by the combination of (a) higher levels of expression of Bi-scFv achieved from mRNA transcripts, and (b) the smaller molecular weight of the active Bi-scFv (~70 kDa) relative to the Bi-NAb and Tri-NAbs (~200 kDa). Thus, on a microgram basis, the Bi-scFv would be estimated to have 3-fold the number of active molecules (antibodies) compared to Bi-NAb and Tri-NAb and would require 3-fold greater dilution to achieve the equivalent molar concentration. This is illustrated

by the difference in IC50 or IC80 potencies of the multispecific antibodies when presented as µg/mL versus nM (Figure 3.9A). Thus, the combination of the relatively high expression of the Bi-scFv and the relatively low molecular weight of the active compound results in the high neutralisation titres (ID50 and ID80) obtained (Figure 3.11A & C). The Bi-NAb demonstrated a 2 to 4-fold higher ID80 when compared to Co-T or sORF-expressed Tri-NAbs, respectively, with significant differences only confirmed against the mRNA sORF-expressed Tri-NAb (Figure 3.11C). Given the similarity in the antibody conformations and hence the molecular weights (~200 kDa), the observed difference in ID80 titres is most likely due to a greater concentration of Bi-NAb in the tested culture supernatants. The difference in Bi-NAb expression over the Tri-NAbs (Co-T and sORF) may stem from the reduced complexity of the Bi-NAb constructs compared to the Tri-NAb mRNA strategies, two mRNA transcripts for the Co-T strategy versus single long transcripts that require *in situ* processing for the sORF. This increased *in situ* processing may also account for the 1.4-fold difference observed in ID80 titre between the Co-T and sORF expressed Tri-NAbs. Our data suggest that the longer, more complicated mRNA transcripts may have reduced protein expression efficiencies at least for multispecific antibody expression and may favour the delivery of scFv tandem bispecific antibody conformations (Bi-scFv and Bi-NAb) *in vivo* (Figure 3.11C).

Interestingly, although the mRNA-expressed Tri-NAb displayed overall lower titres than the Bi-NAb, the Tri-NAb ID50s were higher (Co-T, 971 and sORF, 949) than the Bi-scFv and Bi-NAb ID50s (503 and 600 respectively) against the PGT121-resistant virus CNE8. Once again illustrating the synergistic-enhanced potency achieved by the Tri-NAb conformation against this virus as was reported for the purified Tri-NAb antibodies (Figure 3.9A and Figure 3.11A).

These differences in multispecific antibody expression and concentration within the unpurified cell culture supernatants were consistent with the results obtained from the relative quantification methods (Table 3.2). Disappointingly there was no concordance between ELISA, IC50 x ID50 and WB densitometry concentration estimates of mRNA expressed multispecific antibodies (Table 3.2). The relatively low concentrations estimated by ELISA would imply that an enhanced potency is achieved by the mRNA-expressed multispecific antibodies which cannot be explained. The average concentrations quantified by WB densitometry analysis more closely resembled those

predicted by the *in vitro* neutralisation data (Table 3.2). However, the densitometry analysis had noted discrepancies when correcting for the dilution factor and could not accurately quantify a 2-fold dilution series of the prepared cell culture samples (Table 3.2). The undiluted cell culture supernatants had observed concentrations most closely resembling the highest standard concentration on the respective western blots (Appendix Figure A8).

Despite discrepancies in the concentration estimates between the different quantification methods (ELISA, WB densitometry, IC50 x ID50 neutralisation data – Table 3.2), all methods show a similar pattern. The bispecific antibodies (Bi-scFv and Bi-NAb) were expressed at higher, yet relatively similar concentrations, followed by the Co-T expressed Tri-NAb that was on average 1.4-fold greater than the sORF expressed Tri-NAb. Estimation of the multispecific antibody concentrations using the neutralising IC50 x ID50 methods was deemed the best method, as the determined concentrations reflect the dilution patterns (median ID50 or ID80) of the multispecific antibodies required for equivalent viral inhibition. For example, Bi-scFv: 352.4 µg/mL (average IC50 X ID50 - Table 3.2) / 4 489 or 1 427 (median ID50 or ID80 values - Figure 3.11A) = 0.078 or 0.24 µg/mL, which is close to the determined Bi-scFv median IC50 (0.092 µg/mL) and IC80 (0.22 µg/mL) values (Figure 3.9A). Previous studies quantified human serum antibody titres following passive infusion using the derived IC50 x ID50 estimate from TZM-bl neutralisation assays (measure antibody neutralising activity) or ELISA (measure bound antibody levels) and showed good agreement between the two assays (108,147,350). Assuming that the functional neutralisation activity of the unpurified, mRNA-expressed multispecifics are comparatively similar to the recombinantly expressed and purified multispecific antibodies, then this method would correctly estimate the concentrations within our study (Table 3.2).

Unfortunately, given the discrepancies between the quantification strategies, we are unable to unequivocally provide a concentration of the mRNA-expressed multispecific antibodies but can estimate it to be: Bi-scFv (~150-350 µg/mL), Bi-NAb (125-340 µg/mL), Tri-NAb Co-T (90-155 µg/mL), and Tri-NAb sORF (70-100 µg/mL). If we had more confidence in the quantification of the mRNA-expressed multispecific antibodies, IC50 and IC80 values could have been calculated and corrected for the molecular weight differences of the multispecific antibodies. This would have allowed for more

stringent statistical analysis to be performed to compare the potency of the mRNA-expressed and recombinantly expressed and purified multispecific antibodies.

4.6 Expression discrepancy between the Co-T and sORF expressed Tri-NAb.

Interestingly, the Tri-NAb had better expression efficiency and yield when produced by co-transfection than from the sORF, which was more profound in DNA expression (Table 3.1) than from mRNA expression (Table 3.2). Plasmid DNA size affects mammalian cell transfection efficiency and consequent protein expression. DNA plasmid size has been shown not to influence the DNA lipoplex morphological structure or the efficiency of vector uptake into the cell (378–380), but may influence DNA release from the cationic lipids, the intracellular migration of DNA from the cytoplasm to the nucleus, and/or nuclear import (379,381). Smaller plasmids localise to the nucleus and express their protein products faster than larger plasmids, thus, transfection efficiencies and gene expression for equimolar amounts of plasmid DNA are inversely proportional to plasmid size (378,379,381,382). This was demonstrated by a sharp decrease in luciferase activity resulting from 3.7 kb versus 8.6 kb plasmid DNA sizes (379). Additionally, tricistronic vectors have been reported to have improved (377) or much-reduced protein production efficiency (309,376,383) than combining monocistronic or using bicistronic constructs, which potentially depends on the encoded gene. This may be attributed to the larger size of the tricistronic gene requiring more resources and time for transcription and translation, and co-translational cleavage at the 2A peptide sequences may slow down the translation rate (376) as is the case for the Tri-NAb sORF construct compared to the Co-T.

Alternatively, polycistronic vectors have equal amounts of heavy- and light-chain sequences that can yield equal amounts of protein or potential decreased cleavage efficiency of the second 2A cleavage peptide can reduce translation of the downstream peptide (303). Antibody light chain to heavy chain ratio (LC: HC) influences immunoglobulin assembly and assembly time, and having an abundance of light chain (LC: HC ~1.24–3.43) is required for improved antibody folding, assembly, stability (decreased aggregation that is important for reduced immunogenicity), and expression (384–388). Therefore, a potential reduction in the translation of the 10E8 light chain (third cistron in the Tri-NAb_sORF) and thus the reduced availability of light chain may be a rate-limiting factor of antibody synthesis (389). Since we only observed

assembled and secreted antibodies by western blot, the expression of the Tri-NAb_sORF constituents appeared proportional to each other, with an overall decrease compared to the Tri-NAb Co-T (Figure 3.7E (DNA) and 3.10C (mRNA)). Our experimental workflow was not designed to assess intracellular heavy- and light-chain translational imbalances that may hinder antibody assembly and consequently overall antibody expression. Furthermore, the expression mechanism of antibodies from combined monocistronic versus polycistronic vectors may affect the SP affinity. Co-transfected antibody heavy- and light-chain SPs can be independently but simultaneously recruited to the ER, where the antibody chains may interact while folding and assembling which affects the antibody secretion level (389). Polycistronic constructs have the SP of the upstream heavy chain co-translationally recognised and complexed to the ER membrane translocon before the light chain SP is translated, which may influence the assembly interactions and level of secreted antibody (355,356,389). Given the nature of cistron translation efficiencies being impacted by their relative position in the polycistronic vector, changing the position of the light chain has been shown to improve antibody expression (353). Although an F2A-mediated expression vector with antibody light chain in the first cistron position expressed similar amounts of antibody chains, it was hypothesised that the mRNAs of the different conformations may have different secondary structures such that having light chain in the first position results in higher translation efficiency and yields a higher mAb expression level (353). Therefore, it would be interesting to investigate whether changing cistron positions in the Tri-NAb_sORF, in which the 10E8 light chain encoding region precedes the 10E8 heavy chain encoding region, or the 10E8 light chain is located in the first position followed by the 10E8 heavy chain and then the Bi-NAb, could improve the overall Tri-NAb assembly capacity and expression titres.

Combined, the differing DNA plasmid sizes and the polycistronic nature of the pmRNA_Tri-NAb_sORF (8 385 bp) could explain the reduced Tri-NAb expression achieved by the sORF construct compared to co-transfection pmRNA_Bi-NAb_Ho (6 012 bp) and pmRNA_10E8_Kn (5 994 bp) (measured based on yields post-purification – Table 3.1). However, in the case of mRNA which does not enter the nucleus, the size difference between the Co-T (Bi-NAb_Ho (2 509 bases) and 10E8_Kn (2 491 bases)) and sORF (4 882 bases) mRNA transcripts could have less impact on expression efficiency than for DNA constructs. Thus, mRNA transfection

efficiency and subsequent protein expression may be greater than the equivalent DNA plasmid construct (390). This is consistent with our results, where the mRNA-expressed Tri-NAb sORF titre, although reduced, was not significantly different from the Tri-NAb Co-T (based on neutralisation ID data that relates to antibody expression - Figure 3.11C and Appendix Figure B7B). A direct comparison of mRNA and DNA Tri-NAb Co-T and sORF expression would be required to determine if mRNA expression has more efficient yields.

4.7 Future prospects of mRNA-multispecific antibody delivery for HIV-1 prevention.

The success of immunoprophylaxis strategies against HIV-1 relies on maintaining protective bNAb titres *in vivo* that can neutralise diverse swarms of HIV-1 strains circulating within the local human population. The AMP trial data provided proof of concept that bNAb prophylaxis can be effective for sensitive HIV-1 isolates but highlighted the importance of potent antibody combination therapy for effective HIV-1 prevention (135). Furthermore, the AMP study defined the required serum neutralisation titre for protection, which can be evaluated *in vitro* using an IC80 cut-off of <1 µg/mL to predict the clinical potency and protection of antibodies (135). The multispecific antibodies detailed in this study, comprising VRC01/PGT121 bispecific antibody configurations (Bi-scFv and Bi-NAb) and the VRC01/PGT121/10E8 trispecific (Tri-NAb), had median IC80s between 0.22 – 0.68 µg/mL (~3 nM) with neutralisation coverage of 71-76% at an IC80 <1 µg/mL (Figure 3.9), thus meeting this potential clinical protective criteria (IC80 <1 µg/ml). Whether IVT-mRNA-mediated expression of the HIV-1 bNAbs or multispecific antibodies can achieve sufficient protective titres in humans is currently unknown. It is becoming apparent that IVT mRNA is an efficient means to express antibodies *in vitro* as well as presenting a viable therapeutic/prophylactic/passive immunisation strategy for various biological threats, including viral infections, intoxication, and cancer (391). IVT-mRNA has been shown to be a robust vaccine platform and may represent opportunities for passive immunisation as well, making it advantageous for applications that may require a combination of passive and active immunisation (391) such as HIV-1.

Current delivery of IVT-mRNA is through LNP delivery platforms. Recent SARS-CoV-2 vaccine candidates demonstrated the successful delivery of mRNA vaccine immunogens by LNPs (237,238), however, there is a scarcity of the mRNA/LNP-

mediated expression of antibody studies that have progressed to human clinical trials, with the majority still in preclinical development in mice and NHPs (391–394). Prior to preclinical testing, additional considerations pertaining to the generation and preparation of IVT-mRNA transcripts are required. Primarily the uridine 5'-triphosphate (UTP) is replaced with N1-methyl pseudouridine 5' triphosphate (pseudouridine) that reduces activation of RNA-dependent protein kinase (PKR) and improve the stability and translation capacity of mRNA whilst diminishing its immunogenicity *in vivo* (273,274). In addition during IVT, the T7 RNA polymerase is prone to synthesise smaller oligonucleotides that result from the abortion of initiation (244,283). These short abortive RNA fragments as well as the 3' end of full-length RNA transcripts can prime RNA synthesis generating dsRNA (246,280–282). Double-stranded RNA activates TLR3 pattern recognition receptors and dsRNA-dependent enzymes upon entry into human cells, triggering an immune response and inhibiting intra-cellular protein synthesis (285). Therefore, for improved and efficient translation of administered mRNA and to limit the activation of cytokine production (*in vitro* or *in vivo*), it is necessary to remove the dsRNA contaminant from the IVT mRNA (286). In the current study, this was achieved using a cellulose purification method previously described, that selectively binds dsRNA to cellulose powder in an ethanol-containing buffer, resulting in pure single-stranded mRNA with >95% removal of dsRNA (286). A limitation of the current study was that despite performing the dsRNA-cellulose purification we were unable to confirm the removal of the residual dsRNA contaminates. Prior to clinical advancement, confirmation of the IVT-mRNA purity, LNP formulation and *in vitro* testing would be required.

There is limited published data available mRNA-LNP expression of antibodies *in vivo*. However, two preliminary studies have demonstrated efficacy at *in vivo* delivery of individual (234) and co-expression (301) of anti-HIV-1 bNAbs/scFvs using the mRNA-LNP platforms and reported the following. Nucleoside-modified mRNAs encoding the heavy- and light-chains of bNAb VRC01 encapsulated in LNPs were co-administered in equimolar concentrations by IV injection at a total of 1.4 mg/kg (30 µg) mRNA into BALB/c mice, resulting in VRC01 antibody expression of ~170 µg/mL 24 hours later (234). Furthermore, weekly administrations of 1 mg/kg (30 µg) of mRNA into NOD-scid gamma (NSG) mice was sufficient to maintain VRC01 titres of ~40 µg/mL (234). Surprisingly, 30 µg of VRC01 mRNA resulted in plasma VRC01 levels that were 1.65

times higher than BLT humanised mice injected with 600 µg of purified VRC01 mAb (24 hours post-injection mean titres 204.7 µg/mL and 123.4 µg/mL respectively) and was protective against challenge with the SF162 HIV-1 isolate (234). Alternatively, individual bNAb mRNA-LNP IV administration of (0.5 mg/kg) of PGT121 and PGDM1400 scFvs resulted in systemic titres of >73 µg/mL 24 hours later, and full-length N6 IgG peak titres of 974 µg/mL after 24 hours (301). Co-formulation of mRNAs (1:1:1:0.5) encoding PGT121 scFv, PGDM1400 scFv, and N6 IgG heavy- and light-chain (HC: LC, 2:1) were administered to Tg32 hemizygous mice. The authors extrapolated that a dose of 1 mg/kg (0.3 mg/kg of each bNAb) in mice or 0.2 mg/kg in humans could maintain levels of >10 µg/mL of each antibody up to 90 days (301).

In support of these data, mRNA-LNP *in vivo* delivery of full-length antibodies against the Chikungunya virus have been performed in mice, NHP and humans (392,394), and provides comparative titre data between species. Overall, mRNA-LNP delivery of anti-Chikungunya antibodies achieved protective titres across all species, but reduced serum titres were observed in NHP and human studies: mice (dose 0.5 mg/kg; titre: 14.9 µg/mL), NHP (dose: 0.5 mg/kg; titre: 10.1 µg/mL or repeated dose of 3 mg/kg, titre 1: 16.2 µg/mL, titre 2: 28.8 µg/mL), and human (dose 0.6 mg/kg; titre >1 µg/mL) (392,394). These studies confirm IVT-mRNA-LNP antibody delivery as a passive immunisation strategy *in vivo* and suggest that human clinical trials would likely require >1 mg/kg (IVT-mRNA-LNP) dosing to achieve protective titres. Clinically protective titres against HIV-1 are currently unknown, however, this would depend upon the bNAb potency and the susceptibility of the infecting virus/viral swarm. Current NHP-SHIV challenge models indicate that bNAbs targeting the same conserved epitope that display higher potency against the viral challenge strain are able to protect against infection at lower titres than less potent bNAbs (395). Given the failure of the first AMP trials, the consensus within the field is the requirement for bNAb combinations/multispecifics that will ensure protection within the real-world context. These complexities in bNAb selection, multispecific engineering and construct design may in turn affect IVT-mRNA-LNP dosing.

This study has demonstrated the utility of mRNA-delivery of HIV-1 multispecific antibodies *in vitro* and reports efficient expression of the Bi-scFv, Bi-NAb and Tri-NAb conformations. Furthermore, we demonstrate that multispecific antibodies incorporating heterologous heavy chain assembly can be expressed from single open

reading frame mRNA transcripts (Tri-NAb sORF), simplifying the manufacture and delivery process. We have therefore demonstrated proof-of-principle of mRNA-multispecific antibody delivery *in vitro* and this study provides a basis for the advancement into preclinical testing. Importantly, the IVT-mRNA strategy could be applied to the various established multispecific HIV-1 antibodies that have demonstrated therapeutic and protective efficacy, and improved potency over parental antibodies (Table 1.2). This strategy may provide a significant cost-benefit to those HIV-1 multispecific antibodies that have reached clinical development, 10E8v4/iMAb (195), VRC01/PGDM1400/10E8v4 (198), and 10E8/iMAb and VRC07-523LS (196), and facilitate the large-scale roll-out and may even facilitate the simultaneous delivery of multiple multispecific antibody configurations.

Cognisant of the challenges that arise with *in vivo* delivery of multispecific antibodies, designing multispecific antibodies in which the selected combinations display synergy may be paramount to the multispecific antibody efficacy. Bispecific combinations of N6, CAP256-VRC26.25, PGDM14000, 3BNC117, PGT135, 10E8, and iMAb demonstrate the best combination of potency and neutralisation against HIV-1 subtype C pseudoviruses *in vitro* (141). Thus, elite multispecific antibodies engineered using these specific bNAb combinations, in combination with IVT-mRNA-LNP delivery, may provide a potent HIV-1 prevention strategy that would realise maximum benefit in the sub-Saharan African region (4–7) in which the global HIV-1 infection burden is predominated by the subtype C strains.

4.8 Conclusion.

In the absence of an effective HIV-1 prophylactic vaccine, passive transfer of bNAbs presents a viable alternative. bNAb combinations or engineered multispecific bNAbs are likely required to cope with the extensive diversity of HIV-1 strains in circulation globally. IVT-mRNA-mediated expression of HIV-1 bNAbs/multispecific antibodies may lower the cost of the passive immunisation strategies, promoting large-scale clinical roll-out, particularly in resource-limited countries.

This dissertation describes the generation of IVT-mRNA compatible DNA plasmid constructs for the expression and functional characterisation of previously reported Bi-scFv, Bi-NAb and Tri-NAb multispecific constructs (200). Importantly, we describe the generation of the novel Tri-NAb sORF construct that achieved comparable expression

to traditional co-transfection from IVT-mRNA, simplifying the delivery process for multispecific antibody expression and could further enable the delivery of combinations of multispecific antibodies (i.e. combinations of two bispecifics or multispecifics). Our data demonstrate that all three multispecific antibody conformations could be successfully expressed and assembled from IVT-mRNA transcripts and retained the functional paratopes of each antibody to achieve enhanced neutralisation breadth against a clinically relevant tier 2, HIV-1 pseudovirus panel. Furthermore, the mRNA-expressed multispecific antibodies had a neutralisation coverage comparable to that achieved by the DNA-expressed and purified multispecific antibodies, thus proving the validity of this antibody expression platform *in vitro*.

In conclusion, we have demonstrated proof-of-principle of IVT-mRNA expression of HIV-1 multispecific antibodies encoded by single mRNA transcripts. These data support the advancement into preclinical animal testing to determine if therapeutically relevant titres are attainable *in vivo* following LNP-mediated delivery of these constructs. If successful, IVT-mRNA expression of multispecific antibodies could present a viable strategy for immunoprophylaxis against HIV-1 and other viral infections for which protective vaccines do not yet exist.

References.

1. Gallo RC, Montagnier L. The Discovery of HIV as the Cause of AIDS. N Engl J Med. 2003 Dec 11;349(24):2283–5.

2. Fact sheet - Latest global and regional statistics on the status of the AIDS epidemic. [Internet]. [cited 2024 Mar 13]. Available from: https://www.unaids.org/en/resources/documents/2023/UNAIDS_FactSheet

3. HIV data and statistics [Internet]. [cited 2024 Mar 13]. Available from: https://www.who.int/teams/global-hiv-hepatitis-and-stis-programmes/hiv/strategic-information/hiv-data-and-statistics

4. Murray CJ, Ortblad KF, Guinovart C, Lim SS, Wolock TM, Roberts DA, et al. Global, regional, and national incidence and mortality for HIV, tuberculosis, and malaria during 1990–2013: a systematic analysis for the Global Burden of Disease Study 2013. The Lancet. 2014;384(9947):1005–70.

5. Ortblad KF, Lozano R, Murray CJ. The burden of HIV: insights from the Global Burden of Disease Study 2010. AIDS Lond Engl. 2013;27(13):2003.

6. Murray CJ, Barber RM, Foreman KJ, Ozgoren AA, Abd-Allah F, Abera SF, et al. Global, regional, and national disability-adjusted life years (DALYs) for 306 diseases and injuries and healthy life expectancy (HALE) for 188 countries, 1990–2013: quantifying the epidemiological transition. The Lancet. 2015;386(10009):2145–91.

7. Vos T, Barber RM, Bell B, Bertozzi-Villa A, Biryukov S, Bolliger I, et al. Global, regional, and national incidence, prevalence, and years lived with disability for 301 acute and chronic diseases and injuries in 188 countries, 1990–2013: a systematic analysis for the Global Burden of Disease Study 2013. The lancet. 2015;386(9995):743–800.

8. Watts JM, Dang KK, Gorelick RJ, Leonard CW, Bess Jr JW, Swanstrom R, et al. Architecture and secondary structure of an entire HIV-1 RNA genome. Nature. 2009;460(7256):711–6.

9. van Heuvel Y, Schatz S, Rosengarten JF, Stitz J. Infectious RNA: Human Immunodeficiency Virus (HIV) Biology, Therapeutic Intervention, and the Quest for a Vaccine. Toxins. 2022 Feb;14(2):138.

10. Addo MM, Altfeld M, Rosenberg ES, Eldridge RL, Philips MN, Habeeb K, et al. The HIV-1 regulatory proteins Tat and Rev are frequently targeted by cytotoxic T lymphocytes derived from HIV-1-infected individuals. Proc Natl Acad Sci. 2001;98(4):1781–6.

11. Trono D. HIV accessory proteins: leading roles for the supporting cast. Cell. 1995;82(2):189–92.

12. Turner BG, Summers MF. Structural biology of HIV. J Mol Biol. 1999;285(1):1–32.

13. Ganser-Pornillos BK, Yeager M, Sundquist WI. The structural biology of HIV assembly. Curr Opin Struct Biol. 2008;18(2):203–17.

14. Merk A, Subramaniam S. HIV-1 envelope glycoprotein structure. Curr Opin Struct Biol. 2013;23(2):268–76.

15. Richman DD, Wrin T, Little SJ, Petropoulos CJ. Rapid evolution of the neutralizing antibody response to HIV type 1 infection. Proc Natl Acad Sci. 2003;100(7):4144–9.

16. Cenker JJ, Stultz RD, McDonald D. Brain microglial cells are highly susceptible to HIV-1 infection and spread. AIDS Res Hum Retroviruses. 2017;33(11):1155–65.

17. Douek DC, Brenchley JM, Betts MR, Ambrozak DR, Hill BJ, Okamoto Y, et al. HIV preferentially infects HIV-specific CD4+ T cells. Nature. 2002;417(6884):95–8.

18. Campbell EM, Hope TJ. Live cell imaging of the HIV-1 life cycle. Trends Microbiol. 2008;16(12):580–7.

19. Moore JP, Trkola A, Dragic T. Co-receptors for HIV-1 entry. Curr Opin Immunol. 1997;9(4):551–62.

20. Selyutina A, Persaud M, Lee K, KewalRamani V, Diaz-Griffero F. Nuclear import of the HIV-1 core precedes reverse transcription and uncoating. Cell Rep. 2020;32(13).

21. Cosnefroy O, Murray PJ, Bishop KN. HIV-1 capsid uncoating initiates after the first strand transfer of reverse transcription. Retrovirology. 2016;13(1):1–17.

22. Novikova M, Zhang Y, Freed EO, Peng K. Multiple roles of HIV-1 capsid during the virus replication cycle. Virol Sin. 2019;34:119–34.

23. Dharan A, Bachmann N, Talley S, Zwikelmaier V, Campbell EM. Nuclear pore blockade reveals that HIV-1 completes reverse transcription and uncoating in the nucleus. Nat Microbiol. 2020;5(9):1088–95.

24. Burdick RC, Li C, Munshi M, Rawson JM, Nagashima K, Hu WS, et al. HIV-1 uncoats in the nucleus near sites of integration. Proc Natl Acad Sci. 2020;117(10):5486–93.

25. Larue R, Gupta K, Wuensch C, Shkriabai N, Kessl JJ, Danhart E, et al. Interaction of the HIV-1 intasome with transportin 3 protein (TNPO3 or TRN-SR2). J Biol Chem. 2012;287(41):34044–58.

26. Dharan A, Talley S, Tripathi A, Mamede JI, Majetschak M, Hope TJ, et al. KIF5B and Nup358 cooperatively mediate the nuclear import of HIV-1 during infection. PLoS Pathog. 2016;12(6):e1005700.

27. Krishnan L, Matreyek KA, Oztop I, Lee K, Tipper CH, Li X, et al. The requirement for cellular transportin 3 (TNPO3 or TRN-SR2) during infection maps to human immunodeficiency virus type 1 capsid and not integrase. J Virol. 2010;84(1):397–406.

28. Bryant M, Ratner L. Myristoylation-dependent replication and assembly of human immunodeficiency virus 1. Proc Natl Acad Sci. 1990;87(2):523–7.

29. Usami Y, Popov S, Popova E, Inoue M, Weissenhorn W, G. Göttlinger H. The ESCRT pathway and HIV-1 budding. 2009;

30. de Marco A, Müller B, Glass B, Riches JD, Kräusslich HG, Briggs JA. Structural analysis of HIV-1 maturation using cryo-electron tomography. PLoS Pathog. 2010;6(11):e1001215.

31. Engelman A, Cherepanov P. The structural biology of HIV-1: mechanistic and therapeutic insights. Nat Rev Microbiol. 2012 Apr 1;10(4):279–90.

32. Rolland M, Tovanabutra S, Decamp AC, Frahm N, Gilbert PB, Sanders-Buell E, et al. Genetic impact of vaccination on breakthrough HIV-1 sequences from the STEP trial. Nat Med. 2011;17(3):366–71.

33. Keele BF, Giorgi EE, Salazar-Gonzalez JF, Decker JM, Pham KT, Salazar MG, et al. Identification and characterization of transmitted and early founder virus envelopes in primary HIV-1 infection. Proc Natl Acad Sci. 2008;105(21):7552–7.

34. Naif HM. Pathogenesis of HIV Infection. Infect Dis Rep. 2013 Jun 6;5(Suppl 1):e6.

35. Hernandez-Vargas EA, Middleton RH. Modeling the three stages in HIV infection. J Theor Biol. 2013;320:33–40.

36. Fauci AS. HIV and AIDS: 20 years of science. Nat Med. 2003;9(7):839–43.

37. Gurunathan S, El Habib R, Baglyos L, Meric C, Plotkin S, Dodet B, et al. Use of predictive markers of HIV disease progression in vaccine trials. Vaccine. 2009;27(14):1997–2015.

38. Fiebig EW, Wright DJ, Rawal BD, Garrett PE, Schumacher RT, Peddada L, et al. Dynamics of HIV viremia and antibody seroconversion in plasma donors: implications for diagnosis and staging of primary HIV infection. Aids. 2003;17(13):1871–9.

39. Little SJ, McLean AR, Spina CA, Richman DD, Havlir DV. Viral dynamics of acute HIV-1 infection. J Exp Med. 1999;190(6):841–50.

40. Silvestri G, Cartwright EK. Chapter 9 - HIV and AIDS: Science Wrestles with 10,000 Nucleotides—Points but No Pin. In: Katze MG, Korth MJ, Law GL, Nathanson N, editors. Viral Pathogenesis (Third Edition) [Internet]. Boston: Academic Press; 2016 [cited 2024 Mar 15]. p. 107–23. Available from: https://www.sciencedirect.com/science/article/pii/B9780128009642000094

41. Mellors JW, Rinaldo Jr CR, Gupta P, White RM, Todd JA, Kingsley LA. Prognosis in HIV-1 infection predicted by the quantity of virus in plasma. Science. 1996;272(5265):1167–70.

42. Technical Notes | Volume 26 Number 2 | HIV Surveillance | Reports | Resource Library | HIV/AIDS | CDC [Internet]. 2023 [cited 2024 Mar 13]. Available from: https://www.cdc.gov/hiv/library/reports/hiv-surveillance/vol-26-no-2/content/technical-notes.html

43. Hollingsworth TD, Anderson RM, Fraser C. HIV-1 transmission, by stage of infection. J Infect Dis. 2008;198(5):687–93.

44. Hsu DC, O'Connell RJ. Progress in HIV vaccine development. Hum Vaccines Immunother. 2017;13(5):1018–30.

45. Haynes BF, Wiehe K, Borrow P, Saunders KO, Korber B, Wagh K, et al. Strategies for HIV-1 vaccines that induce broadly neutralizing antibodies. Nat Rev Immunol. 2023;23(3):142–58.

46. Margolis DA, Gonzalez-Garcia J, Stellbrink HJ, Eron JJ, Yazdanpanah Y, Podzamczer D, et al. Long-acting intramuscular cabotegravir and rilpivirine in adults with HIV-1 infection (LATTE-2): 96-week results of a randomised, open-label, phase 2b, non-inferiority trial. The Lancet. 2017;390(10101):1499–510.

47. Flexner C. HIV drug development: the next 25 years. Nat Rev Drug Discov. 2007;6(12):959–66.

48. Volberding PA, Deeks SG. Antiretroviral therapy and management of HIV infection. The Lancet. 2010;376(9734):49–62.

49. Arts EJ, Hazuda DJ. HIV-1 antiretroviral drug therapy. Cold Spring Harb Perspect Med. 2012;2(4):a007161.

50. Volberding PA. HIV Treatment and Prevention: An Overview of Recommendations From the IAS-USA Antiretroviral Guidelines Panel. Top Antivir Med. 2017 Mar;25(1):17–24.

51. Gulick RM, Flexner C. Long-acting HIV drugs for treatment and prevention. Annu Rev Med. 2019;70:137–50.

52. Molina JM, Capitant C, Spire B, Pialoux G, Cotte L, Charreau I, et al. On-demand preexposure prophylaxis in men at high risk for HIV-1 infection. N Engl J Med. 2015;373:2237–46.

53. Baeten JM, Donnell D, Ndase P, Mugo NR, Campbell JD, Wangisi J, et al. Antiretroviral prophylaxis for HIV prevention in heterosexual men and women. N Engl J Med. 2012;367(5):399–410.

54. Abram ME, Ferris AL, Shao W, Alvord WG, Hughes SH. Nature, position, and frequency of mutations made in a single cycle of HIV-1 replication. J Virol. 2010;84(19):9864–78.

55. Gupta RK, Jordan MR, Sultan BJ, Hill A, Davis DH, Gregson J, et al. Global trends in antiretroviral resistance in treatment-naive individuals with HIV after rollout of antiretroviral treatment in resource-limited settings: a global collaborative study and meta-regression analysis. The Lancet. 2012;380(9849):1250–8.

56. Isaac A, Pillay D. New drugs for treating drug resistant HIV-1. Sex Transm Infect. 2003 Jun 1;79(3):176.

57. Preston BD, Poiesz BJ, Loeb LA. Fidelity of HIV-1 reverse transcriptase. Science. 1988;242(4882):1168–71.

58. Hosek SG, Landovitz RJ, Kapogiannis B, Siberry GK, Rudy B, Rutledge B, et al. Safety and feasibility of antiretroviral preexposure prophylaxis for adolescent men who have sex with men aged 15 to 17 years in the United States. JAMA Pediatr. 2017;171(11):1063–71.

59. Bar-On Y, Gruell H, Schoofs T, Pai JA, Nogueira L, Butler AL, et al. Safety and antiviral activity of combination HIV-1 broadly neutralizing antibodies in viremic individuals. Nat Med. 2018;24(11):1701–7.

60. Cohen YZ, Caskey M. Broadly neutralizing antibodies for treatment and prevention of HIV-1 infection. Curr Opin HIV AIDS. 2018;13(4):366–73.

61. Hraber P, Seaman MS, Bailer RT, Mascola JR, Montefiori DC, Korber BT. Prevalence of broadly neutralizing antibody responses during chronic HIV-1 infection. AIDS Lond Engl. 2014;28(2):163.

62. Walker LM, Huber M, Doores KJ, Falkowska E, Pejchal R, Julien JP, et al. Broad neutralization coverage of HIV by multiple highly potent antibodies. Nature. 2011;477(7365):466–70.

63. Klein F, Diskin R, Scheid JF, Gaebler C, Mouquet H, Georgiev IS, et al. Somatic mutations of the immunoglobulin framework are generally required for broad and potent HIV-1 neutralization. Cell. 2013;153(1):126–38.

64. Moore PL, Crooks ET, Porter L, Zhu P, Cayanan CS, Grise H, et al. Nature of nonfunctional envelope proteins on the surface of human immunodeficiency virus type 1. J Virol. 2006;80(5):2515–28.

65. Kwong PD, Doyle ML, Casper DJ, Cicala C, Leavitt SA, Majeed S, et al. HIV-1 evades antibody-mediated neutralization through conformational masking of receptor-binding sites. Nature. 2002;420(6916):678–82.

66. Robertson DL, Sharp PM, McCutchan FE, Hahn BH. Recombination in HIV-1. Nature. 1995;374(6518):124–6.

67. Gaschen B, Taylor J, Yusim K, Foley B, Gao F, Lang D, et al. Diversity considerations in HIV-1 vaccine selection. Science. 2002;296(5577):2354–60.

68. Wei X, Decker JM, Wang S, Hui H, Kappes JC, Wu X, et al. Antibody neutralization and escape by HIV-1. Nature. 2003 Mar 20;422(6929):307–12.

69. Leonard CK, Spellman MW, Riddle L, Harris RJ, Thomas JN, Gregory T. Assignment of intrachain disulfide bonds and characterization of potential glycosylation sites of the type 1 recombinant human immunodeficiency virus envelope glycoprotein (gp120) expressed in Chinese hamster ovary cells. J Biol Chem. 1990;265(18):10373–82.

70. Zhou T, Zheng A, Baxa U, Chuang GY, Georgiev IS, Kong R, et al. A neutralizing antibody recognizing primarily N-linked glycan targets the silent face of the HIV envelope. Immunity. 2018;48(3):500–13.

71. McCoy LE, Burton DR. Identification and specificity of broadly neutralizing antibodies against HIV. Immunol Rev. 2017;275(1):11–20.

72. Wu X, Yang ZY, Li Y, Hogerkorp CM, Schief WR, Seaman MS, et al. Rational design of envelope identifies broadly neutralizing human monoclonal antibodies to HIV-1. Science. 2010;329(5993):856–61.

73. Walker LM, Phogat SK, Chan-Hui PY, Wagner D, Phung P, Goss JL, et al. Broad and potent neutralizing antibodies from an African donor reveal a new HIV-1 vaccine target. Science. 2009;326(5950):285–9.

74. Stamatatos L, Morris L, Burton DR, Mascola JR. Neutralizing antibodies generated during natural HIV-1 infection: good news for an HIV-1 vaccine? Nat Med. 2009;15(8):866–70.

75. Trkola A, Pomales AB, Yuan H, Korber B, Maddon PJ, Allaway GP, et al. Cross-clade neutralization of primary isolates of human immunodeficiency virus type 1 by human monoclonal antibodies and tetrameric CD4-IgG. J Virol. 1995;69(11):6609–17.

76. Burton DR, Pyati J, Koduri R, Sharp SJ, Thornton GB, Parren PW, et al. Efficient neutralization of primary isolates of HIV-1 by a recombinant human monoclonal antibody. Science. 1994;266(5187):1024–7.

77. Parker Miller E, Finkelstein MT, Erdman MC, Seth PC, Fera D. A structural update of neutralizing epitopes on the HIV envelope, a moving target. Viruses. 2021;13(9):1774.

78. Sok D, Burton DR. Recent progress in broadly neutralizing antibodies to HIV. Nat Immunol. 2018;19(11):1179–88.

79. Haynes BF, Burton DR, Mascola JR. Multiple roles for HIV broadly neutralizing antibodies. Sci Transl Med. 2019;11(516).

80. Walsh SR, Seaman MS. Broadly Neutralizing Antibodies for HIV-1 Prevention. Front Immunol. 2021;12:712122.

81. Stewart-Jones GB, Soto C, Lemmin T, Chuang GY, Druz A, Kong R, et al. Trimeric HIV-1-Env structures define glycan shields from clades A, B, and G. Cell. 2016;165(4):813–26.

82. Kwong PD, Wyatt R, Robinson J, Sweet RW, Sodroski J, Hendrickson WA. Structure of an HIV gp120 envelope glycoprotein in complex with the CD4 receptor and a neutralizing human antibody. Nature. 1998;393(6686):648–59.

83. Zhou T, Lynch RM, Chen L, Acharya P, Wu X, Doria-Rose NA, et al. Structural repertoire of HIV-1-neutralizing antibodies targeting the CD4 supersite in 14 donors. Cell. 2015;161(6):1280–92.

84. Rudicell RS, Kwon YD, Ko SY, Pegu A, Louder MK, Georgiev IS, et al. Enhanced potency of a broadly neutralizing HIV-1 antibody in vitro improves protection against lentiviral infection in vivo. J Virol. 2014;88(21):12669–82.

85. Huang J, Kang BH, Ishida E, Zhou T, Griesman T, Sheng Z, et al. Identification of a CD4-binding-site antibody to HIV that evolved near-pan neutralization breadth. Immunity. 2016;45(5):1108–21.

86. Pan R, Gorny MK, Zolla-Pazner S, Kong XP. The V1V2 region of HIV-1 gp120 forms a five-stranded beta barrel. J Virol. 2015;89(15):8003–10.

87. Löving R, Sjöberg M, Wu SR, Binley JM, Garoff H. Inhibition of the HIV-1 spike by single-PG9/16-antibody binding suggests a coordinated-activation model for its three protomeric units. J Virol. 2013;87(12):7000–7.

88. Webb NE, Montefiori DC, Lee B. Dose–response curve slope helps predict therapeutic potency and breadth of HIV broadly neutralizing antibodies. Nat Commun. 2015;6(1):8443.

89. Doria-Rose NA, Bhiman JN, Roark RS, Schramm CA, Gorman J, Chuang GY, et al. New member of the V1V2-directed CAP256-VRC26 lineage that shows increased breadth and exceptional potency. J Virol. 2016;90(1):76–91.

90. Doores KJ, Kong L, Krumm SA, Le KM, Sok D, Laserson U, et al. Two classes of broadly neutralizing antibodies within a single lineage directed to the high-mannose patch of HIV envelope. J Virol. 2015;89(2):1105–18.

91. Walker LM, Huber M, Doores KJ, Falkowska E, Pejchal R, Julien JP, et al. Broad neutralization coverage of HIV by multiple highly potent antibodies. Nature. 2011;477(7365):466–70.

92. Sok D, Pauthner M, Briney B, Lee JH, Saye-Francisco KL, Hsueh J, et al. A prominent site of antibody vulnerability on HIV envelope incorporates a motif associated with CCR5 binding and its camouflaging glycans. Immunity. 2016;45(1):31–45.

93. Wilen CB, Tilton JC, Doms RW. HIV: cell binding and entry. Cold Spring Harb Perspect Med. 2012;2(8).

94. Moore JP, Willey RL, Lewis GK, Robinson J, Sodroski J. Immunological evidence for interactions between the first, second, and fifth conserved domains of the gp120 surface glycoprotein of human immunodeficiency virus type 1. J Virol. 1994;68(11):6836–47.

95. Schoofs T, Barnes CO, Suh-Toma N, Golijanin J, Schommers P, Gruell H, et al. Broad and Potent Neutralizing Antibodies Recognize the Silent Face of the HIV Envelope. Immunity. 2019 Jun;50(6):1513-1529.e9.

96. Blattner C, Lee JH, Sliepen K, Derking R, Falkowska E, de la Peña AT, et al. Structural delineation of a quaternary, cleavage-dependent epitope at the gp41-gp120 interface on intact HIV-1 Env trimers. Immunity. 2014;40(5):669–80.

97. Lee JH, Leaman DP, Kim AS, Torrents de La Peña A, Sliepen K, Yasmeen A, et al. Antibodies to a conformational epitope on gp41 neutralize HIV-1 by destabilizing the Env spike. Nat Commun. 2015;6(1):8167.

98. Huang J, Kang BH, Pancera M, Lee JH, Tong T, Feng Y, et al. Broad and potent HIV-1 neutralization by a human antibody that binds the gp41–gp120 interface. Nature. 2014 Nov;515(7525):138–42.

99. Ananthaswamy N, Fang Q, AlSalmi W, Jain S, Chen Z, Klose T, et al. A sequestered fusion peptide in the structure of an HIV-1 transmitted founder envelope trimer. Nat Commun. 2019;10(1):873.

100. Molinos-Albert LM, Clotet B, Blanco J, Carrillo J. Immunologic insights on the membrane proximal external region: a major human immunodeficiency virus type-1 vaccine target. Front Immunol. 2017;8:1154.

101. Irimia A, Sarkar A, Stanfield RL, Wilson IA. Crystallographic identification of lipid as an integral component of the epitope of HIV broadly neutralizing antibody 4E10. Immunity. 2016;44(1):21–31.

102. Haynes BF, Shaw GM, Korber B, Kelsoe G, Sodroski J, Hahn BH, et al. HIV-host interactions: implications for vaccine design. Cell Host Microbe. 2016;19(3):292–303.

103. Burton DR, Ahmed R, Barouch DH, Butera ST, Crotty S, Godzik A, et al. A blueprint for HIV vaccine discovery. Cell Host Microbe. 2012;12(4):396–407.

104. Haynes BF, Kelsoe G, Harrison SC, Kepler TB. B-cell–lineage immunogen design in vaccine development with HIV-1 as a case study. Nat Biotechnol. 2012;30(5):423–33.

105. Pegu A, Hessell AJ, Mascola JR, Haigwood NL. Use of broadly neutralizing antibodies for HIV-1 prevention. Immunol Rev. 2017;275(1):296–312.

106. Nishimura Y, Gautam R, Chun TW, Sadjadpour R, Foulds KE, Shingai M, et al. Early antibody therapy can induce long-lasting immunity to SHIV. Nature. 2017;543(7646):559–63.

107. Nishimura Y, Martin MA. Of mice, macaques, and men: Broadly neutralizing antibody immunotherapy for HIV-1. Cell Host Microbe. 2017;22(2):207–16.

108. Mendoza P, Gruell H, Nogueira L, Pai JA, Butler AL, Millard K, et al. Combination therapy with anti-HIV-1 antibodies maintains viral suppression. Nature. 2018;561(7724):479–84.

109. Saunders KO, Pegu A, Georgiev IS, Zeng M, Joyce MG, Yang ZY, et al. Sustained delivery of a broadly neutralizing antibody in nonhuman primates confers long-term protection against simian/human immunodeficiency virus infection. J Virol. 2015;89(11):5895–903.

110. Marsden MD. Benefits and limitations of humanized mice in HIV persistence studies. Retrovirology. 2020;17(1):7.

111. Stoddart CA, Galkina SA, Joshi P, Kosikova G, Long BR, Maidji E, et al. Efficacy of broadly neutralizing monoclonal antibody PG16 in HIV-infected humanized mice. Virology. 2014;462:115–25.

112. Gauduin MC, Parren PW, Weir R, Barbas CF, Burton DR, Koup RA. Passive immunization with a human monoclonal antibody protects hu-PBL-SCID mice against challenge by primary isolates of HIV-1. Nat Med. 1997;3(12):1389–93.

113. Parren PW, Ditzel HJ, Gulizia RJ, Binley JM, Barbas III CF, Burton DR, et al. Protection against HIV-1 infection in hu-PBL-SCID mice by passive immunization with a neutralizing human monoclonal antibody against the gp120 CD4-binding site. Aids. 1995;9(6):1–538.

114. Deruaz M, Moldt B, Le KM, Power KA, Vrbanac VD, Tanno S, et al. Protection of humanized mice from repeated intravaginal HIV challenge by passive immunization: a model for studying the efficacy of neutralizing antibodies in vivo. J Infect Dis. 2016;214(4):612–6.

115. Sun M, Li Y, Yuan Z, Lu W, Kang G, Fan W, et al. VRC01 antibody protects against vaginal and rectal transmission of human immunodeficiency virus 1 in hu-BLT mice. Arch Virol. 2016;161:2449–55.

116. Reimann KA, Li JT, Voss G, Lekutis C, Tenner-Racz K, Racz P, et al. An env gene derived from a primary human immunodeficiency virus type 1 isolate confers high in vivo replicative capacity to a chimeric simian/human immunodeficiency virus in rhesus monkeys. J Virol. 1996;70(5):3198–206.

117. Sakuragi S, Shibata R, Mukai R, Komatsu T, Fukasawa M, Sakai H, et al. Infection of macaque monkeys with a chimeric human and simian immunodeficiency virus. J Gen Virol. 1992;73(11):2983–7.

118. Moldt B, Rakasz EG, Schultz N, Chan-Hui PY, Swiderek K, Weisgrau KL, et al. Highly potent HIV-specific antibody neutralization in vitro translates into effective protection against mucosal SHIV challenge in vivo. Proc Natl Acad Sci. 2012;109(46):18921–5.

119. Gautam R, Nishimura Y, Pegu A, Nason MC, Klein F, Gazumyan A, et al. A single injection of anti-HIV-1 antibodies protects against repeated SHIV challenges. Nature. 2016;533(7601):105–9.

120. Pegu A, Yang Z yong, Boyington JC, Wu L, Ko SY, Schmidt SD, et al. Neutralizing antibodies to HIV-1 envelope protect more effectively in vivo than those to the CD4 receptor. Sci Transl Med. 2014;6(243):243ra88-243ra88.

121. Shingai M, Donau OK, Plishka RJ, Buckler-White A, Mascola JR, Nabel GJ, et al. Passive transfer of modest titers of potent and broadly neutralizing anti-HIV monoclonal antibodies block SHIV infection in macaques. J Exp Med. 2014;211(10):2061–74.

122. Julg B, Sok D, Schmidt SD, Abbink P, Newman RM, Broge T, et al. Protective efficacy of broadly neutralizing antibodies with incomplete neutralization activity against simian-human immunodeficiency virus in rhesus monkeys. J Virol. 2017;91(20):10–1128.

123. Julg B, Tartaglia LJ, Keele BF, Wagh K, Pegu A, Sok D, et al. Broadly neutralizing antibodies targeting the HIV-1 envelope V2 apex confer protection against a clade C SHIV challenge. Sci Transl Med. 2017;9(406):eaal1321.

124. Pegu A, Borate B, Huang Y, Pauthner MG, Hessell AJ, Julg B, et al. A meta-analysis of passive immunization studies shows that serum-neutralizing antibody titer associates with protection against SHIV challenge. Cell Host Microbe. 2019;26(3):336–46.

125. Del Prete GQ, Lifson JD, Keele BF. Nonhuman primate models for evaluation of HIV-1 preventative vaccine strategies: model parameter considerations and consequences. Curr Opin HIV AIDS. 2016;11(6):546.

126. Patel P, Borkowf CB, Brooks JT, Lasry A, Lansky A, Mermin J. Estimating per-act HIV transmission risk: a systematic review. AIDS Lond Engl. 2014;28(10):1509.

127. Crowley AR, Ackerman ME. Mind the gap: how interspecies variability in IgG and its receptors may complicate comparisons of human and non-human primate effector function. Front Immunol. 2019;10:697.

128. Pantaleo G, Correia B, Fenwick C, Joo VS, Perez L. Antibodies to combat viral infections: development strategies and progress. Nat Rev Drug Discov. 2022;21(9):676–96.

129. Ward ES, Ober RJ. Multitasking by exploitation of intracellular transport functions: the many faces of FcRn. Adv Immunol. 2009;103:77–115.

130. Roopenian DC, Akilesh S. FcRn: the neonatal Fc receptor comes of age. Nat Rev Immunol. 2007;7(9):715–25.

131. Ko SY, Pegu A, Rudicell RS, Yang Z yong, Joyce MG, Chen X, et al. Enhanced neonatal Fc receptor function improves protection against primate SHIV infection. Nature. 2014;514(7524):642–5.

132. Gilbert PB, Juraska M, DeCamp AC, Karuna S, Edupuganti S, Mgodi N, et al. Basis and statistical design of the passive HIV-1 antibody mediated prevention (AMP) test-of-concept efficacy trials. Stat Commun Infect Dis. 2017;9(1):20160001.

133. Huang Y, Naidoo L, Zhang L, Carpp LN, Rudnicki E, Randhawa A, et al. Pharmacokinetics and predicted neutralisation coverage of VRC01 in HIV-uninfected participants of the Antibody Mediated Prevention (AMP) trials. EBioMedicine. 2021;64.

134. Mayer KH, Seaton KE, Huang Y, Grunenberg N, Isaacs A, Allen M, et al. Safety, pharmacokinetics, and immunological activities of multiple intravenous or subcutaneous doses of an anti-HIV monoclonal antibody, VRC01, administered to HIV-uninfected adults: Results of a phase 1 randomized trial. PLoS Med. 2017 Nov;14(11):e1002435.

135. Corey L, Gilbert PB, Juraska M, Montefiori DC, Morris L, Karuna ST, et al. Two randomized trials of neutralizing antibodies to prevent HIV-1 acquisition. N Engl J Med. 2021;384(11):1003–14.

136. Bar KJ, Sneller MC, Harrison LJ, Justement JS, Overton ET, Petrone ME, et al. Effect of HIV Antibody VRC01 on Viral Rebound after Treatment Interruption. N Engl J Med. 2016 Nov 24;375(21):2037–50.

137. Caskey M, Klein F, Lorenzi JC, Seaman MS, West Jr AP, Buckley N, et al. Viraemia suppressed in HIV-1-infected humans by broadly neutralizing antibody 3BNC117. Nature. 2015;522(7557):487–91.

138. Caskey M, Schoofs T, Gruell H, Settler A, Karagounis T, Kreider EF, et al. Antibody 10-1074 suppresses viremia in HIV-1-infected individuals. Nat Med. 2017;23(2):185–91.

139. Lynch RM, Boritz E, Coates EE, DeZure A, Madden P, Costner P, et al. Virologic effects of broadly neutralizing antibody VRC01 administration during chronic HIV-1 infection. Sci Transl Med. 2015;7(319):319ra206-319ra206.

140. Pace CS, Fordyce MW, Franco D, Kao CY, Seaman MS, Ho DD. Anti-CD4 monoclonal antibody ibalizumab exhibits breadth and potency against HIV-1, with natural resistance mediated by the loss of a V5 glycan in envelope. JAIDS J Acquir Immune Defic Syndr. 2013;62(1):1–9.

141. Wagh K, Seaman MS, Zingg M, Fitzsimons T, Barouch DH, Burton DR, et al. Potential of conventional & bispecific broadly neutralizing antibodies for prevention of HIV-1 subtype A, C & D infections. PLoS Pathog. 2018;14(3):e1006860.

142. Dankwa S, Kosman C, Dennis M, Giorgi EE, Vuong K, Pahountis I, et al. A novel HIV triple broadly neutralizing antibody (bNAb) combination-based passive immunization of infant rhesus macaques achieves durable protective plasma neutralization levels and mediates anti-viral effector functions. bioRxiv. 2023;2023–10.

143. Julg B, Liu PT, Wagh K, Fischer WM, Abbink P, Mercado NB, et al. Protection against a mixed SHIV challenge by a broadly neutralizing antibody cocktail. Sci Transl Med. 2017;9(408):eaao4235.

144. Wagh K, Bhattacharya T, Williamson C, Robles A, Bayne M, Garrity J, et al. Optimal combinations of broadly neutralizing antibodies for prevention and treatment of HIV-1 clade C infection. PLoS Pathog. 2016;12(3):e1005520.

145. Mahomed S, Garrett N, Capparelli EV, Osman F, Mkhize NN, Harkoo I, et al. Safety and pharmacokinetics of escalating doses of neutralising monoclonal antibody CAP256V2LS administered with and without VRC07-523LS in HIV-negative women in South Africa (CAPRISA 012B): a phase 1, dose-escalation, randomised controlled trial. Lancet HIV. 2023 Apr;10(4):e230–43.

146. Julg B, Stephenson KE, Wagh K, Tan SC, Zash R, Walsh S, et al. Safety and antiviral activity of triple combination broadly neutralizing monoclonal antibody therapy against HIV-1: a phase 1 clinical trial. Nat Med. 2022;28(6):1288–96.

147. Cohen YZ, Butler AL, Millard K, Witmer-Pack M, Levin R, Unson-O'Brien C, et al. Safety, pharmacokinetics, and immunogenicity of the combination of the broadly neutralizing anti-HIV-1 antibodies 3BNC117 and 10-1074 in healthy adults: A randomized, phase 1 study. PLoS One. 2019;14(8):e0219142.

148. Sobieszczyk ME, Mannheimer S, Paez CA, Yu C, Gamble T, Theodore DA, et al. Safety, tolerability, pharmacokinetics, and immunological activity of dual-combinations and triple-combinations of anti-HIV monoclonal antibodies PGT121, PGDM1400, 10-1074, and VRC07-523LS administered intravenously to HIV-uninfected adults: a phase 1 randomised trial. Lancet HIV. 2023;10(10):e653–62.

149. Gaudinski MR, Coates EE, Houser KV, Chen GL, Yamshchikov G, Saunders JG, et al. Safety and pharmacokinetics of the Fc-modified HIV-1 human monoclonal antibody VRC01LS: A Phase 1 open-label clinical trial in healthy adults. PLoS Med. 2018;15(1):e1002493.

150. HIV Vaccine Trials Network. Antiretroviral Analytical Treatment Interruption (ATI) to Assess Immunologic and Virologic Responses in Participants Who Initiated ART in Early HIV Infection After Having Received VRC01 or Placebo in HVTN 703/HPTN 081 [Internet]. clinicaltrials.gov; 2023 Aug [cited 2024 Jan 1]. Report No.: NCT04860323. Available from: https://clinicaltrials.gov/study/NCT04860323

151. Gaudinski MR, Houser KV, Doria-Rose NA, Chen GL, Rothwell RSS, Berkowitz N, et al. Safety and pharmacokinetics of broadly neutralising human monoclonal antibody VRC07-523LS in healthy adults: a phase 1 dose-escalation clinical trial. Lancet HIV. 2019;6(10):e667–79.

152. Walsh S, Gay C, Karuna S, Hyrien O, Skalland T, Mayer K, et al. Safety and single-dose pharmacokinetics of VRC07-523LS administered via different routes and doses. J Int AIDS Soc. 2021;24(S1):8–10.

153. Widge A, Houser K, Gaudinski M, Chen G, Carter C, Hickman S, et al. A phase I dose-escalation trial of human monoclonal antibody N6LS in healthy adults. In 2020.

154. Casazza JP, Cale EM, Narpala S, Yamshchikov GV, Coates EE, Hendel CS, et al. Safety and tolerability of AAV8 delivery of a broadly neutralizing antibody in adults living with HIV: a phase 1, dose-escalation trial. Nat Med. 2022;28(5):1022–30.

155. Koup R. Review of bNAbs in Clinical Development. Hiv Res Prev Hivr4p Satell Sess SA04 State Art HIV BNAbs Prev HIV Infect. 2018;

156. Mkhize NN, Yssel AE, Kaldine H, van Dorsten RT, Woodward Davis AS, Beaume N, et al. Neutralization profiles of HIV-1 viruses from the VRC01 Antibody Mediated Prevention (AMP) trials. PLoS Pathog. 2023;19(6):e1011469.

157. Priddy FH, Lewis DJ, Gelderblom HC, Hassanin H, Streatfield C, LaBranche C, et al. Adeno-associated virus vectored immunoprophylaxis to prevent HIV in healthy adults: a phase 1 randomised controlled trial. Lancet HIV. 2019;6(4):e230–9.

158. Stephenson KE, Julg B, Tan CS, Zash R, Walsh SR, Rolle CP, et al. Safety, pharmacokinetics and antiviral activity of PGT121, a broadly neutralizing monoclonal antibody against HIV-1: a randomized, placebo-controlled, phase 1 clinical trial. Nat Med. 2021;27(10):1718–24.

159. Armbruster C, Stiegler GM, Vcelar BA, Jäger W, Michael NL, Vetter N, et al. A phase I trial with two human monoclonal antibodies (hMAb 2F5, 2G12) against HIV-1. Aids. 2002;16(2):227–33.

160. Gaebler C, Nogueira L, Stoffel E, Oliveira TY, Breton G, Millard KG, et al. Prolonged viral suppression with anti-HIV-1 antibody therapy. Nature. 2022 Jun;606(7913):368–74.

161. Huehls AM, Coupet TA, Sentman CL. Bispecific T-cell engagers for cancer immunotherapy. Immunol Cell Biol. 2015;93(3):290–6.

162. Labrijn AF, Janmaat ML, Reichert JM, Parren PW. Bispecific antibodies: a mechanistic review of the pipeline. Nat Rev Drug Discov. 2019;18(8):585–608.

163. Wu X, Demarest SJ. Building blocks for bispecific and trispecific antibodies. Bispecific Antibodies. 2019 Feb 1;154:3–9.

164. Brinkmann U, Kontermann RE. The making of bispecific antibodies. In Taylor & Francis; 2017. p. 182–212.

165. Padte NN, Yu J, Huang Y, Ho DD. Engineering multi-specific antibodies against HIV-1. Retrovirology. 2018;15(1):1–17.

166. Muyldermans S. Nanobodies: natural single-domain antibodies. Annu Rev Biochem. 2013;82:775–97.

167. Li J, Zhou C, Dong B, Zhong H, Chen S, Li Q, et al. Single domain antibody-based bispecific antibody induces potent specific anti-tumor activity. Cancer Biol Ther. 2016;17(12):1231–9.

168. Ward ES, Güssow D, Griffiths AD, Jones PT, Winter G. Binding activities of a repertoire of single immunoglobulin variable domains secreted from Escherichia coli. Nature. 1989;341(6242):544–6.

169. Holt LJ, Herring C, Jespers LS, Woolven BP, Tomlinson IM. Domain antibodies: proteins for therapy. TRENDS Biotechnol. 2003;21(11):484–90.

170. Ahmad ZA, Yeap SK, Ali AM, Ho WY, Alitheen NBM, Hamid M. scFv antibody: principles and clinical application. J Immunol Res. 2012;2012.

171. Röthlisberger D, Honegger A, Plückthun A. Domain interactions in the Fab fragment: a comparative evaluation of the single-chain Fv and Fab format engineered with variable domains of different stability. J Mol Biol. 2005;347(4):773–89.

172. Vidarsson G, Dekkers G, Rispens T. IgG subclasses and allotypes: from structure to effector functions. Front Immunol. 2014;5:520.

173. Klein C, Sustmann C, Thomas M, Stubenrauch K, Croasdale R, Schanzer J, et al. Progress in overcoming the chain association issue in bispecific heterodimeric IgG antibodies. In Taylor & Francis; 2012. p. 653–63.

174. Schaefer W, Regula JT, Bähner M, Schanzer J, Croasdale R, Dürr H, et al. Immunoglobulin domain crossover as a generic approach for the production of bispecific IgG antibodies. Proc Natl Acad Sci. 2011;108(27):11187–92.

175. Klein C, Schaefer W, Regula JT, Dumontet C, Brinkmann U, Bacac M, et al. Engineering therapeutic bispecific antibodies using CrossMab technology. Methods. 2019;154:21–31.

176. Kuglstatter A, Stihle M, Neumann C al, Müller C, Schaefer W, Klein C, et al. Structural differences between glycosylated, disulfide-linked heterodimeric Knob-into-Hole Fc fragment and its homodimeric Knob–Knob and Hole–Hole side products. Protein Eng Des Sel. 2017;30(9):649–56.

177. Atwell S, Ridgway JB, Wells JA, Carter P. Stable heterodimers from remodeling the domain interface of a homodimer using a phage display library. J Mol Biol. 1997 Jul 4;270(1):26–35.

178. Merchant AM, Zhu Z, Yuan JQ, Goddard A, Adams CW, Presta LG, et al. An efficient route to human bispecific IgG. Nat Biotechnol. 1998 Jul;16(7):677–81.

179. Nordstrom JL, Ferrari G, Margolis DM. Bispecific antibody-derived molecules to target persistent HIV infection. J Virus Erad. 2022;8(3):100083.

180. Petrovas C, Ferrando-Martinez S, Gerner MY, Casazza JP, Pegu A, Deleage C, et al. Follicular CD8 T cells accumulate in HIV infection and can kill infected cells in vitro via bispecific antibodies. Sci Transl Med. 2017;9(373):eaag2285.

181. Sengupta S, Board NL, Wu F, Moskovljevic M, Douglass J, Zhang J, et al. TCR-mimic bispecific antibodies to target the HIV-1 reservoir. Proc Natl Acad Sci. 2022;119(15):e2123406119.

182. Promsote W, Xu L, Hataye J, Fabozzi G, March K, Almasri CG, et al. Trispecific antibody targeting HIV-1 and T cells activates and eliminates latently-infected cells in HIV/SHIV infections. Nat Commun. 2023 Jun 22;14(1):3719.

183. Board NL, Yuan Z, Wu F, Moskovljevic M, Ravi M, Sengupta S, et al. Bispecific antibodies promote natural killer cell-mediated elimination of HIV-1 reservoir cells. Nat Immunol. 2024;1–9.

184. Stam JC, de Maat S, de Jong D, Arens M, van Lint F, Gharu L, et al. Directing HIV-1 for degradation by non-target cells, using bi-specific single-chain llama antibodies. Sci Rep. 2022 Aug 4;12(1):13413.

185. Liang J, Zhai L, Liang Z, Chen X, Jiang Y, Lin Y, et al. Rational Design and Characterization of Trispecific Antibodies Targeting the HIV-1 Receptor and Envelope Glycoprotein. Vaccines. 2023;12(1):19.

186. Pace CS, Song R, Ochsenbauer C, Andrews CD, Franco D, Yu J, et al. Bispecific antibodies directed to CD4 domain 2 and HIV envelope exhibit exceptional breadth and picomolar potency against HIV-1. Proc Natl Acad Sci. 2013;110(33):13540–5.

187. Sun M, Pace CS, Yao X, Yu F, Padte NN, Huang Y, et al. Rational design and characterization of the novel, broad and potent bispecific HIV-1 neutralizing antibody iMabm36. J Acquir Immune Defic Syndr 1999. 2014;66(5):473.

188. Asokan M, Rudicell R, Louder M, McKee K, O'dell S, Stewart-Jones G, et al. Bispecific antibodies targeting different epitopes on the HIV-1 envelope exhibit broad and potent neutralization. J Virol. 2015;89(24):12501–12.

189. Bournazos S, Gazumyan A, Seaman MS, Nussenzweig MC, Ravetch JV. Bispecific anti-HIV-1 antibodies with enhanced breadth and potency. Cell. 2016;165(7):1609–20.

190. Huang Y, Yu J, Lanzi A, Yao X, Andrews CD, Tsai L, et al. Engineered bispecific antibodies with exquisite HIV-1-neutralizing activity. Cell. 2016;165(7):1621–31.

191. Moshoette T, Ali SA, Papathanasopoulos MA, Killick MA. Engineering and characterising a novel, highly potent bispecific antibody iMab-CAP256 that targets HIV-1. Retrovirology. 2019 Nov 8;16(1):31.

192. Davis-Gardner ME, Alfant B, Weber JA, Gardner MR, Farzan M. A bispecific antibody that simultaneously recognizes the V2-and V3-glycan epitopes of the HIV-1 envelope glycoprotein is broader and more potent than its parental antibodies. MBio. 2020;11(1):10–1128.

193. Wu X, Guo J, Niu M, An M, Liu L, Wang H, et al. Tandem bispecific neutralizing antibody eliminates HIV-1 infection in humanized mice. J Clin Invest. 2018;128(6):2239–51.

194. Xu L, Pegu A, Rao E, Doria-Rose N, Beninga J, McKee K, et al. Trispecific broadly neutralizing HIV antibodies mediate potent SHIV protection in macaques. Science. 2017;358(6359):85–90.

195. Ho D. A Phase 1 Dose-escalation Study of the Safety, Tolerability, Pharmacokinetics, and Antiviral Activity of the Bispecific Antibody 10E8.4/iMab in HIV-1-infected and Uninfected Individuals [Internet]. clinicaltrials.gov; 2023 Mar [cited 2024 Jan 1]. Report No.: NCT03875209. Available from: https://clinicaltrials.gov/study/NCT03875209

196. Ho D. Phase 1b Single Dose Clinical Trial of a Novel Long-Acting Bispecific Antibody in People With HIV to Inform Development for HIV Pre- and Post-Exposure Prophylaxis [Internet]. clinicaltrials.gov; 2023 Dec [cited 2024 Jan 1]. Report No.: NCT05890963. Available from: https://clinicaltrials.gov/study/NCT05890963

197. National Institute of Allergy and Infectious Diseases (NIAID). A Phase I, First-in-Human Study of SAR441236, a Tri-specific Broadly Neutralizing Antibody, in Participants With HIV [Internet]. clinicaltrials.gov; 2024 Jan [cited 2024 Jan 1]. Report No.: NCT03705169. Available from: https://clinicaltrials.gov/study/NCT03705169

198. A First-in-Human Study of the Trispecific HIV-1 Broadly Neutralizing Antibody, SAR441236 - CROI Conference [Internet]. 2024 [cited 2024 Mar 7]. Available from: https://www.croiconference.org/abstract/a-first-in-human-study-of-the-trispecific-hiv-1-broadly-neutralizing-antibody-sar441236/

199. Khan SN, Sok D, Tran K, Movsesyan A, Dubrovskaya V, Burton DR, et al. Targeting the HIV-1 spike and coreceptor with bi-and trispecific antibodies for single-component broad inhibition of entry. J Virol. 2018;92(18):10–1128.

200. Steinhardt JJ, Guenaga J, Turner HL, McKee K, Louder MK, O'Dell S, et al. Rational design of a trispecific antibody targeting the HIV-1 Env with elevated anti-viral activity. Nat Commun. 2018;9(1):1–12.

201. Strokappe NM, Hock M, Rutten L, Mccoy LE, Back JW, Caillat C, et al. Super Potent Bispecific Llama VHH Antibodies Neutralize HIV via a Combination of gp41 and gp120 Epitopes. Antibodies Basel Switz. 2019 Jun 18;8(2):38.

202. Moshoette T, Papathanasopoulos MA, Killick MA. HIV-1 bispecific antibody iMab-N6 exhibits enhanced breadth but not potency over its parental antibodies iMab and N6. Virol J. 2022;19(1):143.

203. Hernandez I, Bott SW, Patel AS, Wolf CG, Hospodar AR, Sampathkumar S, et al. Pricing of monoclonal antibody therapies: higher if used for cancer? Am J Manag Care. 2018 Feb;24(2):109–12.

204. Dugdale CM, Ufio O, Alba C, Permar SR, Stranix-Chibanda L, Cunningham CK, et al. Cost-effectiveness of broadly neutralizing antibody prophylaxis for HIV-exposed infants in sub-Saharan African settings. J Int AIDS Soc. 2023 Jan;26(1):e26052.

205. Sterling J. GEN - Genetic Engineering and Biotechnology News. 2022 [cited 2024 Mar 10]. Tech Innovation Needed to Boost Capacity and Cut mAb Production Costs. Available from: https://www.genengnews.com/insights/tech-innovation-needed-to-boost-capacity-and-cut-mab-production-costs/

206. Kelley B, Renshaw T, Kamarck M. Process and operations strategies to enable global access to antibody therapies. Biotechnol Prog. 2021;37(3):e3139.

207. Hollevoet K, Declerck PJ. State of play and clinical prospects of antibody gene transfer. J Transl Med. 2017;15(1):1–19.

208. Schambach A, Zychlinski D, Ehrnstroem B, Baum C. Biosafety features of lentiviral vectors. Hum Gene Ther. 2013;24(2):132–42.

209. Muthumani K, Flingai S, Wise M, Tingey C, Ugen KE, Weiner DB. Optimized and enhanced DNA plasmid vector based in vivo construction of a neutralizing anti-HIV-1 envelope glycoprotein Fab. Hum Vaccines Immunother. 2013;9(10):2253–62.

210. Joseph A, Zheng JH, Chen K, Dutta M, Chen C, Stiegler G, et al. Inhibition of in vivo HIV infection in humanized mice by gene therapy of human hematopoietic stem cells with a lentiviral vector encoding a broadly neutralizing anti-HIV antibody. J Virol. 2010;84(13):6645–53.

211. Brady JM, Baltimore D, Balazs AB. Antibody gene transfer with adeno-associated viral vectors as a method for HIV prevention. Immunol Rev. 2017;275(1):324–33.

212. Gao G, Vandenberghe LH, Wilson JM. New recombinant serotypes of AAV vectors. Curr Gene Ther. 2005;5(3):285–97.

213. Srivastava A, Lusby E, Berns KI. Nucleotide sequence and organization of the adeno-associated virus 2 genome. J Virol. 1983;45(2):555–64.

214. Ogden PJ, Kelsic ED, Sinai S, Church GM. Comprehensive AAV capsid fitness landscape reveals a viral gene and enables machine-guided design. Science. 2019;366(6469):1139–43.

215. Chavda VP, Bezbaruah R, Valu D, Patel B, Kumar A, Prasad S, et al. Adenoviral Vector-Based Vaccine Platform for COVID-19: Current Status. Vaccines. 2023 Feb 13;11(2):432.

216. Kates J, Cox C, Published JM. How Much Could COVID-19 Vaccines Cost the U.S. After Commercialization? [Internet]. KFF. 2023 [cited 2024 Mar 10]. Available from: https://www.kff.org/coronavirus-covid-19/issue-brief/how-much-could-covid-19-vaccines-cost-the-u-s-after-commercialization/

217. VFC | Current CDC Vaccine Price List | CDC [Internet]. 2024 [cited 2024 Mar 11]. Available from: https://www.cdc.gov/vaccines/programs/vfc/awardees/vaccine-management/price-list/index.html

218. Dong JY, Fan PD, Frizzell RA. Quantitative Analysis of the Packaging Capacity of Recombinant Adeno-Associated Virus. Hum Gene Ther. 1996 Nov 10;7(17):2101–12.

219. Balazs AB, Chen J, Hong CM, Rao DS, Yang L, Baltimore D. Antibody-based protection against HIV infection by vectored immunoprophylaxis. Nature. 2012 Jan 1;481(7379):81–4.

220. Balazs AB, Ouyang Y, Hong CM, Chen J, Nguyen SM, Rao DS, et al. Vectored immunoprophylaxis protects humanized mice from mucosal HIV transmission. Nat Med. 2014 Mar 1;20(3):296–300.

221. Calcedo R, Vandenberghe LH, Gao G, Lin J, Wilson JM. Worldwide epidemiology of neutralizing antibodies to adeno-associated viruses. J Infect Dis. 2009;199(3):381–90.

222. Boutin S, Monteilhet V, Veron P, Leborgne C, Benveniste O, Montus MF, et al. Prevalence of serum IgG and neutralizing factors against adeno-associated virus (AAV) types 1, 2, 5, 6, 8, and 9 in the healthy population: implications for gene therapy using AAV vectors. Hum Gene Ther. 2010;21(6):704–12.

223. Ronzitti G, Gross DA, Mingozzi F. Human Immune Responses to Adeno-Associated Virus (AAV) Vectors. Front Immunol. 2020;11:670.

224. Manno CS, Pierce GF, Arruda VR, Glader B, Ragni M, Rasko JJ, et al. Successful transduction of liver in hemophilia by AAV-Factor IX and limitations imposed by the host immune response. Nat Med. 2006;12(3):342–7.

225. Gardner MR, Kattenhorn LM, Kondur HR, Von Schaewen M, Dorfman T, Chiang JJ, et al. AAV-expressed eCD4-Ig provides durable protection from multiple SHIV challenges. Nature. 2015;519(7541):87–91.

226. Johnson PR, Schnepp BC, Zhang J, Connell MJ, Greene SM, Yuste E, et al. Vector-mediated gene transfer engenders long-lived neutralizing activity and protection against SIV infection in monkeys. Nat Med. 2009;15(8):901–6.

227. Fuchs SP, Martinez-Navio JM, Piatak Jr M, Lifson JD, Gao G, Desrosiers RC. AAV-delivered antibody mediates significant protective effects against SIVmac239 challenge in the absence of neutralizing activity. PLoS Pathog. 2015;11(8):e1005090.

228. Saunders KO, Wang L, Joyce MG, Yang ZY, Balazs AB, Cheng C, et al. Broadly neutralizing human immunodeficiency virus type 1 antibody gene transfer protects nonhuman primates from mucosal simian-human immunodeficiency virus infection. J Virol. 2015;89(16):8334–45.

229. Martinez-Navio JM, Fuchs SP, Mendes DE, Rakasz EG, Gao G, Desrosiers RC. Long-Term Delivery of an Anti-SIV Monoclonal Antibody With AAV. Front Immunol [Internet]. 2020 Mar 17 [cited 2024 Mar 11];11. Available from: https://www.frontiersin.org/journals/immunology/articles/10.3389/fimmu.2020.00449/full

230. Martinez-Navio JM, Fuchs SP, Pantry SN, Lauer WA, Duggan NN, Keele BF, et al. Adeno-Associated Virus Delivery of Anti-HIV Monoclonal Antibodies Can Drive Long-Term Virologic Suppression. Immunity. 2019 Mar;50(3):567-575.e5.

231. Spalding KL, Bhardwaj RD, Buchholz BA, Druid H, Frisén J. Retrospective Birth Dating of Cells in Humans. Cell. 2005 Jul 15;122(1):133–43.

232. Schlake T, Thess A, Thran M, Jordan I. mRNA as novel technology for passive immunotherapy. Cell Mol Life Sci. 2019;76(2):301–28.

233. Schlake T, Thran M, Fiedler K, Heidenreich R, Petsch B, Fotin-Mleczek M. mRNA: a novel avenue to antibody therapy? Mol Ther. 2019;27(4):773–84.

234. Pardi N, Secreto AJ, Shan X, Debonera F, Glover J, Yi Y, et al. Administration of nucleoside-modified mRNA encoding broadly neutralizing antibody protects humanized mice from HIV-1 challenge. Nat Commun. 2017;8(1):14630.

235. Sahin U, Karikó K, Türeci Ö. mRNA-based therapeutics — developing a new class of drugs. Nat Rev Drug Discov. 2014 Oct;13(10):759–80.

236. Stadler CR, Bähr-Mahmud H, Celik L, Hebich B, Roth AS, Roth RP, et al. Elimination of large tumors in mice by mRNA-encoded bispecific antibodies. Nat Med. 2017;23(7):815–7.

237. Pardi N, Hogan MJ, Porter FW, Weissman D. mRNA vaccines—a new era in vaccinology. Nat Rev Drug Discov. 2018;17(4):261–79.

238. Park JW, Lagniton PNP, Liu Y, Xu RH. mRNA vaccines for COVID-19: what, why and how. Int J Biol Sci. 2021;17(6):1446–60.

239. Light DW, Lexchin J. The costs of coronavirus vaccines and their pricing. J R Soc Med. 2021 Nov 1;114(11):502–4.

240. COVID vaccine manufacturers set list price between $120-$130 per dose. Reuters [Internet]. 2023 Sep 12 [cited 2024 Mar 10]; Available from: https://www.reuters.com/business/healthcare-pharmaceuticals/covid-vaccine-manufacturers-set-list-price-between-120-130-per-dose-2023-09-12/

241. Gilbert PB, Juraska M, deCamp AC, Karuna S, Edupuganti S, Mgodi N, et al. Basis and Statistical Design of the Passive HIV-1 Antibody Mediated Prevention (AMP) Test-of-Concept Efficacy Trials. Stat Commun Infect Dis. 2017 Jan;9(1):20160001.

242. Patel A, Bah MA, Weiner DB. In Vivo Delivery of Nucleic Acid-Encoded Monoclonal Antibodies. BioDrugs. 2020 Jun 1;34(3):273–93.

243. Kang DD, Li H, Dong Y. Advancements of in vitro transcribed mRNA (IVT mRNA) to enable translation into the clinics. Adv Drug Deliv Rev. 2023 Aug 1;199:114961.

244. Milligan JF, Groebe DR, Witherell GW, Uhlenbeck OC. Oligoribonucleotide synthesis using T7 RNA polymerase and synthetic DNA templates. Nucleic Acids Res. 1987;15(21):8783–98.

245. Conrad T, Plumbom I, Alcobendas M, Vidal R, Sauer S. Maximizing transcription of nucleic acids with efficient T7 promoters. Commun Biol. 2020 Aug 14;3(1):1–8.

246. Gholamalipour Y, Karunanayake Mudiyanselage A, Martin CT. 3′ end additions by T7 RNA polymerase are RNA self-templated, distributive and diverse in character—RNA-Seq analyses. Nucleic Acids Res. 2018;46(18):9253–63.

247. Ramanathan A, Robb GB, Chan SH. mRNA capping: biological functions and applications. Nucleic Acids Res. 2016;44(16):7511–26.

248. Shatkin A. Capping of eucaryotic mRNAs. Cell. 1976;9(4):645–53.

249. Galloway A, Cowling VH. mRNA cap regulation in mammalian cell function and fate. Biochim Biophys Acta BBA - Gene Regul Mech. 2019 Mar 1;1862(3):270–9.

250. Daffis S, Szretter KJ, Schriewer J, Li J, Youn S, Errett J, et al. 2′-O methylation of the viral mRNA cap evades host restriction by IFIT family members. Nature. 2010 Nov;468(7322):452–6.

251. Devarkar SC, Wang C, Miller MT, Ramanathan A, Jiang F, Khan AG, et al. Structural basis for m7G recognition and 2′-O-methyl discrimination in capped RNAs by the innate immune receptor RIG-I. Proc Natl Acad Sci. 2016;113(3):596–601.

252. Henderson JM, Ujita A, Hill E, Yousif-Rosales S, Smith C, Ko N, et al. Cap 1 Messenger RNA Synthesis with Co-transcriptional CleanCap® Analog by In Vitro Transcription. Curr Protoc. 2021;1(2):e39.

253. Pesole G, Mignone F, Gissi C, Grillo G, Licciulli F, Liuni S. Structural and functional features of eukaryotic mRNA untranslated regions. Gene. 2001;276(1–2):73–81.

254. Leppek K, Das R, Barna M. Functional 5′ UTR mRNA structures in eukaryotic translation regulation and how to find them. Nat Rev Mol Cell Biol. 2018;19(3):158–74.

255. Araujo PR, Yoon K, Ko D, Smith AD, Qiao M, Suresh U, et al. Before it gets started: regulating translation at the 5′ UTR. Int J Genomics. 2012;2012.

256. Presnyak V, Alhusaini N, Chen YH, Martin S, Morris N, Kline N, et al. Codon optimality is a major determinant of mRNA stability. Cell. 2015;160(6):1111–24.

257. Hanson G, Coller J. Codon optimality, bias and usage in translation and mRNA decay. Nat Rev Mol Cell Biol. 2018;19(1):20–30.

258. Mao Y, Dong L, Liu XM, Guo J, Ma H, Shen B, et al. m6A in mRNA coding regions promotes translation via the RNA helicase-containing YTHDC2. Nat Commun. 2019;10(1):5332.

259. Choi J, Ieong KW, Demirci H, Chen J, Petrov A, Prabhakar A, et al. N 6-methyladenosine in mRNA disrupts tRNA selection and translation-elongation dynamics. Nat Struct Mol Biol. 2016;23(2):110–5.

260. Eyler DE, Franco MK, Batool Z, Wu MZ, Dubuke ML, Dobosz-Bartoszek M, et al. Pseudouridinylation of mRNA coding sequences alters translation. Proc Natl Acad Sci. 2019;116(46):23068–74.

261. Andreassi C, Riccio A. To localize or not to localize: mRNA fate is in 3′ UTR ends. Trends Cell Biol. 2009;19(9):465–74.

262. Brown BD, Gentner B, Cantore A, Colleoni S, Amendola M, Zingale A, et al. Endogenous microRNA can be broadly exploited to regulate transgene expression according to tissue, lineage and differentiation state. Nat Biotechnol. 2007;25(12):1457–67.

263. Lytle JR, Yario TA, Steitz JA. Target mRNAs are repressed as efficiently by microRNA-binding sites in the 5′ UTR as in the 3′ UTR. Proc Natl Acad Sci. 2007;104(23):9667–72.

264. Lai WJC, Zhu M, Belinite M, Ballard G, Mathews DH, Ermolenko DN. Intrinsically Unstructured Sequences in the mRNA 3' UTR Reduce the Ability of Poly (A) Tail to Enhance Translation. J Mol Biol. 2022;434(24):167877.

265. Mockey M, Gonçalves C, Dupuy FP, Lemoine FM, Pichon C, Midoux P. mRNA transfection of dendritic cells: Synergistic effect of ARCA mRNA capping with Poly(A) chains *in cis* and *in trans* for a high protein expression level. Biochem Biophys Res Commun. 2006 Feb 24;340(4):1062–8.

266. Park J, Kim M, Yi H, Baeg K, Choi Y, Lee YS, et al. Short poly (A) tails are protected from deadenylation by the LARP1–PABP complex. Nat Struct Mol Biol. 2023;30(3):330–8.

267. Passmore LA, Coller J. Roles of mRNA poly (A) tails in regulation of eukaryotic gene expression. Nat Rev Mol Cell Biol. 2022;23(2):93–106.

268. Zhao J, Hyman L, Moore C. Formation of mRNA 3′ ends in eukaryotes: mechanism, regulation, and interrelationships with other steps in mRNA synthesis. Microbiol Mol Biol Rev. 1999;63(2):405–45.

269. Chaudhary N, Weissman D, Whitehead KA. mRNA vaccines for infectious diseases: principles, delivery and clinical translation. Nat Rev Drug Discov. 2021;20(11):817–38.

270. Karikó K, Buckstein M, Ni H, Weissman D. Suppression of RNA recognition by Toll-like receptors: the impact of nucleoside modification and the evolutionary origin of RNA. Immunity. 2005;23(2):165–75.

271. Expression of therapeutic proteins after delivery of chemically modified mRNA in mice | Nature Biotechnology [Internet]. [cited 2024 Mar 11]. Available from: https://www.nature.com/articles/nbt.1733

272. Li B, Luo X, Dong Y. Effects of chemically modified messenger RNA on protein expression. Bioconjug Chem. 2016;27(3):849–53.

273. Karikó K, Muramatsu H, Welsh FA, Ludwig J, Kato H, Akira S, et al. Incorporation of pseudouridine into mRNA yields superior nonimmunogenic vector with increased translational capacity and biological stability. Mol Ther. 2008;16(11):1833–40.

274. Anderson BR, Muramatsu H, Nallagatla SR, Bevilacqua PC, Sansing LH, Weissman D, et al. Incorporation of pseudouridine into mRNA enhances translation by diminishing PKR activation. Nucleic Acids Res. 2010;38(17):5884–92.

275. Thess A, Grund S, Mui BL, Hope MJ, Baumhof P, Fotin-Mleczek M, et al. Sequence-engineered mRNA Without Chemical Nucleoside Modifications Enables an Effective Protein Therapy in Large Animals. Mol Ther. 2015 Sep 1;23(9):1456–64.

276. Courel M, Clément Y, Bossevain C, Foretek D, Vidal Cruchez O, Yi Z, et al. GC content shapes mRNA storage and decay in human cells. Elife. 2019;8:e49708.

277. von Roretz C, Marco SD, Mazroui R, Gallouzi I. Turnover of AU-rich-containing mRNAs during stress: a matter of survival. Wiley Interdiscip Rev RNA. 2011;2(3):336–47.

278. Kudla G, Lipinski L, Caffin F, Helwak A, Zylicz M. High guanine and cytosine content increases mRNA levels in mammalian cells. PLoS Biol. 2006;4(6):e180.

279. Mauger DM, Cabral BJ, Presnyak V, Su SV, Reid DW, Goodman B, et al. mRNA structure regulates protein expression through changes in functional half-life. Proc Natl Acad Sci. 2019;116(48):24075–83.

280. Krupp G. Unusual promoter-independent transcription reactions with bacteriophage RNA polymerases. Nucleic Acids Res. 1989;17(8):3023–36.

281. Cazenave C, Uhlenbeck OC. RNA template-directed RNA synthesis by T7 RNA polymerase. Proc Natl Acad Sci. 1994;91(15):6972–6.

282. Triana-Alonso FJ, Dabrowski M, Wadzack J, Nierhaus KH. Self-coded 3′-extension of run-off transcripts produces aberrant products during in vitro transcription with T7 RNA polymerase. J Biol Chem. 1995;270(11):6298–307.

283. Martin CT, Muller DK, Coleman JE. Processivity in early stages of transcription by T7 RNA polymerase. Biochemistry. 1988;27(11):3966–74.

284. Chen YG, Hur S. Cellular origins of dsRNA, their recognition and consequences. Nat Rev Mol Cell Biol. 2022;23(4):286–301.

285. Hartmann G. Nucleic acid immunity. Adv Immunol. 2017;133:121–69.

286. Baiersdörfer M, Boros G, Muramatsu H, Mahiny A, Vlatkovic I, Sahin U, et al. A facile method for the removal of dsRNA contaminant from in vitro-transcribed mRNA. Mol Ther-Nucleic Acids. 2019;15:26–35.

287. Dousis A, Ravichandran K, Hobert EM, Moore MJ, Rabideau AE. An engineered T7 RNA polymerase that produces mRNA free of immunostimulatory byproducts. Nat Biotechnol. 2023;41(4):560–8.

288. Wu MZ, Asahara H, Tzertzinis G, Roy B. Synthesis of low immunogenicity RNA with high-temperature in vitro transcription. Rna. 2020;26(3):345–60.

289. Mu Z, Haynes BF, Cain DW. HIV mRNA Vaccines—Progress and Future Paths. Vaccines. 2021 Feb;9(2):134.

290. Gay CL, DeBenedette MA, Tcherepanova IY, Gamble A, Lewis WE, Cope AB, et al. Immunogenicity of AGS-004 dendritic cell therapy in patients treated during acute HIV infection. AIDS Res Hum Retroviruses. 2018;34(1):111–22.

291. Routy JP, Boulassel MR, Yassine-Diab B, Nicolette C, Healey D, Jain R, et al. Immunologic activity and safety of autologous HIV RNA-electroporated dendritic cells in HIV-1 infected patients receiving antiretroviral therapy. Clin Immunol. 2010 Feb 1;134(2):140–7.

292. Allard SD, De Keersmaecker B, de Goede AL, Verschuren EJ, Koetsveld J, Reedijk ML, et al. A phase I/IIa immunotherapy trial of HIV-1-infected patients with Tat, Rev and Nef expressing dendritic cells followed by treatment interruption. Clin Immunol. 2012;142(3):252–68.

293. Van Gulck E, Vlieghe E, Vekemans M, Van Tendeloo VF, Van De Velde A, Smits E, et al. mRNA-based dendritic cell vaccination induces potent antiviral T-cell responses in HIV-1-infected patients. Aids. 2012;26(4):F1–12.

294. Gandhi RT, Kwon DS, Macklin EA, Shopis JR, McLean AP, McBrine N, et al. Immunization of HIV-1-infected persons with autologous dendritic cells transfected with mRNA encoding HIV-1 Gag and Nef: results of a randomized, placebo-controlled clinical trial. JAIDS J Acquir Immune Defic Syndr. 2016;71(3):246–53.

295. Jacobson JM, Routy JP, Welles S, DeBenedette M, Tcherepanova I, Angel JB, et al. Dendritic cell immunotherapy for HIV-1 infection using autologous HIV-1 RNA: a randomized, double-blind, placebo-controlled clinical trial. JAIDS J Acquir Immune Defic Syndr. 2016;72(1):31–8.

296. Walsh EE, Frenck Jr RW, Falsey AR, Kitchin N, Absalon J, Gurtman A, et al. Safety and immunogenicity of two RNA-based Covid-19 vaccine candidates. N Engl J Med. 2020;383(25):2439–50.

297. Anderson EJ, Rouphael NG, Widge AT, Jackson LA, Roberts PC, Makhene M, et al. Safety and immunogenicity of SARS-CoV-2 mRNA-1273 vaccine in older adults. N Engl J Med. 2020;383(25):2427–38.

298. Saunders KO, Pardi N, Parks R, Santra S, Mu Z, Sutherland L, et al. Lipid nanoparticle encapsulated nucleoside-modified mRNA vaccines elicit polyfunctional HIV-1 antibodies comparable to proteins in nonhuman primates. Npj Vaccines. 2021 Apr 9;6(1):1–14.

299. Pardi N, Hogan MJ, Porter FW, Weissman D. mRNA vaccines—a new era in vaccinology. Nat Rev Drug Discov. 2018;17(4):261–79.

300. Pardi N, LaBranche CC, Ferrari G, Cain DW, Tombácz I, Parks RJ, et al. Characterization of HIV-1 nucleoside-modified mRNA vaccines in rabbits and rhesus macaques. Mol Ther-Nucleic Acids. 2019;15:36–47.

301. Narayanan E, Falcone S, Elbashir SM, Attarwala H, Hassett K, Seaman MS, et al. Rational design and in vivo characterization of mRNA-encoded broadly neutralizing antibody combinations against HIV-1. Antibodies. 2022;11(4):67.

302. Huang J, Ofek G, Laub L, Louder MK, Doria-Rose NA, Longo NS, et al. Broad and potent neutralization of HIV-1 by a gp41-specific human antibody. Nature. 2012;491(7424):406–12.

303. Liu Z, Chen O, Wall JBJ, Zheng M, Zhou Y, Wang L, et al. Systematic comparison of 2A peptides for cloning multi-genes in a polycistronic vector. Sci Rep. 2017;7(1):2193.

304. Ho SCL, Bardor M, Feng H, Mariati, Tong YW, Song Z, et al. IRES-mediated Tricistronic vectors for enhancing generation of high monoclonal antibody expressing CHO cell lines. J Biotechnol. 2012 Jan 1;157(1):130–9.

305. Felipe P de, Luke GA, Hughes LE, Gani D, Halpin C, Ryan MD. E unum pluribus: multiple proteins from a self-processing polyprotein. Trends Biotechnol. 2006 Feb 1;24(2):68–75.

306. Kim JH, Lee SR, Li LH, Park HJ, Park JH, Lee KY, et al. High cleavage efficiency of a 2A peptide derived from porcine teschovirus-1 in human cell lines, zebrafish and mice. PloS One. 2011;6(4):e18556.

307. Szymczak AL, Vignali DA. Development of 2A peptide-based strategies in the design of multicistronic vectors. Expert Opin Biol Ther. 2005 May 1;5(5):627–38.

308. Ryan MD, King AM, Thomas GP. Cleavage of foot-and-mouth disease virus polyprotein is mediated by residues located within a 19 amino acid sequence. J Gen Virol. 1991;72(11):2727–32.

309. Wang Y, Wang F, Wang R, Zhao P, Xia Q. 2A self-cleaving peptide-based multi-gene expression system in the silkworm Bombyx mori. Sci Rep. 2015;5(1):16273.

310. De Felipe P, Ryan MD. Targeting of proteins derived from self-processing polyproteins containing multiple signal sequences. Traffic. 2004;5(8):616–26.

311. Ibrahimi A, Velde GV, Reumers V, Toelen J, Thiry I, Vandeputte C, et al. Highly efficient multicistronic lentiviral vectors with peptide 2A sequences. Hum Gene Ther. 2009;20(8):845–60.

312. Daniels RW, Rossano AJ, Macleod GT, Ganetzky B. Expression of multiple transgenes from a single construct using viral 2A peptides in Drosophila. PloS One. 2014;9(6):e100637.

313. Fang J, Qian JJ, Yi S, Harding TC, Tu GH, VanRoey M, et al. Stable antibody expression at therapeutic levels using the 2A peptide. Nat Biotechnol. 2005;23(5):584–90.

314. Shapiro J, Sciaky N, Lee J, Bosshart H, Angeletti RH, Bonifacino JS. Localization of endogenous furin in cultured cell lines. J Histochem Cytochem. 1997;45(1):3–12.

315. Matthews DJ, Goodman LJ, Gorman CM, Wells JA. A survey of furin substrate specificity using substrate phage display. Protein Sci. 1994;3(8):1197–205.

316. Binley JM, Sanders RW, Clas B, Schuelke N, Master A, Guo Y, et al. A recombinant human immunodeficiency virus type 1 envelope glycoprotein complex stabilized by an intermolecular disulfide bond between the gp120 and gp41 subunits is an antigenic mimic of the trimeric virion-associated structure. J Virol. 2000;74(2):627–43.

317. Tumba NL, Owen GR, Killick MA, Papathanasopoulos MA. Immunization with HIV-1 trimeric SOSIP. 664 BG505 or founder virus C (FVCEnv) covalently complexed to two-domain CD4S60C elicits cross-clade neutralizing antibodies in New Zealand white rabbits. Vaccine X. 2022;12:100222.

318. Killick MA, Grant ML, Cerutti NM, Capovilla A, Papathanasopoulos MA. Env–2dCD4S60C complexes act as super immunogens and elicit potent, broadly neutralizing antibodies against clinically relevant human immunodeficiency virus type 1 (HIV-1). Vaccine. 2015;33(46):6298–306.

319. Wu X, Yang ZY, Li Y, Hogerkorp CM, Schief WR, Seaman MS, et al. Rational design of envelope identifies broadly neutralizing human monoclonal antibodies to HIV-1. Science. 2010 Aug 13;329(5993):856–61.

320. Kwon YD, Georgiev IS, Ofek G, Zhang B, Asokan M, Bailer RT, et al. Optimization of the Solubility of HIV-1-Neutralizing Antibody 10E8 through Somatic Variation and Structure-Based Design. J Virol. 2016 Jul 1;90(13):5899–914.

321. Wei X, Decker JM, Liu H, Zhang Z, Arani RB, Kilby JM, et al. Emergence of resistant human immunodeficiency virus type 1 in patients receiving fusion inhibitor (T-20) monotherapy. Antimicrob Agents Chemother. 2002 Jun;46(6):1896–905.

322. Derdeyn CA, Decker JM, Sfakianos JN, Wu X, O'Brien WA, Ratner L, et al. Sensitivity of human immunodeficiency virus type 1 to the fusion inhibitor T-20 is modulated by coreceptor specificity defined by the V3 loop of gp120. J Virol. 2000 Sep;74(18):8358–67.

323. Platt EJ, Wehrly K, Kuhmann SE, Chesebro B, Kabat D. Effects of CCR5 and CD4 cell surface concentrations on infections by macrophagetropic isolates of human immunodeficiency virus type 1. J Virol. 1998 Apr;72(4):2855–64.

324. Platt EJ, Bilska M, Kozak SL, Kabat D, Montefiori DC. Evidence that ecotropic murine leukemia virus contamination in TZM-bl cells does not affect the outcome of neutralizing antibody assays with human immunodeficiency virus type 1. J Virol. 2009 Aug;83(16):8289–92.

325. Takeuchi Y, McClure MO, Pizzato M. Identification of gammaretroviruses constitutively released from cell lines used for human immunodeficiency virus research. J Virol. 2008 Dec;82(24):12585–8.

326. Wang S, Zhou Q, Chen X, Luo RH, Li Y, Liu X, et al. Modification of N-terminal α-amine of proteins via biomimetic ortho-quinone-mediated oxidation. Nat Commun. 2021 Apr 15;12(1):2257.

327. Kumar R, Deshpande S, Sewall LM, Ozorowski G, Cottrell CA, Lee WH, et al. Elicitation of potent serum neutralizing antibody responses in rabbits by immunization with an HIV-1 clade C trimeric Env derived from an Indian elite neutralizer. PLoS Pathog. 2021 Apr;17(4):e1008977.

328. deCamp A, Hraber P, Bailer RT, Seaman MS, Ochsenbauer C, Kappes J, et al. Global panel of HIV-1 Env reference strains for standardized assessments of vaccine-elicited neutralizing antibodies. J Virol. 2014 Mar;88(5):2489–507.

329. Kulkarni SS, Lapedes A, Tang H, Gnanakaran S, Daniels MG, Zhang M, et al. Highly complex neutralization determinants on a monophyletic lineage of newly transmitted subtype C HIV-1 Env clones from India. Virology. 2009 Mar 15;385(2):505–20.

330. Li M, Gao F, Mascola JR, Stamatatos L, Polonis VR, Koutsoukos M, et al. Human immunodeficiency virus type 1 env clones from acute and early subtype B infections for standardized assessments of vaccine-elicited neutralizing antibodies. J Virol. 2005 Aug;79(16):10108–25.

331. Revilla A, Delgado E, Christian EC, Dalrymple J, Vega Y, Carrera C, et al. Construction and phenotypic characterization of HIV type 1 functional envelope clones of subtypes G and F. AIDS Res Hum Retroviruses. 2011 Aug;27(8):889–901.

332. Shang H, Han X, Shi X, Zuo T, Goldin M, Chen D, et al. Genetic and neutralization sensitivity of diverse HIV-1 env clones from chronically infected patients in China. J Biol Chem. 2011 Apr 22;286(16):14531–41.

333. Williamson C, Morris L, Maughan MF, Ping LH, Dryga SA, Thomas R, et al. Characterization and selection of HIV-1 subtype C isolates for use in vaccine development. AIDS Res Hum Retroviruses. 2003 Feb;19(2):133–44.

334. Li M, Salazar-Gonzalez JF, Derdeyn CA, Morris L, Williamson C, Robinson JE, et al. Genetic and neutralization properties of subtype C human immunodeficiency virus type 1 molecular env clones from acute and early heterosexually acquired infections in Southern Africa. J Virol. 2006 Dec;80(23):11776–90.

335. Blish CA, Jalalian-Lechak Z, Rainwater S, Nguyen MA, Dogan OC, Overbaugh J. Cross-subtype neutralization sensitivity despite monoclonal antibody resistance among early subtype A, C, and D envelope variants of human immunodeficiency virus type 1. J Virol. 2009 Aug;83(15):7783–8.

336. Long EM, Rainwater SMJ, Lavreys L, Mandaliya K, Overbaugh J. HIV type 1 variants transmitted to women in Kenya require the CCR5 coreceptor for entry, regardless of the genetic complexity of the infecting virus. AIDS Res Hum Retroviruses. 2002 May 20;18(8):567–76.

337. Rademeyer C, Korber B, Seaman MS, Giorgi EE, Thebus R, Robles A, et al. Features of Recently Transmitted HIV-1 Clade C Viruses that Impact Antibody Recognition: Implications for Active and Passive Immunization. PLoS Pathog. 2016 Jul;12(7):e1005742.

338. Hraber P, Rademeyer C, Williamson C, Seaman MS, Gottardo R, Tang H, et al. Panels of HIV-1 Subtype C Env Reference Strains for Standardized Neutralization Assessments. J Virol. 2017 Oct 1;91(19):e00991-17.

339. Gibson DG, Glass JI, Lartigue C, Noskov VN, Chuang RY, Algire MA, et al. Creation of a bacterial cell controlled by a chemically synthesized genome. science. 2010;329(5987):52–6.

340. Gibson DG, Young L, Chuang RY, Venter JC, Hutchison CA, Smith HO. Enzymatic assembly of DNA molecules up to several hundred kilobases. Nat Methods. 2009;6(5):343–5.

341. Moshoette T, Papathanasopoulos MA, Killick MA. HIV-1 bispecific antibody iMab-N6 exhibits enhanced breadth but not potency over its parental antibodies iMab and N6. Virol J. 2022 Sep 7;19(1):143.

342. Mizote Y, Masumi-Koizumi K, Katsuda T, Yamaji H. Production of an antibody Fab fragment using 2A peptide in insect cells. J Biosci Bioeng. 2020;130(2):205–11.

343. Georgiev IS, Joyce MG, Yang Y, Sastry M, Zhang B, Baxa U, et al. Single-chain soluble BG505. SOSIP gp140 trimers as structural and antigenic mimics of mature closed HIV-1 Env. J Virol. 2015;89(10):5318–29.

344. Raymond C, Tom R, Perret S, Moussouami P, L'Abbé D, St-Laurent G, et al. A simplified polyethylenimine-mediated transfection process for large-scale and high-throughput applications. Methods. 2011;55(1):44–51.

345. Gupta R, Brunak S. Prediction of glycosylation across the human proteome and the correlation to protein function. Pac Symp Biocomput Pac Symp Biocomput. 2002;310–22.

346. Seaman MS, Janes H, Hawkins N, Grandpre LE, Devoy C, Giri A, et al. Tiered categorization of a diverse panel of HIV-1 Env pseudoviruses for assessment of neutralizing antibodies. J Virol. 2010;84(3):1439–52.

347. Yoon H, Macke J, West AP, Foley B, Bjorkman PJ, Korber B, et al. CATNAP: a tool to compile, analyze and tally neutralizing antibody panels. Nucleic Acids Res. 2015 Jul 1;43(W1):W213-219.

348. Li M, Gao F, Mascola JR, Stamatatos L, Polonis VR, Koutsoukos M, et al. Human immunodeficiency virus type 1 env clones from acute and early subtype B infections for standardized assessments of vaccine-elicited neutralizing antibodies. J Virol. 2005;79(16):10108–25.

349. Killick M, Capovilla A, Papathanasopoulos MA. Generation and characterization of an HIV-1 subtype C transmitted and early founder virus consensus sequence. AIDS Res Hum Retroviruses. 2014;30(10):1001–5.

350. Caskey M, Klein F, Lorenzi JCC, Seaman MS, West AP, Buckley N, et al. 3BNC117 a Broadly Neutralizing Antibody Suppresses Viremia in HIV-1-Infected Humans. Nature. 2015 Jun 25;522(7557):487–91.

351. Guttman M, Padte NN, Huang Y, Yu J, Rocklin GJ, Weitzner BD, et al. The influence of proline isomerization on potency and stability of anti-HIV antibody 10E8. Sci Rep. 2020;10(1):14313.

352. Do Kwon Y, Wang XE, Bender MF, Yang R, Li Y, McKee K, et al. Structures of HIV-1 neutralizing antibody 10E8 delineate the mechanistic basis of its multi-peak behavior on size-exclusion chromatography. Antibodies. 2021;10(2):23.

353. Ho SC, Bardor M, Li B, Lee JJ, Song Z, Tong YW, et al. Comparison of internal ribosome entry site (IRES) and Furin-2A (F2A) for monoclonal antibody expression level and quality in CHO cells. PloS One. 2013;8(5):e63247.

354. Chng J, Wang T, Nian R, Lau A, Hoi KM, Ho SC, et al. Cleavage efficient 2A peptides for high level monoclonal antibody expression in CHO cells. In Taylor & Francis; 2015. p. 403–12.

355. Torres M, Hussain H, Dickson AJ. The secretory pathway–the key for unlocking the potential of Chinese hamster ovary cell factories for manufacturing therapeutic proteins. Crit Rev Biotechnol. 2023;43(4):628–45.

356. Nyathi Y, Wilkinson BM, Pool MR. Co-translational targeting and translocation of proteins to the endoplasmic reticulum. Biochim Biophys Acta BBA-Mol Cell Res. 2013;1833(11):2392–402.

357. Paetzel M, Karla A, Strynadka NCJ, Dalbey RE. Signal Peptidases. Chem Rev. 2002 Dec 1;102(12):4549–80.

358. von Heijne G. The signal peptide. J Membr Biol. 1990;115:195–201.

359. Arakawa T, Kita Y, Sato H, Ejima D. MEP chromatography of antibody and Fc-fusion protein using aqueous arginine solution. Protein Expr Purif. 2009;63(2):158–63.

360. Shukla AA, Hinckley PJ, Gupta P, Yigzaw Y, Hubbard B. Strategies to address aggregation during protein A chromatography. BioProcess Int. 2005;3(5):36–43.

361. Shukla AA, Gupta P, Han X. Protein aggregation kinetics during Protein A chromatography: case study for an Fc fusion protein. J Chromatogr A. 2007;1171(1–2):22–8.

362. Kinderman F, Yerby B, Jawa V, Joubert MK, Joh NH, Malella J, et al. Impact of precipitation of antibody therapeutics after subcutaneous injection on pharmacokinetics and immunogenicity. J Pharm Sci. 2019;108(6):1953–63.

363. Arnold JN, Wormald MR, Sim RB, Rudd PM, Dwek RA. The impact of glycosylation on the biological function and structure of human immunoglobulins. Annu Rev Immunol. 2007;25:21–50.

364. Boune S, Hu P, Epstein AL, Khawli LA. Principles of N-linked glycosylation variations of IgG-based therapeutics: pharmacokinetic and functional considerations. Antibodies. 2020;9(2):22.

365. Zheng K, Bantog C, Bayer R. The impact of glycosylation on monoclonal antibody conformation and stability. In Taylor & Francis; 2011. p. 568–76.

366. van de Bovenkamp FS, Derksen NIL, Ooijevaar-de Heer P, Rispens T. The enzymatic removal of immunoglobulin variable domain glycans by different glycosidases. J Immunol Methods. 2019 Apr 1;467:58–62.

367. Parsons MS, Lee WS, Kristensen AB, Amarasena T, Khoury G, Wheatley AK, et al. Fc-dependent functions are redundant to efficacy of anti-HIV antibody PGT121 in macaques. J Clin Invest. 2019;129(1):182–91.

368. Zhou T, Georgiev I, Wu X, Yang ZY, Dai K, Finzi A, et al. Structural basis for broad and potent neutralization of HIV-1 by antibody VRC01. Science. 2010;329(5993):811–7.

369. Li Y, O'Dell S, Walker LM, Wu X, Guenaga J, Feng Y, et al. Mechanism of neutralization by the broadly neutralizing HIV-1 monoclonal antibody VRC01. J Virol. 2011;85(17):8954–67.

370. van Dorsten RT, Lambson BE, Wibmer CK, Weinberg MS, Moore PL, Morris L. Neutralization Breadth and Potency of Single-Chain Variable Fragments Derived from Broadly Neutralizing Antibodies Targeting Multiple Epitopes on the HIV-1 Envelope. J Virol. 2020 Jan 6;94(2):10.1128/jvi.01533-19.

371. van Dorsten RT, Reh L, Trkola A, Morris L, Moore PL. Single-Chain Variable Fragments of Broadly Neutralizing Antibodies Prevent HIV Cell-Cell Transmission. J Virol. 2022 Feb 23;96(4):e01934-21.

372. Mahomed S. Broadly neutralizing antibodies for HIV prevention: a comprehensive review and future perspectives. Clin Microbiol Rev. 2024 Apr 30;37(2):e00152-22.

373. Klein JS, Bjorkman PJ. Few and far between: how HIV may be evading antibody avidity. PLoS Pathog. 2010;6(5):e1000908.

374. Pan AC, Borhani DW, Dror RO, Shaw DE. Molecular determinants of drug–receptor binding kinetics. Drug Discov Today. 2013 Jul 1;18(13):667–73.

375. Schreiber G, Haran G, Zhou HX. Fundamental aspects of protein− protein association kinetics. Chem Rev. 2009;109(3):839–60.

376. Meas S, Mekvichitsaeng P, Roshorm YM. Co-expression of self-cleaved multiple proteins derived from Porcine Reproductive and Respiratory Syndrome Virus by bi-cistronic and tri-cistronic DNA vaccines. Protein Expr Purif. 2021 Jan 1;177:105763.

377. Mathison M, Singh VP, Gersch RP, Ramirez MO, Cooney A, Kaminsky SM, et al. "Triplet" polycistronic vectors encoding Gata4, Mef2c, and Tbx5 enhances postinfarct ventricular functional improvement compared with singlet vectors. J Thorac Cardiovasc Surg. 2014 Oct 1;148(4):1656-1664.e2.

378. McLenachan S, Sarsero JP, Ioannou PA. Flow-cytometric analysis of mouse embryonic stem cell lipofection using small and large DNA constructs. Genomics. 2007 Jun 1;89(6):708–20.

379. Kreiss P, Mailhe P, Scherman D, Pitard B, Cameron B, Rangara R, et al. Plasmid DNA size does not affect the physicochemical properties of lipoplexes but modulates gene transfer efficiency. Nucleic Acids Res. 1999 Oct 1;27(19):3792–8.

380. Janich C, Ivanusic D, Giselbrecht J, Janich E, Pinnapireddy SR, Hause G, et al. Efficient Transfection of Large Plasmids Encoding HIV-1 into Human Cells—A High Potential Transfection System Based on a Peptide Mimicking Cationic Lipid. Pharmaceutics. 2020 Aug 25;12(9):805.

381. Bai H, Lester GMS, Petishnok LC, Dean DA. Cytoplasmic transport and nuclear import of plasmid DNA. Biosci Rep. 2017 Nov 29;37(6):BSR20160616.

382. Campeau P, Chapdelaine P, Seigneurin-Venin S, Massie B, Tremblay JP. Transfection of large plasmids in primary human myoblasts. Gene Ther. 2001 Sep;8(18):1387–94.

383. Wu CY, Huang CW, Nai YS, Chu PY, Wang CH, Ding ST. A newly designed EGFP-2A peptide monocistronic baculoviral vector for concatenating the expression of recombinant proteins in insect cells. Processes. 2019;7(5):291.

384. Yang Y, Mariati, Ho SC, Yap MG. Mutated polyadenylation signals for controlling expression levels of multiple genes in mammalian cells. Biotechnol Bioeng. 2009;102(4):1152–60.

385. Gonzalez R, Andrews BA, Asenjo JA. Kinetic model of BiP-and PDI-mediated protein folding and assembly. J Theor Biol. 2002;214(4):529–37.

386. Ho SC, Koh EY, van Beers M, Mueller M, Wan C, Teo G, et al. Control of IgG LC: HC ratio in stably transfected CHO cells and study of the impact on expression, aggregation, glycosylation and conformational stability. J Biotechnol. 2013;165(3–4):157–66.

387. Schlatter S, Stansfield SH, Dinnis DM, Racher AJ, Birch JR, James DC. On the optimal ratio of heavy to light chain genes for efficient recombinant antibody production by CHO cells. Biotechnol Prog. 2005;21(1):122–33.

388. Koh EY, Ho SC, Mariati, Song Z, Bi X, Bardor M, et al. An internal ribosome entry site (IRES) mutant library for tuning expression level of multiple genes in mammalian cells. PLoS One. 2013;8(12):e82100.

389. Lin J, Neo SH, Ho SC, Yeo JH, Wang T, Zhang W, et al. Impact of Signal Peptides on Furin-2A Mediated Monoclonal Antibody Secretion in CHO Cells. Biotechnol J. 2017;12(9):1700268.

390. Zou S, Scarfo K, Nantz MH, Hecker JG. Lipid-mediated delivery of RNA is more efficient than delivery of DNA in non-dividing cells. Int J Pharm. 2010 Apr 15;389(1):232–43.

391. Thran M, Mukherjee J, Pönisch M, Fiedler K, Thess A, Mui BL, et al. mRNA mediates passive vaccination against infectious agents, toxins, and tumors. EMBO Mol Med. 2017;9(10):1434–47.

392. August A, Attarwala HZ, Himansu S, Kalidindi S, Lu S, Pajon R, et al. A phase 1 trial of lipid-encapsulated mRNA encoding a monoclonal antibody with neutralizing activity against Chikungunya virus. Nat Med. 2021;27(12):2224–33.

393. Sabnis S, Kumarasinghe ES, Salerno T, Mihai C, Ketova T, Senn JJ, et al. A novel amino lipid series for mRNA delivery: improved endosomal escape and sustained pharmacology and safety in non-human primates. Mol Ther. 2018;26(6):1509–19.

394. Kose N, Fox JM, Sapparapu G, Bombardi R, Tennekoon RN, De Silva AD, et al. A lipid-encapsulated mRNA encoding a potently neutralizing human monoclonal antibody protects against chikungunya infection. Sci Immunol. 2019;4(35):eaaw6647.

395. Julg B, Tartaglia LJ, Keele BF, Wagh K, Pegu A, Sok D, et al. Broadly neutralizing antibodies targeting the HIV-1 envelope V2 apex confer robust protection against a clade C SHIV challenge. Sci Transl Med. 2017 Sep 6;9(406):eaal1321.

396. Sambrook J, Russell DW. The inoue method for preparation and transformation of competent E. coli:“ultra-competent” cells. Csh Protoc. 2006;2006(1):10–1101.

Appendix A: General laboratory techniques and Kit protocols.

A1 Preparation of chemically competent cells.

Chemically competent *Escherichia coli* (*E.coli)* DH5α cells were prepared using the Inoue methods previously described (396). Chemically competent DH5α *E. coli* cells were streaked (to isolate a single bacterial colony for expansion) on Luria Bertani (LB) nutrient agar plates (2% (w/v) yeast extract, 5% (w/v) peptone, 5% (w/v) NaCl, 15% (w/v) agar) and incubated at 37°C overnight. A single colony was inoculated into 30 mL of super optimal broth (SOB) media (85 mM NaCl, 20% (w/v) tryptone, 5% (w/v) yeast extract, 2.5 mM KCl) in a 250 mL Erlenmeyer flask and incubated at 37°C, 200 rpm overnight. From this starter culture, three 1 L Erlenmeyer flasks containing 200 mL SOB media were inoculated with increasing volumes of starter culture (4 mL, 8 mL, and 20 mL) and incubated overnight at 18°C, 200 rpm. The OD600 of the cultures was monitored the following morning until one of the three cultures reached an OD600 of 0.4-0.45. The culture was placed in an ice-bath for 10 minutes. The bacteria cells were harvested by centrifugation at 2 500 x g for 10 minutes at 4°C, the media supernatant was discarded, and the bacterial cell pellet was gently resuspended and washed in 40 mL of chilled Inoue transformation buffer (55 mM $MnCl_2.4H_2O$; 15 mM $CaCl_2.2H_2O$; 250 mM KCl; 10 mM piperazine-1,2-bis (PIPES) solution, pH 6.7; sterile filtered through a 0.22 µm filter (Pall) insert reference). The bacterial cells were harvested by centrifugation at 2 500 x g for 10 minutes at 4°C, the Inoue transformation buffer was discarded, and the cell pellet was gently resuspended in an additional 20 mL of chilled Inoue transformation buffer. Dimethylsulfoxide (DMSO - 1.5 mL, final concentration 7.5% v/v) was added to the bacterial suspension and swirled to mix before incubating on ice for 10 minutes. Aliquots (50 - 100 µL) were dispensed into chilled, sterile 1.5 mL microfuge tubes kept on ice, and stored at -80°C.

A2 Isolation and purification of DNA.

A2.1 DNA extraction from agarose gel.

DNA was extracted from 0.8% agarose gels using the QIAquick Gel Extraction Kit (Qiagen, Hilden, Germany), according to the manufacturer's instructions with slight alterations. The gel fragments containing the DNA of interest was excised from the

agarose gel and three volumes of solubilisation Buffer QG (composition unavailable) were added to one weight-volume of gel (100 mg gel ~ 100 µL) and incubated at 50°C for 10 minutes to completely dissolve the gel slice. One gel volume of isopropanol was added to the sample, mixed, and loaded into the QIAquick spin column and centrifuged at 16 000 x g for one minute to allow the DNA to bind to the silica membrane in the high-salt buffer. The flow-through was discarded and 500 µL of Buffer QG (composition unavailable) was added to the column and centrifuged for one minute at 16 000 x g (recommended if the DNA will be used for sequencing or *in vitro* transcription). The flow-through was discarded and the bound DNA was washed with 750 µL of Buffer PE (composition unavailable), incubated at room temperature for 2 to 5 minutes, and centrifuged at 16 000 x g for 1 minute. The flow-through was discarded and the wash procedure was repeated with 500 µL of Buffer PE. After discarding the second wash buffer PE flow-through, the empty column was centrifuged at 16 000 x g for an additional 1 minute to remove any residual wash buffer. The DNA was eluted with a low-salt buffer into a clean 1.5 mL microfuge tube with 30 µL of Buffer EB (10 mM Tris-Cl, pH 8.5) applied to the centre of the membrane, incubated at room temperature for 2 to 4 minutes, and centrifuged at 16 000 x g for 2 minutes. The purified DNA fragments were quantified by UV absorption at A_{260nm} on a NanoDrop® Spectrophotometer ND-1000, software version 3.8.1 (Thermo Fisher Scientific, Waltham, MA, USA), initiated with nuclease-free water and blanked against the appropriate Buffer EB. Purified DNA was stored at 4°C short term or -20°C long term.

A2.2 PCR DNA amplicon purification.

PCR amplified DNA products were purified via a silica-based membrane column using the GeneJET PCR Purification Kit (Invitrogen, Thermo Fisher Scientific, Waltham, MA, USA, not all buffer compositions were available) to remove primers, dNTPs, enzymes, and salts from the DNA prior to downstream cloning and ligation reactions. A 1:1 volume of Binding Buffer (containing chaotropic agents to denature proteins and promote DNA binding to the silica membrane in the column) was added to the PCR mixture, mixed, transferred into the GeneJET purification column, and centrifuged at 12 000 x g for 1 minute. The flow-through was discarded and bound DNA was washed with 700 µL of Wash Buffer (diluted 1:5 with ethanol) and centrifuged at 12 000 x g for 1 minute. The flow-through was discarded and the empty column was centrifuged for an additional 2 minutes to remove any residual wash buffer. The DNA products were

eluted into a clean 1.5 mL microfuge tube in 30 µL of Elution Buffer (10 mM Tris-HCl, pH 8.5) applied to the centre of the membrane, incubated at room temperature for 2 minutes and centrifuged at 12 000 x g for 2 minutes. The purified DNA products were quantified by UV absorption at A_{260nm} on the NanoDrop® Spectrophotometer ND-1000, software version 3.8.1 (Thermo Fisher Scientific, Waltham, MA, USA) which was initiated with nuclease-free water and blanked against the appropriate Elution Buffer. Purified DNA products were stored at 4°C (short term) or -20°C (long term).

A2.3 Plasmid DNA isolation (Mini prep).

Plasmid DNA was extracted from 6 mL of overnight *E. coli* culture using the High Pure Plasmid Isolation Kit (Roche Group, Basel, Switzerland) according to the manufacturer's instructions. Culture was harvested by centrifugation at 4 500 x g for 10 minutes, the media supernatant was discarded, and the cell pellet was resuspended in 250 µL of chilled RNase-containing Suspension Buffer (50 mM Tris-HCl, 10 mM EDTA, 0.01% (w/v) RNase A, pH 8.0). The solution was transferred to a clean 1.5 mL microfuge tube and 250 µL of Lysis Buffer (0.2 M NaOH, 1% (v/v) SDS) was added, mixed gently, and incubated at room temperature for 5 minutes to ensure adequate lysis of the bacterial cells. Chilled Binding Buffer (350 µL – 4 M CH_5N_3.HCl, 0.5 M CH_3CO_2K, pH 4.2) was added, mixed gently, and incubated on ice for 5 minutes to precipitate genomic DNA and proteins before being centrifuged at 16 000 x g for 10 minutes. The debris pellet was discarded, and the supernatant was transferred to the High Pure filter tube and centrifuged at 16 000 x g for 1 minute to allow DNA binding to the membrane. The flow-through was discarded and the bound DNA was washed with 500 µL of Wash Buffer I diluted in ethanol (5 M CH_3N_3.HCl; 20 mM Tris-HCl; 60% (v/v) ethanol, pH 6.6) and centrifuged at 13 000 x g for 1 minute. The flow-through was discarded and an additional wash was performed with 700 µL of Wash Buffer II diluted in ethanol (20 mM NaCl; 2 mM Tris-HCl; 80% (v/v) ethanol, pH 7.5), centrifuged at 13 000 x g for 1 minute and an additional 2-minute centrifugation after the wash buffer flow-through was discarded. The DNA was eluted into a clean 1.5 mL microfuge tube with 100 µL of Elution Buffer (10 mM Tris, pH 8.5) added to the centre of the membrane, incubated at room temperature for 2 minutes and centrifuged at 13 000 x g for 2 minutes. The purified plasmid DNA was quantified by UV absorption at A_{260nm} on the NanoDrop® Spectrophotometer ND-1000, software version 3.8.1 (Thermo

Fisher Scientific, Waltham, MA, USA) which was initiated with nuclease-free water and blanked against the appropriate Elution Buffer. Purified DNA was stored at -20°C.

A2.4 Plasmid DNA isolation (Midi and Maxi preps).

Plasmid DNA was isolated from 50 mL (Midi) or 150 mL (Maxi) of *E. coli* culture using a modified alkaline-lysis method followed by ion exchange chromatography using the QIAGEN Plasmid Midi and Maxi Kits (Qiagen, Hilden, Germany) according to the manufacturer's instructions with slight modifications. The bacterial culture was harvested by centrifugation at 6 000 x g for 15 minutes at 4°C (Eppendorf Centrifuge 5804 R – Eppendorf, Hamburg, Germany), and the media supernatant was discarded. The bacterial cell pellet was resuspended in 4 mL (Midi) or 10 mL (Maxi) of chilled resuspension buffer (P1 resuspension buffer: 50 mM Tris-Cl; 10 mM EDTA; 100 µg/mL RNase A, pH 8.0), the bacterial cells were lysed in 4 mL (Midi) or 10 mL (Maxi) lysis buffer (P2 lysis buffer: 200 mM NaOH; 1% (w/v) SDS), mixed, and incubated at room temperature for 5 minutes. The reaction was neutralised with 4 mL (Midi) or 10 mL (Maxi) chilled neutralisation buffer (P3 neutralisation buffer: 3 M CH_3CO_2K, pH 5.5), mixed and incubated on ice for 15 minutes (Midi) or 20 minutes (Maxi). The lysate was removed by centrifugation at 4 500 x g for 15 minutes and filtered through nylon filter wool (available at any aquarium store). The supernatant containing plasmid DNA was added to the anion-exchange QIAGEN-tip100 (Midi) or QIAGEN-tip500 (Maxi) (all buffers passed through the QIAGEN-tips by gravity flow), pre-equilibrated with 4 mL (Midi) or 10 mL (Maxi) equilibration buffer (QBT equilibration buffer: 750 mM NaCl; 50 mM MOPS, 15% (v/v) isopropanol; 0.15% (v/v) Triton® X-100, pH 7.0) that facilitated selective DNA binding to the resin. The bound DNA was washed with a high-salt buffer to remove RNA, proteins, and other impurities with 2 x 10 mL (Midi) or 2 x 30 mL (Maxi) of wash buffer (QC: 1 M NaCl; 50 mM Tris-Cl; 15% (v/v) isopropanol, pH 7.0). The DNA was eluted from the resin in 5 mL (Midi) or 15 mL (Maxi) of elution buffer (QF: 1.25 mM NaCl; 50 mM Tris-Cl; 15% (v/v) isopropanol, pH 8.5), precipitated with 3.5 mL (Midi) or 10.5 mL (Maxi) isopropanol and mixed. For the Midi prep, the eluate mixture was divided among four 2 mL microfuge tubes and centrifuged at 16 000 x g for 30 minutes at 4°C (Eppendorf Centrifuge 5415 R – Eppendorf, Hamburg, Germany). The supernatant was carefully discarded, the DNA pellets were each washed with 0.5 mL of 70% ethanol and centrifuged at 16 000 x g for 10 minutes at 4°C (Eppendorf Centrifuge 5415 R – Eppendorf, Hamburg, Germany). The

supernatant was carefully aspirated, the DNA pellets were air-dried for 5-10 minutes and resuspended in 100 µL endotoxin-free TE buffer (10 mM Tris-Cl; 1 mM EDTA, pH 8.0). The Maxi prep eluate mixture was centrifuged at 15 000 x g for 30 minutes at 4°C (Eppendorf Centrifuge 5415 R – Eppendorf, Hamburg, Germany). The supernatant was carefully discarded, and the DNA pellet was washed with 5 mL of 70% ethanol and centrifuged at 15 000 x g for 10 minutes at 4°C (Eppendorf Centrifuge 5415 R – Eppendorf, Hamburg, Germany). The supernatant was carefully discarded, and the DNA pellet was air-dried for 5-10 minutes and resuspended in 500 µL endotoxin-free TE buffer (10 mM Tris-Cl; 1 mM EDTA, pH 8.0). The DNA concentration was determined by UV absorption at A_{260nm} on a NanoDrop Spectrophotometer ND-1000, software version 3.8.1 (Thermo Fisher Scientific, Waltham, MA, USA) which was initiated with nuclease-free water and blanked against the TE buffer. Purified plasmid DNA was diluted to 0.5 µg/µL with TE buffer and stored at -20°C.

A3 Thermocycling.

Polymerase chain reactions (PCRs) were performed according to the cycling conditions described in Table A1. PCR thermocycling and temperature incubations were performed on the GeneAmp® PCR System 9700 (Applied Biosystems, Thermo Fisher Scientific, Waltham, MA, USA) or C1000 Touch™ Thermal Cycler (BIO-RAD Laboratories, Hercules, CA, USA).

A4 Agarose gel electrophoresis.

Agarose (0.8 - 2% (w/v)) was dissolved in 1x tris, acetic acid, EDTA (TAE) Electrophoresis Buffer (40 mM Tris, 20 mM acetic acid, 1 mM EDTA) (Thermo Fisher Scientific, Waltham, MA, USA) with 40 µg (final concentration 0.8 µg/µL) of Ethidium Bromide Solution (BIO-RAD Laboratories, Hercules, CA, USA) for nucleic acid visualisation by agarose gel electrophoresis. DNA samples were prepared with 6x Orange DNA Loading Dye (Thermo Fisher Scientific, Waltham, MA, USA), diluted to a final 1x concentration, and resolved along the GeneRuler DNA Ladder Mix, ready-to-use SM0333 (Thermo Fisher Scientific, Waltham, MA, USA) or the O'GeneRuler 50 bp DNA Ladder, ready-to-use SM1133 (Thermo Fisher Scientific, Waltham, MA, USA) depending on the anticipated size, according to the manufacturer's instructions.

Samples of IVT-mRNA transcripts pre- and post-purification were diluted in DEPC-treated water and prepared in 2x RNA Loading Dye R0641 (Thermo Fisher Scientific,

Waltham, MA, USA), heated at 70°C for 10 minutes to denature the RNA secondary structure, chilled on ice for 3 minutes and resolved along the RiboRuler High Range RNA Ladder, ready-to-use SM1823 (Thermo Fisher Scientific, Waltham, MA, USA) that had been denatured in parallel with the samples. Agarose gel electrophoresis was performed in a multiSUB tank (Cleaver Scientific, Thistle Scientific Ltd, Warwickshire, UK) resolved at 80 V for approximately 1 hour and visualised using the ChemiDoc™ MP Imaging System and the Quantity One® software, version 4.6.9 (BIO-RAD Laboratories, Hercules, CA, USA) under Trans UV light exposure.

A5 Sanger sequencing.

In-house Sanger sequencing was performed using the BigDye™ Terminator v3.1 Cycle Sequencing Kit (Applied Biosystems, Thermo Fisher Scientific, Waltham, MA, USA) on a 3730xl DNA Analyzer (Applied Biosystems, Thermo Fisher Scientific, Waltham, MA, USA) according to the manufacturer's instructions with the following modifications. A final volume of 10 µL per well was used in a MicroAmp™ Optical 96-well Reaction plate (Applied Biosystems, Thermo Fisher Scientific, Waltham, MA, USA), comprising: 2 µl of 5x Sequencing Buffer, 1 µl of BigDye™ Terminator v3.1 Ready Reaction Mix, 1.5 µl of 3.5 µM primer, 300 ng of purified plasmid template DNA and PCR grade water to make up the remaining reaction volume. Various primer sets were used to sequence the forward and reverse direction to cover the area/s of interest (Table A1). The sequencing plate was centrifuged at 2 000 x g for 2 minutes and the thermal cycling was performed on the PCR System 9700 GeneAmp Thermocycler (Applied Biosystems, Thermo Fisher Scientific, Waltham, MA, USA) using the following conditions: 96°C for 1 minute, followed by 25 cycles of 96°C for 10 seconds, 50°C for 5 seconds, 60°C for 4 minutes, and held at 4°C (Table A1). The sequencing reaction was purified by precipitation by adding 50 µL ethanol-sodium acetate solution (3 M sodium acetate, pH 5.25: 100% ethanol = 1:25) to each well prior to centrifugation at 2 000 x g for 30 minutes at 4°C to pellet the amplicons. The plate was inverted and centrifuged at 100 x g for 20 seconds to remove the sodium acetate-ethanol solution, 150 µL of chilled 70% ethanol was added to each well and the plate was centrifuged at 2 000 x g for 5 minutes. The plate was inverted and centrifuged at 500 x g for 30 seconds to remove the ethanol and incubated at 95°C for 3 minutes to evaporate any remaining ethanol. Hi-Di™ Formamide (Applied Biosystems, Thermo Fisher Scientific, Waltham, MA, USA) was added to the plate (10 µL per well). The reactions were

incubated at 65°C for 5 minutes, vortexed, the plate was centrifuged at 1 000 x g for 30 seconds and loaded into the 3730xl DNA Analyser (Applied Biosystems, Thermo Fisher Scientific, Waltham, MA, USA) to be sequenced. The sequences were analysed using SnapGene® 3.1.2, the sequence reads were trimmed on the 5' and 3' ends to remove low-quality sequences and aligned to an *in silico* reference plasmid sequence generated in SnapGene® 3.1.2 to confirm the DNA constructs.

A6 SDS-PAGE.

Protein samples were analysed by SDS-PAGE and/or western blot. SDS-PAGE gels (10% acrylamide as described in Table A2) were cast in-house using the BIO-RAD Mini-Protean system (BIO-RAD Laboratories, Hercules, CA, USA). Protein samples (clarified cell culture supernatant or purified antibody) were prepared in reducing sample buffer (4x stock diluted to a final 1x: 0.025 M Tris-HCl, pH 6.8; 2% (w/v) SDS; 5% (v/v) glycerol; 0.1% (v/v) *B*-Mercaptoethanol; 0.0125 M ethylenediaminetetraacetic acid (EDTA); 0.02% (w/v) Bromophenol Blue) and heated at 80°C for 5 minutes. SDS-PAGE gels were resolved in 1x tank buffer (0.025 M Tris, 0.192 M Glycine, 0.1% (w/v) SDS) at 30 mA per gel for approximately 1 hour. NuPAGE™ 4-12% Bis-Tris Precast Gels (Invitrogen, Thermo Fisher Scientific, Waltham, MA, USA) were also used for protein sample analyses. Protein samples (clarified cell culture supernatant or purified antibody) were prepared in NuPAGE™ LDS Sample Buffer (4x) (Invitrogen, Thermo Fisher Scientific, Waltham, MA, USA) for non-reducing conditions and NuPAGE™ LDS Sample Buffer (4x) supplemented with 0.5 M dithiothreitol (DTT)- LDS sample buffer: DTT = 2.5:1) for reducing conditions and were heated at 70°C for 10 minutes. NuPAGE gels were resolved using 1x NuPAGE™ MOPS SDS Running Buffer (20x) (final concentration 1x: 50 mM MOPS, 50 mM Tris Base, 0.1% SDS, 1 mM EDTA, pH 7.7 - Invitrogen, Thermo Fisher Scientific, Waltham, MA, USA) performed in the Invitrogen Novex Mini-Cell system at 200 V for approximately 35 minutes. The samples were resolved along with the Color Protein Standard Broad Range P7719S or P7712S (New England Biolabs, Ipswich, MA, USA). Resolved protein bands were visualised using an overnight comassie blue staining (50% (v/v) methanol, 10% (v/v) acetic acid, 0.025% (w/v) Coomassie R250)/ followed by destaining (5% (v/v) ethanol, 7% (v/v) acetic acid) protocol and were imaged on the ChemiDoc™ MP Imaging System and the Quantity One® software, version 4.6.9 (BIO-RAD Laboratories, Hercules, CA, USA) under Trans UV light exposure.

A7 Western Blot.

SDS-PAGE resolved antibodies were transferred onto a Hybond™-C Extra nitrocellulose membrane (Amersham Biosciences, GE Healthcare, Amersham, UK) using the XCell II ™ Blot Module at 30 V for 1 hour, using NuPAGE® Transfer Buffer (20x) (final 1x concentration: 0.5 M Bicine, 0.5 M Bis-Tris, 20.5 mM EDTA free acid, 10% (v/v) methano, pH 7.2 - Thermo Fisher Scientific, Waltham, MA, USA). The nitrocellulose membrane was blocked overnight in 5% milk powder prepared in Tris Buffered Saline with Tween-20 (TTBS - 1% Tris, 0.01% Tween 20, pH 7.4). The blocking buffer was washed off the membrane with two 30 mL TTBS washes and placed flush on a clean glass surface for the development incubations. Resolved antibodies containing an intact Fc domain (parental antibodies; PGT121/122, VRC01 or 10E8v4 and multispecifics; Bi-NAb and Tri-NAb (Co-T & sORF)), were detected by incubating the membrane with secondary antibody for 1 hour at room temperature. Initial western blots used ECL™ anti-human IgG horseradish peroxidase linked whole antibody (from sheep) (Cat. NA933V, GE Healthcare UK Limited, Buckinghamshire, UK) diluted 1:2 000 in TTBS, subsequent western blots used anti-Human-IgG (Fc specific)-horseradish peroxidase (HRP) produced in goat (Cat. A0170, Merck Group, Darmstadt, Germany) diluted 1:3 000 in TTBS. Transferred His tagged proteins (4dCD4 (control) and Bi-scFv) were detected by incubating the blocked membranes for 1 hour at room temperature in Penta-His HRP Conjugate diluted 1:2 000 in Penta-His Blocking Buffer (0.5% (w/v) Blocking Reagent, 0.1% (v/v) Tween-20 - Qiagen, Hilden, Germany), or His-Probe-HRP conjugate (4 µg/mL - Thermo Fisher Scientific, Waltham, MA, USA) diluted 1:1 000 in Penta-His Blocking Buffer. Residual HRP-linked antibody was washed off the membrane with 5 x 3-minute washes in 50 mL of TTBS. The membrane was developed using an HRP substrate for enhanced chemiluminescence (ECL) - (Pierce™ ECL Western Blotting Substrate (Thermo Fisher Scientific, Waltham, MA, USA)), according to the manufacturer's instructions. A 1:1 mix of peroxide solution and luminol enhancer solution was prepared, added to the membrane surface, and incubated for 5 minutes at room temperature. The membrane was imaged on the ChemiDoc™ MP Imaging System and the Quantity One® software, version 4.6.9 (BIO-RAD Laboratories, Hercules, CA, USA) on the chemiluminescence setting with no filter for maximal exposure.

Table A1. Primers and thermocycling conditions used in this study.

Construct	Experimental Procedure and Section	Primer name	Primer Sequence (5' to 3')	PCR Conditions	Amplicon Size (bp)
Bi-scFv	Amplify Bi-scFv sequence (section 2.3.2.2)	CMV_FOR Bi-scFv_REV	AGGTCTATATAAGCAGAGCTCGG CAGGGGCCCTCATCAGTGATGGTGATGGTGGTGGCCGGAGCCGCTGC	98°C for 10s; 30 cycles of: 98°C for 10s, 65°C for 15s, and 72°C for 45s; 72°C for 5 min; 4°C hold.	1 696
Bi-NAb	**Mutagenesis**				
	Silence *Bpi* I in CH2 domain of pmRNA_Bi-NAb (section 2.4)	BpiI_SDM_FOR BpiI_SDM_REV	AACAATCTCCAAGGCCAAGGG TTCTCGATTGGGGCAGGC	98°C for 30s; 25 cycles of: 98°C for 20s, 69°C for 15s, and 72°C for 3 min 30s; 72°C for 5 min; 4°C hold.	6 012
	Assembly				
	Gibson Assemble Bi-NAb and CH3_Hole (section 2.5.1)	CH3_Ho_FOR CH3_Ho_REV Bi-NAb_Linear_FOR Bi-NAb_Linear_REV	GACTGGCTGAACGGCAAGGAG CAGGCTCTTCTGGGTGTAGTG CACTACACCCAGAAGAGCCTG CTCCTTGCCGTTCAGCCAGTC	98°C for 30s; 30 cycles of: 98°C for 10s, 65°C for 15s, and 72°C for 30s; 72°C for 5 min; 4°C hold. 98°C for 30s; 30 cycles of: 98°C for 20s, 70°C for 15s, and 72°C for 2 min; 72°C for 5 min; 4°C hold.	390 3 889
	Sanger sequencing				
	* Bi-NAb *Bpi* I CH2 silenced (section 2.4.1)	CH3_Ho_FOR CH3_Ho_REV	GACTGGCTGAACGGCAAGGAG CAGGCTCTTCTGGGTGTAGTG	N/A	N/A
	pmRNA_Bi-NAb_Ho assembled (section 2.5.1.1)	CH3_Ho_Screen_FOR CH3_Ho_REV	GAGCCTGAGCTGCGCC CAGGCTCTTCTGGGTGTAGTG	96°C for 1 min; 25 cycles of: 96°C for 10s, 50°C for 5s, and 60°C for 4 min; 4°C hold.	
Tri-NAb	**Assembly**				
	Generate P2A cleavage peptide template DNA (section 2.5.2)	Cleavage_peptide_FOR Cleavage_peptide_REV	GGCTCCGGCCGACGAAGAAGGCGACGAGGAAGCGGAGCTACTAACTTCAGCCTG AGGTCCAGGGTTCTCCTCCACGTCTCCAGCCTGCTTCAGCAGGCTGAAGTTAGTAGCTC	98°C for 30s; 5 cycles of: 98°C for 10s, 63°C for 5s, and 72°C for 10s; 72°C for 5 min; 4°C hold.	93
	Gibson Assemble pmRNA_ Tri-NAb_sORF (section 2.5.2)	Bi-NAb_Ho_linear_FOR Bi-NAb_Ho_linear_REV 10E8_Kn_linear_FOR 10E8_Kn_linear_pmRNA_REV Cleavage_peptide_AMP_FOR Cleavage_peptide_AMP_REV	GGGCCCGTTTAAACGCTG CTTGCCAGGAGACAGGGA GTGGAGGAGAACCCTGGACCTATGGCGACGGGTTCAAGA AGGCAGCGTTTAAACGGGCCCTTAGCTGCACTCGGTAGGG CTGTCCCTGTCTCCTGGCAAGGGCTCCGGCCGACGAAG AGGTCCAGGGTTCTCCTCC	98°C for 30s; 25 cycles of: 98°C for 20s, 62°C for 15s, and 72°C for 4 min; 72°C for 5 min; 4°C hold. 98°C for 30s; 30 cycles of: 98°C for 20s, 68°C for 15s, and 72°C for 1 min 10s; 72°C for 5 min; 4°C hold. 98°C for 30s; 30 cycles of: 98°C for 20s, and 70°C for 15s; 72°C for 5 min; 4°C hold.	6 006 2 322 114
	Sanger sequencing				
	pmRNA_Tri-NAb_sORF (section 2.5.2)	CH3_Ho_Screen_FOR	GAGCCTGAGCTGCGCC	96°C for 1 min; 25 cycles of: 96°C for 10s, 50°C for 5s, and 60°C for 4 min; 4°C hold.	N/A
	Mutagenesis				
	SDM furin in 10E8_Kn (section 2.5.3.1)	10E8_Kn_furin_SDM_FOR 10E8_Kn_furin SDM_REV	CGAAGAAGGAGAAGATCAGGTTCGGGT TCGGCCAGGGCTCAG	98°C for 30s; 25 cycles of: 98°C for 20s, 65°C for 15s, and 72°C for 4 min 10s; 72°C for 5 min; 4°C hold.	6 177
	SDM furin in 10E8_Kn of Tri-NAb_sORF (section 2.5.3.3)	10E8_Kn_furin_SDM_FOR 10E8_Kn_furin SDM_REV	CGAAGAAGGAGAAGATCAGGTTCGGGT TCGGCCAGGGCTCAG	98°C for 30s; 10 cycles of: 98°C for 20s, 63°C for 15s, and 72°C for 5 min; 15 cycles of: 98°C for 20s, 69°C for 15s, and 72°C for 5 min; 72°C for 5 min; 4°C hold.	8 385
	Assembly				
	Gibson Assemble 10E8_Kn_Δfurin into pmRNA (section 2.5.3.2)	10E8_Kn_linear_pmRNA_FOR 10E8_Kn_linear_pmRNA_REV Bi-NAb_Ho_linear_FOR pmRNA_linear_REV	AGAAGAAATATAGCCGCCACCATGGCGACGGGTTCAAGA AGGCAGCGTTTAAACGGGCCCTTAGCTGCACTCGGTAGGG GGGCCCGTTTAAACGCTG GGTGGCGGCTATATTTCTTC	98°C for 30s; 30 cycles of: 98°C for 20s, 68°C for 15s, and 72°C for 1 min 15s; 72°C for 5 min; 4°C hold. 98°C for 30s; 30 cycles of: 98°C for 20s, 64°C for 15s, and 72°C for 2 min 30s; 72°C for 5 min; 4°C hold.	2 285 3 638
	Sanger sequencing				
	pmRNA_Tri-NAb_sORF_Δfurin (section 2.5.3.3)	CMV_FOR CH3_Ho_Screen_FOR 10E8_Kn_CP_seq_FOR 10E8_Kn_CP_seq_REV	AGGTCTATATAAGCAGAGCTCGG GAGCCTGAGCTGCGCC TTCCTGTACAGCAAGCTG CCAGGGCCACTGACAC	96°C for 1 min; 25 cycles of: 96°C for 10s, 50°C for 5s, and 60°C for 4 min; 4°C hold.	
	10E8_Kn_Δfurin (section 2.5.3.1)	10E8_Kn_CP_seq_FOR 10E8_Kn_CP_seq_REV	TTCCTGTACAGCAAGCTG CCAGGGCCACTGACAC	96°C for 1 min; 25 cycles of: 96°C for 10s, 50°C for 5s, and 60°C for 4 min; 4°C hold.	N/A
	pmRNA_10E8_Kn_Δfurin (section 2.5.3.2)	CMV_FOR 10E8_Kn_CP_seq_FOR 10E8_Kn_CP_seq_REV	AGGTCTATATAAGCAGAGCTCGG TTCCTGTACAGCAAGCTG CCAGGGCCACTGACAC	96°C for 1 min; 25 cycles of: 96°C for 10s, 50°C for 5s, and 60°C for 4 min; 4°C hold.	
Firefly luciferase	**Assembly**				
	Gibson Assemble Fluc into pmRNA (section 2.6)	Fluc_FOR Fluc_REV Bi-NAb_Ho_linear_FOR pmRNA_linear_REV	AGAAGAAATATAGCCGCCACCATGGCCGATGCTAAGAAC AGGCAGCGTTTAAACGGGCCCTTACACGGCGATCTTGC GGGCCCGTTTAAACGCTG GGTGGCGGCTATATTTCTTC	98°C for 30s; 30 cycles of: 98°C for 20s, 63°C for 15s, and 72°C for 1 min 5s; 72°C for 5 min; 4°C hold. 98°C for 30s; 30 cycles of: 98°C for 20s, 64°C for 15s, and 72°C for 2 min 30s; 72°C for 5 min; 4°C hold.	1 695 3 638
	Sanger sequencing				
	pmRNA_Fluc (section 2.6)	CMV_FOR	AGGTCTATATAAGCAGAGCTCGG	96°C for 1 min; 25 cycles of: 96°C for 10s, 50°C for 5s, and 60°C for 4 min; 4°C hold.	N/A

*Indicates Sanger sequencing performed by Inqaba Biotech; red text indicates incorporated His tag and *Apa*I restriction site; blue text indicates the incorporated mutation; green text indicates corresponding homologous overlap. N/A, not applicable.

Table A2a. Composition of 10% Separating PAGE gel to cast two 1 mm gels.

Solution (composition)	Volume (mL)
30% Acrylamide/2.7% Bisacrylamide monomer	5.0
4x Separating Gel Buffer (1.5 M Tris-HCl, pH 8.8)	3.75
10% SDS	0.15
Water	6.5
10% APS (make up fresh)	0.075
TEMED	0.0075

Table A2b. Composition of 4% Stacking PAGE gel to cast two 1 mm gels.

Solution (composition)	Volume (mL)
30% Acrylamide/2.7% Bisacrylamide monomer	1.33
4x Stacking Gel Buffer (0.5 M Tris-HCl, pH 6.8)	2.5
10% SDS	0.1
Water	6.0
10% APS (make up fresh)	0.075
TEMED	0.0075

SDS, sodium dodecyl sulphate; APS, Ammonium Persulfate; TEMED, N, N, N', N'-tetramethylethylene-diamine

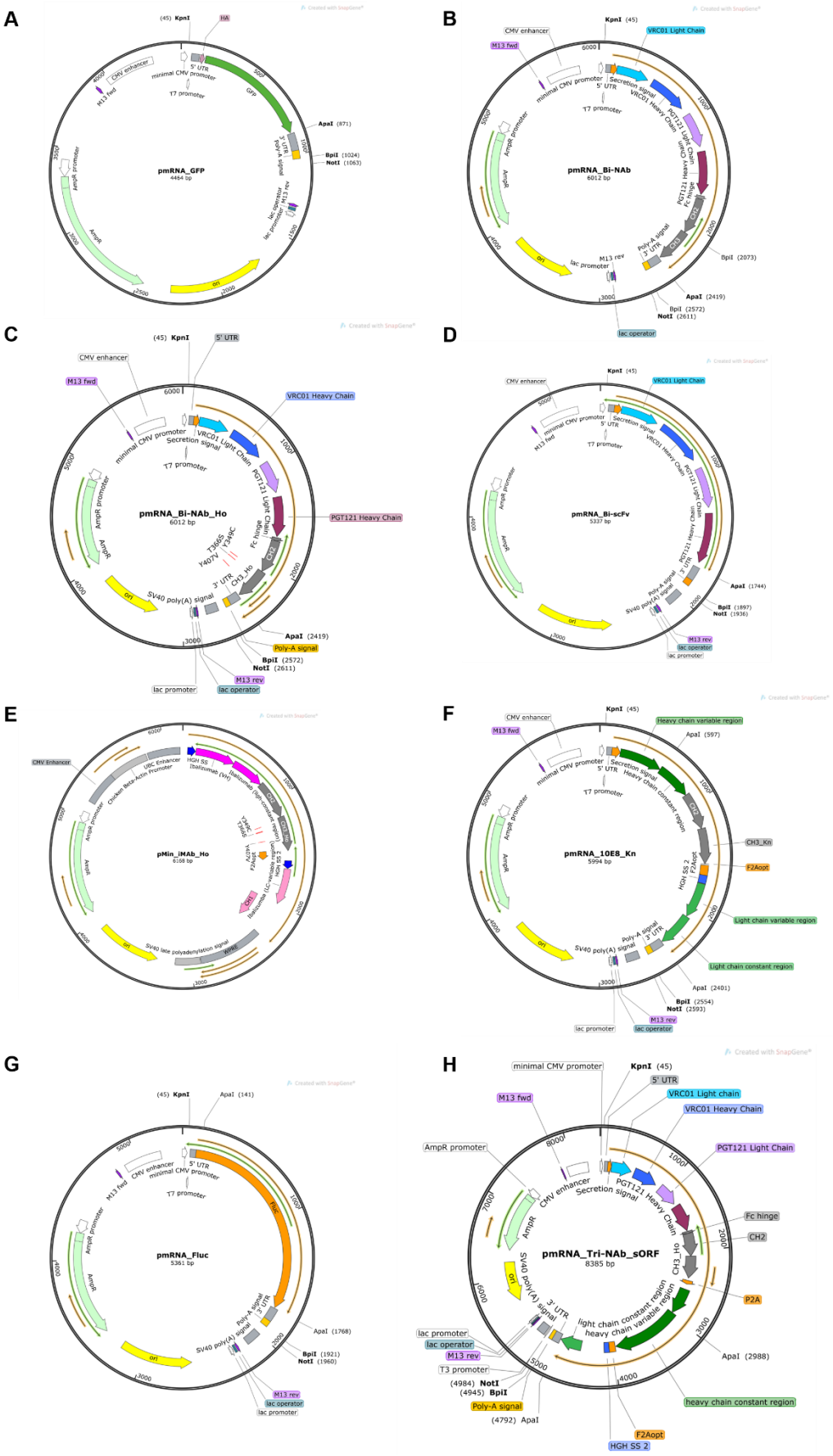


Figure A1. Plasmid maps for the final pmRNA expression constructs encoding the multispecific antibodies (Bi-scFv, Bi-NAb, Bi-NAb_Ho, 10E8_Kn, and Tri-NAb_sORF, as well as green fluorescent protein (GFP) and firefly luciferase (Fluc) (controls for mRNA-mediated expression, and pMin_iMAb_Ho as an assembly control.

For the pmRNA multispecific antibody constructs, the 5' UTR, multispecific antibody amino acid sequence, and 3' UTR sequences are given below, with the main features indicated as follows: Minimal CMV promoter, T7 promoter, secretion signal, VRC01 light chain variable region, VRC01 heavy chain variable region, PGT121 light chain variable region, PGT121 heavy chain variable region, **His tag**, Fc domain, P2A cleavage peptide, 10E8 heavy chain variable region, 10E8 heavy chain constant region, F2Aopt, 10E8 light chain variable region, 10E8 light chain constant region, poly-A signal, glycine-serine linkers.

>pmRNA_Bi-scFv

ggtaggcgtgtacggtgggaggtctatataagcagagctcggtacctaatacgactcactatagggaaataagaga
gaaaagaagagtaagaagaaatatagccgccaccMGWSCIILFLVATATGVHSSLTQSPGTLSLS
PGETAIISCRTSQYGSLAWYQQRPGQAPRLVIYSGSTRAAGIPDRFSGSRWGPDYN
LTISNLESGDFGVYYCQQYEFFGQGTKVQVDIGGGGSGGGGSGGGGSQVQLVQS
GGQMKKPGESMRISCRASGYEFIDCTLNWIRLAPGKRPEWMGWLKPRGGAVNYA
RPLQGRVTMTRDVYSDTAFLELRSLTVDDTAVYFCTRGKNCDYNWDFEHWGRGTP
VIVSSGGGGSGGGGSGGGGSGGGGSGGGGSSDISVAPGETARISCGEKSLGSRA
VQWYQHRAGQAPSLIIYNNQDRPSGIPERFSGSPDSPFGTTATLTITSVEAGDEADY
YCHIWDSRVPTKWVFGGGTTLTVLGGGGSGGGGSGGGGSQMQLQESGPGLVKP
SETLSLTCSVSGASISDSYWSWIRRSPGKGLEWIGYVHKSGDTNYSPSLKSRVNLS
LDTSKNQVSLSLVAATAADSGKYYCARTLHGRRIYGIVAFNEWFTYFYMDVWGNGT
QVTVSSGSG**HHHHHH****gggcccgtttaaacgctgccttctgcggggcttgccttctggccatgcccttcttctc
tcccttgcacctgtacctcttggtctttgaataaagcctgagtaggaaggctagaaaaaaaaaaaaaaaaaaaaa
aaaaaaaaaaaaaaaaaaaaaaaaaaaaaa

>pmRNA_Bi-NAb

ggtaggcgtgtacggtgggaggtctatataagcagagctcggtacctaatacgactcactatagggaaataagaga
gaaaagaagagtaagaagaaatatagccgccaccMGWSCIILFLVATATGVHSSLTQSPGTLSLS
PGETAIISCRTSQYGSLAWYQQRPGQAPRLVIYSGSTRAAGIPDRFSGSRWGPDYN
LTISNLESGDFGVYYCQQYEFFGQGTKVQVDIGGGGSGGGGSGGGGSQVQLVQS
GGQMKKPGESMRISCRASGYEFIDCTLNWIRLAPGKRPEWMGWLKPRGGAVNYA
RPLQGRVTMTRDVYSDTAFLELRSLTVDDTAVYFCTRGKNCDYNWDFEHWGRGTP
VIVSSGGGGSGGGGSGGGGSGGGGSGGGGSSDISVAPGETARISCGEKSLGSRA
VQWYQHRAGQAPSLIIYNNQDRPSGIPERFSGSPDSPFGTTATLTITSVEAGDEADY
YCHIWDSRVPTKWVFGGGTTLTVLGGGGSGGGGSGGGGSQMQLQESGPGLVKP
SETLSLTCSVSGASISDSYWSWIRRSPGKGLEWIGYVHKSGDTNYSPSLKSRVNLS
LDTSKNQVSLSLVAATAADSGKYYCARTLHGRRIYGIVAFNEWFTYFYMDVWGNGT
QVTVSSGSGMVRSDKTHTCPPCPAPELLGGPSVFLFPPKPKDTLMISRTPEVTCVV
VDVSHEDPEVKFNWYVDGVEVHNAKTKPREEQYNSTYRVVSVLTVLHQDWLNGK
EYKCKVSNKALPAPIEKTISKAKGQPREPQVYTLPPSREELTKNQVSLTCLVKGFYP
SDIAVEWESNGQPENNYKTTPPVLDSDGSFFLYSKLTVDKSRWQQGNVFSCSVMH
EALHNHYTQKSLSLSPGK**gggcccgtttaaacgctgccttctgcggggcttgccttctggccatgcccttctt
ctctcccttgcacctgtacctcttggtctttgaataaagcctgagtaggaaggctagaaaaaaaaaaaaaaaaaaaa
aaaaaaaaaaaaaaaaaaaaaaaaaaaaaa

>pmRNA_10E8_Kn

ggtaggcgtgtacggtgggaggtctatataagcagagctcggtacctaatacgactcactatagggaaataagaga
gaaaagaagagtaagaagaaatatagccgccaccMATGSRTSLLLAFGLLCLPWLQEGSAEVQ
LVESGGGLVKPGGSLRLSCSASGFDFDNAWMTWVRQPPGKGLEWVGRITGPGEG
WSVDYAAPVEGRFTISRLNSINFLYLEMNNLRMEDSGLYFCARTGKYYDFWSGYPP
GEEYFQDWGRGTLVTVSSASTKGPSVFPLAPSSKSTSGGTAALGCLVKDYFPEPVT
VSWNSGALTSGVHTFPAVLQSSGLYSLSSVVTVPSSSLGTQTYICNVNHKPSNTKV
DKRVEPKSCDKTHTCPPCPAPELLGGPSVFLFPPKPKDTLMISRTPEVTCVVVDVS
HEDPEVKFNWYVDGVEVHNAKTKPREEQYNSTYRVVSVLTVLHQDWLNGKEYKC
KVSNKALPAPIEKTISKAKGQPREPQVYTLPPCRDELTKNQVSLWCLVKGFYPSDIA
VEWESNGQPENNYKTTPPVLDSDGSFFLYSKLTVDKSRWQQGNVFSCSVMHEAL
HNHYTQKSLSLSPGRRRRRRSGSGAPVKQTLNFDLLKLAGDVESNPGPMATGSRT
SLLLAFGLLCLPWLQEGSASYELTQETGVSVALGRTVTITCRGDSLRSHYASWYQK
KPGQAPILLFYGKNNRPSGVPDRFSGSASGNRASLTISGAQAEDDAEYYCSSRDKS
GSRLSVFGGGTKLTVLSQPKAAPSVTLFPPSSEELQANKATLVCLISDFYPGAVTVA
WKADSSPVKAGVETTTPSKQSNNKYAASSYLSLTPEQWKSHRSYSCQVTHEGSTV
EKTVAPTECS*gggcccgtttaaacgctgccttctgcggggcttgccttctggccatgcccttcttctctcccttgcac
ctgtacctcttggtctttgaataaagcctgagtaggaaggctagaaaaaaaaaaaaaaaaaaaaaaaaaaaaaa
aaaaaaaaaaaaaaaaaaaaaa

>pmRNA_Tri-NAb_sORF

ggtaggcgtgtacggtgggaggtctatataagcagagctcggtacctaatacgactcactatagggaaataagaga
gaaaagaagagtaagaagaaatatagccgccaccMGWSCIILFLVATATGVHSSLTQSPGTLSLS
PGETAIISCRTSQYGSLAWYQQRPGQAPRLVIYSGSTRAAGIPDRFSGSRWGPDYN
LTISNLESGDFGVYYCQQYEFFGQGTKVQVDIGGGGSGGGGSGGGGSQVQLVQS
GGQMKKPGESMRISCRASGYEFIDCTLNWIRLAPGKRPEWMGWLKPRGGAVNYA
RPLQGRVTMTRDVYSDTAFLELRSLTVDDTAVYFCTRGKNCDYNWDFEHWGRGTP
VIVSSGGGGSGGGGSGGGGSGGGGSGGGGSSDISVAPGETARISCGEKSLGSRA
VQWYQHRAGQAPSLIIYNNQDRPSGIPERFSGSPDSPFGTTATLTITSVEAGDEADY
YCHIWDSRVPTKWVFGGGTTLTVLGGGGSGGGGSGGGGSQMQLQESGPGLVKP
SETLSLTCSVSGASISDSYWSWIRRSPGKGLEWIGYVHKSGDTNYSPSLKSRVNLS
LDTSKNQVSLSLVAATAADSGKYYCARTLHGRRIYGIVAFNEWFTYFYMDVWGNGT
QVTVSSGSGMVRSDKTHTCPPCPAPELLGGPSVFLFPPKPKDTLMISRTPEVTCVV
VDVSHEDPEVKFNWYVDGVEVHNAKTKPREEQYNSTYRVVSVLTVLHQDWLNGK
EYKCKVSNKALPAPIEKTISKAKGQPREPQVYTLPPSREELTKNQVSLTCLVKGFYP
SDIAVEWESNGQPENNYKTTPPVLDSDGSFFLYSKLTVDKSRWQQGNVFSCSVMH
EALHNHYTQKSLSLSPGKGSGRRRRRRGSGATNFSLLKQAGDVEENPGPMATGS
RTSLLLAFGLLCLPWLQEGSAEVQLVESGGGLVKPGGSLRLSCSASGFDFDNAWM
TWVRQPPGKGLEWVGRITGPGEGWSVDYAAPVEGRFTISRLNSINFLYLEMNNLR
MEDSGLYFCARTGKYYDFWSGYPPGEEYFQDWGRGTLVTVSSASTKGPSVFPLA
PSSKSTSGGTAALGCLVKDYFPEPVTVSWNSGALTSGVHTFPAVLQSSGLYSLSSV
VTVPSSSLGTQTYICNVNHKPSNTKVDKRVEPKSCDKTHTCPPCPAPELLGGPSVF
LFPPKPKDTLMISRTPEVTCVVVDVSHEDPEVKFNWYVDGVEVHNAKTKPREEQY
NSTYRVVSVLTVLHQDWLNGKEYKCKVSNKALPAPIEKTISKAKGQPREPQVYTLPP

CRDELTKNQVSLWCLVKGFYPSDIAVEWESNGQPENNYKTTPPVLDSDGSFFLYSK
LTVDKSRWQQGNVFSCSVMHEALHNHYTQKSLSLSPGRRRRRRRSGSGAPVKQTL
NFDLLKLAGDVESNPGPMATGSRTSLLLAFGLLCLPWLQEGSASYELTQETGVSVA
LGRTVTITCRGDSLRSHYASWYQKKPGQAPILLFYGKNNRPSGVPDRFSGSASGN
RASLTISGAQAEDDAEYYCSSRDKSGSRLSVFGGGTKLTVLSQPKAAPSVTLFPPS
SEELQANKATLVCLISDFYPGAVTVAWKADSSPVKAGVETTTPSKQSNNKYAASSYL
SLTPEQWKSHRSYSCQVTHEGSTVEKTVAPTECS*gggcccgtttaaacgctgccttctgcggg
gcttgccttctggccatgcccttcttctctcccttgcacctgtacctcttggtctttgaataaagcctgagtaggaaggctag
aaaaaaaaaaaaaaaaaaaaaaaaaaaaaaaaaaaaaaaaaaaaaaaaaaaaaa

For control constructs, the 5' UTR, amino acid sequence, and 3' UTR sequences are given below, with the main features indicated as follows: Minimal CMV promoter, T7 promoter, green fluorescent protein (GFP), Firefly luciferase (Fluc), poly-A signal.

>pmRNA_GFP

ggtaggcgtgtacggtgggaggtctatataagcagagctcggtacctaatacgactcactataggggaaataagaga
gaaaagaagagtaagaagaaatatagccgccaccMGYPYDVPDYASRVSKGEELFTGVVPILVE
LDGDVNGHKFSVSGEGEGDATYGKLTLKFICTTGKLPVPWPTLVTTLTYGVQCFSR
YPDHMKQHDFFKSAMPEGYVQERTIFFKDDGNYKTRAEVKFEGDTLVNRIELKGID
FKEDGNILGHKLEYNYNSHNVYIMADKQKNGIKVNFKIRHNIEDGSVQLADHYQQNT
PIGDGPVLLPDNHYLSTQSALSKDPNEKRDHMVLLEFVTAAGITLGMDELYK*
gggcccgtttaaacgctgccttctgcggggcttgccttctggccatgcccttcttctctcccttgcacctgtacctcttggtctt
tgaataaagcctgagtaggaaggctagaaaaaaaaaaaaaaaaaaaaaaaaaaaaaaaaaaaaaaaaaaaaaaaaa
aaaaaaaaa

>pmRNA_Fluc

ggtaggcgtgtacggtgggaggtctatataagcagagctcggtacctaatacgactcactataggggaaataagaga
gaaaagaagagtaagaagaaatatagccgccaccMADAKNIKKGPAPFYPLEDGTAGEQLHKA
MKRYALVPGTIAFTDAHIEVDITYAEYFEMSVRLAEAMKRYGLNTNHRIVVCSENSLQ
FFMPVLGALFIGVAVAPANDIYNERELLNSMGISQPTVVFVSKKGLQKILNVQKKLPII
QKIIIMDSKTDYQGFQSMYTFVTSHLPPGFNEYDFVPESFDRDKTIALIMNSSGSTG
LPKGVALPHRTACVRFSHARDPIFGNQIIPDTAILSVVPFHHGFGMFTTLGYLICGFR
VVLMYRFEEELFLRSLQDYKIQSALLVPTLFSFFAKSTLIDKYDLSNLHEIASGGAPLS
KEVGEAVAKRFHLPGIRQGYGLTETTSAILITPEGDDKPGAVGKVVPFFEAKVVDLDT
GKTLGVNQRGELCVRGPMIMSGYVNNPEATNALIDKDGWLHSGDIAYWDEDEHFFI
VDRLKSLIKYKGYQVAPAELESILLQHPNIFDAGVAGLPDDDAGELPAAVVVLEHGKT
MTEKEIVDYVASQVTTAKKLRGGVVFVDEVPKGLTGKLDARKIREILIKAKKGGKIAV*
gggcccgtttaaacgctgccttctgcggggcttgccttctggccatgcccttcttctctcccttgcacctgtacctcttggtctt
tgaataaagcctgagtaggaaggctagaaaaaaaaaaaaaaaaaaaaaaaaaaaaaaaaaaaaaaaaaaaaaaaaa
aaaaaaaaa

Appendix B: Supplementary result figures.

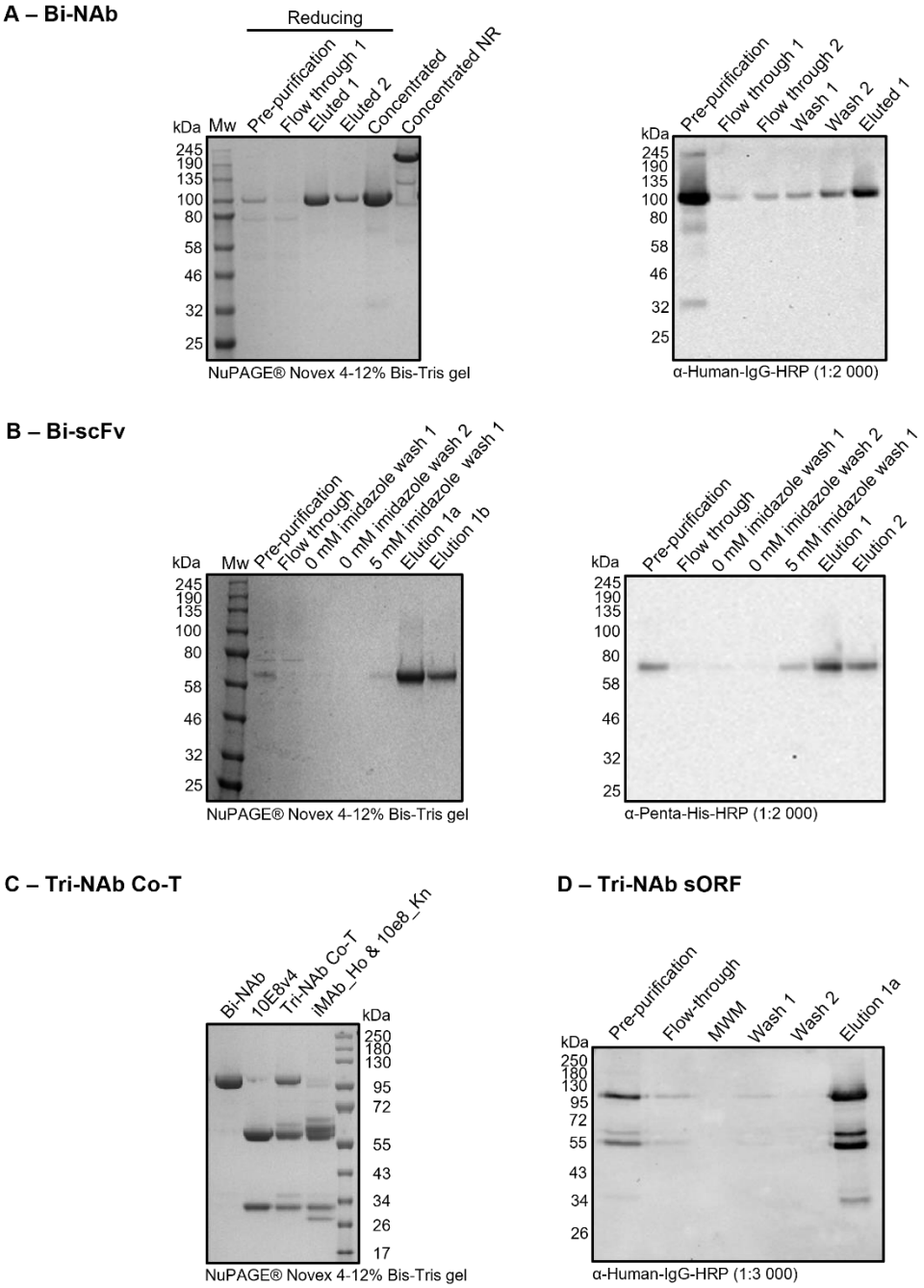


Figure B1. Recombinantly expressed multispecific and parental antibodies were purified by standard affinity chromatography procedures. (A) Antibody conformations containing an Fc domain (Bi-NAb, Tri-NAb, and parental VRC01, PGT121, and 10E8v4) were purified using protein A affinity chromatography. Two rounds of purification were performed to maximise yields of pure antibody (Bi-NAb purification is given as an example, the other antibodies displayed similar results). **(B)** The Bi-scFv antibody was purified by immobilised metal-ion affinity chromatography via its C-terminal His tag. Increasing wash concentrations of Imidazole eluted non-specific proteins and two rounds of elution incubations maximised the yield of pure Bi-scFv. SDS-PAGE gels (right side) resolved the antibody purification samples under reducing conditions on NuPAGE® Novex 4-12% Bis-Tris gels. Initial purification of the Tri-NAb Co-T **(C)** and the Tri-NAb sORF **(D)** demonstrated that the high molecular weight 10E8 heavy chain band (~65 kDa) was not removed during purification, further necessitating the need to improve the furin cleavage efficiency. Additionally, there was a 10E8 light chain high molecular weight band (~35 kDa) likely resulting from inefficient cleavage of the F2Aopt and a F2Aopt-tag attached to the C-terminus of the 10E8 light chain. Western blots had the samples resolved in parallel to the SDS-PAGE gels and transferred onto nitrocellulose membranes and developed using ECL™ anti-human IgG horseradish peroxidase (HRP) linked whole antibody (1: 2 000 - A), α-Human-IgG-HRP (1:3 000 - **D**) and α-Penta-His-HRP (1:2 000 - **B**). The protein ladder is the Color Protein Standard Broad Range P7719S (New England Biolabs, Ipswich, MA, USA).

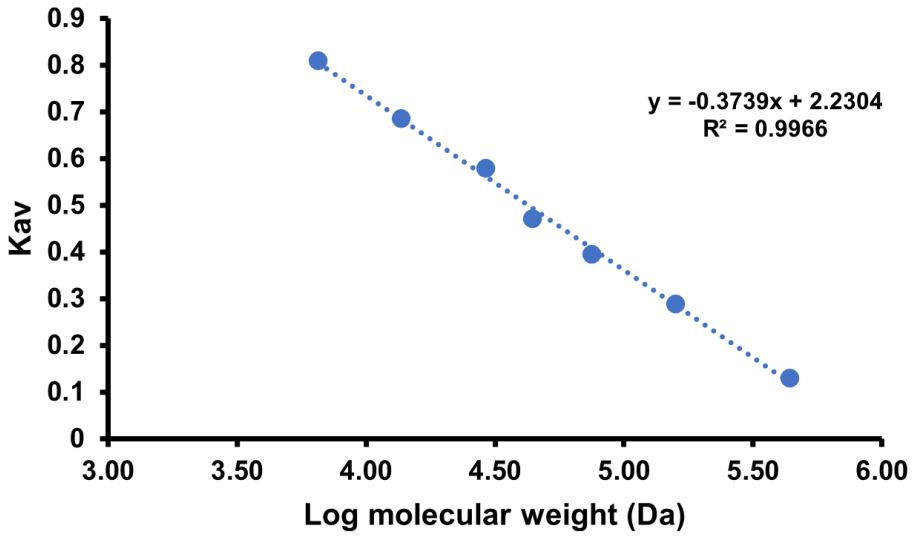


Figure B2. Molecular weight protein standard calibration curve. Chromatographic separation and a calibration curve for the HiLoad 16/600 Superdex 200pg column were generated using Blue Dextran and a mixture of low and high molecular weight standard proteins (aprotinin (6 500 Da), ribonuclease A (13 700 Da), carbonic anhydrase (29 000 Da), ovalbumin (44 000 Da), conalbumin (75 000 DA), aldolase (158 000 Da), ferritin (440 000 Da)). The Kav values of each protein standard was determined from the protein retention volumes of the size exclusion chromatography profile and plotted against the log of the protein standards molecular weight (Da). The calibration curve equation was used to determine the molecular weight of the parental and multispecific antibodies by substituting their Kav values and solving for x.

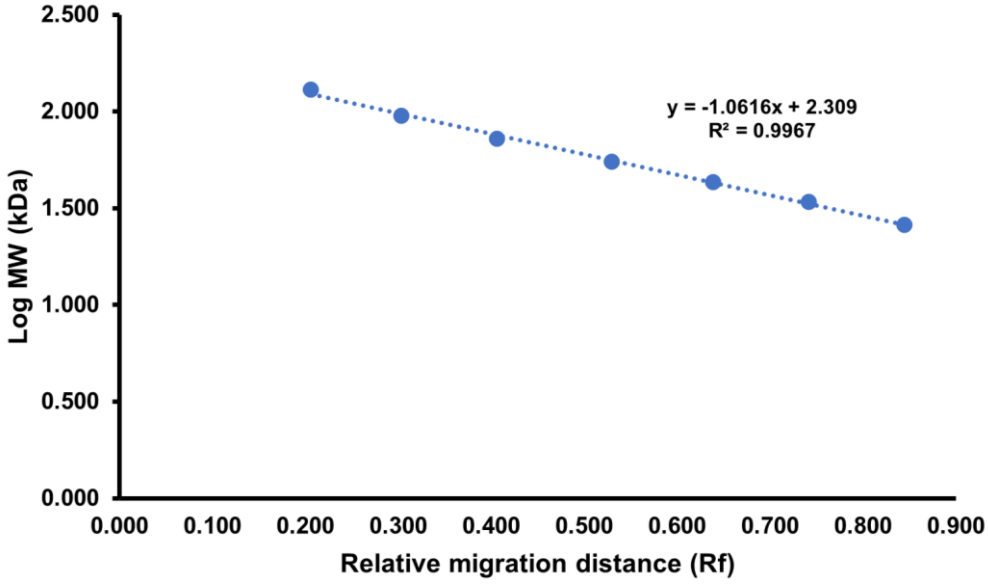


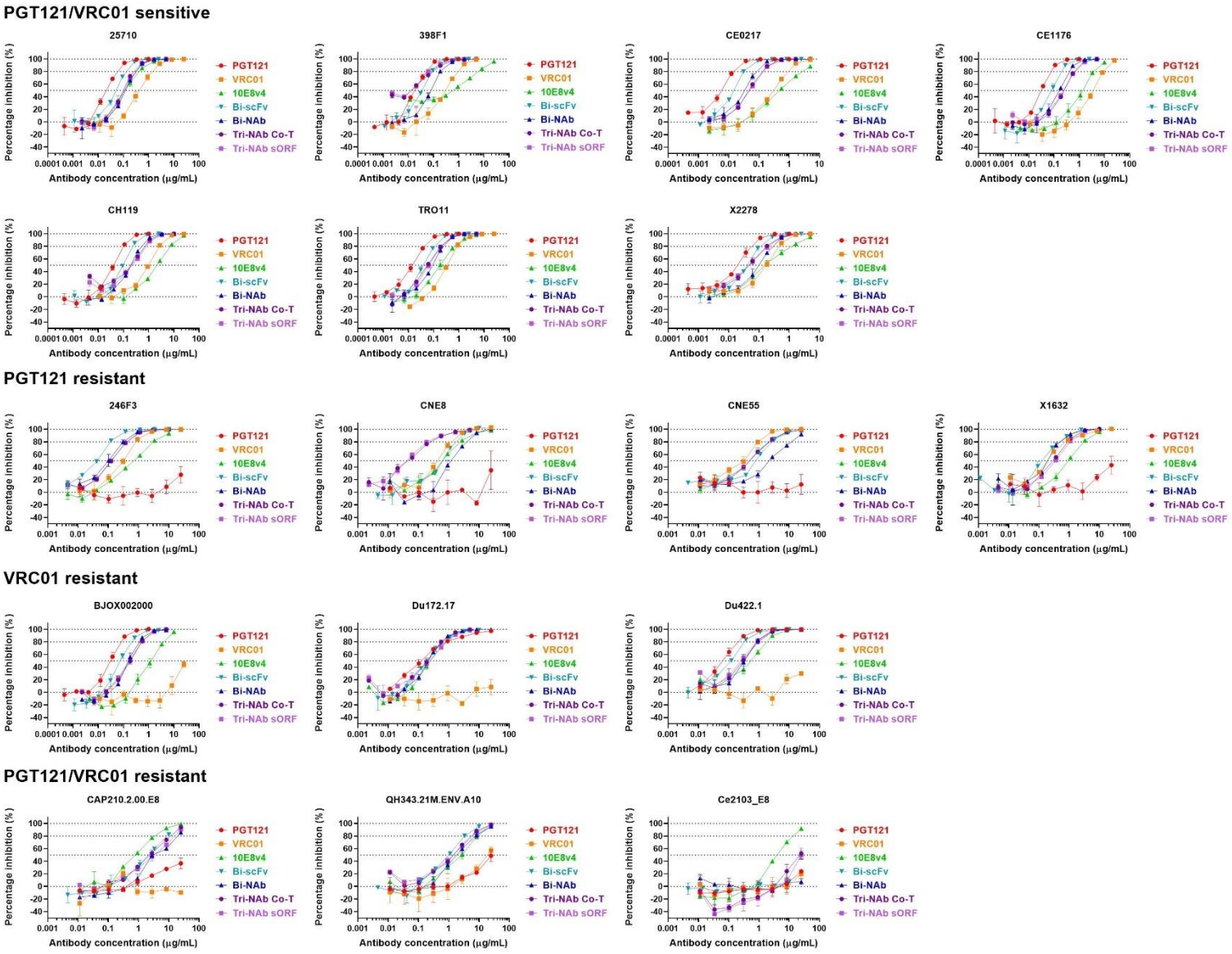
Figure B3. Relative migration distance of the protein molecular weights. The parental and multispecific antibodies were resolved on a 4-12% Bis-Tris gel (Figure 3.8B) alongside the Color Protein Standard Broad Range P7719S (New England Biolabs, Ipswich, MA, USA). The relative migration distance (Rf) of each molecular weight marker band was determined (migration distance of the protein/migration distance of the dye front) and plotted against the log molecular weight (MW) of the protein. The generated standard curve was used to determine the relative molecular weight of the reduced parental and multispecific antibody polypeptides, calculated from the standard curve by substituting their Rf values. This standard curve was less accurate at predicting the non-reducing sizes; therefore, the native antibody molecular weights were only calculated from the size exclusion standard calibration curve.

Table B1. Molecular weights of the parental and multispecific antibodies. Antibody molecular weights (kDa) were calculated from the respective relative migration distance (Rf) of the reduced and SDS-PAGE resolved polypeptides. Published molecular weights are from the SDS-PAGE results of Steinhardt *et. al.* (200). The native molecular weights were calculated from the calibration curve from the size exclusion chromatography (SEC) profiles. The predicted molecular weights the predicted N-linked glycosylation sites were computed from the antibody amino acid sequences (excluding the secretion signal sequence) using online computing tools.

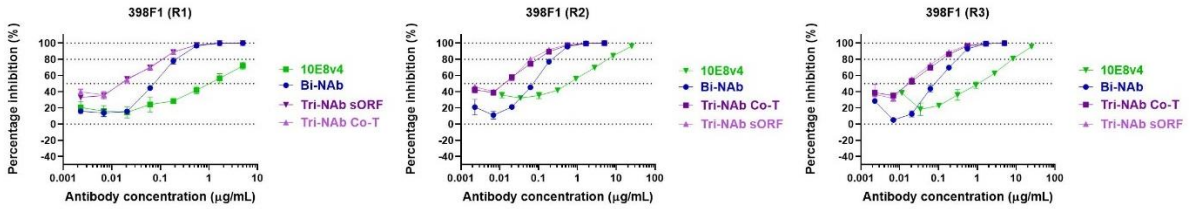
	Antibody state	**PGT121**	**VRC01**	**10E8v4**	**Bi-scFv**	**Bi-NAb**	**Tri-NAb**
Calculated from Rf values (kDa)	Reduced	HC (~64); LC (~30)	HC (~59); LC (~31)	HC (~61); LC (~31)	~71	~96	Bi-NAb (~96), 10E8: HC (~61), LC (~31)
Published (kDa)	Reduced	N/A	N/A	N/A	~58	~95	Bi-NAb (~85), 10E8: HC (~52), LC (~22)
	Non-reduced	N/A	N/A	N/A	~60	~170	~165
Calculated from SEC profiles (kDa)	Native	~195.9	~185.3	~136.4 (*adjusted to ~190.7)	~60.6	~219	~187.3
Predicted molecular weight (kDa)	Amino acid sequence	HC (~50.6); LC (~22.6)	HC (49.9); LC (23.1)	HC (~50.8); LC (~22.9)	~55.1	~80.3	Bi-NAb (~80.3), 10E8: HC (~51.2), LC (~29)
Predicted number of glycosylation sites	Amino acid sequence	3	2	1	3	4	6

*Molecular weight compensation for the non-specific hydrophobic interaction of 10E8v4 with SEC resin. See section 3.5.2 for details.

A


PGT121/VRC01 sensitive
25710
398F1
CE0217
CE1176
CH119
TRO11
X2278
PGT121 resistant
246F3
CNE8
CNE55
X1632
VRC01 resistant
BJOX002000
Du172.17
Du422.1
PGT121/VRC01 resistant
CAP210.2.00.E8
QH343.21M.ENV.A10
Ce2103_E8
Percentage inhibition (%)
Antibody concentration (μg/mL)
PGT121
VRC01
10E8v4
Bi-scFv
Bi-NAb
Tri-NAb Co-T
Tri-NAb sORF

B

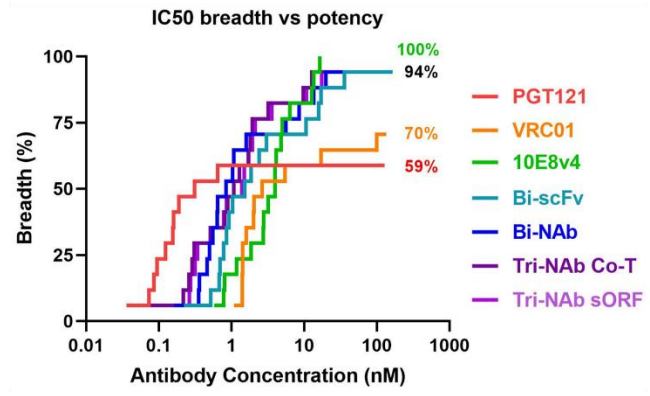


C

	10E8v4 IC50 (µg/mL)	10E8v4 IC80 (µg/mL)
398F1 (R1)	1.005	9.123*
398F1 (R2)	0.521	6.284
398F1 (R3)	1.142	8.452
Average	0.889	7.953

Figure B4. Parental and multispecific purified antibody viral inhibition profiles against a panel of 17 tier 2 HIV-1 pseudoviruses. (A) Neutralisation curves indicating the percentage viral inhibition achieved at the various concentration of antibody. The 50% and 80% viral inhibition achieved by each antibody relative to the virus-only control were used to generate the IC50/IC80 depicted date respectively. **(B)** The dual PGT121/VRC01 sensitive virus 398F1 plateaued at ~40% viral inhibition for the 10E8v4 parental and the Tri-NAb antibodies. The assay was repeated three times with no adjustment to the Tri-NAb (Co-T and sORF) profile, but slight differences in the 10E8v4 profiles. **(C)** The 10E8v4 IC50 and IC80 values determined for the 398F1 repeat neutralisation assays, indicating slight variation but no greater than a two-fold difference in values. Repeat 2 (R2) was used for the results. *Extrapolated IC80 value as this was not reached at the maximum concentration for that assay.

A



B

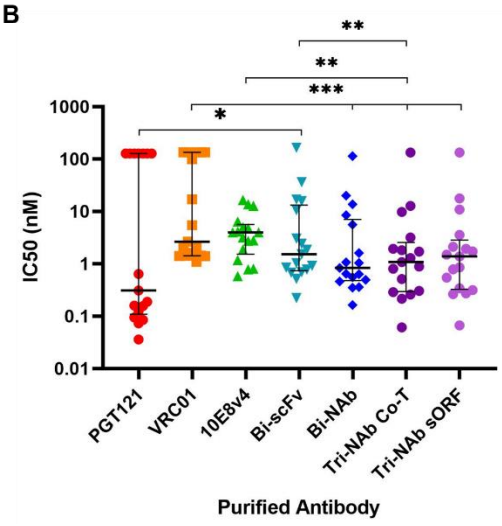


Figure B5. Neutralisation IC50 breadth and potency comparison of purified parental and multispecific antibodies against a panel of 17 HIV-1 pseudoviruses. IC50 depicted data (corrected to nM concentration) for the purified monoclonal parental and multispecific antibodies (Bi-scFv, Bi-NAb, and Tri-NAb generated from co-transfection (Co-T) and from the single open reading frame (sORF)). **(A)** Breadth-potency curve of parental and multispecific IC50 values (nM) indicating the enhanced neutralisation breadth of the multispecific antibodies over the parental antibodies VRC01 and PGT121. **(B)** Scatterplots depicting median IC50 values and interquartile range obtained for the parental and multispecific antibodies. Median IC50 values, demonstrating the enhanced potency of the multispecific antibodies over VRC01 and 10E8v4 parental antibodies but the potency of the PGT121 parental antibody was not conserved. Statistical differences were determined using a Friedman test with Dunns correction post hoc, level of significance indicated as follows: * <0.05, ** <0.01, *** <0.001.

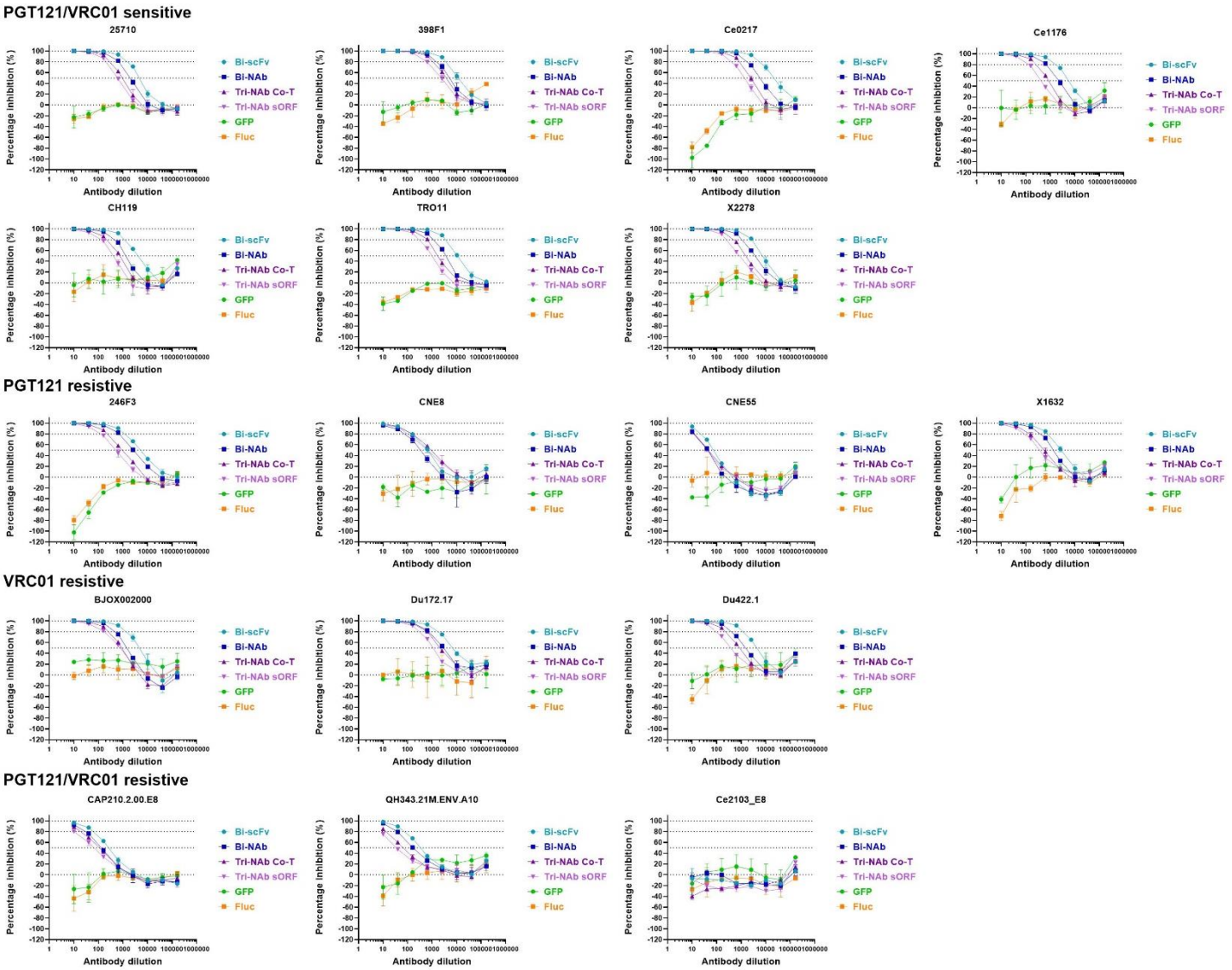


Figure B6. IVT-mRNA expressed multispecific antibody viral inhibition profiles against a panel of 17 tier 2 HIV-1 pseudoviruses. Neutralisation curves indicating the percentage viral inhibition achieved at the dilutions of mRNA-expressed clarified cell culture supernatant. The 50% and 80% viral inhibition achieved by each antibody relative to the virus-only control were used to generate the ID50/ID80 depicted date respectively.

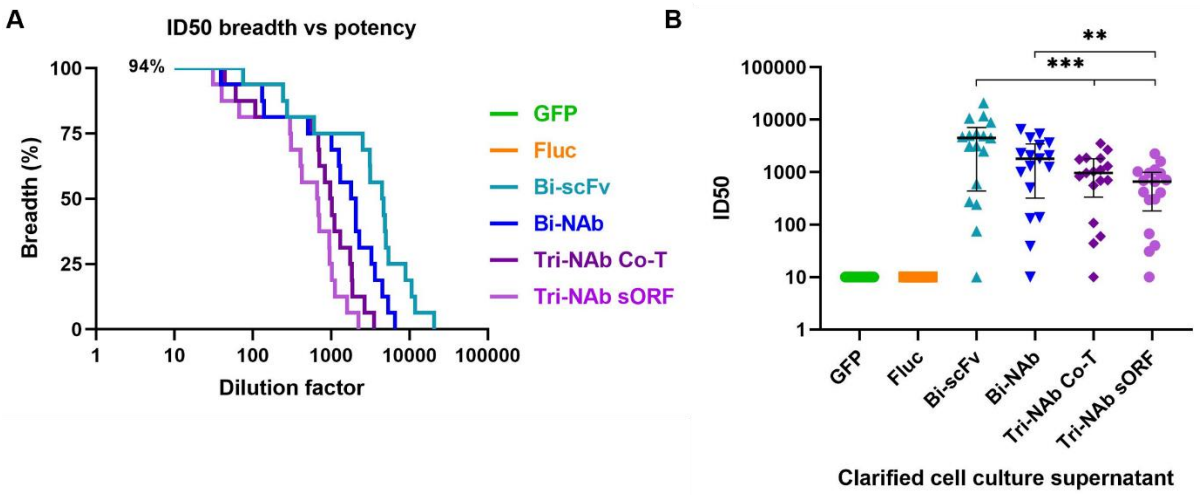


Figure B7. Neutralisation ID50 breadth and potency comparison of IVT-mRNA expressed multispecific antibodies against a panel of 17 HIV-1 pseudoviruses. ID50 depicted data for the mRNA-expressed controls (green fluorescent protein (GFP) and firefly luciferase (Fluc)) and multispecific antibodies (Bi-scFv, Bi-NAb, and Tri-NAb generated from co-transfection (Co-T) and from the single open reading frame (sORF)). **(A)** Breadth-potency curve of the ID50 values indicating the enhanced neutralisation breadth of the multispecific antibodies. **(B)** Scatter plots depicting median ID50 values obtained for the multispecific antibodies. Median and interquartile ranges (IQR) are shown, demonstrating the potency of the multispecific antibodies achieved from mRNA expression. Statistical differences were determined using a Friedman test with Dunns correction post hoc, level of significance indicated as follows: * <0.05, ** <0.01, *** <0.001.

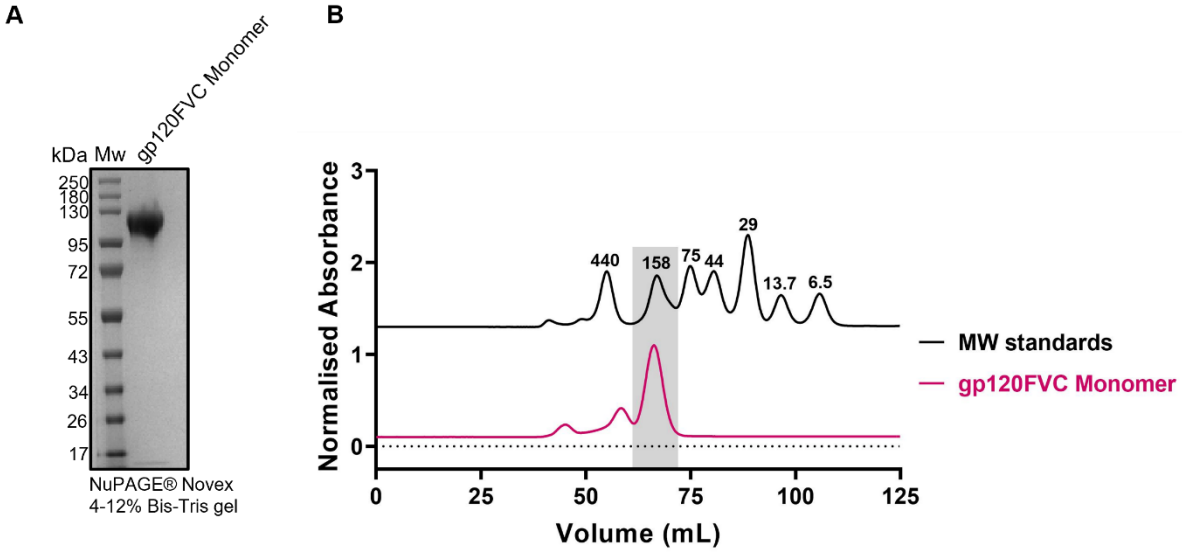


Figure B8. Affinity chromatography purification of HIV-1 Env gp120FVC Monomer glycoprotein. Gp120 founder virus consensus C (gp120FVC) Monomer was recombinantly expressed in mammalian 293F cells. **(A)** An optimised lectin-affinity chromatography procedure purified harvested culture supernatant containing the expressed protein and SDS-PAGE analysed the concentrated eluate (5 µg) under reducing conditions (+DTT). **(B)** Size exclusion chromatography was performed on the HiLoad 16/600 Superdex 200pg column to isolate the monomeric fraction (shaded grey). The protein ladder is the Color Protein Standard Broad Range P7719S (New England Biolabs, Ipswich, MA, USA). SDS-PAGE, sodium dodecyl sulphate-polyacrylamide gel electrophoreses; MW, molecular weight.

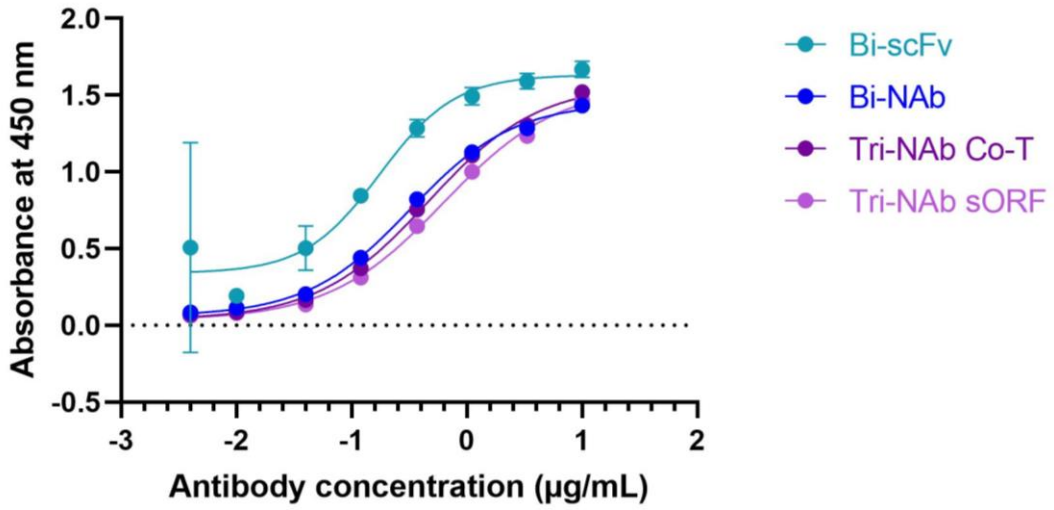


Figure B9. Representation of the multispecific antibody standard curves used to relatively quantify the mRNA-expressed multispecific antibody titres. A three-fold serial dilution ranging from 10 – 0.004 µg/mL of recombinantly expressed and purified Bi-scFv, Bi-NAb, or Tri-NAb (expressed from co-transfection (Co-T) and single open reading frame (sORF)) multispecific antibodies were run in triplicate in an ELISA. To generate the standard curve, the sigmoidal, 4PL equation on GraphPad prism 8 was used. R^2 values for the Bi-scFv was 0.85, the Bi-NAb and Tri-NAbs (Co-T and sORF) were 0.998.

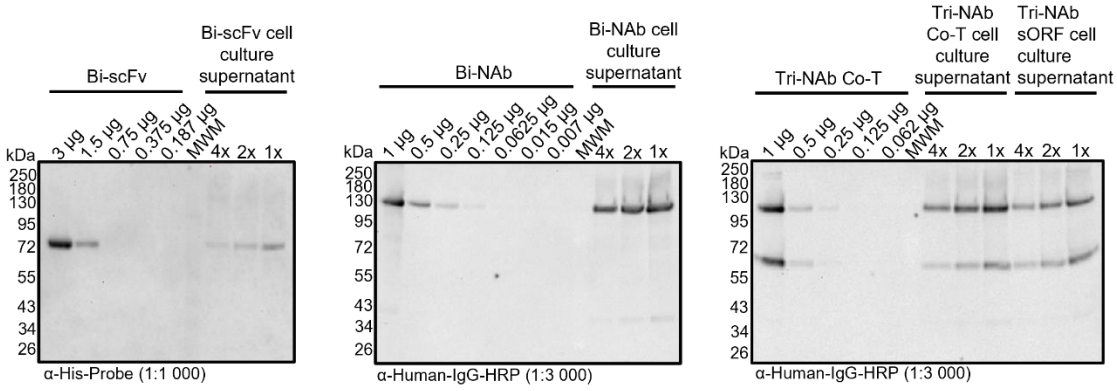


Figure B10. Western blot images analysed by densitometry to quantify the amount of mRNA-expressed multispecific antibodies in the clarified cell culture supernatant. Purified multispecific antibodies were used to make the standards with known loaded amounts of protein to generate a standard curve. Clarified cell culture supernatant from mRNA-expressed multispecific antibodies were diluted and quantified relative to the respective standard curves. Western blots were transferred onto nitrocellulose membranes and developed using His-probe horseradish peroxidase (HRP) conjugate (4 µg/mL - Thermo Fisher Scientific, Waltham, MA, USA) and anti-Human-IgG (Fc specific)-HRP produced in goat (1:3 000 - Cat. A0170, Merck Group, Darmstadt, Germany). The protein ladder is the Color Protein Standard Broad Range P7719S (New England Biolabs, Ipswich, MA, USA).

Appendix C: Ethics waiver.

UNIVERSITY OF THE WITWATERSRAND, JOHANNESBURG	HUMAN RESEARCH ETHICS COMMITTEE (MEDICAL)

Office of the Deputy Vice-Chancellor (Research & Innovation)

TO: Ms C O'Connor
School: Pathology
Department: Molecular Medicine and Haematology
HIV Pathogenesis Research Unit
Medical School
University
E-mail: 1842025@students.wits.ac.za

CC: Supervisor: Dr M Killick <Mark.Killick@wits.ac.za>
and <HREC-Medical.ResearchOffice@wits.ac.za>

FROM: Mr Iain Burns
Human Research Ethics Committee (Medical)
Tel: 011 717 1252

E-mail: Iain.Burns@wits.ac.za

DATE: 05/05/2022

REF: *R14/49*

PROTOCOL NO: W-CBP-220505-01 (This is your ethics application study reference number. Please quote this reference number in all correspondence relating to this study)

PROJECT TITLE: *mRNA-mediated delivery of anti-HIV-1 multispecific antibodies as a passive immunization strategy*

Please find attached the Ethics Waiver Certificate for the above project. I hope it goes well and that an article in a recognized publication comes out of it. This will reflect well on your professional standing and contribute to the Government funding of the University.

MSWorks2000/Iain0007/ClearScanWaiver.wps

UNIVERSITY OF THE WITWATERSRAND, JOHANNESBURG	HUMAN RESEARCH ETHICS COMMITTEE (MEDICAL)

Office of the Deputy Vice-Chancellor (Research & Innovation)

05/05/2022

Ref: W-CBP-220505-01

TO WHOM IT MAY CONCERN

Waiver: This certifies that the following research does not require clearance from the Human Research Ethics Committee (Medical)

Investigator: Ms C O'Connor
Student No. (if appropriate): 1842025
Staff No. (if appropriate):

Supervisor: Dr M Killick

School: Pathology
Department: Molecular Medicine and Haematology
HIV Pathogenesis Research Unit
Medical School
University

Project title: *mRNA-mediated delivery of anti-HIV-1 multispecific antibodies as a passive immunization strategy*

Reason: In vitro laboratory study
No human participants will be involved in the study

CB Penny

Dr CB Penny
Chairperson: Human Research Ethics Committee (Medical)

Research Office Secretariat:
Third Floor, Phillip Tobias Building, corner of St Andrews and York Roads, Parktown, Johannesburg 2193
Postal address: Private Bag 3, Wits 2050
Tel Nos: +27 (0)11 717 1234/1252/2656/2700
Office E-mail: HREC-Medical.ResearchOffice@wits.ac.za
Website:
https://www.wits.ac.za/research/researcher-support/research-ethics/ethics-committees/